A posteriori error analysis for some problems related to fuel cells simulations

Hussein Albazzal

Thèse de doctorat préparée à l'Université de Franche-Comté

par

Hussein ALBAZZAL

Pour obtenir le grade de
Docteur en Mathématiques de l'Université Bourgogne Franche-Comté

Analyse d'erreur *a posteriori* pour certains problèmes liés aux simulations de piles à combustible

Thèse soutenue à Besançon le 26/09/2023, devant le jury composé de :

Martin VOHRALIK	Directeur de recherche, Inria Paris	Président
Martin VOHRALIK	Directeur de recherche, Inria Paris	Rapporteur
Jérôme POUSIN	Professeur, Université de Lyon	Rapporteur
Véronique MARTIN	Maîtresse de Conférences, Université de Picardie Jules Verne	Examinatrice
Toni SAYAH	Professeur, Université Saint Joseph de Beyrouth, Liban	Examinateur
Alexei LOZINSKI	Professeur, Université Bourgogne Franche-Comté	Directeur
Roberta TITTARELLI	Maîtresse de Conférences, SUPMICROTECH-ENSMM	Co-encadrante
Samir JEMEI	Professeur, Université de Franche-Comté	Invité

Thèse de doctorat préparée à l'Université de Franche-Comté

par

Hussein ALBAZZAL

Pour obtenir le grade de
Docteur en Mathématiques de l'Université Bourgogne Franche-Comté

A posteriori error analysis for certain problems related to fuel cell simulations

Thèse soutenue à Besançon le 26/09/2023, devant le jury composé de :

Martin VOHRALIK	Directeur de recherche, Inria Paris	Président
Martin VOHRALIK	Directeur de recherche, Inria Paris	Rapporteur
Jérôme POUSIN	Professeur, Université de Lyon	Rapporteur
Véronique MARTIN	Maîtresse de Conférences, Université de Picardie Jules Verne	Examinatrice
Toni SAYAH	Professeur, Université Saint Joseph de Beyrouth, Liban	Examinateur
Alexei LOZINSKI	Professeur, Université Bourgogne Franche-Comté	Directeur
Roberta TITTARELLI	Maîtresse de Conférences, SUPMICROTECH-ENSMM	Co-encadrante
Samir JEMEI	Professeur, Université de Franche-Comté	Invité

Titre: Analyse d'erreur *a posteriori* pour certains problèmes liés aux simulations de piles à combustible.

Mots Clés: Estimation d'erreur *a posteriori*, couplage dimensionnel mixte, algorithme adaptatif, Méthode des Éléments Finis, FreeFEM.

Résumé: La principale motivation de cette thèse est le besoin de simulations numériques efficaces des écoulements de gaz dans les canaux serpentins des piles à combustible à membrane échangeuse de protons. Nous considérons les modèles de Poisson et de Stokes dans un domaine 2D composé de plusieurs longues sections rectangulaires droites et de plusieurs coudes. Afin d'accélérer la résolution et de réduire les coûts de calcul, nous proposons des modèles 0D (un profil parabolique fixe pour l'équation de Poisson et l'écoulement de Poiseuille pour les équations de Stokes), et nous résolvons par éléments finis le modèle 2D dans les coudes. Afin d'atteindre la tolérance souhaitée de l'erreur entre la solution exacte et la solution approchée provenant du modèle couplé 0D/2D, nous devons surmonter un double défi : comment détecter la position appropriée de l'interface entre les modèles 0D et 2D et comment contrôler l'erreur de discrétisation dans les coudes. Pour cela, nous avons développé des estimateurs d'erreur a posteriori basés sur la reconstruction de flux équilibré dans les sous-domaines où la méthode des éléments finis est appliquée. Dans le modèle couplé 0D/2D pour Poisson, les estimations donnent une borne supérieure calculable garantie globale de la norme d'énergie de la solution. Dans le modèle couplé 0D/2D pour Stokes, les estimations donnent une borne supérieure garantie globale pour l'erreur H1 en vitesse et l'erreur L2 en pression sur le domaine entier. Dans ce dernier cas, l'estimateur fait intervenir la constante inf-sup qui est en général inconnue (dans nos cas de test, elle est cependant connue qu'elle est très petite), ce qui rend l'estimateur pas complètement calculable en pratique. Nous avons également étudié l'influence de la constante inf-sup sur l'efficacité des estimations d'erreur a posteriori et nous avons poursuivi quelques idées pour construire de nouveaux estimateurs garantis indépendants de la constante inf-sup. Des bornes inférieures globales pour l'erreur sont également dérivées pour les modèles de Poisson et de Stokes. Les estimateurs proposés peuvent être scindés en deux parties : une première indiquant l'erreur due à la position de l'interface et une seconde indiquant l'erreur due à la discrétisation. A l'aide de ces estimateurs, un algorithme est proposé pour choisir la position de l'interface et effectuer un raffinement adaptatif du maillage afin d'équilibrer les deux sources d'erreur et d'atteindre la précision souhaitée. Les estimateurs et l'algorithme adaptatif sont validés numériquement.

Title: *A posteriori* error analysis for certain problems related to fuel cell simulations.
Keywords: *A posteriori* error estimate, mixed dimensional coupling, adaptive algorithm, Finite Element Method, FreeFEM.

Abstract: The main motivation of this thesis is the need for efficient numerical simulations of the gas flows in the serpentine channels of the proton-exchange membrane fuel cells. We consider Poisson and Stokes models in a 2D domain which is composed of several long straight rectangular sections and several bends. In order to speed up the resolution and to reduce the computational costs, we propose 0D models (a fixed parabolic profile for Poisson equation and Poiseuille flow for Stokes equations), and we apply a finite element resolution for the 2D model in the bends. In order to achieve the desired tolerance of the error between the exact solution and the approximated solution coming from the 0D/2D coupled model, we have to overcome a double challenge: how to detect the suitable position of the interface between the 0D and 2D models and how to control the discretization error in the bends. For this purpose, we have developed *a posteriori* error estimators based on equilibrated flux reconstruction in the subdomains where the finite element method is applied. In the coupled 0D/2D model for Poisson, the estimates give a global guaranteed computable upper bound of the energy norm of the solution. In the coupled 0D/2D model for Stokes, the estimates give a global guaranteed upper bound for the H1-error in velocity and the L2-error in pressure on the whole domain. In the latter case, the estimator involves the inf-sup constant which is in general unknown (in our test cases, it is known to be very small though), thus making the estimator not completely computable in practice. We have also studied the influence of the inf-sup constant on the efficiency of *a posteriori* error estimates and we have pursued some ideas to construct new guaranteed estimators which are independent of the inf-sup constant. Global lower bounds for the error are also derived for Poisson and Stokes model. The proposed estimators can be split into two parts: a first one indicating the error due to the position of the interface and a second one indicating the error due to the discretization. Using these estimators, an algorithm is proposed to choose the interface position and to make adaptive mesh refinement in order to balance the two sources of the error and to achieve the desired accuracy. The estimators and the adaptive algorithm are validated numerically.

Codes AMS: 65N15; 65N30 ; 65N50.

UBFC
UNIVERSITÉ
BOURGOGNE FRANCHE-COMTÉ

Acknowledgement

Between scientific rigor and industrial pragmatism, this thesis is the result of multiple discussions, scientific and technical reflections within the framework of Laboratoire de Mathématiques de Besançon (LMB). I would like to thank from the bottom of my heart Prof. Alexei LOZINSKI, my thesis's director, as well as Prof. Roberta TITTIRALLI, my co-director, for the trust they placed inside me with a good orientation that allowed me to make my own experience. I have learned a lot, from the point of scientific view as well as, from a personal point of view. I would like to express my gratitude for their invaluable support and effort throughout all this fruitable journey. I would like to thank Prof. Geneviève Dusson for the funding and the material's support. All my gratitude also goes to Prof. Martin VOHRALIK for the contribution in this work and for the course that he has discussed regarding "a posteriori error estimator" that was so beneficial for me. Also, I would like to thank Prof. Martin VOHRALIK and Prof. Jérôme POUSIN for the interest they have shown in our work by accepting honorary to be the reporters of the thesis. I would also like to thank Prof. Toni SAYAH and Prof. Véronique MARTIN for the interest they have shown in our work by accepting honorary to be the examiners of the thesis. In addition, I would like to express my gratitude to Prof. Samir JEMEI for accepting our invitation and to Prof. Fei GAO for his help and contribution to the project and the progress of my thesis. I would like to express my gratitude to Prof. Ayman Mourad who taught me at the Lebanese University, for his wise, advices and his support during all my journey of Study. I would like to thank those who have come a long way by my side, especially my colleagues in Laboratoire de Mathématiques de Besançon. I would like to thank all the professors who taught me at Limoges, Toulouse and at the Lebanese University. Finally, I would like to thank all my family members and my friends who have supported me, and who really know how challenging it was for me at the beginning till the end, the difficulties I passed by, and the nights I spent working on this PHD that make me nowadays so proud for speaking about it.

Contents

Introduction

The present work is motivated by models of the serpentine cathode-anode flow channels in Proton Exchange Membrane Fuel Cells (PEMFC), cf. [51]. A quite acceptable model proposed to describe the flow distribution in these channels is the steady-state incompressible Navier-Stokes equations (but in function of the application more complete and complex models can be adopted, as the compressible and/or unsteady equations) and one hurdle is to make efficient computations in these very stretched rectangular regions linked by relatively small bends. To have an idea of these channels, one can see layers 1 and 7 of Figure 1.1 at page 17. In particular, we deal with the 2D cross–sectional area (when the plate is sliced parallel to the channels). Since the numerical resolution implies a high computation complexity, in this thesis we want to propose an approach to simplify its resolution based on the geometry of channels and overall based on error estimates which can be used to choose a compromise between reduced time of computation and accuracy. In this thesis we focus on the Poisson and Stokes equations to lay a foundation in view of a generalization to the incompressible Navier-Stokes. Following typical boundary conditions in PEMFC, cf. for example [81], we choose the Poiseuille flow as boundary conditions on the inlet and outlet boundaries of the channel, and no-slip boundary condition on the wall.

In order to speed up the computations, the idea is to split the resolution as follows: in the rectangular regions of the domain, the flow is approximated by simple analytical solutions, namely the Poiseuille flow which is accurate if the flow is sufficiently far from the bends (we call this 0D model), in the bend regions we keep the original governing equations and approximate them by the finite element (FE) method (we call this the 2D model). We refer to this as the 0D/2D model. There exists different ways to derive a coupled model. In [42, 43, 63], 0D/3D coupling is obtained for the time dependent Navier-Stokes system by assuming the dominance of the axial velocity and integrating the governing equations on a section. In [46] and in [57] an asymptotic analysis is used to get respectively the 0D/3D and 0D/2D coupled simplified models for time dependent Navier-Stokes equations. A 0D/2D coupled model for Poisson equation is derived in [70] and [59] by the asymptotic analysis. In the thesis we derive the 0D model using the asymptotic analysis. Indeed, we work with the domain Ω, which is one serpentine of the channel, as showed in Figure 1.3 at page 19, knowing that we can iterate the ideas developed in Ω for all the other serpentines (as we show *e.g.* in Section 2.4). So, the stretched rectangular portion of the domain Ω, which we call in this thesis Ω' and refer to it as the 0D domain, cf. Fig. 1.4, the solution is approximated by a simple explicit expression (the analogue of the Poiseuille velocity). In the remaining part of the domain, denoted by $\tilde{\Omega} = \Omega \backslash \Omega'$ and referred to it as the 2D domain, we approximate the solution of the Poisson or Stokes equation (the 2D model) using the FE method. The 0D and 2D domains are separated by an interface γ. For the Poisson 0D/2D model the coupling condition on the interface γ is the continuity of the velocity, while for the Stokes 0D/2D model we find a quite natural coupling condition which is derived from the variational formulation, that is the continuity of the normal average force on the interface γ with an appropriate weight. For numerical implementation,

also a simpler coupling condition is explored, which gives similar numerical results. After coupling, we observe that the error between "0D/2D simplified model" and "original 2D non simplified model" is affected by the mesh size and the position of the interface so, the error between the "original 2D non simplified model" and the "0D/2D simplified model" is due to the discretization error and the error that comes from the position of the interface. We want to extend the area where we want to impose 0D model and since we do not know the exact solution of the Poisson and Stokes equations, we have studied an *a posteriori* estimator in order to get a computable upper bound for the error between the proposed simplified 0D/2D model and the original non coupled 2D model.

In order to study the error between the exact solution of a partial differential equation (PDE) and the approximated numerical solution we have two main estimations of the error which are very important in numerical analysis. The first one is represented by *a priori* estimation of the error while the second one is named by *a posteriori* error estimation. *A priori* estimation is qualitative while *a posteriori* estimation is quantitative. In general, the main goal of using *a priori* estimation is to prove the optimal order of convergence for the error under quite smooth hypothesis. For example in [68] the authors prove the optimal convergence of the error in $H^1 - norm$ and sub-optimal order of convergence in $L^2 - norm$ for linear elliptic interface problems. In [62], *a priori* estimation is used in order to reduce the rate of convergence for the discontinuous Galerkin method when applied to the Poisson problem. There is many articles which deal with *a priori* error estimation such as [10, 24, 25, 50, 67]. A limit of *a priori* error estimation is the dependence of the upper bound of the error on the exact solution which is unknown and consequently we get an uncomputable upper bound. In reality the exact solution is unknown and sometimes it is singular, *e.g.* as in L-shaped domains, then using *a priori* analysis can not help to use adaptive strategies in order to obtain an optimal convergence and for this reason we need to study *a posterori* error estimation. As we do not know the exact solution, *a posteriori* error estimation gives a computable upper bound of the numerical error between the exact and the approximated solution and this upper bound depends on known quantities only, such as the approximated solution and the *data* of the problem, some remarkable works in this subject are done by Verfürth [74], Ainsworth and Oden [1], Babuška and Strouboulis [8], Neittaanmäki and Repin [58], Han [48], or Repin [64]. *A posteriori* error estimation is widely used in FE discretization methods, some pioneer works are done by Babuška and Rheinboldt [4–7, 9]. Among all these *a posteriori* error estimators we will focus in the thesis on so-called *equilibrated flux*. The main concepts of the equilibrated fluxes estimates is related to Prager–Synge equality [61] and the hypercircle method as in Synge [69]. There are many research studies about equilibrated fluxes estimators such as Repin [66], Destuynder and Métivet [30], Luce and Wohlmuth [55], Ladevèze and Leguillon [54], Korotov [53], Vejchodský [72], or Braess and Schöberl [16], Fierro and Veeser [41].

We propose an *a posteriori* error analysis for the coupled Poisson equation, then we extend it for the coupled steady Stokes equations, and the perspective is to enlarge the analysis for a coupled steady incompressible Navier-Stokes system. The main contribution in our study is that we adapt the approach of Vohralik *et al.* [39, 78] in the context of the coupled 0D/2D model in order to detect the suitable position of the interface between 0D and 2D model and also to adapt the mesh for the FE 2D model in the bend. The approach of Vohralik *et al.* is based on a flux/stress reconstruction on a whole domain

where a PDE is discretized with a numerical method. In this work, we introduce a new definition of the reconstructed flux/stress σ_h, in order to be able to estimate the error of the discretization for the 2D model but also for the choice of the interface position. Indeed, we have divided the estimator into two parts, the first contribution estimates the error caused by the position of the interface and another contribution is related to the FE error in the 2D domain. The main contributions this PhD thesis are specified in the following paragraph.

Thesis contributions

For *a posteriori* error we separate the estimator into two types: the first type comes from the error due to the position of the interface and the second type comes from the error of the numerical discretization in the 2D domain. The idea is to use these contributions in order to determine a suitable position of the interface and a suitable mesh, according to some tolerance.

The first goal is to device coupling models fot the Poisson and Stokes equations using asymptotic analysis as in [45, 59, 70].

The derivation of *a posteriori* error estimator depends on the flux reconstruction which is introduced by Vohralik *et al.* [28, 32, 38, 39, 60]. The second goal is to introduce a new definition of the flux reconstruction σ_h to be defined on the whole domain Ω which is computed in a way for the 0D model and in another way for the 2D model in a similar way of Vohralik *et al.* in order to introduce the estimator which inform us about the error about coupling and discretizing.

Finally, the third goal, that is deeply related to the previous goal, is to prove the reliability (upper bound for the error by the estimator) and the efficiency (lower bound for the error by the estimator), if it is possible, of the proposed estimators. We remark that the efficiency has to be global in what concerns the error produced by the 0D/2D coupling: once we choose an interface to make the coupling problem, that impacts the solution globally.

Throughout the thesis we also pay attention to validate the estimators numerically and to design adaptive algorithms to use them successfully.

Plan of the Thesis

We have three chapters and these chapters are constructed as the following.

Chapter 1. In this chapter we present the context, we consider a polygonal domain Ω and we talk about the physical model, the derivation of the coupled 0D/2D of Poisson and Stokes equations. Moreover we give a general presentation about equilibrated *a posteriori* error estimators on a simple and standard model where there is no coupling condition.

Chapter 2. In this chapter we deal with the Poisson equation on the polygonal domain Ω. We introduce a first attempt of the definition of the flux reconstruction of the coupled 0D/2D model, and this estimator is called "simple *a posteriori* estimator". We

prove the guaranteed upper bound (reliability) of the estimator, but the lower bound (efficiency) seems impossible to be proved and we explain the reason. So, we introduce a second definition of the flux reconstruction with gives to us a guaranteed upper bound and a lower bound (efficiency) of the error between the coupled 0D/2D model and the 2D non coupled model. We make a numerical comparison between the two estimators of the two fluxes. We make adaptation of the mesh in order to get an optimal convergence or to improve the convergence of the error and estimator. At the end of this chapter we present briefly an extension of this work for multiple channels (with many interfaces and coupling).

Chapter 3. In this chapter we consider the Stokes equation. Here, a new problematic is added: the Stokes problem involves the β constant, that is the constant in the inf-sup condition that ensures that the Stokes problem is well-posed, and this constant is in general in the equilibrated error estimators. The value of this constant is in general unknown, but we know that for long strechted channels this value is small. We define a stress reconstruction for the 0D/2D Stokes model in order to get "a simple *a posteriori* estimator and we prove the guaranteed upper bound estimate (reliablity), but the lower bound (efficiency) is not proved for the first stress reconstruction. We also introduce a second stress reconstruction and we prove the global upper bound and the local lower bound (local efficiency) but we have assumed that $\left\|\tilde{\Omega}\right\| \leq CR^2$ where $\tilde{\Omega}$ is the domain related to 2D model and R represents the width of the inlet in the channel. Since the estimators of the coupled 0D/2D stokes model depends on the inf-sup constant, we will consider instead the 2D non coupled Stokes equation and we will introduce a new idea to develop an estimator for which we have proved the upper and lower bounds for the non coupled 2D Stokes equation that is independent of the inf-sup condition. The study that we make is for the non coupled Stokes equation to prove the (upper and lower) bounds of the error without the usage of the value β of the inf-sup condition and it is applicable for the coupled 0D/2D Stokes model (but due to time restriction we did not make it). At the end of this chapter we have made a section related to conclusion and perspectives.

1. Context and model problems

1.1. Physical model and its simplifications

Fuel cell is an electrochemical device that converts the chemical energy of reactants into electricity and heat. In this study we focus on a Ballard NEXA 2-D PEMFC (Proton Exchange Membrane Fuel Cells), as in [83]. It can be seen from Figure 1.1 that a single cell consists of 7 individual layers: 1) cathode gas supply channel, 2) cathode gas diffusion layer (GDL), 3) cathode catalyst layer, 4) membrane, 5) anode catalyst layer, 6) anode gas diffusion layer (GDL) and 7) anode gas supply channel. The actual geometry form of cathode gas channel is represented in Figure 1.2.

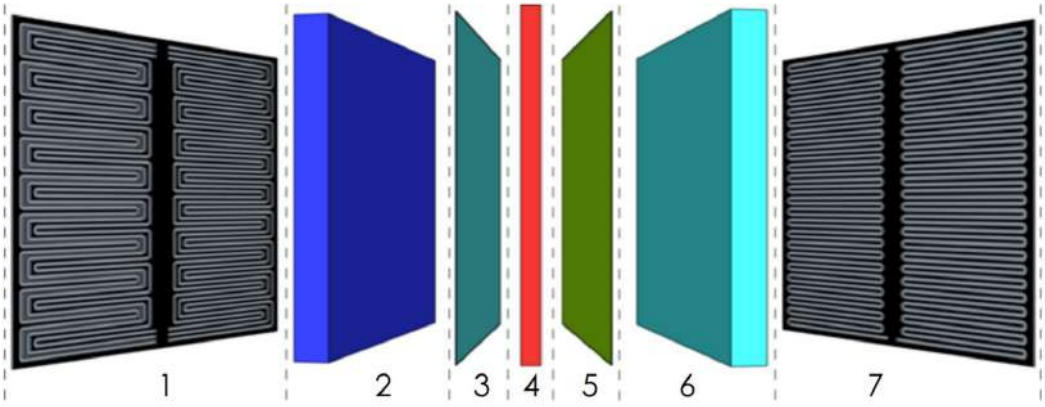

Figure 1.1.: Stucture of a single cell of of PEMFC stack [83]

Figure 1.2.: Actual geometry form of cathode gas supply channel [83]

A complete model of PEMFC should take into account several complex interconnected phenomena described by several branches of physics and chemistry, such as electrochemistry, flow in porous media, multiphase flow. The present thesis is only concerned by a small part of this rich physics: modeling the gas flow in the cathode channels of PEMFC. In particular, we exclude from our study the gas diffusion layer and the membrane electrode assembly. In real PEMFC, the unavoidable water from humidified gas streams and electrochemical reactions, leads to gas-liquid two-phase flow in the flow channels of fuel cell. As a first approximation, one can assume though a single phase (gas) flow.

More drastic simplifying assumptions can be found in the literature, such as:

- The gas in the cathode channels is modelled as a Newtonian fluid with constant viscosity μ.
- The fluid is supposed incompressible, i.e. the density ρ is constant and the velocity u satisfies $\nabla \cdot u = 0$, cf. [51]. We note however that the case of variable density is also considered in this article.
- Parabolic profiles are assumed for the inlet and outlet velocities of the fluid, cf. [81].
- As mentioned above, a single phase flow is assumed (no liquid water in the channel).
- The flow is laminar, since typically it low Reynolds number: $Re < 250$, as detected in [12].

Geometrical simplifications

In addition to the physical assumptions listed above, we shall make here some drastic geometrical simplifications. Most notably, the geometrical setting considered in the thesis is always 2D. More specifically, we shall mostly consider the 2D domain Ω depicted in Figure 1.3, representing a typical portion of the whole cathode gas channel (although, in some simulations, we will also deal with more complicated domains as depicted in Figure 1.3 on the right, representing the whole channel, reassembling the entire cathode channels in Figure 1.2). As seen at Figure 1.3, we shall always assume that our domains Ω are polygonal, although the real geometry of the cathode channel can have some curved parts, cf. Figure 1.2). A possible adaptation of our techniques to the case of curved boundary will be only briefly outlined in Appendix D, but is mostly out of the scope of the present thesis.

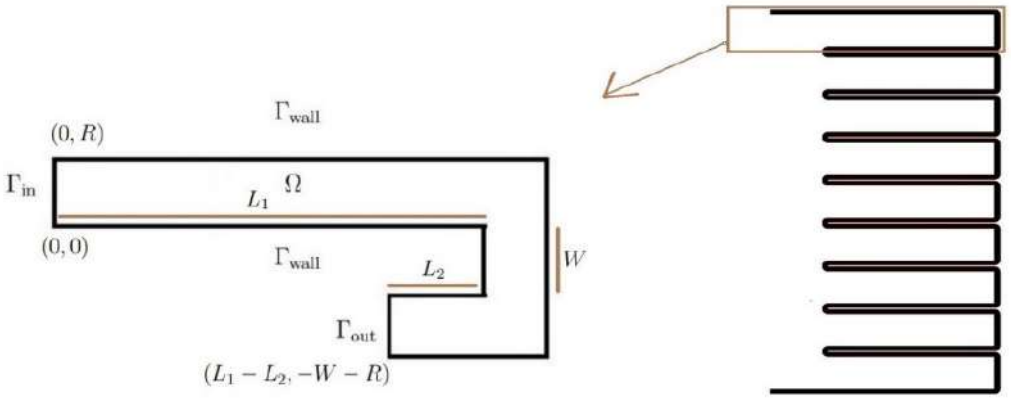

Figure 1.3.: Computational domain Ω (on the left) representing a portion of the whole cathode channel (on the right).

Let us explain some geometrical notations in relation to the domain Ω from Figure 1.3. We denote by Γ_{in} the inlet border where the inlet parabolic profile is imposed on the velocity, Γ_{out} the same for the outlet border, and Γ_{wall} the portion of $\partial\Omega$ corresponding to the wall of the channel where the no slip condition $u = 0$ is imposed on the velocity. We have thus $\Gamma_{\text{wall}} = \partial\Omega \backslash \big(\Gamma_{\text{in}} \cup \Gamma_{\text{out}}\big)$. In all the numerical experimental measurements below (unless stated otherwise) we shall use the following geometrical parameters: $R = 0.5,\ L_1 = 5.1,\ L_2 = 0.3$ and $W = 0.9$, cf. Figure 1.3.

Navier-Stokes equations for the gas flow in the cathode channel

In view of the above mentioned physical and geometrical assumptions, the gas flow can be described by the incompressible steady (time independent) Navier-Stokes equations in the 2D domain Ω of Figure 1.3:

$$\begin{cases} \rho(u \cdot \nabla)u - \mu\Delta u + \nabla p = 0 & & \text{in} \quad \Omega, \\ \operatorname{div} u = 0 & & \text{in} \quad \Omega, \\ u_1 = S(y), & u_2 = 0 & \text{on} \quad \Gamma_{in}, \\ u_1 = -S(y + W + R), & u_2 = 0 & \text{on} \quad \Gamma_{out}, \\ u = 0 & & \text{on} \quad \Gamma_{wall}. \end{cases} \tag{1.1}$$

with

$$S(y) = \frac{6u_{av}}{R^2} y(R-y) \tag{1.2}$$

Here R and W are some lengths detected in Figure 1.3, $u = (u_1, u_2)$ represents the fluid velocity vector ($cm \cdot s^{-1}$) and p the pressure. $S(y)$ is the parabolic Poiseuille profile with the average velocity u_{av}, i.e. the unique quadratic polynomials vanishing at $y = 0$ and $y = R$, and having the average u_{av} over the interval $(0, R)$.

The following physical parameters are proposed in [51]: the density is given by $\rho = \rho_{\text{air}} = 1.031401 \quad kg{\cdot}m^{-3}$, the dynamic viscosity is given by $\mu = \mu_{\text{air}} = 2.018{\times}10^{-5} \quad kg{\cdot}m^{-1}{\cdot}s^{-1}$, and the average velocity is taken as $u_{av} = 0.1 \quad cm \cdot s^{-1}$.

The characteristic feature of flows in the domains like those in Figure 1.3 is that they can be very accurately described by a simple expression, i.e. the Poiseuille flow, in the long straight portions of the channels, cf. the flow depiction at Figure 1.7 (a solution to the Stokes equations is plotted there, but qualitatively the Navier-Stokes solution looks the same). If one wants to approximate such a flow numerically, by the finite element method, one can do the computations only in the bent portions of the channel, while imposing the Poiseuille profile in the straight portions. The crucial question is then where to put the interface between the two portions. This is indeed the central theme of the present thesis. We shall not attempt here to answer this question in the case of *non-linear* incompressible Navier-Stokes equations above. We shall content ourselves with the simpler *linear* governing equations — the scalar Poisson equation and Stokes system. Hopefully, our results can be adapted to the Navier-Stokes case, and then to more complicated models (variable density and viscosity, coupling with the gas diffusion layer, etc).

1.2. Derivation of simplified models for Poisson and Stokes equations

In this section, we consider the boundary value problems for Poisson and Stokes equations posed in a domain Ω as depicted in Figure 1.3. We shall refer to the problem with original governing equation as the 2D model, and shall introduce a simplified 0D model in a portion of the whole domain. The latter will be referred to as the 0D model since the solution there will be given by simple expressions involving at most 1 scalar parameter. The coupling of these two models will be referred to as 0D/2D model.

The geometrical notation for 0D/2D coupling are presented at Figure 1.4. We denote by Ω' the subdomain where the 0D models will be set, and by $\tilde{\Omega}$ the subdomain where the original governing equations (the 2D model) will be kept. The two subdomains are separated by the interface $\gamma := \overline{\Omega'} \cap \overline{\tilde{\Omega}}$, which is taken to be a vertical line placed at the horizontal coordinate $x = x_\gamma$. Thus, $\Omega = \Omega' \cup \gamma \cup \tilde{\Omega}$.

For both Poisson and Stokes problems, the goal is take the subdomain Ω' as big as possible in order to reduce the computational cost while not compromizing the overall accuracy, since a numerical approximation (using finite elements) is needed only in $\tilde{\Omega}$.

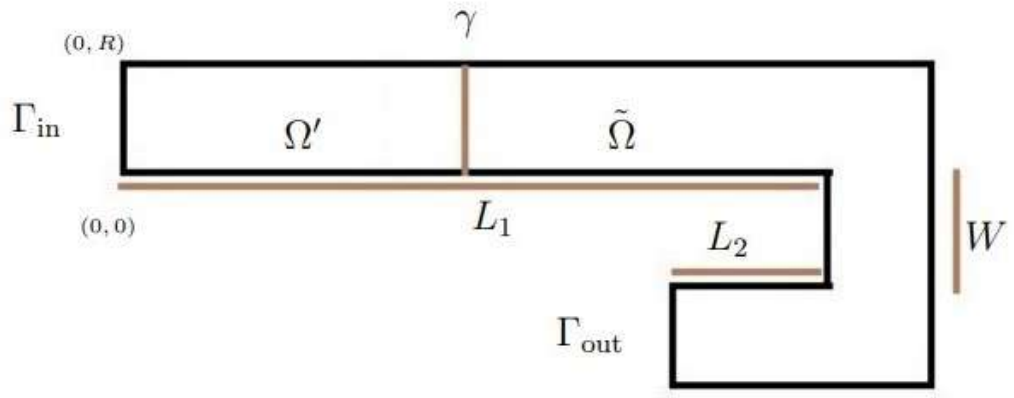

Figure 1.4.: Representation of the global domain Ω splitted in two regions: region Ω' (where the 0D model is proposed), region $\tilde{\Omega}$ (where the 2D model is proposed) and the interface γ

1.2.1. Derivation of the simplified 0D/2D model of Poisson

We begin with a derivation of a 0D/2D coupled model for the very simple problem involving the Poisson equation. Let us consider the boundary value problem for a scalar function u on domain Ω from Figure 1.3:

$$-\Delta u = f, \qquad \text{in} \quad \Omega, \tag{1.3a}$$
$$u = u_{\text{in}}, \qquad \text{on} \quad \Gamma_{\text{in}}, \tag{1.3b}$$
$$u = u_{\text{out}}, \qquad \text{on} \quad \Gamma_{\text{out}}, \tag{1.3c}$$
$$u = 0 \qquad \text{on} \quad \Gamma_{\text{wall}}. \tag{1.3d}$$

where

$$u_{\text{in}} = S(y), \quad u_{\text{out}} = S(y + W + R), \quad f = \frac{12 u_{av}}{R^2} = -S''(y)$$

with $S(y)$ defined by (1.2). Here, u_{av} is a positive parameter measuring the average of u on the inflow/outflow. The formulas for u_{in} and u_{out} represent thus quadratic polynomials vanishing at the junctions of $\Gamma_{\text{in/out}}$ and Γ_{wall} and having the prescribed average u_{av}. The inflow/outflow are chosen to mimic the boundary conditions of the more physical case of Navier-Stokes equations (1.1). The expression for the constant right-hand side f is chosen in a consistent manner with the inflow profile, as will be seen below.

The weak formulation of system (1.3) is represented by finding $u \in H_g^1(\Omega)$ such that:

$$(\nabla u, \nabla v)_\Omega = (f, v)_\Omega \quad \forall v \in H_0^1(\Omega), \tag{1.4}$$

where

$$H_0^1(\Omega) := \{u \in H^1(\Omega); \quad u = 0 \quad \text{on} \quad \partial\Omega\},$$
$$H_g^1(\Omega) := \{u \in H^1(\Omega); \quad u = u_g \quad \text{on} \quad \partial\Omega\},$$

$$u_g = \begin{cases} u_{in} & \text{on} \quad \Gamma_{\text{in}}, \\ u_{out} & \text{on} \quad \Gamma_{\text{out}}, \\ 0 & \text{on} \quad \Gamma_{\text{wall}}, \end{cases}$$

and $(\cdot\ ,\ \cdot)$ denote the L^2-scalar product.

We have plotted in Figure 1.5 an approximate solution to problem (1.3) obtained by a standard finite element approximation with $\mathbb{P}_2$ continuous elements on a mesh of size $h \approx 0.02$. We observe that this solution has indeed a very simple form in the rectangular region between the inflow and the bent region. Our goal is thus to determine explicitly this form.

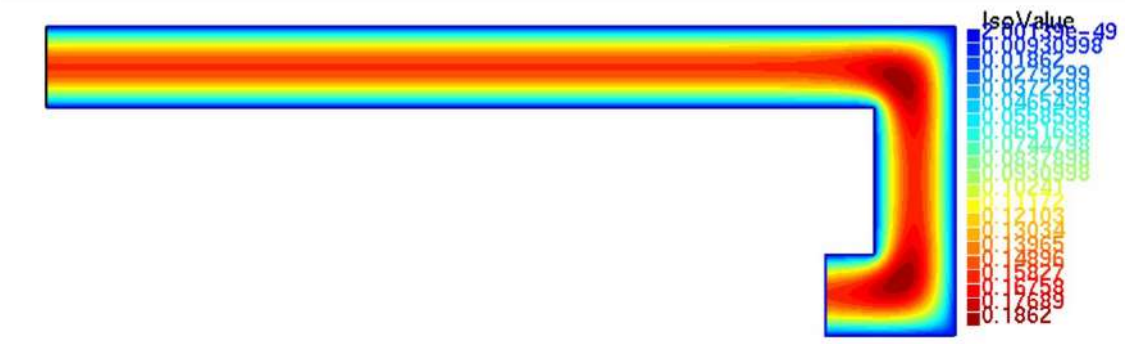

Figure 1.5.: The approximate numerical solution u_h for the Poisson problem on Ω (1.3).

Simplified Model

Using techniques in [45] and in [70], we want to derive 0D model on $\Omega' = (0, x_\gamma) \times (0, R)$ which is represented in Figure 1.4, where x_γ is the abscissa of the interface γ. We have $R << L_1$ and we consider that $U = u_{av}$ is the characteristic dimension for the u (this is its average on the inflow). Let us introduce $\epsilon = \frac{R}{L_1}$ as $R << L_1$. Let us consider the dimensionless quantities:

$$\tilde{u} = \frac{u}{U}, \quad \tilde{x} = \frac{x}{L_1}, \quad \tilde{y} = \frac{y}{R},$$

then, let us substitute the quantities $u = U\tilde{u}, \quad x = L_1\tilde{x}, \quad y = R\tilde{y}, \quad$ in system (1.3) that gives the following system:

$$-(\epsilon^2 \partial^2_{\tilde{x}\tilde{x}}\tilde{u} + \partial^2_{\tilde{y}\tilde{y}}\tilde{u}) = \tilde{f} \quad \text{for} \quad \tilde{x}, \tilde{y} \in (0,1), \tag{1.5}$$

with $\tilde{f} = \frac{R^2}{U} f = 12$ (since $U = u_{av}$). Now, let $\epsilon \to 0$ and recover the variables with dimensions by substituting $\tilde{u} = \frac{u}{U}$, $\tilde{x} = \frac{x}{L_1}$, $\tilde{y} = \frac{y}{R}$ and in system (1.5) to get

$$-\partial^2_{yy} u = f \quad \text{in} \quad \Omega'. \tag{1.6}$$

From equation (1.6) and by integrating twice we get $u(y) = -\frac{12u_{av}}{2R^2}y^2 + c_1 y + c_2$ for some constants $c_1(x)$ and $c_2(x)$ depend of x only. From boundary condition (1.3d) of system (1.3), we fix the constants as $u = 0$ for $y = 0$ and $y = R$ to get $c_2 = 0$ and $c_1 = \frac{6u_{av}}{R}$, thus $u(x, y) = 6u_{av}\frac{(R-y)y}{R^2}$. Finally our simplified model in Ω' gives

$$u' := u'(x, y) = 6u_{av}\frac{(R-y)y}{R^2} = S(y) \quad \text{in} \quad \Omega'. \tag{1.7}$$

Coupled Model

Let us introduce the simplified 0D model in Ω', the non simplified 2D model in $\tilde{\Omega}$ and let γ be the interface between Ω' and $\tilde{\Omega}$ such that $\Omega = \Omega' \cup \tilde{\Omega} \cup \gamma$. Let $\Gamma' \subset \Gamma_{\text{wall}}$ be the wall of Ω' and $\tilde{\Gamma} \subset \Gamma_{\text{wall}}$ be the wall of $\tilde{\Omega}$. The coupled domain is represented in Figure 1.4. The simplified model is:

$$u' = S(y) \quad \text{in} \quad \Omega'. \tag{1.8}$$

The non simplified model in $\tilde{\Omega}$ is to find $\tilde{u}$ such that:

$$\begin{cases} -\Delta \tilde{u} = f & \text{in} \quad \tilde{\Omega}, \\ \tilde{u} = S(y), & \text{on} \quad \gamma, \\ \tilde{u} = u_{out}, & \text{on} \quad \Gamma_{\text{out}}, \\ \tilde{u} = 0 & \text{on} \quad \tilde{\Gamma}. \end{cases} \tag{1.9}$$

The coupling condition is thus

$$u' = \tilde{u} \quad \text{on } \gamma. \tag{1.10}$$

The variational formulation of system (1.9) is : Find $\tilde{u} \in H^1_g(\tilde{\Omega})$ such that

$$(\nabla \tilde{u}, \nabla \tilde{v})_{\tilde{\Omega}} = (f, \tilde{v})_{\tilde{\Omega}} \qquad \forall \tilde{v} \in H^1_0(\tilde{\Omega}) \tag{1.11}$$

where,

$$H^1_g(\tilde{\Omega}) := \{\tilde{u} \in H^1(\tilde{\Omega}); \quad \tilde{u} = \tilde{u}_g \quad \text{on} \quad \partial\tilde{\Omega}\}$$

and

$$\tilde{u}_g = \begin{cases} S(y) & \text{on} \quad \gamma, \\ u_{out} & \text{on} \quad \Gamma_{out}, \\ 0 & \text{on} \quad \tilde{\Gamma}. \end{cases}$$

1.2.2. Discretization of the 0D/2D model for Poisson

Let $\tilde{\mathcal{T}}_h$ be a triangular mesh on $\tilde{\Omega}$ regular in the sense of [29] . Introduce the FE spaces
$\tilde{V}_h := \{\tilde{v}_h \quad \text{continuous on} \quad \tilde{\Omega} \quad \text{s.t:} \quad v_h|_K \in \mathbb{P}_k(K)\ \forall K \in \tilde{\mathcal{T}}_h)\}$,
$\tilde{V}_h^g := \{v_h \in \tilde{V}_h \quad \text{such that:} \quad v_h|_{\partial\tilde{\Omega}} = \tilde{u}_g\}$,
$\tilde{V}_h^0 := \{v_h \in \tilde{V}_h \quad \text{such that:} \quad v_h|_{\partial\tilde{\Omega}} = 0\}$,
where $\mathbb{P}_k(K)$ is the set of polynomials of degree $\leqslant k$ on a triangle $K \in \tilde{\mathcal{T}}_h$. Now, we discretize the problem (1.11) above as: find $\tilde{u}_h \in \tilde{V}_h^g$, such that

$$(\nabla \tilde{u}_h, \nabla \tilde{v}_h)_{\tilde{\Omega}} = (f, \tilde{v}_h)_{\tilde{\Omega}} \quad \forall \tilde{v}_h \in \tilde{V}_h^0. \tag{1.12}$$

Then the approximated solution on the whole Ω is reconstructed as

$$u_h^s = \begin{cases} u' \text{ in } \overline{\Omega'}, \\ \tilde{u}_h \text{ in } \tilde{\Omega}. \end{cases} \tag{1.13}$$

A numerical illustration

In this section, we numerically test the 0D/2D model for the Poisson equation using the finite elements of degree $k = 2$. We explore the error in the energy norm between the approximated solution u_h^s, defined by (1.13), and the solution u to (1.4)

$$\|\nabla(u_h^s - u)\|_\Omega. \tag{1.14}$$

with respect to different positions of the interface γ. The exact solution u is in fact unknown, and we replace it by a reference solution, i.e. a finite element approximation on a sufficiently fine mesh on Ω.

Let us fix a mesh size of $\tilde{\Omega}$ by $h \approx 0.08$, $h \approx 0.04$ and $h \approx 0.02$, we want to see the variation of the energy norm between the simplified approximated solution u_h^s and the reference solution u, with respect to different positions of the interface i.e. $x_\gamma \in [0.1, L_1 - 0.1]$ and for each mesh sizes as it is showed in Figure 1.6.

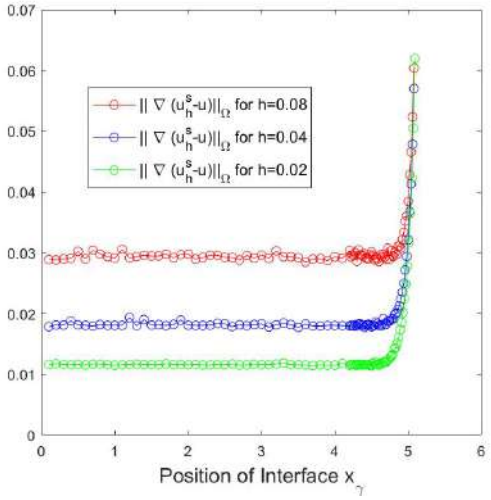

Figure 1.6.: The variation of the coupled error $||\nabla u_h^s - \nabla u||_\Omega$ with respect to different positions of the interface x_γ and for each mesh size $h \approx 0.08$, $h \approx 0.04$ and $h \approx 0.02$.

We see from Figure 1.6 that the error of the coupled 0D/2D model is affected by the position of the interface. As the position of the interface becomes near the bend region as the error $||\nabla u_h^s - \nabla u||_\Omega$ becomes bigger.

1.2.3. Derivation of the simplified 0D/2D model of Stokes

We now want to derive a simplified coupled 0D/2D model for the Stokes equation, i.e. equations (1.1) with $\rho = 0$. To simplify the notations, we redefine p/μ as p. We thus consider the following problem for the velocity u and the pressure p on domain Ω as in

Figure 1.3:

$$-\Delta u + \nabla p = 0 \quad \text{in} \quad \Omega, \tag{1.15a}$$
$$\operatorname{div} u = 0 \quad \text{in} \quad \Omega, \tag{1.15b}$$
$$u_1 = S(y), \quad u_2 = 0 \quad \text{on} \quad \Gamma_{\text{in}}, \tag{1.15c}$$
$$u_1 = -S(y + W + R), \quad u_2 = 0 \quad \text{on} \quad \Gamma_{\text{out}}, \tag{1.15d}$$
$$u = 0 \quad \text{on} \quad \Gamma_{\text{wall}}. \tag{1.15e}$$

If p is a solution of system (1.15), then $p + c$ is also a solution. So, let us fix this constant c by the condition

$$\int_\Omega p = 0. \tag{1.16}$$

The weak formulation of system (1.15) is represented by finding $(u, p) \in \mathbf{H}^1_g(\Omega) \times L^2_0(\Omega)$, cf the notations below, such that:

$$\begin{cases} (\nabla u, \nabla v)_\Omega - (\nabla \cdot v, p)_\Omega = 0 & \forall v \in [H^1_0(\Omega)]^2, \\ -(\nabla \cdot u, q)_\Omega = 0 & \forall q \in L^2_0(\Omega). \end{cases} \tag{1.17}$$

System (1.17) is well posed [47] due to the inf-sup condition:

$$\inf_{q \in L^2_0(\Omega)} \sup_{v \in [H^1_0(\Omega)]^2} \frac{(q, \nabla \cdot v)_\Omega}{||q||_\Omega ||\nabla v||_\Omega} = \beta > 0. \tag{1.18}$$

We have plotted in Figure 1.7 an approximate solution to problem (1.15) obtained by a standard Taylor-Hood finite element approximation (i.e. using $\mathbb{P}_2$ continuous elements for the velocity, and $\mathbb{P}_1$ continuous elements for the pressure) on a mesh of size $h \approx 0.02$. We observe that this solution has indeed a very simple form in the rectangular region between the inflow and the bent region. The velocity vector is horizontal there and its profile is independent of x. The pressure is an affine function of x. Our goal is thus to determine explicitly the expressions giving velocity and pressure there.

Notations

Let us define the following notations.

- $L^2_0(\Omega) = \{f \in L^2(\Omega); \int_\Omega f = 0\}$.
- $u_g = \begin{cases} (S(y), 0) & \text{on} \quad \Gamma_{in}, \\ (-S(y + W + R), 0) & \text{on} \quad \Gamma_{out}, \\ (0, 0) & \text{on} \quad \Gamma_{wall}. \end{cases}$
- $\mathbf{H}^1_g(\Omega) := \{u \in [H^1(\Omega)]^2; \quad u = u_g \quad \text{on} \quad \partial\Omega\}$.
- $[H^1_0(\Omega)]^2 := \{u \in [H^1(\Omega)]^2; \quad u = 0 \quad \text{on} \quad \partial\Omega\}$.
- $H(\operatorname{div}, \Omega) := \{u \in [L^2(\Omega)]^2; \quad \nabla \cdot u \in L^2(\Omega)\}$.
- $(u, v)_\Omega = \int_\Omega uv$.

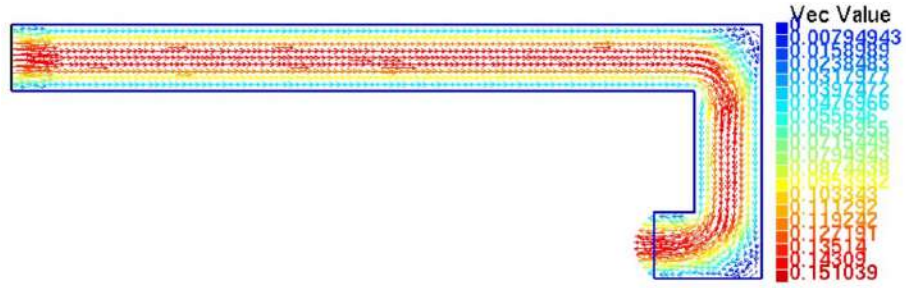

(a) The approximate velocity u_h

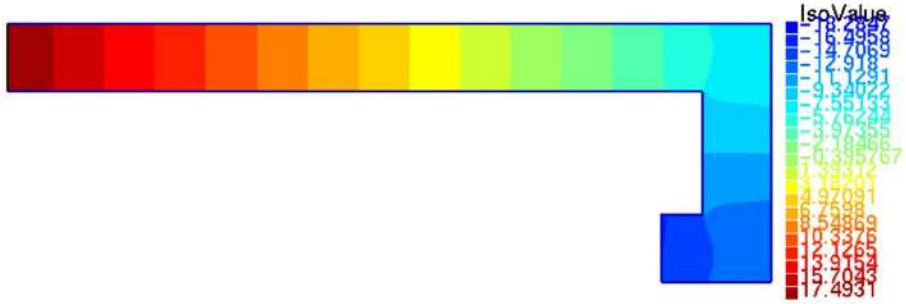

(b) The approximate pressure p_h

Figure 1.7.: A numerical approximation for velocity and pressure given by Stokes problem (1.15) on Ω.

Simplified Model

We want to impose a simplified 0D model on $\Omega' = (0, x_\gamma) \times (0, R)$ which is represented in Figure 1.4, , where x_γ is the abscissa of the interface γ. We have $R << L_1$ and we consider that $U_2 << U_1$, where U_1 is the characteristic dimension for horizontal velocity and U_2 is the characteristic dimension for vertical velocity. Let us introduce the following relations: $\epsilon = \frac{R}{L_1}$ as $R << L_1$, $U_1 = u_{av}$ where u_{av} is the average velocity, $U_2 = \epsilon U_1$ and the characteristic dimension for pressure $\Pi = \frac{U_1 L_1}{R^2}$. So, let us consider the dimensionless quantities:

$$\tilde{u}_1 = \frac{u_1}{U_1}, \quad \tilde{u}_2 = \frac{u_2}{U_2}, \quad \tilde{x} = \frac{x}{L_1}, \quad \tilde{y} = \frac{y}{R}, \quad \tilde{p} = \frac{p}{\Pi},$$

then, let us substitute the quantities $u_1 = U_1\tilde{u}_1, \quad u_2 = U_2\tilde{u}_2, \quad x = L_1\tilde{x}, \quad y = R\tilde{y}, \quad p = \Pi\tilde{p}$ in system (1.15) that gives the following system:

$$\begin{cases} -(\epsilon^2\partial^2_{\tilde{x}\tilde{x}}\tilde{u}_1 + \partial^2_{\tilde{y}\tilde{y}}\tilde{u}_1) + \partial_{\tilde{x}}\tilde{p} = 0 \\ \partial_{\tilde{y}}\tilde{p} = \epsilon^4\partial^2_{\tilde{x}\tilde{x}}\tilde{u}_2 + \epsilon^2\partial^2_{\tilde{y}\tilde{y}}\tilde{u}_2 \\ \partial_{\tilde{x}}\tilde{u}_1 + \partial_{\tilde{y}}\tilde{u}_2 = 0 \end{cases} \quad \text{in} \quad (0,1)^2. \tag{1.19}$$

Now, let $\epsilon \to 0$ and recover the variables with dimensions by substituting $\tilde{u}_1 = \frac{u_1}{U_1}$, $\tilde{u}_2 = \frac{u_2}{U_2}$, $\tilde{x} = \frac{x}{L_1}$, $\tilde{y} = \frac{y}{R}$ and $\tilde{p} = \frac{p}{\Pi}$ in system (1.19) to get:

$$-\partial^2_{yy} u_1 + \partial_x p = 0 \tag{1.20a}$$
$$\partial_y p = 0 \qquad \text{in} \quad \Omega'. \tag{1.20b}$$
$$\partial_x u_1 + \partial_y u_2 = 0 \tag{1.20c}$$

Eq. (1.20b) gives

$$p = p(x)$$

so that (1.20a) implies that $\partial^2_{yy} u_1$ is a function of x only. Thus, $\partial^2_{yy} u_1$ is constant for any fixed x, so that $u_1(x, y)$ is a quadratic polynomial of y with coefficients depending on x. Since u_1 should vanish at $y = 0$ and $y = R$, we see that u_1 should be proportional to $y(R - y)$ with the coefficient of proportionality dependent on x. Substituting this to (1.20a) gives

$$u_1(x, y) = -\frac{1}{2} y(R - y) \frac{dp}{dx}(x)$$

Substituting this to (1.20c) gives

$$-\frac{1}{2} y(R - y) \frac{d^2 p}{dx^2}(x) + \partial_y u_2(x, y) = 0$$

Take any x, integrate this in y from 0 to R, and observe $\int_0^R \partial_y u_2(x, y) dy = u_2(x, R) - u_2(x, 0) = 0$. This implies $\frac{d^2 p}{dx^2} = 0$, i.e.

$$p = -Px + e$$

with some constants P and e. It also means that $\partial_y u_2 = 0$, hence $u_2 = 0$ due to the boundary conditions on $y = 0$. Finally, imposing the average of u_1 at any given x to be u_{av} gives $u_1 = S(y)$ as defined by (1.2), and we identify the pressure gradient as $P = \frac{12 u_{av}}{R^2}$. Our simplified model in Ω' is thus

$$u_1(x, y) = S(y) \tag{1.21a}$$
$$u_2(x, y) = 0 \qquad \text{in} \quad \Omega'. \tag{1.21b}$$
$$p(x, y) = -\frac{12 u_{av}}{R^2} x + c \tag{1.21c}$$

with some $c \in \mathbb{R}$.

Coupled Model

Let us introduce the simplified 0D model in Ω', the non simplified 2D model in $\tilde{\Omega}$ and let γ be the interface between Ω' and $\tilde{\Omega}$ such that $\Omega = \Omega' \cup \tilde{\Omega} \cup \gamma$. Let $\Gamma' \subset \Gamma_{\text{wall}}$ be the wall of Ω' and $\tilde{\Gamma}_{\text{wall}} \subset \Gamma_{\text{wall}}$ be the wall of $\tilde{\Omega}$. The coupled domain is represented in Figure 1.4. The simplified model in Ω' is:

$$\begin{cases} u'_1(x, y) = S(y), \\ u'_2(x, y) = 0, \\ p'(x, y) = -Px + c_{\Omega'}, \end{cases} \qquad \text{in} \quad \Omega' \tag{1.22}$$

with $S(y)$ the Poiseuille profile (1.2), $P = \frac{12 u_{av}}{R^2}$ and $c_{\Omega'}$ some constant to be determined.

In $\tilde{\Omega}$, we keep the original governing equations: find $\tilde{u}$ and $\tilde{p}$ such that:

$$\begin{cases} -\Delta\tilde{u} + \nabla\tilde{p} = 0 & & \text{in} \quad \tilde{\Omega}, \\ \operatorname{div}\tilde{u} = 0 & & \text{in} \quad \tilde{\Omega}, \\ \tilde{u}_1 = S(y), & \tilde{u}_2 = 0 & \text{on} \quad \gamma, \\ \tilde{u}_1 = -S(y+W+R), & \tilde{u}_2 = 0 & \text{on} \quad \Gamma_{\text{out}}, \\ \tilde{u} = 0 & & \text{on} \quad \tilde{\Gamma}_{\text{wall}}. \end{cases} \tag{1.23}$$

Note that we have already assumed here the coupling condition for the velocity on the interface

$$u_1' = \tilde{u}_1 \quad \text{and} \quad u_2' = \tilde{u}_2 \quad \text{on} \quad \gamma\,. \tag{1.24}$$

Remark that if $\tilde{p}$ is a solution of system (1.23), then $\tilde{p} + K$ is also a solution of system (1.23) in $\tilde{\Omega}$ for any $K \in \mathbb{R}$. Let $p^0 \in L_0^2(\tilde{\Omega})$ be a particular unique solution of system (1.23). The existence and uniqueness of $(\tilde{u}, p^0) \in [H^1(\tilde{\Omega})]^2 \times L_0^2(\tilde{\Omega})$ as a weak solution of system (1.23) is related to the inf-sup condition, cf. [47, Theorem 5.1, page 80]. More specifically, this solution is characterized by: find $(\tilde{u}, p^0) \in \mathbf{H}_g^1(\tilde{\Omega}) \times L_0^2(\tilde{\Omega})$ such that

$$\begin{cases} (\nabla\tilde{u}, \nabla\tilde{v})_{\tilde{\Omega}} - (\nabla\cdot\tilde{v}, p^0)_{\tilde{\Omega}} = 0 & \forall\tilde{v} \in [H_0^1(\tilde{\Omega})]^2, \\ -(\nabla\cdot\tilde{u}, \tilde{q})_{\tilde{\Omega}} = 0 & \forall\tilde{q} \in L_0^2(\tilde{\Omega}), \end{cases} \tag{1.25}$$

where

$$\mathbf{H}_g^1(\tilde{\Omega}) := \{\tilde{u} \in [H^1(\tilde{\Omega})]^2; \quad \tilde{u} = \tilde{u}_g \quad \text{on} \quad \partial\tilde{\Omega}\}$$

and

$$\tilde{u}_g = \begin{cases} (S(y), 0) & \text{on} \quad \gamma, \\ (-S(y+W+R), 0) & \text{on} \quad \Gamma_{out}, \\ (0,0) & \text{on} \quad \tilde{\Gamma}_{\text{wall}}. \end{cases}$$

The general solution for the pressure in (1.23) is then given by

$$\tilde{p} = p^0 + c_{\tilde{\Omega}} \tag{1.26}$$

with the constant $c_{\tilde{\Omega}}$ to be determined.

So, for the moment we have two additive constants: $c_{\Omega'}$ in (1.23) and $c_{\tilde{\Omega}}$ in (1.26). To eliminate one of these constants, we propose the following coupling condition

$$\int_\gamma (\nabla u' - p' I) n \cdot S(y) n = \int_\gamma (\nabla\tilde{u} - \tilde{p} I) n \cdot S(y) n. \tag{1.27}$$

Physically, this reflects the continuity of the normal force on both sides of γ, taking the average with the weight $S(y)$. Mathematically, eq. (1.27) makes perfect sense for $(\tilde{u}, \tilde{p}) \in \mathbf{H}_g^1(\tilde{\Omega}) \times L^2(\tilde{\Omega})$ since (1.25) implies that $(\nabla\tilde{u} - \tilde{p}I) \in H(\operatorname{div}, \tilde{\Omega})^2$ so that its normal trace on γ is well defined. The multiplication by $S(y)$ in (1.27) may seem somewhat arbitrary. We shall see however that this equation comes from a natural variational formulation of the coupled problem, cf. the paragraph below. Moreover, it is this coupling condition that allows us to develop the reliable and efficient *a posteriori* error bounds in Chapter 3.

Adding to the coupling condition above the requirement that the integral of pressure over all of Ω is 0, i.e.

$$\int_{\Omega'} p' + \int_{\tilde{\Omega}} \tilde{p} = 0 \tag{1.28}$$

closes the system of equations. We have now two scalar equations for two additive constants $c_{\Omega'}$ and $c_{\tilde{\Omega}}$. This enables us to define the unique solution to the coupled system (1.22)–(1.23)–(1.27)–(1.28).

Remark 1.1. *We have also considered a slightly simpler alternative to the coupling condition* (1.27)*, which consists in imposing that the average pressure is the same on both sides of the interface* γ*:*

$$\int_\gamma p' = \int_\gamma \tilde{p} \tag{1.29}$$

The coupled system (1.22)–(1.23)–(1.29)–(1.28) *also allows us to define a unique solution on* Ω *and works well in practice, cf. the numerical results below. However, mathematically,* (1.29) *is not satisfactory since* $\tilde{p}$ *is by definition in* $L^2(\tilde{\Omega})$ *so that it does not necessarily have a trace on* γ*.*

A variational characterization of the coupled problem (1.22)–(1.23)–(1.27)–(1.28)

We present here another derivation of the coupled problem, starting from a variational problem taking into account the essential features of the solution predicted by the asymptotic analysis, and leading to the coupling condition (1.27) together with the simplified model (1.22). We start by recalling that the asymptotic analysis suggests that the velocity in Ω' can be approximated by an expression of the form $(\alpha(x)S(y), 0)$ with $S(y)$ given by (1.2) and some $\alpha(x)$, and the pressure in Ω' can be approximated by a function of x only. Let us introduce the spaces of functions on Ω that satisfy these constraints on Ω':

$$V^s = \{v \in [H^1(\Omega]^2 : v|_{\Omega'} = (\beta(x)S(y), 0) \text{ with } \beta \in H^1(0, x_\gamma)\}, \tag{1.30}$$

$$M^s = \{q \in L^2_0(\Omega : q|_{\Omega'} = \chi(x) \text{ with } \chi \in L^2(0, x_\gamma)\}, \tag{1.31}$$

and restrict the variational formulation (1.17) of the Stokes problem to produce a plausible approximation to the velocity and pressure, simplified on Ω'. We thus search for $(u^s, p^s) \in V^s \times M^s$ such that $u = u_g$ on $\partial\Omega$ and

$$\begin{cases} (\nabla u^s, \nabla v^s)_\Omega - (\nabla \cdot v^s, p^s)_\Omega = 0 & \forall v^s \in V^s \cap [H^1_0(\Omega)]^2, \\ -(\nabla \cdot u^s, q^s)_\Omega = 0 & \forall q^s \in M^s. \end{cases} \tag{1.32}$$

This produces indeed the coupled solution introduced above.

Lemma 1.2. *Problem* (1.32) *has the unique solution which is given by*

$$u^s = \begin{cases} u' \text{ on } \Omega', \\ \tilde{u} \text{ on } \tilde{\Omega}, \end{cases} \tag{1.33}$$

$$p^s = \begin{cases} p' \text{ on } \Omega', \\ \tilde{p} \text{ on } \tilde{\Omega}. \end{cases} \tag{1.34}$$

with $u', \tilde{u}, p', \tilde{p}$ *given by* (1.22)–(1.23)–(1.27)–(1.28)*.*

Proof. Let $(u^s, p^s) \in V^s \times M^s$ be a solution to (1.32) veryfying $u^s = u_g$ on $\partial\Omega$, $u^s = (\alpha(x)S(y), 0)$ on Ω', and $p^s = \pi(x)$ on Ω'. Take the test function q^s in the second equation of (1.32) as

$$q^s(x, y) = \chi(x) = \frac{u_{av}}{R}\alpha'(x) \quad \text{on } \Omega'$$

and $q^s = \nabla \cdot u^s$ on $\tilde{\Omega}$. Note that $q^s \in M^s$ since

$$\int_\Omega q^s = \int_0^R S(y)dy \int_0^{x_\gamma} \alpha'(x)dx + \int_{\tilde{\Omega}} \nabla \cdot u^s = \int_\Omega \nabla \cdot u^s = \int_{\partial\Omega} u_g = 0.$$

The second equation of (1.32) now gives

$$0 = (\nabla \cdot u^s, q^s)_\Omega = \frac{u_{av}}{R} \int_0^R S(y)dy \int_0^{x_\gamma} \alpha'(x)^2 dx + (\nabla \cdot u^s, \nabla \cdot u^s)_{\tilde{\Omega}} = \frac{u_{av}^2}{R} \|\alpha'\|^2_{(0,x_\gamma)} + \|\nabla \cdot u^s\|^2_{\tilde{\Omega}}$$

hence $\alpha(x) = \text{const} = 1$ (by boundary conditions on Γ_{in}) and $\nabla \cdot u^s = 0$ on $\tilde{\Omega}$. Thus $u^s = (S(y), 0)$ on Ω'.

The first equation of (1.32) with any test function v^s of the form $\beta(x)S(y)$ on Ω' can be now written as

$$\int_0^R S'(y)^2 dy \int_0^{x_\gamma} \beta(x)dx - \int_0^R S(y)dy \int_0^{x_\gamma} \pi(x)\beta'(x)dx + (\nabla u^s, \nabla v^s)_{\tilde{\Omega}} - (\nabla \cdot v^s, p^s)_{\tilde{\Omega}} = 0$$

Taking $\beta = 0$ gives immediately $\text{div}(\nabla u^s - p^s I) = 0$ on $\tilde{\Omega}$. On the other hand, taking $\beta \in H_0^1(0, x_\gamma)$ and $v^s = 0$ on $\tilde{\Omega}$ gives

$$P \int_0^{x_\gamma} \beta(x)dx - \int_0^{x_\gamma} \pi(x)\beta'(x)dx = 0$$

since $-S''(y) = P$. Hence $\pi' = -P$ on $(0, x_\gamma)$. We have thus proven that (u^s, p^s) is of the form (1.22) on Ω' and satisfies (1.23) on $\tilde{\Omega}$. Now, taking any test function $v^s \in V^s$ with $v^s = S(y)$ on Ω' and integrating by parts on Ω' and on $\tilde{\Omega}$ gives

$$\int_\gamma [(\nabla u^s)n - p^s n] \cdot S(y) = 0$$

which is equivalent to the coupling condition (1.27). Thus, (u^s, p^s) can be represented as (1.33)–(1.34) with $u', \tilde{u}, p', \tilde{p}$ given by (1.22)–(1.23)–(1.27)–(1.28).

Vice-versa, let $u', \tilde{u}, p', \tilde{p}$ be given by (1.22)–(1.23)–(1.27)–(1.28). Combining them in (u^s, p^s) as in (1.33)–(1.34), we see immediately $u^s \in V^s$, $p^s \in M^s$ and $\text{div}(\nabla u^s - p^s I) = 0$, $\nabla \cdot u^s = 0$ on both Ω' and $\tilde{\Omega}$. Taking any $v^s \in V^s$ of the form $\beta(x)S(y)$ on Ω', we observe

$$(\nabla u^s, \nabla v^s)_\Omega - (\nabla \cdot v^s, p^s)_\Omega = \beta(x_\gamma) \int_\gamma [(\nabla u^s)n - p^s n] \cdot S(y) = 0$$

by integration by parts on Ω' and on $\tilde{\Omega}$, and the coupling condition (1.27). This means that (u^s, p^s) satisfies (1.32). ■

1.2.4. Discretization of the 0D/2D model for Stokes

Let $\tilde{\mathcal{T}}_h$ be a regular triangular mesh on $\tilde{\Omega}$ in the sense of [29]. Introduce the FE spaces
$\tilde{V}_h := \{v_h = (v_h^1, v_h^2) \quad \text{continuous on} \quad \tilde{\Omega} \quad \text{s.t.} \quad v_h|_K \in \mathbb{P}_2(K)\ \forall K \in \tilde{\mathcal{T}}_h\}$,
$\tilde{V}_h^g := \{v_h \in \tilde{V}_h \quad \text{s.t.} \quad v_h|_{\partial\tilde{\Omega}} = \tilde{u}_g\}$,
$\tilde{V}_h^0 := \{v_h \in \tilde{V}_h \quad \text{s.t.} \quad v_h|_{\partial\tilde{\Omega}} = 0\}$,
$\tilde{M}_h := \{q_h \quad \text{continuous on} \quad \tilde{\Omega} \quad \text{s.t.} \quad q_h|_K \in \mathbb{P}_1(K)\ \forall K \in \tilde{\mathcal{T}}_h \quad \text{and} \quad \int_{\tilde{\Omega}} q_h = 0\}$,

Now, we discretize (1.25) as: find $\tilde{u}_h \in \tilde{V}_h^g$, $\tilde{p}_h^0 \in \tilde{M}_h$ such that

$$\begin{cases} (\nabla \tilde{u}_h, \nabla \tilde{v}_h)_{\tilde{\Omega}} - (\nabla \cdot \tilde{v}_h, \tilde{p}_h^0)_{\tilde{\Omega}} = 0 & \forall \tilde{v}_h \in \tilde{V}_h^0, \\ -(\nabla \cdot \tilde{u}_h, \tilde{q}_h)_{\tilde{\Omega}} = 0 & \forall \tilde{q}_h \in \tilde{M}_h, \end{cases} \tag{1.35}$$

set

$$\tilde{p}_h = \tilde{p}_h^0 + c_{\tilde{\Omega},h} \tag{1.36}$$

and couple it with the approximation on Ω'

$$\begin{cases} u_1'(x,y) = S(y), \\ u_2'(x,y) = 0, \\ p_h'(x,y) = -Px + c_{\Omega',h}, \end{cases} \quad \text{in} \quad \Omega' \tag{1.37}$$

through the conditions

$$\int_\gamma (\nabla u' - p_h' I) n \cdot S(y) n = \int_\gamma (\nabla \tilde{u}_h - \tilde{p}_h I) n \cdot S(y) n, \tag{1.38}$$

$$\int_{\Omega'} p_h' + \int_{\tilde{\Omega}} \tilde{p}_h = 0. \tag{1.39}$$

Note that p_h' is different from p' since $c_{\Omega',h} \neq c_{\Omega'}$. Then the approximate solution on the whole Ω is reconstructed as

$$u_h^s = \begin{cases} u' \text{ on } \Omega', \\ \tilde{u}_h \text{ on } \tilde{\Omega}, \end{cases} \tag{1.40}$$

$$p_h^s = \begin{cases} p_h' \text{ on } \Omega', \\ \tilde{p}_h \text{ on } \tilde{\Omega}. \end{cases} \tag{1.41}$$

A numerical illustration

In this section, we numerically test the 0D/2D model for the Stokes equations. We explore the error in the energy norm between the approximated velocity u_h^s and pressure p_h^s, defined by (1.40) and (1.41) respectively, and the exact velocity and pressure given by (1.15), with respect to different positions of the interface γ. We shall report thus the following quantities:

$$\|\nabla(u_h^s - u)\|_\Omega \quad \text{and} \quad \|p_h^s - p\|_\Omega \tag{1.42}$$

The exact solution (u, p) is in fact unknown, and we replace it by a reference solution, i.e. a finite element approximation on a sufficiently fine mesh on Ω, using continuous $\mathbb{P}_4/\mathbb{P}_4$ finite elements for velocity/pressure.

Let us fix a mesh size of $\tilde{\Omega}$ by $h \approx 0.064$, $h \approx 0.032$ and $h \approx 0.016$, we want to see the variation of the energy norm between the simplified approximated solution u_h^s and the reference solution u, i.e. $||\nabla u_h^s - \nabla u||_\Omega$ and the variation of the L^2-norm between the simplified approximated solution p_h^s and the reference solution p, i.e. $||p_h^s - p||_\Omega$ with respect to different positions of the interface i.e. $x_\gamma \in [0.1, L_1 - 0.1]$ and for each mesh sizes as it is showed in Figure 1.8.

We see from Figure 1.8 that the error of the coupled 0D/2D model is affected by the position of the interface. As the position of the interface becomes near the bend region as the errors $||\nabla u_h^s - \nabla u||_\Omega$ and $||p_h^s - p||_\Omega$ become bigger.

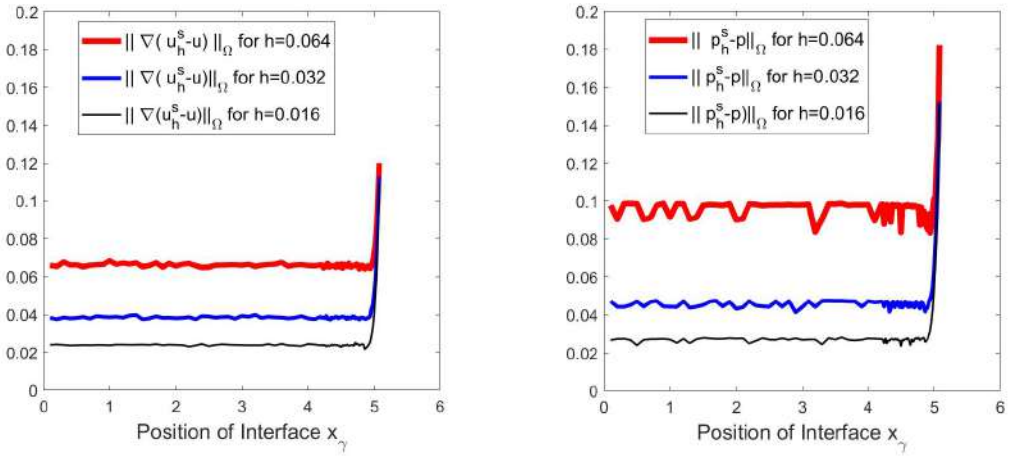

Figure 1.8.: The variation of the coupled errors $||\nabla u_h^s - \nabla u||_\Omega$ and $||p_h^s - p||_\Omega$ with respect to different positions of the interface x_γ and for each mesh size $h \approx 0.064$, $h \approx 0.032$ and $h \approx 0.016$.

Remark 1.3. *As announced in Remark 1.1, the coupling condition* (1.27) *can be replaced in practice by another one* (1.29)*. The results produced by the two variants are indeed very close one to another. This is reported in Figure 1.9. We plot there the pressure error* $\|p_h^s - p\|_\Omega$ *produced by the two variants on meshes of size* $h \approx 0.064$*, as function of the position of interface* γ*. Note the velocity approximation* u_h^s *is not affected by the choice of the coupling condition, so that there is no need to compare the velocity errors.*

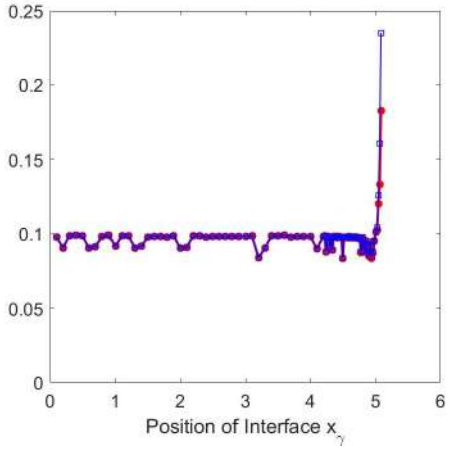

Figure 1.9.: The variation of $||p_h^s - p||_\Omega$ using the two coupling conditions. Red: condition (1.29); blue: condition (1.27).

1.3. A posteriori error Estimation

The main core of the thesis (Chapters 2 and 3) will be devoted to the construction of *a posteriori* error estimators for the coupled 0D/2D models for Poisson and Stokes equation,

as derived in the preceding section, using finite elements to discretize the original 2D equation on the “not simplified" subdomain $\tilde{\Omega}$. These estimators will in particular take into account the “modeling" error due to the replacement of the original problem by the coupled 0D/2D model. Prior to presenting our estimators for coupled problems, let us give here a general background about *a posteriori* error estimation in the context of usual boundary value problems.

A posteriori error estimators are obtained from some computable quantities on the patches of the mesh elements or on the mesh elements themselves. These computable local quantities on the mesh element K are denoted by η_K, which represent a local estimators on K and usually depends on the numerical computable solution u_h, quantify the local discretization error. Now, the global estimator η is defined by

$$\eta^2 := \sum_{K \in \mathcal{T}_h} \eta_K^2 \tag{1.43}$$

Let us denote the exact solution by u and the approximated solution by u_h, then among the desirable properties for the optimal *a posteriori* error estimator η, we can cite:

i) **guaranteed upper bound**, which represents the global reliability in which we have a fully computable upper bound, that depends on the approximated solution u_h, of the numerical error between the exact and the approximated solution i.e. there exists a (known) constant $C > 0$ which is independent from the exact solution u, from the approximate solution u_h and from the mesh size h such that

$$\|u - u_h\| \leq C\eta + osc \tag{1.44}$$

where *osc* are the data oscillations, measures the discretization error of some data function $f \in L^2(\Omega)$. When $C = 1$ the *a posteriori* error estimator is called an guaranteed estimator.

ii) **local efficiency**, at which the local estimator η_K gives a local lower bound for the actual error up to a generic constant i.e. there exists a constant $c > 0$, which does not depend on u and u_h, such that

$$c\eta_K \leq \left\| u_{|\omega_K} - u_{h|\omega_K} \right\|_{\omega_K} + osc_{|\omega_K}, \tag{1.45}$$

where the patch ω_K is a collection of elements K that share the same vertex a. Here, $u_{|\omega_K}$, $u_{h|\omega_K}$ and $osc_{|\omega_K}$ represent the restriction of the exact solution u, the approximated u_h and the data oscillation *osc* on the patch ω_K respectively. Usually, the constant c is unknown.

iii) **asymptotic exactness**, the efficiency index which is the ratio $\frac{\eta}{\|u-u_h\|}$ tends to one as we refine the mesh.

$$\frac{\eta}{\|u - u_h\|} \to 1 \tag{1.46}$$

iv) **robustness**, where the previous properties are independent from the parameters of the problem i.e. the constants C, c and the efficiency index do not depend on the parameters of the problem and their variation.

v) **low computational cost**, where the computation of η can be done locally in order to obtain a low computational cost.

Optimally, an estimator should satisfy (1.44) and (1.45) with constants C and c very close to 1 as much as possible. From this we obtain two things, the estimator is a good approximation of the exact error i.e. $\eta \approx \|u - u_h\|$ and the estimator detects locally where the error is big across the mesh $\mathcal{T}_h$, which is important in adaptive mesh refinement algorithms. Usually, the norm $\|\cdot\|$ in Properties i) to iii) is the energy norm of the associated problem.

In order to study Properties i) to v), for linear elliptic PDEs problems, we refer the reader to the following works [2, 20, 23, 34–36, 58, 64, 74, 77]. There are many types of *a posteriori* error but the most known estimator is the explicit *residual estimates*, which is introduced initially by Babuška and Rheinboldt in [4, 7, 9]. Many studies verified that these explicit *residual estimators* satisfy the properties i) as in [3], ii) as in [73] for Stokes and [74] for Poisson equation, iv) as in [75, 76] for the reaction-diffusion and convection-diffusion equations, and they satisfy in general the property v). The constant C in the upper bound in i) is in general not known for the residual error estimators, although there are some explicit estimates for it in the literature, eg. Carstensen and Funken [21], Carstensen and Klose [22], and in Veeser and Verfürth [71]. Certainly, we cannot hope that $C = 1$. The residual error estimators are thus said to be reliable and not guaranteed. There are many other types of *a posteriori* error estimates such as *equilibrated residual estimates* as Ainsworth and Oden [1], *Averaging estimates* as Zienkiewicz–Zhu [84] and Carstensen [18,19], *Functional a posteriori error estimates* as Neittaanmäki and Repin [58] and Repin [64], *hierarchical estimates* as Bank and Smith [11] and finally *geometric a posteriori error estimates* as Castro- Díaz and Hecht in [26] or Frey and Alauzet [44].
Among all the techniques, we focus on the guaranteed because the constants in upper bound is known and it allows us to estimate error knowing the magnitude of the error. In this thesis we will focus on so-called *equilibrated fluxes estimates*.

Equilibrated fluxes estimators

Fluxes of the solution u are usually the gradient of u i.e $-\nabla u$ (in Poisson problems for example) and are sometimes stresses quantities i.e $\nabla u - pI$ (where u represents the velocity and p represents the pressure in the Stokes problems for example). The idea of reconstruction of fluxes from the approximated finite element solution u_h comes from the fact that we want to reconstruct a flux which satisfies the properties of the exact flux $-\nabla u$ since, for example in Poisson equation $-\Delta u = f$ on the domain Ω, the approximated flux $-\nabla u_h$ does not belong to $H(\mathrm{div}, \Omega)$ and $-\Delta u_h \neq f$ while ∇u belongs to $H(\mathrm{div}, \Omega)$ space and $\nabla \cdot (-\nabla u) = f$, where $H(\mathrm{div}, \Omega)$ is the space which contains vector functions in $L^2(\Omega)$ and its divergence also belong to $L^2(\Omega)$. For this reason we make a reconstructed flux σ_h which belongs to $H(\mathrm{div}, \Omega)$ and get an estimation of the actual error $\|\nabla u - \nabla u_h\|_\Omega$. These estimators represents the norm between the fluxes of the finite element solution u_h and the reconstructed ones σ_h i.e $\|\nabla u_h + \sigma_h\|_\Omega$.
The idea of equilibrated fluxes estimates is related to Prager–Synge equality [61] and the hypercircle method as Synge [69]. Their are many research studies about *equilibrated fluxes estimators* such as Repin [66], Destuynder and Métivet [30], Luce and Wohlmuth [55], Ladevèze and Leguillon [54], Korotov [53], Vejchodský [72], or Braess and Schöberl [16], Fierro and Veeser [41]. The robust with respect to the polynomial degree is proved by Braess et

al. in [14]. This distinguishes them from the other types of estimates.
In the next section we will explain the idea of *equilibrated fluxes estimators* using the Vohralik techniques in [39] .

1.4. An a posteriori error estimator for the non coupled 2D Poisson Model

In order to understand better some ideas of the technique of equilibrated fluxes for *a posteriori* error estimation, we will give a simple theoretical analysis and some numerical illustration in the case of a Poisson problem with Neumann boundary condition. We make the flux reconstruction by similar strategies as [39] giving "pedagogical" motivation for it. We shall contend ourselves here with a simpler proof of the efficiency, without attempting to prove the "p-robustness".

Let us consider the problem posed in domain $\Omega \subset \mathbb{R}^d$ with $d = 2$ or 3:

$$-\Delta u = f \text{ in } \Omega,$$

$$\frac{\partial u}{\partial n} = 0 \text{ on } \partial\Omega.$$

We suppose $f \in L^2(\Omega)$ and Ω a bounded polygonal/polyhedral domain. Note that we prefer to treat here the problem with Neumann boundary conditions since they turn out to be slightly simpler with respect to the a posteriori analysis than the Dirichlet ones (the changes that should be made in the Dirichlet case are outlined at the end of the section, see *Remark* 1.8). The solution u is defined up to an additive constant. To make the solution unique, we impose $\int_\Omega u = 0$.
Let $\mathcal{T}_h$ be a regular mesh on Ω consisting of triangles/tetrahedra. Let V_h be the usual $\mathbb{P}_k$ finite element space on this mesh (the space of continuous functions on Ω given by poynomials of degree $\leqslant k$ on every $K \in \mathcal{T}_h$). The discrete problem is to find $u_h \in V_h$ such that for any $v_h \in V_h$

$$\int_\Omega \nabla u_h \cdot \nabla v_h = \int_\Omega f v_h. \tag{1.47}$$

Our goal is to provide an a posteriori estimate for $\|\nabla u - \nabla u_h\|_\Omega$. First of all, we note the following bound: for any $\sigma \in H(\mathrm{div}, \Omega)$ such that $\mathrm{div}\,\sigma = f$ on Ω, $\sigma \cdot n = 0$ on $\partial\Omega$, we have

$$\|\nabla u - \nabla u_h\|_\Omega \leqslant \|\sigma + \nabla u_h\|_\Omega. \tag{1.48}$$

Indeed, setting $e = u - u_h$

$$\|\nabla u - \nabla u_h\|_\Omega^2 = (\nabla u - \nabla u_h, \nabla e) = (f, e) - (\nabla u_h, \nabla e) = (\mathrm{div}\,\sigma, e) - (\nabla u_h, \nabla e)$$

$$= (-\sigma - \nabla u_h, \nabla e) \leqslant \|\sigma + \nabla u_h\|_\Omega \|\nabla e\|_\Omega,$$

so that the announced estimate follows by dividing on both sides by $\|\nabla u - \nabla u_h\|_\Omega = \|\nabla e\|_\Omega$. Let us emphasize that (1.48) holds for any « flux » σ with $\mathrm{div}\,\sigma = f$, and the idea of what follows is to give a recepee to construct such a flux in a way easily implementatble on a computer. Another thing to keep in mind is that this σ should be kept as close as possible to $-\nabla u_h$, in order to minimize the over-prediction of the error in (1.48). Let us start from

the observation that there is an ideal flux (of no practical use) given by $\sigma^{\text{ideal}} = -\nabla u$. For this flux, (1.48) is a trivial identity. This σ^{ideal} satisfies

$$\sigma^{\text{ideal}} = -\nabla u,$$

$$\operatorname{div} \sigma^{\text{ideal}} = f,$$

$$\sigma^{\text{ideal}} \cdot n = 0 \operatorname{on} \partial\Omega.$$

Now, let us introduce the localized version of σ^{ideal} : $\sigma^a = -(\nabla u)\psi^a$ where ψ^a is the $\mathbb{P}_1$ finite element basis function (the hat function) associated to any mesh node a. This σ^a satisfies on the patch $\omega^a = \operatorname{supp}(\psi^a)$

$$\sigma^a = -(\nabla u)\psi^a \operatorname{on} \omega^a,$$

$$\operatorname{div} \sigma^a = f\psi^a - \nabla u \cdot \nabla \psi^a \operatorname{on} \omega^a,$$

$$\sigma^a \cdot n = 0 \operatorname{on} \partial\omega^a.$$

Note that

$$\sigma^{\text{ideal}} = \sum_a \sigma^a \operatorname{on} \Omega$$

since $\sum_a \psi^a = 1$ (we imply the summation over all the mesh nodes in such expressions). Let us discretize the problem for σ^a. We do it first on a very formal level. We introduce some finite element space $\Sigma_h^a \subset H(\operatorname{div}, \omega^a)$ and seek for $\sigma_h^a \in \Sigma_h^a$ such that

$$\sigma_h^a \approx -(\nabla u_h)\psi^a \operatorname{on} \omega^a, \tag{1.49}$$

$$\operatorname{div} \sigma_h^a \approx f\psi^a - \nabla u_h \cdot \nabla \psi^a \operatorname{on} \omega^a, \tag{1.50}$$

$$\sigma_h^a \cdot n = 0 \operatorname{on} \partial\omega^a. \tag{1.51}$$

We define then

$$\sigma_h = \sum_a \sigma_h^a. \tag{1.52}$$

Both (1.49) and (1.50) introduce some approximations with respect to the exact σ^a, most notably u is replaced by u_h there. But the role of these approximations is quite different from (1.49) to (1.50). In the case of (1.50), replacing u by u_h does not affect our primary goal, i.e. to construct a flux with $\operatorname{div} \sigma = f$. Indeed, if (1.50) were satisfied exacly, then one would have

$$\operatorname{div} \sigma_h = \sum_a \operatorname{div} \sigma_h^a = f \sum_a \psi^a - \nabla u_h \cdot \nabla \left(\sum_a \psi^a \right) = f. \tag{1.53}$$

We want thus to satisfy (1.50) as accurately as possible. In our final construction (1.50) will be imposed almost exactly with the small modification that f will be replaced by a piecewise polynomial approximation f_h (otherwise, it would be impossible to satisfy (1.50) since $\operatorname{div} \sigma_h^a$ is piecewise polynomial).
On the other hand, (1.49) cannot be made precise even in principle since $(\nabla u_h)\psi^a \notin H(\operatorname{div}, \omega^a)$. We want however to make the difference between σ_h^a and $-(\nabla u_h)\psi^a$ as small as possible, in order to minimize the over-prediction of the error in (1.48).

Motivated by the discussion above, we give now the precise formulation for σ_h^a in (1.49)–(1.51): find $\sigma_h^a \in \Sigma_h^a$ such that

$$\sigma_h^a = \arg \min_{\substack{s_h^a \in \Sigma_h^a \\ \operatorname{div} s_h^a = \Pi_{Q_h^a}(f\psi^a - \nabla u_h \cdot \nabla \psi^a)}} \|s_h^a + (\nabla u_h)\psi^a\|_{\omega^a} \tag{1.54}$$

where $\Sigma_h^a \in H(\operatorname{div}, \omega^a)$ incorporates already the boundary conditions (1.51) and is given by

$$\Sigma_h^a = \{\sigma_h \in H(\operatorname{div}, \omega^a), \sigma_h|_K \in \mathrm{RT}_p(K) \quad \forall K \in \omega^a, [[\sigma_h]]_F \cdot n_F \text{ on any facet inside } \omega^a, \sigma_h \cdot n = 0 \text{ on } \partial\omega^a\}$$

and

$$Q_h^a = \operatorname{div} \Sigma_h^a = \left\{ q_h \in L^2(\omega^a), q_{h|_K} \in \mathbb{P}_p(K) \quad \forall K \in \omega^a, \quad \text{and} \int_{\omega^a} q_h = 0 \right\}$$

with $\mathbb{P}_p(K)$ the set of polynomials of degree $\leqslant p$ on K. Here $\mathrm{RT}_p(K)$ is the set of Raviart-Thomas (vector-valued) finite elements on a cell K which is defined by

$$\mathrm{RT}_p(K) := \mathbb{P}_p(K)^2 + x\tilde{\mathbb{P}}_p(K) \tag{1.55}$$

where, $\tilde{\mathbb{P}}_p(K)$ represents the set of homogeneous polynomials of degree p on K. Note also that the constraint $\int_{\omega^a} q_h = 0$ is introduced in Q_h^a in accordance with $\sigma_h \cdot n = 0$ on $\partial\omega^a$ in the definition of Σ_h^a. Let us summarize some important properties of the Raviart-Thimas space used here after.

Remark 1.4. *The space* $\mathrm{RT}_p(K)$ *is characterized by the following properties.*

- $\mathrm{RT}_p(K)$ *contains all the vector-valaued polynomial functions of degree* $\leqslant p$ *(plus other things).*
- *Let* $\Gamma_0, \ldots, \Gamma_d$ *be the sides of* ∂K, $\alpha_0, \ldots, \alpha_d$ *any polynomials of degree* $\leqslant p$ *on* $\Gamma_0, \ldots, \Gamma_d$ *respectively, and* β *any polynomial of degree* $\leqslant p$ *on* K *such that* $\sum_{i=0}^d \int_{\Gamma_i} \alpha_i = \int_K \beta$. *Then there exists* $\gamma \in \mathrm{RT}_p(K)$ *such that*

$$\gamma \cdot n = \alpha_i \text{ on } \Gamma_i, \quad i = 0, \ldots, d$$

$$\operatorname{div} \gamma = \beta \text{ on } K.$$

We now give the Euler-Lagrange equations that give the solution to (1.54): find $\sigma_h^a \in \Sigma_h^a$ and $p_h^a \in Q_h^a$ such that for all $\tau_h \in \Sigma_h^a$ and $q_h \in Q_h^a$

$$\int_{\omega^a} \sigma_h^a \cdot \tau_h + \int_{\omega^a} p_h^a \operatorname{div} \tau_h = -\int_{\omega^a} (\nabla u_h)\psi^a \cdot \tau_h, \tag{1.56}$$

$$\int_{\omega^a} q_h \operatorname{div} \sigma_h^a = \int_{\omega^a} (f\psi^a - \nabla u_h \cdot \nabla \psi^a) q_h. \tag{1.57}$$

Existance of the solution to this problem is given by the following well-known result.

Lemma 1.5. *Consider the problem: find $\sigma_h \in \Sigma_h^a$ and $p_h \in Q_h^a$ such that for all $\tau_h \in \Sigma_h^a$ and $q_h \in Q_h^a$*

$$\int_{\omega^a} \sigma_h \cdot \tau_h + \int_{\omega^a} p_h \operatorname{div} \tau_h = -\int_{\omega^a} F \cdot \tau_h,$$
$$\int_{\omega^a} q_h \operatorname{div} \sigma_h = \int_{\omega^a} G q_h.$$

This problem has the unique solution for any given $F \in L^2(\omega^a)^d$ and $G \in L^2(\omega^a)$. Moreover,

$$\|\sigma_h\|_{\omega^a}^2 + h_a^2 \|\operatorname{div} \sigma_h\|_{\omega^a}^2 + \frac{1}{h_a^2}\|p_h\|_{\omega^a}^2 \leqslant C(\|F\|_{\omega^a}^2 + h_a^2 \|G\|_{\omega^a}^2).$$

The proof of this Lemma can be found in several textbooks on mixed finite element methods. The prefactors with the powers of the mesh size h_a stem from a rescaling from a reference patch configuration. The flux reconstruction σ_h is thus defined by (1.52) with σ_h^a given by (1.56)–(1.57) and the a posteriori error estimator is defined by $\|\sigma_h + \nabla u_h\|_\Omega$, cf. (1.48).

Theorem 1.6. *Assume $p \geqslant k$. The error estimator $\|\sigma_h + \nabla u_h\|_\Omega$ with σ_h defined by (1.56)-(1.57)-(1.52) satisfies*

$$\|\nabla u - \nabla u_h\|_\Omega \leqslant \|\sigma_h + \nabla u_h\|_\Omega + h.o.t. \tag{1.58}$$

$$\|\sigma_h + \nabla u_h\|_\Omega \leqslant C\|\nabla u - \nabla u_h\|_\Omega + h.o.t. \tag{1.59}$$

with C depending only on the mesh regularity and on polynomial degrees k and p, and h.o.t. standing for higher order terms, i.e. the contributions of order $o(h^k)$, at least if f is sufficiently smooth, and thus negligible. More specifically,

$$h.o.t. \leqslant C\sqrt{\sum_{K \in \mathcal{T}_h} h_K^2 \|f - f_h\|_K^2}$$

where $f_h|_K$ is the orthogonal projection of $f|_K$ on the space $\mathbb{P}_p(K)$ of polynomials of degree $\leqslant p$ on K.

Proof. The upper estimate (1.58) is aready almost proved, cf. (1.48). However, we do not have exactly $\operatorname{div} \sigma_h = f$, but rather $\operatorname{div} \sigma_h = f_h$ with f_h described in the statement above. To see this, we recall (1.57) which is valid for piecewise $\mathbb{P}_p$ polynomials q_h under the constraint $\int_{\omega^a} q_h = 0$. In fact, (1.57) is satisfied with $q_h = 1$ as well. Indeed,

$$\int_{\omega^a} \operatorname{div} \sigma_h^a = 0 = \int_{\omega^a} (f\psi^a - \nabla u_h \cdot \nabla \psi^a)$$

since $\sigma_h^a \cdot n = 0$ on $\partial\omega^a$ and thanks to (1.47) with $v_h = \psi^a$. Thus, (1.57) is valid for any piecewise $\mathbb{P}_p$ polynomial q_h without constraints. We can also write it separately on any mesh cell $K \in \mathcal{T}_h$ since q_h are discontinuous:

$$\int_K q_h \operatorname{div} \sigma_h^a = \int_K q_h(f\psi^a - \nabla u_h \cdot \nabla \psi^a), \quad \forall q_h \in \mathbb{P}_p(K).$$

Summing this over all the vertices a gives, cf (1.53),

$$\int_K q_h \operatorname{div} \sigma_h = \int_K q_h f, \quad \forall q_h \in \mathbb{P}_p(K)$$

so that $\operatorname{div}\sigma_h = f_h$ on K. We now modify the proof of (1.48): introducing $\bar{e}_K$ as the mean of $e = u - u_h$ on K

$$\|\nabla u - \nabla u_h\|_\Omega^2 = (\nabla u - \nabla u_h, \nabla e) = (f - f_h, e) + (f_h, e) - (\nabla u_h, \nabla e)$$

$$= (f - f_h, e) + (\operatorname{div}\sigma_h, e) - (\nabla u_h, \nabla e) = \sum_{K\in\mathcal{T}_h} (f - f_h, e - \bar{e}_K)_K - (\sigma_h + \nabla u_h, \nabla e)$$

$$\leqslant \sqrt{\sum_{K\in\mathcal{T}_h} h_K^2 \|f - f_h\|_K^2}\sqrt{\sum_{K\in\mathcal{T}_h} \frac{1}{h_K^2}\|e - \bar{e}_K\|_K^2} + \|\sigma_h + \nabla u_h\|_\Omega \|\nabla e\|_\Omega.$$

This proves (1.58) since $\|e - \bar{e}_K\|_K \leqslant C h_K \|\nabla e\|_K$. We turn now to (1.59). We want to prove first its localized version

$$\|\sigma_h^a + (\nabla u_h)\psi^a\|_{\omega^a} \leqslant C\|\nabla(u - u_h)\|_{\omega^a} + Ch_a\|f - f_h\|_{\omega^a}. \tag{1.60}$$

To this end, introduce $\tilde{\sigma}_h^a \in \Sigma_h^a$ by

$$\tilde{\sigma}_h^a = \sigma_h^a + (\nabla u_h)\psi^a + c_h$$

with c_h to be specified shortly. The idea is to recast the problem (1.56)-(1.57) in terms of $\sigma_h^a + (\nabla u_h)\psi^a$ since this is our quantity of interest now. Note that $(\nabla u_h)\psi^a$ is a polynomial of degree $\leqslant k$ on any mesh cell K, so that $(\nabla u_h)\psi^a|_K \in \mathrm{RT}_p(K)$ provided $p \geqslant k$. However, $(\nabla u_h)\psi^a \notin \Sigma_h^a$ since the normal derivatives of u_h jump accross the mesh facets. We want thus to add a correction c_h to compensate these jumps. We set c_h as a piecewise polynomial on the mesh on ω^a with $c_h|_K \in \mathrm{RT}_p(K\ )$ for any cell $K \in \omega^a$, $c_h \cdot n = 0$ on $\partial\omega^a$, and $[[c_h]]_F \cdot n_F = -[[\nabla u_h]]_F \psi^a \cdot n_F$ on any $F \in \mathcal{F}^a$ where $\mathcal{F}^a$ denotes the set of mesh facets inside ω^a. We achieve this by setting on any side $F \in \mathcal{F}^a$ of any cell $K \in \omega^a$

$$c_h = \frac{1}{2}[[\nabla u_h]]_F \psi^a \cdot n. \tag{1.61}$$

Here c_h should be understood as $c_h|_K$ and n should be understood as the unit normal looking outside of K. Note that $[[\nabla u_h]]_F \psi^a \cdot n$ is a polynomial of degree $\leqslant k$ on any facet F, so that (1.61) can be indeed prescribed provided $p \geqslant k$. Prescription of c_h on ∂K does not fully determine c_h on K. But the details of the construction of c_h are not important. We should only insure that

$$\|c_h\|_K + h_a\|\operatorname{div} c_h\|_K \leqslant C\sqrt{h_a}\|c_h\|_{\partial K} \tag{1.62}$$

which can be done by constructing c_h first on the reference element and then rescaling. Now, (1.56)-(1.57) can be rewritten as

$$\int_{\omega^a} \tilde{\sigma}_h^a \cdot \tau_h + \int_{\omega^a} p_h^a \operatorname{div}\tau_h = \int_{\omega^a} c_h \cdot \tau_h, \tag{1.63}$$

$$\int_{\omega^a} q_h \operatorname{div}\tilde{\sigma}_h^a = \sum_{K\in\omega^a}\int_K (f + \Delta u_h)\psi^a q_h + \sum_{K\in\omega^a}\int_K q_h \operatorname{div} c_h. \tag{1.64}$$

Lemma 1.5 gives

$$\|\tilde{\sigma}_h^a\|_{\omega^a}^2 \leqslant C\left(\|c_h\|_{\omega^a}^2 + h_a^2 \sum_{K\in\omega^a}\|f + \Delta u_h\|_K^2 + h_a^2 \sum_{K\in\omega^a}\|\operatorname{div} c_h\|_K^2\right).$$

Thus, in view of (1.61) and (1.62),

$$\|\sigma_h^a + (\nabla u_h)\psi^a\|_{\omega^a}^2 \leqslant C\left(\sum_{K\in\omega^a} h_K^2\|f+\Delta u_h\|_K^2 + \sum_{F\in\mathcal{F}^a} h_F\,\|[[\nabla u_h]]\cdot n_F\|_F^2\right). \qquad (1.65)$$

We are now going to bound the two terms in (1.65) using Verfurth's technique of bubble functions. Introducing a bubble function b_K on K (a polynomial such that $b_K = 0$ on ∂K and $\|b_K\|_{L^\infty(K)} = 1$) and using an appropriate inverse inequality (i.e. a bound on polynomials which can be proved by equivalence of norms and scaling), we get

$$\|f_h+\Delta u_h\|_K^2 \leqslant C\int_K (f_h+\Delta u_h)^2 b_K \leqslant C\|f-f_h\|_K\|f_h+\Delta u_h\|_K + C\int_K (f_h+\Delta u_h)(f+\Delta u_h)b_K.$$

We recall that $f = -\Delta u$ in a weak sense and intergrate by parts

$$\int_K (f_h+\Delta u_h)(f+\Delta u_h)b_K = \int_K (-\Delta(u-u_h))(f_h+\Delta u_h)b_K = \int_K \nabla(u-u_h)\cdot\nabla\left((f_h+\Delta u_h)b_K\right)$$

$$\leqslant \|\nabla(u-u_h)\|_K\|\nabla(f_h+\Delta u_h)\|_K\|b_K\|_{L^\infty(K)} + \|\nabla(u-u_h)\|_K\|f_h+\Delta u_h\|_K\|\nabla b_K\|_{L^\infty(K)}$$

$$\leqslant \frac{C}{h_K}\|\nabla(u-u_h)\|_K\|f_h+\Delta u_h\|_K$$

using some some inverse inequalities and $\|b_K\|_{L^\infty(K)} = 1$. Thus,

$$\|f_h+\Delta u_h\|_K \leqslant \frac{C}{h_K}\|\nabla(u-u_h)\|_K + C\|f-f_h\|_K$$

and

$$h_K\|f_h+\Delta u_h\|_K \leqslant C\|\nabla(u-u_h)\|_K + Ch_K\|f-f_h\|_K. \qquad (1.66)$$

Similarly, for any mesh facet F shared by two cells K_1, K_2, we introduce a bubble function b_F (a polynomial on K_1, K_2 such that $b_F = 0$ on $\partial(\overline{K_1\cup K_2})$ and $\|b_F\|_{L^\infty(K_1\cup K_2)} = 1$). Let also Π_{K_i} denote a natural extension of polynomials from F to K_i. In the same spirit as before,

$$\|[[\nabla u_h]]\cdot n_F\|_F^2 \leqslant C\int_F \left([[\nabla u_h]]\cdot n_F\right)^2 b_F = C\int_F \left([[\nabla\left(u_h-u\right)]]\cdot n_F\right)\left([[\nabla u_h]]\cdot n_F\right) b_F$$

$$= C\sum_{i=1}^2 \int_{\partial K_i} \left(\nabla\left(u_h-u\right)\cdot n\right)\Pi_{K_i}\left([[\nabla u_h]]\cdot n_F\right) b_F$$

$$= C\sum_{i=1}^2 \left[\int_{K_i} \nabla\left(u_h-u\right)\cdot\nabla\left(\Pi_{K_i}\left([[\nabla u_h]]\cdot n_F\right) b_F\right) + \int_{K_i} \Delta\left(u_h-u\right)\left(\Pi_{K_i}\left([[\nabla u_h]]\cdot n_F\right) b_F\right)\right].$$

We remark

$$\|\Pi_{K_i}\left([[\nabla u_h]]\cdot n_F\right) b_F\|_{K_i} \leqslant C\sqrt{h_F}\,\|[[\nabla u_h]]\cdot n_F\|_F$$

$$\|\nabla\left(\Pi_{K_i}\left([[\nabla u_h]]\cdot n_F\right) b_F\right)\|_{K_i} \leqslant \frac{C}{\sqrt{h_F}}\,\|[[\nabla u_h]]\cdot n_F\|_F$$

and conclude

$$\|[[\nabla u_h]]\cdot n_F\|_F \leqslant \frac{C}{\sqrt{h_F}}\|\nabla(u-u_h)\|_{K_1\cup K_2} + C\sqrt{h_F}\|f+\Delta u_h\|_{K_1\cup K_2}.$$

In view of (1.66), this gives

$$\sqrt{h_F}\,\|[[\nabla u_h]]\cdot n_F\|_F \leqslant C\|\nabla(u-u_h)\|_{K_1\cup K_2} + Ch_F\|f-f_h\|_{K_1\cup K_2}. \tag{1.67}$$

Substituting (1.66) and (1.67) into (1.65) gives (1.60).
It remains to sum (1.60) over all the nodes a:

$$\begin{aligned}\|\sigma_h+\nabla u_h\|_\Omega &= \left\|\sum_a(\sigma_h^a+(\nabla u_h)\psi^a)\right\|_\Omega\\ &\leqslant \sum_a\|\sigma_h^a+(\nabla u_h)\psi^a\|_{\omega^a}\\ &\leqslant C\sum_a\|\nabla(u-u_h)\|_{\omega^a}+C\sum_a h_a\|f-f_h\|_{\omega^a}.\end{aligned}$$

This yields (1.59) since each patch ω^a contains a bounded number of mesh cells K. Here are the details for the h.o.t.:

$$\left(\sum_a h_a\|f-f_h\|_{\omega^a}\right)^2 \leqslant C\sum_a\sum_{K\in\omega^a}h_K^2\|f-f_h\|_K^2 \leqslant C\sum_{K\in\mathcal{T}_h}h_K^2\|f-f_h\|_K^2.$$

with C depends on the maximum of the constants where the patches intersect. ■

Remark 1.7. *The proofs above are not optimal with respect to the polynomial order p. Our constants do depend (in principle) on p. But it can be in fact proven that they are p-independent, cf. the article by Braess et al. [14] and the subsequent papers by Vohralik and Ern.*

Remark 1.8. *All the above can be easily applied to the case of Dirichlet boundary conditions for the PDE $-\Delta u = f$. The flux σ_h will be still defined as the sum of local contribution (1.52), each of which is defined by (1.56)–(1.57), but one should adapt the definitions of Σ_h^a and Q_h^a there. If the patch ω^a does not touch the boundary $\partial\Omega$ or interescts it in only one point (or an edge in 3D), then nothing changes. However if $|\partial\omega^a\cap\partial\Omega|>0$ then one should not prescribe $\sigma_h\cdot n=0$ on this common part of $\partial\omega^a$ and $\partial\Omega$ in the definition of Σ_h^a. Note that we still have $\sigma_h\cdot n=0$ on the remaining part of $\partial\omega^a$. Accordingly, we no longer have $\int_{\omega^a}\operatorname{div}\sigma_h=0$ for $\sigma_h\in\Sigma_h^a$ on such a patch ω^a. Thus there is no need for the constraint $\int_{\omega^a}q_h=0$ in the definition of Q_h. Once the definitions of Σ_h^a and Q_h^a are modified accordingly, all the estimates above remain valid in the Dirichlet case.*

1.4.1. Numerical Results

The goal here is to validate the upper bound estimator in (1.58) of a posteriori error to the L-shaped domain $\Omega=(-1,1)\times(-1,1)\backslash[0,1]\times[-1,0]$ of the following Poisson problem

$$-\Delta u = f \text{ in } \Omega$$

$$u = u_e \text{ on } \partial\Omega$$

with the exact solution u_e written, in polar coordinates, as

$$u_e(r,\theta) = r^{\frac{2}{3}}\sin(2\theta/3). \tag{1.68}$$

We remark that we consider here $\theta \in (0, 3\pi/2)$. The corresponding source term $f = 0$. The exact solution u_e given by (1.68) is singular, $u \in H^{1+\frac{1}{2}-\epsilon}(\Omega)$ for any $\epsilon > 0$ only, with the gradient exploding at the corner $(0, 0)$. Since $f = 0$, then $h.o.t. = 0$ in the estimator in (1.58) and we get

$$\|\nabla u - \nabla u_h\|_\Omega \leqslant \|\sigma_h + \nabla u_h\|_\Omega. \tag{1.69}$$

Let V_h be the usual $\mathbb{P}_1$ finite element space on the uniform triangulation mesh $\mathcal{T}_h$ of this L-shaped Ω. For every element $K \in \mathcal{T}_h$ we plot in Figure 1.10 the Elementwise errors $\|\nabla(u - u_h)\|_K$ (left) and Equilibrated fluxes estimators $\|\sigma_h + \nabla u_h\|_K$ (right).

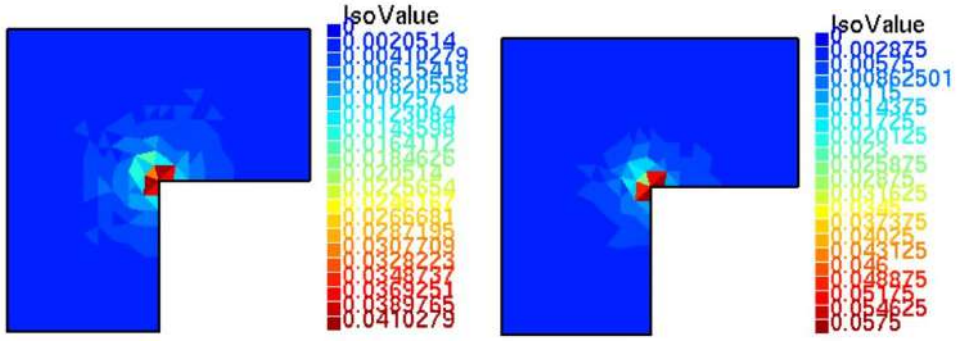

Figure 1.10.: Elementwise errors $\|\nabla(u - u_h)\|_K$ (left) and Equilibrated fluxes estimators $\|\sigma_h + \nabla u_h\|_K$ (right) for u_h in $\mathbb{P}_1$ finite element space.

Now let V_h be the usual $\mathbb{P}_2$ finite element space on the uniform triangulation mesh $\mathcal{T}_h$ of this L-shaped Ω. For every element $K \in \mathcal{T}_h$ we plot in Figure 1.11 the Elementwise errors $\|\nabla(u - u_h)\|_K$ (left) and Equilibrated fluxes estimators $\|\sigma_h + \nabla u_h\|_K$ (right).

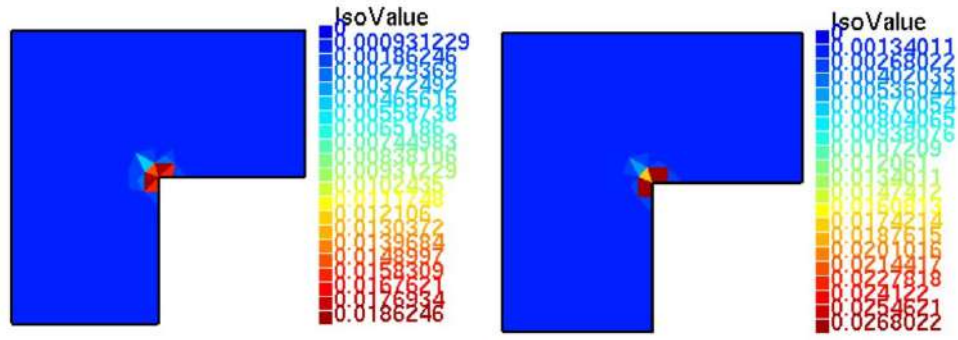

Figure 1.11.: Elementwise errors $\|\nabla(u - u_h)\|_K$ (left) and Equilibrated fluxes estimators $\|\sigma_h + \nabla u_h\|_K$ (right) for u_h in $\mathbb{P}_2$ finite element space.

In the Figure 1.10 and Figure 1.11 , we see that the Elementwise errors $\|\nabla(u - u_h)\|_K$ (left) and Equilibrated fluxes estimators $\|\sigma_h + \nabla u_h\|_K$ (right) are distributed equivalently in a way that the error and the estimator have the biggest values in the triangles which are concentrated at the corner. For this reason we should introduce an adaptive algorithm to refine the mesh more at the triangles where the estimator $\|\sigma_h + \nabla u_h\|_K$ is big in order to obtain an optimal convergence. The results for this example using adaptive algorithm are introduced in the **Appendix A**.

2. A posteriori estimator for the coupled 0D/2D Poisson equation

In this chapter we are going to talk about a posteriori error of the approximated solution u_h^s defined in (1.8)–(1.12)–(1.13) for the coupled 0D/2D model of the Poisson equation (1.3) on $\Omega = \Omega' \cup \gamma \cup \tilde{\Omega}$ which is represented in Figure 1.4. We will introduce two possibilities of reconstructing the flux σ_h on Ω of the coupled 0D/2D model. In Section 2.1, we will construct the first attempt of defining the flux reconstruction where the upper bound is guaranteed (reliability of the estimator) while the lower bound (efficiency of the estimator) is not satisfied (or it is very difficult to be proved). In Section 2.2, we will construct the second attempt of defining the flux reconstruction where the upper bound (reliability of the estimator) and the lower bound (efficiency of the estimator) are guaranteed and proved. In Section 2.3 we have made an adaptive algorithm that enables us to choose a good position for the interface γ and to optimize the mesh on $\tilde{\Omega}$.

Let us recall first some basic notions related to the technique of equilibrated fluxes.

Definition 2.1 (Flux σ)**.** *Let u be the solution of system (1.4) then, we denote the flux by $\sigma := -\nabla u$.*

Theorem 2.2 (Properties of weak solution of system (1.4))**.** *Let u be solution of system (1.4) and let σ be defined as in Definition 2.1. Then, $u \in H_g^1(\Omega)$, $\sigma \in H(\mathrm{div}, \Omega)$ and $\nabla \cdot \sigma = f$ with $f = \frac{12 u_{av}}{R^2}$.*

Proof. See Theorem 7.1.3 in [78]. ■

Remark 2.3 (Properties of approximate solution u_h^s)**.** *Let u_h^s be the approximated solution given by (1.8)–(1.12)–(1.13). Then, $u_h^s \in H_g^1(\Omega)$, $-\nabla u_h^s \notin H(\mathrm{div}, \Omega)$ and $\nabla \cdot (-\nabla u_h^s) \neq f$ in general.*

This remark tells us that the straightforward flux approximation $-\nabla u_h^s$ does not retain the properties of the flux σ. We want thus to construct another flux, named σ_h, starting from u_h^s such that $\sigma_h \in H(\mathrm{div}, \Omega)$ and $\nabla \cdot \sigma_h = f$. This will be achieved in the next section, cf. Theorem 2.2.

2.1. A simple a posteriori estimator with guaranteed upper bound only

2.1.1. Flux reconstruction

Let u_h^s be the approximate solution given by (1.8)–(1.12)–(1.13). Ideally, we could look for a flux $\sigma_h^{\mathrm{ideal}} \in \Sigma_h^\Omega \subset H(\mathrm{div}, \Omega)$ such that:

$$\sigma_h^{\mathrm{ideal}} := \underset{\substack{v_h \in \Sigma_h^\Omega, \\ \mathrm{div}\, v_h = f \text{ on } \Omega}}{\arg\min} ||\nabla u_h^s + v_h||_{L^2(\Omega)} \tag{2.1}$$

taking Σ_h^{Ω} as the RT_k space on $\tilde{\Omega}$ and $(-\nabla u')$ on Ω'. Computing σ_h^{ideal} would be too costly, so we localize this minimization to the patches of each node of the mesh on $\tilde{\Omega}$. This can be done in a completely standard way at the interior nodes, cf. for example the exposition in Section 1.4. Note in particular that this localization relies on the finite element discretization of the governing equation at these nodes. The construction is also standard at the nodes on the wall part of the boundary and on the outflow, cf. Remark 1.8, and relies on the observation that the stress can be kept free on these parts of the boundary. On the contrary, we have a non standard situation at the nodes on the interface γ. Indeed, in order to preserve continuity of the normal component, we should have there $\sigma_h \cdot n = -\nabla u' \cdot n = 0$ on γ, as if this is a part of the boundary where the Neumann conditions are imposed. But this is not the case: Dirichlet boundary conditions are prescribed at these nodes in the finite element discretization. Our way to circumvent this problem is to enlarge the patch attached to the interface γ, as explained below.

For each vertex $a \in \tilde{\Omega}$ we consider a patch ω^a to be the collection of all triangles that share this vertex a. Let $\mathcal{V}_h^*$ be the vertices of $\overline{\tilde{\Omega}} \backslash \bar{\gamma}$. Our notations are shown in Figure 2.1.

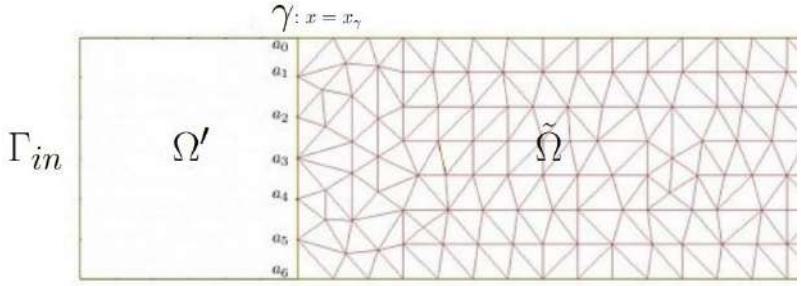

Figure 2.1.: Simplified region Ω', vertices a_i of patches ω^{a_i} at the interface γ in the non simplified region $\tilde{\Omega}$

Let

$$\omega^\gamma = \bigcup_{a_i \in \gamma} \omega^{a_i}$$

as in Figure 2.2.

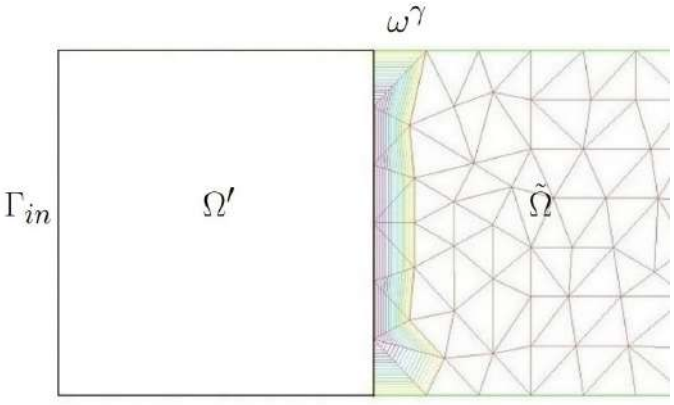

Figure 2.2.: Patch ω^γ which represents the union of all patches of vertices located on γ

We introduce the partition of unity:

$$\begin{aligned}\mathbb{1}_{\Omega} &= \mathbb{1}_{\Omega'} + \mathbb{1}_{\tilde{\Omega}} \\ &= \mathbb{1}_{\Omega'} + \sum_{a \,:\, \text{vertices in } \tilde{\Omega}} \psi^a \\ &= \mathbb{1}_{\Omega'} + \underbrace{\sum_{a \,\in\, \gamma} \psi^a}_{\psi^\gamma :=} + \sum_{a \,\in\, \mathcal{V}_h^*} \psi^a \\ &= \mathbb{1}_{\Omega'} + \psi^\gamma + \sum_{a \,\in\, \mathcal{V}_h^*} \psi^a,\end{aligned}$$

where, ψ^a and ψ^γ are $\mathbb{P}_1$ finite element functions. In particular, ψ^a is the hat function for any mesh node excluding those in γ. By construction ψ^γ is 1 on γ and 0 on all nodes not on γ.
Now, we replace σ_h^{ideal} by

$$\sigma_h = \sigma_h^\gamma + \sum_{a \in \mathcal{V}_h^*} \sigma_h^a + (-\nabla u')\mathbb{1}_{\Omega'} = \tilde{\sigma}_h + \sigma', \tag{2.2}$$

where, $\sigma' = -\nabla u'$ in Ω', see equation (1.8), and $\tilde{\sigma}_h$ is defined by

$$\tilde{\sigma}_h := \sigma_h^\gamma + \sum_{a \in \mathcal{V}_h^*} \sigma_h^a. \tag{2.3}$$

For each $a \in \mathcal{V}_h^*$, we define $\sigma_h^a \in \Sigma_h^a$ by

$$\sigma_h^a := \underset{\substack{v_h^a \in \Sigma_h^a, \\ \operatorname{div} v_h^a = \Pi_{Q_h^a}\left(\psi^a f - \nabla\psi^a \cdot \nabla \tilde{u}_h\right)}}{\arg\min} ||v_h^a + \psi^a \nabla \tilde{u}_h||_{L^2(\omega^a)}$$

and $\sigma_h^\gamma \in \Sigma_h^\gamma$ by

$$\sigma_h^\gamma := \underset{\substack{v_h^\gamma \in \Sigma_h^\gamma, \\ \operatorname{div} v_h^\gamma = \Pi_{Q_h^\gamma}\left(\psi^\gamma \cdot f - \nabla\psi^\gamma \cdot \nabla \tilde{u}_h\right)}}{\arg\min} ||v_h^\gamma + \psi^\gamma \nabla \tilde{u}_h||_{L^2(\omega^\gamma)} \tag{2.4}$$

Where,
Case 1: a in an internal node of $\tilde{\Omega}$
$\Sigma_h^a := \{\sigma_h \in RT_k(K)\ \forall K \in \omega^a, \sigma_h \cdot n = 0 \quad \text{on} \quad \partial\omega^a\}$
$Q_h^a := \{q_h \in L^2(\omega^a), q_h|_K \in \mathbb{P}_k(K), \forall K \in \omega^a, \int_{\omega^a} q_h = 0\}$
Case 2: a on the wall of $\tilde{\Omega}\backslash\gamma$
$\Sigma_h^a := \{\sigma_h \in RT_k(K)\ \forall K \in \omega^a, \sigma_h \cdot n = 0 \quad \text{on} \quad \partial\omega^a \backslash \partial\tilde{\Omega}\}$
$Q_h^a := \{q_h \in L^2(\omega^a), q_h|_K \in \mathbb{P}_k(K), \forall K \in \omega^a\}$
Case 3: $a = \gamma$
$\Sigma_h^\gamma := \{\sigma_h \in RT_k(K)\ \forall K \in \omega^\gamma, \sigma_h \cdot n = 0 \quad \text{on} \quad \partial\omega^\gamma \backslash \partial\tilde{\Omega} \quad \text{and} \quad \sigma_h \cdot n = (-\nabla u') \cdot n = 0 \quad \text{on} \quad \gamma\}$
$Q_h^\gamma := \{q_h \in L^2(\omega^\gamma), q_h|_K \in \mathbb{P}_k(K), \forall K \in \omega^\gamma\}$

$\Pi_{Q_h^a}$ is the $L^2(\omega_a)$-orthogonal projection and $\Pi_{Q_h^\gamma}$ is the $L^2(\omega^\gamma)$-orthogonal projection. We remark that the minimization problems above are equivalent to the following variational problems. Find $\sigma_h^\gamma \in \Sigma_h^\gamma$ and $r_h^\gamma \in Q_h^\gamma$ such that

$$\begin{cases} (\sigma_h^\gamma, v_h)_{\omega^\gamma} - (r_h^\gamma, \nabla \cdot v_h)_{\omega^\gamma} = (-\psi^\gamma \nabla \tilde{u}_h, v_h)_{\omega^\gamma} & \forall v_h \in \Sigma_h^\gamma, \\ (\nabla \cdot \sigma_h^\gamma, q_h)_{\omega^\gamma} = (\psi^\gamma f - \nabla \psi^\gamma \cdot \nabla \tilde{u}_h, q_h)_{\omega^\gamma} & \forall q_h \in Q_h^\gamma, \end{cases} \tag{2.5}$$

And for all vertices $a \in \mathcal{V}_h^*$, find $\sigma_h^a \in \Sigma_h^a$ and $r_h^a \in Q_h^a$ such that:

$$\begin{cases} (\sigma_h^a, v_h)_{\omega^a} - (r_h^a, \nabla \cdot v_h)_{\omega^a} = -(\psi^a \nabla \tilde{u}_h, v_h)_{\omega^a} & \forall v_h \in \Sigma_h^a, \\ (\nabla \cdot \sigma_h^a, q_h)_{\omega^a} = (\psi^a f - \nabla \psi^a \cdot \nabla \tilde{u}_h, q_h)_{\omega^a} & \forall q_h \in Q_h^a, \end{cases} \tag{2.6}$$

Proposition 2.4. *Let σ_h defined by equation (2.2) and σ_h^γ by equation* (2.4) *. We have $\tilde{\sigma}_h = \sigma_h^\gamma + \sum_{a \in \mathcal{V}_h^*} \sigma_h^a$, then $\nabla \cdot \tilde{\sigma}_h = \Pi_{Q_h}(f) = f$ on $\tilde{\Omega}$ and consequently $\nabla \cdot \sigma_h = f$ on Ω where, $f = \frac{12 u_{av}}{R^2}$ and $Q_h = \mathbb{P}_k(\tilde{\mathcal{T}}_h)$.*

Proof. $\tilde{\sigma}_h \in H(\mathrm{div}, \tilde{\Omega})$ as all the individual components σ_h^γ and σ_h^a belong to $H(\mathrm{div}, \tilde{\Omega})$ for all $a \in \mathcal{V}_h^*$, since by extension we can go from $H(\mathrm{div}, \omega^\gamma)$ and $H(\mathrm{div}, \omega^a)$ to $H(\mathrm{div}, \tilde{\Omega})$, and $\tilde{\sigma}_h$ is the sum of all these components. Now, to show that $\nabla \cdot \sigma_h = f$ in Ω, we will deal with the following three cases:
Case 1: a is internal node of $\tilde{\Omega}$:
$\forall a \in \mathcal{V}_h^*$ we have: $(\nabla \cdot \sigma_h^a, q_h)_{\omega^a} = (\psi^a f - \nabla \psi^a \cdot \nabla \tilde{u}_h, q_h)_{\omega^a}$ for all $q_h \in Q_h^a$, then we have $\int_{\omega^a} q_h = 0$ and we have $(\nabla \cdot \sigma_h^a, 1)_{\omega^a} = 0$ as $\sigma_h^a \cdot n = 0$ on $\partial\omega^a$ and using the divergence theorem. From Eq (1.12), we have $(\nabla \tilde{u}_h, \nabla \tilde{v}_h)_{\tilde{\Omega}} = (f, \tilde{v}_h)_{\tilde{\Omega}}$ for all $\tilde{v}_h \in \tilde{V}_h^0$ so, let us take the following particular cases for the test function $\tilde{v}_h \in \tilde{V}_h^0$:

- If we take $\tilde{v}_h = \psi^a$, then $(\nabla \tilde{u}_h \cdot \nabla \psi^a, 1)_{\tilde{\Omega}} = (f \psi^a, 1)_{\tilde{\Omega}}$ since $\tilde{v}_h = \psi^a \in \tilde{V}_h^0$ as a is an internal node of $\tilde{\Omega}$.

Let us define $Q_h(\omega^a) := \{q_h \in L^2(\omega^a); q_h \in \mathbb{P}_k(K) \quad \forall K \in \omega^a\}$, then for all $a \in \mathcal{V}_h^*$ we have $(\nabla \cdot \sigma_h^a, q_h)_{\omega^a} = (\psi^a f - \nabla \tilde{u}_h \cdot \nabla \psi^a, q_h)_{\omega^a}$ for all $q_h \in Q_h(\omega^a)$ and not only for the vector-valued function with zero mean value.
Case 2: a is on wall of $\tilde{\Omega} \backslash \gamma$:
We have $(\nabla \cdot \sigma_h^a, q_h)_{\omega^a} = (\psi^a f - \nabla \psi^a \cdot \nabla \tilde{u}_h, q_h)_{\omega^a}$ for all $q_h \in Q_h^a = Q_h(\omega^a)$.
Case 3: $a = \gamma$:
We have $(\nabla \cdot \sigma_h^\gamma, q_h)_{\omega^\gamma} = (\psi^\gamma f - \nabla \psi^\gamma \cdot \nabla \tilde{u}_h, q_h)_{\omega^\gamma}$ for all $q_h \in Q_h^\gamma = Q_h(\omega^\gamma)$.

Let now $\tilde{q}_h \in Q_h = \mathbb{P}_k(\tilde{\mathcal{T}}_h)$ then,

$$\begin{aligned} (\nabla \cdot \tilde{\sigma}_h, \tilde{q}_h)_{\tilde{\Omega}} &= \left(\nabla \cdot \sigma_h^\gamma, \tilde{q}_h\right)_{\tilde{\Omega}} + \left(\nabla \cdot (\sum_{a \in \mathcal{V}_h^*} \sigma_h^a), \tilde{q}_h\right)_{\tilde{\Omega}} \\ &= \left((\psi^\gamma f - \nabla \psi^\gamma \cdot \nabla \tilde{u}_h, \tilde{q}_h\right)_{\tilde{\Omega}} + \sum_{a \in \mathcal{V}_h^*} \left(\psi^a f - \nabla \psi^a \cdot \nabla \tilde{u}_h, \tilde{q}_h\right)_{\tilde{\Omega}} \\ &= \left(f(\psi^\gamma + \sum_{a \in \mathcal{V}_h^*} \psi^a) - \nabla \tilde{u}_h \cdot \nabla(\psi^\gamma + \sum_{a \in \mathcal{V}_h^*} \psi^a), \tilde{q}_h\right)_{\tilde{\Omega}} \\ &= \left(f \mathbb{1}_{\tilde{\Omega}} - \nabla \tilde{u}_h \cdot \nabla(\mathbb{1}_{\tilde{\Omega}}), \tilde{q}_h\right)_{\tilde{\Omega}} \\ &= (f, \tilde{q}_h)_{\tilde{\Omega}} \end{aligned}$$

Since $\nabla \cdot (RT_k(K)) = Q_h(K) = \mathbb{P}_k(K)$ for all $K \in \tilde{\mathcal{T}}_h$, we get $\nabla \cdot \tilde{\sigma}_h = \Pi_{Q_h}(f) = f$ where, Π_{Q_h} is the $L^2(\tilde{\Omega})$-orthogonal projection onto Q_h and finally, we get

$$\nabla \cdot \tilde{\sigma}_h = f \qquad \text{on} \quad \tilde{\Omega}.$$

■

2.1.2. Reliability of the *a posteriori* error estimate based on (2.2)

We adapt here a general result about the reliability of equilibrated flux *a posteriori* error estimates.

Theorem 2.5 (A general a posterior error estimate)**.** *Let u be the weak solution defined by system (1.4). Let u_h^s be given by (1.8)–(1.12)–(1.13) and σ_h the flux reconstruction* (2.2)*. Recalling $\tilde{\mathcal{T}}_h$ the mesh on $\tilde{\Omega}$, define $\forall K \in \tilde{\mathcal{T}}_h$ the local flux estimator $\eta_{F,K} := ||\nabla \tilde{u}_h + \tilde{\sigma}_h||_K$. Then,*

$$||\nabla(u - u_h^s)||_\Omega^2 \leq \sum_{K \in \tilde{\mathcal{T}}_h} \eta_{F,K}^2 \tag{2.7}$$

Proof. First, $u - u_h^s \in H_0^1(\Omega)$, thus as

$$||\nabla v|| = \sup_{\phi \in H_0^1(\Omega), ||\nabla \phi|| = 1,} (\nabla v, \nabla \phi) \qquad \forall v \in H_0^1(\Omega)$$

then,

$$||\nabla(u - u_h^s)|| = \sup_{\phi \in H_0^1(\Omega), ||\nabla \phi|| = 1,} (\nabla(u - u_h^s), \nabla \phi) \qquad \forall \phi \in H_0^1(\Omega).$$

Now, let $\phi \in H_0^1(\Omega)$ and $||\nabla \phi||_\Omega = 1$ be fixed. Then, by using the weak formulation (1.4), we get:

$$(\nabla(u - u_h^s), \nabla \phi)_\Omega = (f, \phi)_\Omega - (\nabla u_h^s, \nabla \phi)_\Omega.$$

Now, adding and subtracting $(\sigma_h, \nabla \phi)_\Omega$ where, $\sigma_h = \tilde{\sigma} + \sigma'$ we get:

$$\begin{aligned}
(\nabla(u - u_h^s), \nabla \phi)_\Omega &= (\nabla(u - u_h^s) + \sigma_h - \sigma_h, \nabla \phi)_\Omega \\
&= (\nabla(u - u_h^s), \nabla \phi)_\Omega + (\sigma_h, \nabla \phi)_\Omega - (\sigma_h, \nabla \phi)_\Omega \\
&= (f, \phi)_\Omega - (\nabla u_h^s, \nabla \phi)_\Omega - (\nabla \cdot \sigma_h, \phi)_\Omega - (\sigma_h, \nabla \phi)_\Omega \\
&= (f - \nabla \cdot \sigma_h, \phi)_\Omega - (\nabla u_h^s + \sigma_h, \nabla \phi)_\Omega \\
&= -(\nabla u_h^s + \sigma_h, \nabla \phi)_\Omega \\
&= -(\nabla u' + \sigma', \nabla \phi)_{\Omega'} - (\nabla \tilde{u}_h + \tilde{\sigma}_h, \nabla \phi)_{\tilde{\Omega}} \\
&= -(\nabla \tilde{u}_h + \tilde{\sigma}_h, \nabla \phi)_{\tilde{\Omega}} \\
&\leq \sum_{K \in \tilde{\mathcal{T}}_h} \eta_{F,K} ||\nabla \phi||_K \\
&\leq \Big(\sum_{K \in \tilde{\mathcal{T}}_h} \eta_{F,K}^2 \Big)^{\frac{1}{2}} \Big(\sum_{K \in \tilde{\mathcal{T}}_h} ||\nabla \phi||_K^2 \Big)^{\frac{1}{2}} \\
&\leq \Big(\sum_{K \in \tilde{\mathcal{T}}_h} \eta_{F,K}^2 \Big)^{\frac{1}{2}} ||\nabla \phi||.
\end{aligned}$$

So,

$$\Big(\nabla(u-u_h^s),\nabla\phi\Big)_\Omega \leq \Big(\sum_{K\in\mathcal{T}_h}\eta_{F,K}^2\Big)^{\frac{1}{2}},$$

then,

$$||\nabla(u-u_h^s)||_\Omega = \sup_{\phi\in H_0^1(\Omega),||\nabla\phi||=1}(\nabla(u-u_h^s),\nabla\phi) \leq \Big(\sum_{K\in\tilde{\mathcal{T}}_h}\eta_{F,K}^2\Big)^{\frac{1}{2}}.$$

Finally,

$$||\nabla(u-u_h^s)||_\Omega^2 \leq \sum_{K\in\tilde{\mathcal{T}}_h}\eta_{F,K}^2.$$

■

2.1.3. Lack of efficiency

We report here on our attempt to establish the efficiency of the *a posteriori* error estimate of (2.7) following the lines of Ern and Vohralik in [39]. We shall see that this leads to some unsolvable issues, indicating that the flux reconstruction introduced in Section 2.1.1 does not lead to an efficient error indicator.

We want thus to see if we can show that these estimators give a "local" lower bound for the error $||\nabla(u-u_h^s)||_\Omega^2$ up to a generic constant only depending on the shape-regularity parameter. To be able to make this lower bound, we will introduce the following two lemmas. Let us introduce a new domain $\omega' \subset \Omega'$ and $\omega^\gamma \subset \tilde{\Omega}$, as shown in Figure 2.3 below, where the abscissa $x_2 < x_\gamma$ and x_γ is very near to x_2.

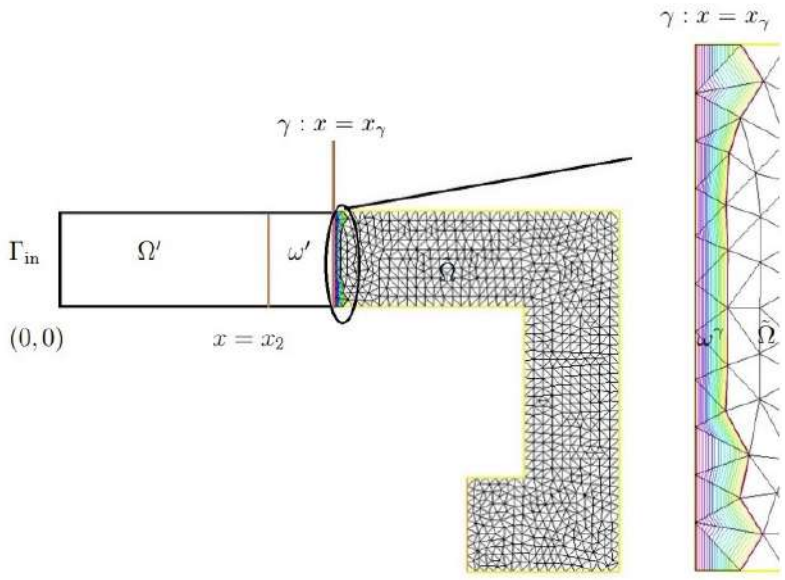

Figure 2.3.: The coupled 0D/2D domain with new local domain $\omega' \subset \Omega_1'$

Lemma 2.6. *Let u be the exact solution on the whole domain Ω defined by (1.4). Let u_h^s be the approximate solution on Ω defined by (1.8)–(1.12)–(1.13). Let γ be the interface between the 2D and 0D models at $x = x_\gamma > 0$ as being shown in the Figure 2.3. Here we want to distinguish between the following two cases.*

- *Case 1: if the vertex $a \in \gamma$ we have the patch $\omega^\gamma = \cup_{a\in\gamma}\omega^a$ as shown in Figure 2.3. Let $r^\gamma \in H^1_*(\omega^\gamma)$ solves:*

$$(\nabla r^\gamma, \nabla v)_{\omega^\gamma} = -(\psi^\gamma \nabla \tilde{u}_h, \nabla v)_{\omega^\gamma} + (\psi^\gamma f - \nabla\psi^\gamma \cdot \nabla\tilde{u}_h, v)_{\omega^\gamma}, \forall v \in H^1_*(\omega^\gamma), \quad (2.8)$$

  where,

  - $H^1_*(\omega^\gamma) := \{v \in H^1(\omega^\gamma); v = 0$ *on* $\partial\omega^\gamma \cap \partial\Omega\}$,
  - $\psi^\gamma = \sum_{a\in\gamma}\psi^a$.

  Then, there exists a positive constant $C_\gamma(\frac{R}{h}) > 0$ which depends on shape regularity and mesh size h such that:

$$||\nabla r^\gamma||_{\omega^\gamma} \leq C_\gamma\left(\frac{R}{h}\right)||\nabla(u - u_h^s)||_{\omega^\gamma\cup\omega'}, \quad (2.9)$$

  where, $\omega' \subset \Omega'$ such that $\omega' = [x_2, x_\gamma] \times [0, R]$ and x_2 is very near to x_γ such that: $|x_\gamma - x_2| > 0$.

- *Case 2: if $a \in \tilde{\Omega}\backslash\gamma = \mathcal{V}_h^*$, we have the patch ω^a be collection of all elements that intersect with this vertex a.*
  Let $r^a \in H^1_*(\omega^a)$ solves:

$$(\nabla r^a, \nabla v)_{\omega^a} = -(\psi^a \nabla \tilde{u}_h, v)_{\omega^a} + (\psi^a f - \nabla\psi^a \cdot \nabla\tilde{u}_h, v)_{\omega^a}, \forall v \in H^1_*(\omega^a), \quad (2.10)$$

  where,

  - $H^1_*(\omega^a) := \{v \in H^1(\omega^a); (v, 1)_{\omega^a} = 0\}$ *for all* $a \in \mathcal{V}_h^{int} = \mathcal{V}_h^* \cap \tilde{\Omega}$,
  - $H^1_*(\omega^a) := \{v \in H^1(\omega^a); v = 0$ *on* $\partial\omega^a \cap \partial\tilde{\Omega}$ $\}$ *for all* $a \in \mathcal{V}_h^{ext} = \mathcal{V}_h^* \cap \partial\tilde{\Omega}$.

  Then, there exists a positive constant $C_{cont,PF} > 0$ only depending on shape regularity such that:

$$||\nabla r^a||_{\omega^a} \leq C_{cont,PF}||\nabla(u - \tilde{u}_h)||_{\omega^a}. \quad (2.11)$$

Proof. • Case 1: for $a \in \gamma$, we have $\psi^\gamma = \sum_{a\in\gamma}\psi^a$ is a polynomial of degree 1 and equal to 1 on γ and 0 on all nodes not on γ.
Let us define Ψ^Γ by:

$$\Psi^\Gamma = \begin{cases} \psi^\gamma & \text{on} \quad \omega^\gamma, \\ \theta & \text{on} \quad \omega' = [x_2, x_\gamma] \times [0, R], \\ 0 & \text{on} \quad \Omega'\backslash\omega'. \end{cases}$$

Where, x_γ is the abscissa of γ which represents the interface at $x = x_\gamma$ and $x_2 < x_\gamma$ and $\theta(x, y) := \frac{x-x_2}{x_\gamma - x_2}$. We have that Ψ^Γ is continuous on γ since:

- $\Psi^\Gamma|_{x=x_\gamma^+} = \psi^\gamma|_{x_\gamma} = 1$,
- $\Psi^\Gamma|_{x=x_\gamma^-} = \theta(x_\gamma, y) = \frac{x_\gamma - x_2}{x_\gamma - x_2} = 1$.

Ψ_Γ is also continuous at x_2 and finally it is continuous on $\Omega' \cup \omega^\gamma$. As $r^\gamma \in H^1_*(\omega^\gamma)$ solves equation (2.8) then,

$$||\nabla r^\gamma||_{\omega^\gamma} = \sup_{\substack{v \in H^1_*(\omega^\gamma), \\ ||\nabla v||_{\omega^\gamma}=1}} (\nabla r^\gamma, \nabla v)_{\omega^\gamma}.$$

Let $v \in H^1_*(\omega^\gamma)$ and $||\nabla v||_{\omega^\gamma} = 1$, then v can be extended to Ω' by any $v' \in H^1(\Omega')$ such that $v'|_\gamma = v|_\gamma$ and $v' = 0$ on $\partial\Omega' \backslash \gamma$ and $||\nabla v||_{\Omega'} = 1$ or $||\nabla v||_{\Omega'} = c$ where, c is a constant.

$$\tilde{v} = \begin{cases} v & \text{on} \quad \omega^\gamma, \\ v' & \text{on} \quad \Omega'. \end{cases}$$

Now, $\tilde{v} \in H^1(\omega^\gamma \cup \Omega')$ so,

$$\begin{aligned}
(\nabla r^\gamma, \nabla v)_{\omega^\gamma} &= -(\psi^\gamma \nabla \tilde{u}_h, \nabla v)_{\omega^\gamma} + (\psi^\gamma f - \nabla \psi^\gamma \cdot \nabla \tilde{u}_h, v)_{\omega^\gamma} \\
&= -(\psi^\gamma \nabla \tilde{u}_h, \nabla v)_{\omega^\gamma} + (\psi^\gamma f - \nabla \psi^\gamma \cdot \nabla \tilde{u}_h, v)_{\omega^\gamma} - (\nabla u', \nabla(\Psi^\Gamma \tilde{v}))_{\omega'} + (f, \Psi^\Gamma \tilde{v})_{\omega'} \\
&= (f, \psi^\gamma v)_{\omega^\gamma} + (f, \Psi^\Gamma \tilde{v})_{\omega'} - (\nabla \tilde{u}_h, \nabla(\psi^\gamma v))_{\omega^\gamma} - (\nabla u', \nabla(\Psi^\Gamma \tilde{v}))_{\omega'} \\
&= (f, \Psi^\Gamma \tilde{v})_{\omega^\gamma \cup \omega'} - (\nabla u_h^s, \nabla(\Psi^\Gamma \tilde{v}))_{\omega^\gamma \cup \omega'}
\end{aligned}$$

Since $\Psi^\Gamma \tilde{v} \in H^1_0(\omega^\gamma \cup \omega')$ then, we can extend by zero outside $\omega^\gamma \cup \omega'$ to integrate on Ω.

$$\begin{aligned}
(\nabla r^\gamma, \nabla v)_{\omega^\gamma} &= (f, \Psi^\Gamma \tilde{v})_\Omega - (\nabla u_h^s, \nabla(\Psi^\Gamma \tilde{v}))_{\omega^\gamma \cup \omega'} \\
&= \left(\nabla u, \nabla(\Psi^\Gamma \tilde{v})\right)_\Omega - \left(\nabla u_h^s, \nabla(\Psi^\Gamma \tilde{v})\right)_{\omega^\gamma \cup \omega'} \\
&= \left(\nabla u, \nabla(\Psi^\Gamma \tilde{v})\right)_{\omega^\gamma \cup \omega'} - \left(\nabla u_h^s, \nabla(\Psi^\Gamma \tilde{v})\right)_{\omega^\gamma \cup \omega'} \\
&= (\nabla(u - u_h^s), \nabla(\Psi^\Gamma \tilde{v}))_{\omega^\gamma \cup \omega'} \\
&= (\nabla(u - \tilde{u}_h), \nabla(\psi^\gamma \tilde{v}))_{\omega^\gamma} + (\nabla(u - u'), \nabla(\theta v'))_{\omega'} \\
&\leq ||\nabla(u - \tilde{u}_h)||_{\omega^\gamma} ||\nabla(\psi^\gamma v)||_{\omega^\gamma} + ||\nabla(u - u')||_{\omega'} ||\nabla(\theta v')||_{\omega'}
\end{aligned}$$

Next, $||\nabla(\psi^\gamma v)||_{\omega^\gamma} = ||\nabla \psi^\gamma v + \psi^\gamma \nabla v||_{\omega^\gamma} \leq ||\nabla \psi^\gamma||_{\infty,\omega^\gamma} ||v||_{\omega^\gamma} + ||\psi^\gamma||_{\infty,\omega^\gamma} ||\nabla v||_{\omega^\gamma}$
Now, using Friedrichs inequality, we get:

$$||v||_{\omega^\gamma} \leq C_{F,\omega^\gamma} h_{\omega^\gamma} ||\nabla v||_{\omega^\gamma}.$$

Where, h_{ω^γ} is the diameter of ω^γ.Then

$$\begin{aligned}
||\nabla(\psi^\gamma v)||_{\omega^\gamma} &\leq ||\nabla v||_{\omega^\gamma} \left(C_{F,\omega^\gamma} h_{\omega^\gamma} ||\nabla \psi^\gamma||_{\infty,\omega^\gamma} + ||\psi^\gamma||_{\infty,\omega^\gamma} \right) \\
&= C_{F,\omega^\gamma} h_{\omega^\gamma} ||\nabla \psi^\gamma||_{\infty,\omega^\gamma} + 1
\end{aligned}$$

and $||\nabla(\theta v')||_{\omega'} = ||\nabla \theta v' + \theta \nabla v'||_{\omega'} \leq ||\nabla \theta||_{\infty,\omega'} ||v'||_{\omega'} + ||\theta||_{\infty,\omega'} ||\nabla v'||_{\omega'}$.

Now, using Friedrichs inequality we get:

$$||v'||_{\omega'} \leq C_{F,\omega'} h_{\omega'} ||\nabla v'||_{\omega'},$$

where, $h_{\omega'}$ is the diameter of ω'. Then

$$\begin{aligned} ||\nabla(\theta v')||_{\omega'} &\leq ||\nabla v'||_{\omega'} \Big(C_{F,\omega'} h_{\omega'} ||\nabla\theta||_{\infty,\omega'} + ||\theta||_{\infty,\omega'} \Big) \\ &\leq C_{F,\omega'} h_{\omega'} ||\nabla v||_{\infty,\omega'} + 1. \end{aligned}$$

Finally,

$$\begin{aligned} ||\nabla r^\gamma||_{\omega^\gamma} \leq & \Big(C_{F,\omega^\gamma} h_{\omega^\gamma} ||\nabla\psi^\gamma||_{\infty,\omega^\gamma} + 1 \Big) ||\nabla(u - \tilde{u}_h)||_{\omega^\gamma} \\ & + \Big(C_{F,\omega'} h_{\omega'} ||\nabla\theta||_{\infty,\omega'} + 1 \Big) ||\nabla(u - u')||_{\omega'}. \end{aligned}$$

As $\theta(x) = \frac{x - x_2}{x_\gamma - x_2}$, then $\theta'(x) = \frac{1}{x_\gamma - x_2}$ and $h_{\omega'} = \sqrt{(x_\gamma - x_2)^2 + R^2}$ so, $h_{\omega'} ||\theta'||_{\infty,\omega'} = \frac{1}{x_\gamma - x_2} \sqrt{(x_\gamma - x_2)^2 + R^2} \approx \sqrt{2}$ if $x_\gamma - x_2 = R$, we also have $h_{\omega^\gamma} ||\nabla\psi^\gamma||_{\infty,\omega_{\gamma_1}} \approx \frac{R}{h}$, where h is the mesh size. Finally, there exists a positive constant $C_\gamma(\frac{R}{h}) > 0$ which depends on the mesh size h and the shape regularity such that:

$$||\nabla r^\gamma||_{\omega^\gamma} \leq C_\gamma \left(\frac{R}{h} \right) ||\nabla(u - u_h^s)||_{\omega^\gamma \cup \omega'} \tag{2.12}$$

- Case 2: for $a \in \tilde{\Omega} \backslash \gamma = \mathcal{V}_h^*$, we have ψ^a is a polynomial of degree 1 and equal to 1 on vertex a and 0 on all other nodes. Here we will proceed in a similar way of [39]. We have $r^a \in H_*^1(\omega^a)$ solves equation (2.10) then,

$$||\nabla r^a||_{\omega^a} = \sup_{\substack{v \in H_*^1(\omega^a), \\ ||\nabla v||_{\omega^a} = 1}} (\nabla r^a, \nabla v)_{\omega^a}.$$

Let $v \in H_*^1(\omega^a)$ and $||\nabla v||_{\omega^a} = 1$, then

$$\begin{aligned} (\nabla r^a, \nabla v)_{\omega^a} &= -(\psi^a \nabla \tilde{u}_h, \nabla v)_{\omega^a} + (\psi^a f - \nabla\psi^a \cdot \nabla \tilde{u}_h, v)_{\omega^a} \\ &= -(\nabla \tilde{u}_h, \psi^a \nabla v)_{\omega^a} + (f, \psi^a v)_{\omega^a} - (\nabla \tilde{u}_h, \nabla\psi^a v)_{\omega^a} \\ &= (f, \psi^a v)_{\omega^a} - (\nabla \tilde{u}_h, \nabla(\psi^a v))_{\omega^a}. \end{aligned}$$

But, $\psi^a v \in H_0^1(\omega^a)$ so, it can be extended by 0 outside ω^a to be defined on whole Ω. Then,

$$\begin{aligned} (\nabla r^a, \nabla v)_{\omega^a} &= (f, \psi^a v)_\Omega - (\nabla u_h^s, \nabla(\psi^a v))_{\omega^a} \\ &= (\nabla u, \nabla(\psi^a v))_\Omega - (\nabla u_h^s, \nabla(\psi^a v))_{\omega^a} \\ &= (\nabla u, \nabla(\psi^a v))_{\omega^a} - (\nabla u_h^s, \nabla(\psi^a v))_{\omega^a} \\ &= (\nabla(u - u_h^s), \nabla(\psi^a v))_{\omega^a} \\ &\leq ||\nabla(u - u_h^s)||_{\omega^a} ||\nabla(\psi^a v)||_{\omega^a} \end{aligned}$$

Now, splitting the cases $a \in \mathcal{V}_h^{int}$ and $a \in \mathcal{V}_h^{ext}$.
If $a \in \mathcal{V}_h^{int}$: use Poincaré inequality on the patch ω^a as $v_{\omega^a} := \frac{(v,1)_{\omega^a}}{|\omega^a|} = 0$:

$$||v - v_{\omega^a}||_{\omega^a} \leq C_{p,\omega^a} h_{\omega^a} ||\nabla v||_{\omega^a}.$$

If $a \in \mathcal{V}_h^{ext}$: use Friedrichs inequality on the patch ω^a :

$$||v||_{\omega^a} \leq C_{F,\omega^a} h_{\omega^a} ||\nabla v||_{\omega^a}$$

and using $||\nabla v||_{\omega^a} = 1$ and $||\psi^a||_{\infty,\omega^a} = 1$ we get:

$$\begin{aligned} ||\nabla(\psi^a v)||_{\omega^a} &= ||\nabla\psi^a v + \psi^a \nabla v||_{\omega^a} \\ &\leq ||\nabla\psi^a||_{\infty,\omega^a} ||v||_{\omega^a} + ||\psi^a||_{\infty,\omega^a} ||\nabla v||_{\omega^a} \\ &\leq ||\nabla v||_{\omega^a} \Big(C_{PF,\omega^a} h_{\omega^a} ||\nabla\psi^a||_{\infty,\omega^a} + ||\psi^a||_{\infty,\omega^a} \Big) \\ &\leq 1 + C_{PF,\omega^a} h_{\omega^a} ||\nabla\psi^a||_{\infty,\omega^a} \end{aligned}$$

where,

$$C_{PF,\omega^a} := \begin{cases} C_{p,\omega^a} & \text{if} \quad a \in \mathcal{V}_h^{int}, \\ C_{F,\omega^a} & \text{if} \quad a \in \mathcal{V}_h^{ext}. \end{cases}$$

Then,

$$\begin{aligned} ||\nabla r^a||_{\omega^a} &\leq \big(1 + C_{PF,\omega^a} h_{\omega^a} ||\nabla\psi^a||_{\infty,\omega^a}\big) ||\nabla(u - u_h^s)||_{\omega^a} \\ &\leq \max_{a \in \mathcal{V}_h^*} \big(1 + C_{PF,\omega^a} h_{\omega^a} ||\nabla\psi^a||_{\infty,\omega^a}\big) ||\nabla(u - u_h^s)||_{\omega^a}, \end{aligned}$$

so,

$$||\nabla r^a||_{\omega^a} \leq C_{cont,PF} ||\nabla(u - u_h^s)||_{\omega^a},$$

where, $C_{cont,PF} = \max_{a \in \mathcal{V}_h^*} \{1 + C_{PF,\omega^a} h_{\omega^a} ||\nabla\psi^a||_{\infty,\omega^a}\ \}$ and for "nice" meshes $h_{\omega^a} ||\nabla\psi^a||_{\infty,\omega^a} \approx 2$ see [39, Remark 3.24].

■

Let us assume that the following theorem which is showed in [14, Theorem 7] is applicable for the patch ω^γ and that is an essential result for the next results.

Theorem 2.7. *Let us define $\omega := \omega^\gamma$, $RT_k(K) := \{\tau : \tau(x) = q_K + s_K x, q_K \in (\mathbb{P}_k)^2, s_K \in \mathbb{P}_k\}$ and $RT^k_{-1,0}(\omega) := \{\tau \in L_2(\omega) : \tau|_K \in RT_k(K), \forall K \in \omega, \tau \cdot n = 0$ on $\partial\omega\}$. Let r be the residual which is defined by*

$$\langle r, v \rangle := \sum_{K \in \omega} \int_K r_K v + \sum_{E \in \omega} \int_E r_E v$$

with $r_K \in \mathbb{P}_k(K)$ and $r_E \in \mathbb{P}_k(E)$. If $\langle r, 1 \rangle = 0$, then there exists a constant C independent of k and mesh size h such that

$$\inf_{\substack{\sigma \in RT^k_{-1,0}(\omega), \\ \operatorname{div}(\sigma) = r}} ||\sigma||_\omega \leq C ||r||_{[H^1(\omega)/R]^*}.$$

Remark 2.8. *We will not take care about if Theorem 2.7 can be proved or not since even if we suppose that Theorem 2.7 can be proved, we will not be able to prove the efficiency according to Theorem 2.10 below since the constant of the efficiency depends on the mesh size. The drawback of the first suggestion of the reconstructed flux is that this C_γ, and consequently the efficiency, depends on the mesh size h. If we try to improve this constant of efficiency to be independent from the mesh size by taking out the big patch ω^γ and define many patches that are centered at each node $a \in \gamma$ as we did for each patch with nodes a located in the wall of $\tilde{\Omega}\backslash\gamma$, then we will loose the compatibility condition in the definition of the stress reconstruction in system (2.6). In this study we have only proved the upper bound which is good in order to deduce later that the error depends on the position of the interface and on the discretization.*

Corollary 2.9. *We will distinguish between the following two cases:*

- *Case 1: if $a \in \gamma$ and we deal with the patch ω^γ: let $\tau_h^\gamma = \psi^\gamma \nabla \tilde{u}_h$ and $g^\gamma = \psi^\gamma f - \nabla\psi^\gamma \cdot \nabla \tilde{u}_h$. Let $\mathcal{T}^\gamma = \cup_{K\cap\gamma\neq\emptyset} K$. Suppose that $\tau_h^\gamma|_K \in \Sigma_h(K)$ and $g^\gamma|_K \in Q_h(K)$ for all $K \in \mathcal{T}^\gamma$ where, $\Sigma_h = RT_k = RT_k(\tilde{\mathcal{T}}_h) \cap H(\mathrm{div}, \tilde{\Omega})$ and $Q_h = \mathbb{P}_k(\tilde{\mathcal{T}}_h)$.*
  Let $r^\gamma \in H^1_*(\omega^\gamma)$ solves equation (2.8) and let σ_h^γ be the solution of system (2.5) and if we suppose that Theorem 2.7 (below) can be verified, then there exists a positive real number $C^1_{st} > 0$ that depends only on the shape regularity such that:

$$||\sigma_h^\gamma + \tau_h^\gamma||_{\omega^\gamma} \leq C^1_{st} ||\nabla r^\gamma||_{\omega^\gamma}.$$

- *Case 2: if $a \in \tilde{\Omega}\backslash\gamma = \mathcal{V}_h^*$ and we deal with the patch ω^a: let $\tau_h^a = \psi^a \nabla \tilde{u}_h$ and $g^a = \psi^a f - \nabla\psi^a \cdot \nabla \tilde{u}_h$. Let $\mathcal{T}^a = \cup_{K\cap\{a\}\neq\emptyset} K$. Suppose that $\tau_h^a|_K \in \Sigma_h(K)$ and $g^a|_K \in Q_h(K)$ for all $K \in \mathcal{T}^a$ where, $\Sigma_h = RT_k = RT_k(\tilde{\mathcal{T}}_h) \cap H(\mathrm{div}, \tilde{\Omega})$ and $Q_h = \mathbb{P}_k(\tilde{\mathcal{T}}_h)$. Let $r^a \in H^1_*(\omega^a)$ solves equation (2.10) and let σ_h^a be the solution of system (2.6), then there exists a positive real number $C^2_{st} > 0$ that depends only on the shape regularity such that:*

$$||\sigma_h^a + \tau_h^a||_{\omega^a} \leq C^2_{st} ||\nabla r^a||_{\omega^a}.$$

Proof. • Case 1: for $a \in \gamma$, we have $\mathcal{T}^\gamma = \cup_{K\cap\gamma\neq\emptyset} K$. Let $\mathcal{E}_h^\gamma$ be the set of all edges in $\mathcal{T}^\gamma$ and let us define the jump by $[[v]] = (v_{|K})_{|e} - (v_{|K'})_{|e}$ if $e \in \mathcal{E}_h^{int,\gamma}$ and $[[v]] = v_{|e}$ if $e \in \mathcal{E}_h^{ext,\gamma}$ where, $\mathcal{E}_h^{int,\gamma}$ and $\mathcal{E}_h^{ext,\gamma}$ be the interior and exterior edges respectively in the patch ω^γ.

$$\begin{aligned}
||\nabla r^\gamma||_{\omega^\gamma} &= \sup_{\substack{v\in H^1_*(\omega^\gamma),\\ ||\nabla v||_{\omega^\gamma}=1}} \{-(\psi^\gamma \nabla\tilde{u}_h, \nabla v)_{\omega^\gamma} + (\psi^\gamma f - \nabla\psi^\gamma\cdot\nabla\tilde{u}_h, v)_{\omega^\gamma}\} \\
&= \sup_{\substack{v\in H^1_*(\omega^\gamma),\\ ||\nabla v||_{\omega^\gamma}=1}} \{-(\tau_h^\gamma, \nabla v)_{\omega^\gamma} + (g^\gamma, v)_{\omega^\gamma}\} \\
&= \sup_{\substack{v\in H^1_*(\omega^\gamma),\\ ||\nabla v||_{\omega^\gamma}=1}} \{\sum_{K\in\mathcal{T}^\gamma} -(\tau_h^\gamma, \nabla v)_K + (g^\gamma, v)_K\} \\
&= \sup_{\substack{v\in H^1_*(\omega^\gamma),\\ ||\nabla v||_{\omega^\gamma}=1}} \{\sum_{e\in\mathcal{E}_h^\gamma} \langle[[-\tau_h^\gamma\cdot n_e]], v\rangle_e + \sum_{K\in\mathcal{T}^\gamma} (\nabla\cdot\tau_h^\gamma + g^\gamma, v)_K\}.
\end{aligned}$$

We have

$$||\sigma_h^\gamma + \tau_h^\gamma||_{\omega^\gamma} = \inf_{\substack{v_h \in \Sigma_h^\gamma, \\ \nabla \cdot v_h = g^\gamma}} ||v_h + \tau_h^\gamma||_{\omega^\gamma}$$

Let $\delta_h^\gamma = \sigma_h^\gamma + \tau_h^\gamma$ then,

$$||\sigma_h^\gamma + \tau_h^\gamma||_{\omega^\gamma} = ||\delta_h^\gamma||_{\omega^\gamma} = \inf_{\substack{v_h \in \Sigma_h^\gamma(\mathcal{T}^\gamma), \\ \nabla \cdot v_{h|_K} = (\nabla \cdot \tau_h^\gamma + g^\gamma)_{|_K}, \forall K \in \mathcal{T}^\gamma}} ||v_h||_{\omega^\gamma}$$

Where, $\Sigma_h^\gamma(\mathcal{T}^\gamma)$ is a broken version of Σ_h^γ. Now, by supposing that in [14, Theorem 7] is applicable to our patch ω^γ (i.e. if we suppose that Theorem 2.7 below can be proved), then there exists some positive constant $C_{st}^1 > 0$ only depending on shape regularity parameter such that:

$$||\sigma_h^\gamma + \tau_h^\gamma||_{\omega^\gamma} \leq C_{st}^1 ||\nabla r^\gamma||_{\omega^\gamma}.$$

- Case 2: for $a \in \tilde{\Omega} \backslash \gamma = \mathcal{V}_h^*$, we have $\mathcal{T}^a = \cup_{K \cap \{a\} \neq \emptyset} K$. Let $\mathcal{E}_h$ be the set of all edges in $\tilde{\mathcal{T}_h}$, let $\mathcal{E}_h^a$ be the set of all edges in patch ω^a and let us define the jump by $[[v]] = (v_{|_K})|_e - (v_{|_{K'}})|_e$ if $e \in \mathcal{E}_h^{int}$ and $[[v]] = v_{|_e}$ if $e \in \mathcal{E}_h^{ext}$. So

$$\begin{aligned}
||\nabla r^a||_{\omega^a} &= \sup_{\substack{v \in H_*^1(\omega^a), \\ ||\nabla v||_{\omega^a} = 1}} \{-(\psi^a \nabla \tilde{u}_h, \nabla v)_{\omega^a} + (\psi^a f - \nabla \psi^a \cdot \nabla \tilde{u}_h, v)_{\omega^a}\} \\
&= \sup_{\substack{v \in H_*^1(\omega^a), \\ ||\nabla v||_{\omega^a} = 1}} \{-(\tau_h^a, \nabla v)_{\omega^a} + (g^a, v)_{\omega^a}\} \\
&= \sup_{\substack{v \in H_*^1(\omega^a), \\ ||\nabla v||_{\omega^a} = 1}} \{\sum_{K \in \mathcal{T}^a} -(\tau_h^a, \nabla v)_K + (g^a, v)_K\} \\
&= \sup_{\substack{v \in H_*^1(\omega^a), \\ ||\nabla v||_{\omega^a} = 1}} \{\sum_{e \in \mathcal{E}_h^a} \langle [[-\tau_h^a \cdot n_e]], v \rangle_e + \sum_{K \in \mathcal{T}^a} (\nabla \cdot \tau_h^a + g^a, v)_K\}.
\end{aligned}$$

We have

$$||\sigma_h^a + \tau_h^a||_{\omega^a} = \inf_{\substack{v_h \in \Sigma_h^a, \\ \nabla \cdot v_h = g^a}} ||v_h + \tau_h^a||_{\omega^a}.$$

Let $\delta_h^a = \sigma_h^a + \tau_h^a$ then,

$$||\sigma_h^a + \tau_h^a||_{\omega^a} = ||\delta_h^a||_{\omega^a} = \inf_{\substack{v_h \in \Sigma_h^a(\mathcal{T}^a), \\ \nabla \cdot v_h|_K = (\nabla \cdot \tau_h^a + g^a)|_K, \forall K \in \mathcal{T}^a}} ||v_h||_{\omega^a}.$$

Where, $\Sigma_h^a(\mathcal{T}^a)$ is a broken version of Σ_h^a. Now, [14, Theorem 7] is applicable to our patch ω_a, so there exists some positive constant $C_{st}^2 > 0$ only depending on shape regularity parameter such that:

$$||\sigma_h^a + \tau_h^a||_{\omega^a} \leq C_{st}^2 ||\nabla r^a||_{\omega^a}.$$

■

Theorem 2.10. *(Local Efficiency) Let u be the exact solution on the whole domain Ω defined by (1.4). Let u_h^s be the approximate solution on Ω defined by (1.8)–(1.12)–(1.13). Let $\tilde{\sigma}_h$ defined as in (2.3). Let $(\psi^\gamma \nabla \tilde{u}_h)_{|_K} \in \Sigma_h(K)$ and $(\nabla\psi^\gamma \cdot \nabla \tilde{u}_h)_{|_K} \in Q_h(K)\ \forall K \in \mathcal{T}^\gamma$. Let $(\psi^a \nabla \tilde{u}_h)_{|_K} \in \Sigma_h(K)$ and $(\nabla\psi^a \cdot \nabla \tilde{u}_h)_{|_K} \in Q_h(K)\ \forall K \in \mathcal{T}^a$ where, $\Sigma_h = RT_k = RT_k(\tilde{\mathcal{T}_h}) \cap H(\mathrm{div}, \tilde{\Omega})$ and $Q_h = \mathbb{P}_k(\tilde{\mathcal{T}_h})$.*
Then, if $K \subset \omega^\gamma$

$$||\nabla \tilde{u}_h + \tilde{\sigma}_h||_K \leq C_{st}^2 C_{cont,PF} \sum_{a \in \mathcal{V}_k} ||\nabla(u - u_h^s)||_{\omega^a} + C_{st}^1 C_\gamma \left(\frac{R}{h}\right) ||\nabla(u - u_h^s)||_{\omega^\gamma \cup \omega'}, \quad (2.13)$$

and if $K \subset \tilde{\Omega} \backslash \omega^\gamma$ then,

$$||\nabla \tilde{u}_h + \tilde{\sigma}_h||_K \leq C_{st}^2 C_{cont,PF} \sum_{a \in \mathcal{V}_k} ||\nabla(u - \tilde{u}_h)||_{\omega^a}.$$

Proof. We have $\tilde{\sigma_h}_{|_K} = {\sigma_h^\gamma}_{|_K} + \sum_{a \in \mathcal{V}_K} {\sigma_h^a}_{|_K}$ where, $\mathcal{V}_K$ represents the vertices of the triangle K. Then,

$$\begin{aligned} ||\nabla \tilde{u}_h + \tilde{\sigma}_h||_K &= || \sum_{a \in \mathcal{V}_k} (\psi^a \nabla \tilde{u}_h + \sigma_h^a)|_K + (\psi^\gamma \nabla \tilde{u}_h + \sigma_h^\gamma)|_K||_K \\ &\leq \sum_{a \in \mathcal{V}_K} ||\psi^a \nabla \tilde{u}_h + {\sigma_h}^a||_{\omega^a} + ||\psi_\gamma \nabla \tilde{u}_h + \sigma_h^\gamma||_{\omega^\gamma} \end{aligned}$$

Thanks to Corollary 2.9 and Lemma 2.6, we have:

$$||\psi^a \nabla \tilde{u}_h + {\sigma_h}^a||_{\omega^a} \leq C_{st}^2 ||\nabla r^a||_{\omega^a} \leq C_{st}^2 C_{cont,PF} ||\nabla(u - \tilde{u}_h)||_{\omega^a}$$

and

$$||\psi^\gamma \nabla \tilde{u}_h + {\sigma_h}^\gamma||_{\omega^\gamma} \leq C_{st}^1 ||\nabla r^\gamma||_{\omega^\gamma} \leq C_{st}^1 C_\gamma \left(\frac{R}{h}\right) ||\nabla(u - u_h^s)||_{\omega^\gamma \cup \omega'}$$

Finally,

$$||\nabla \tilde{u}_h + \tilde{\sigma}_h||_K \leq C_{st}^2 C_{cont,PF} \sum_{a \in \mathcal{V}_k} ||\nabla(u - \tilde{u}_h)||_{\omega^a} + C_{st}^1 C_\gamma \left(\frac{R}{h}\right) ||\nabla(u - u_h^s)||_{\omega^\gamma \cup \omega'}$$

■

Conclusion. From Theorem 2.10, we conclude that we can not prove the efficiency since the constant $C_\gamma\left(\frac{R}{h}\right)$ in (2.13) depends on the mesh size. In order to be able to prove the efficiency we will build a new flux reconstruction in the Section 2.2 .

2.1.4. Numerical results using the flux reconstruction (2.2)

We will take in this section $RT_k = RT_2$ and $\mathbb{P}_k = \mathbb{P}_2$. We have obtained in Theorem 2.5 that $||\nabla(u - u_h^s)||_\Omega^2 \leq \sum_{K \in \tilde{\mathcal{T}_h}} \eta_{F,K}^2$ and we want to plot the error:

$$Error := ||\nabla(u - u_h^s)||_\Omega = \sqrt{||\nabla(u - u_1')||_{\Omega_1'}^2 + ||\nabla(u - \tilde{u}_h)||_{\tilde{\Omega}}^2}$$

and the estimator:

$$Estimator := \sqrt{\sum_{K \in \tilde{\mathcal{T}}_h} \eta^2_{F,K}}$$

with respect to different positions of interface γ which has the position $x = x_\gamma$ in a way that x_γ goes form the position very near to the inlet i.e. $x_\gamma = x^i_\gamma = 0.1$ to the position very near to the corner of the channel i.e. $x_\gamma = x^f_\gamma = L_1 - 0.02 = 5.08$ where, x^i_γ and x^f_γ are located in Figure 2.4 below.

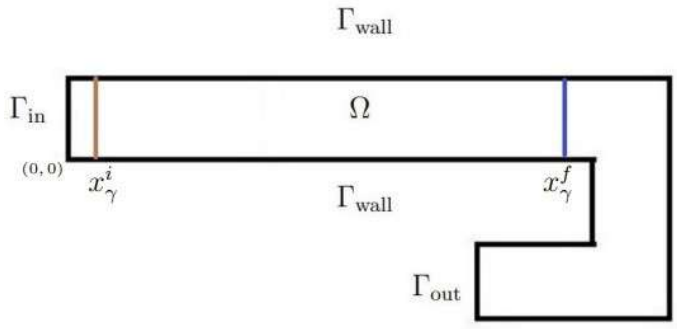

Figure 2.4.: Direction of the interface γ from position $x = x^i_\gamma$ to $x = x^f_\gamma$

For fixed mesh size $h = 0.07$, we plot the error and the estimator in the Theorem 2.5 for different positions of the interfaces and we obtain the graph in Figure 2.5.

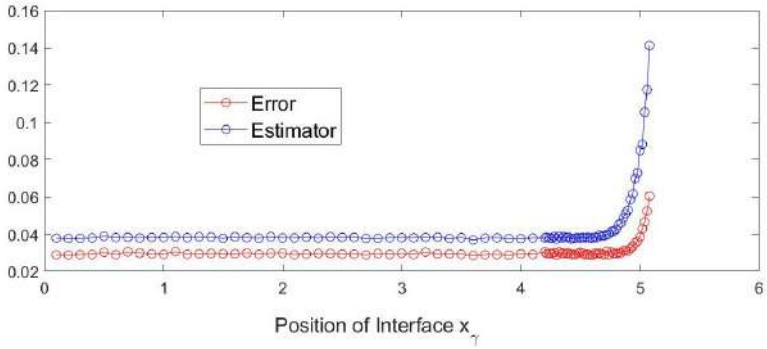

Figure 2.5.: Error on Ω and Estimator on $\tilde{\Omega}$ in Theorem 2.5 for mesh size $h = 0.07$

Now, let us decrease the mesh size to $h = 0.02$ and plot the error and the estimator in the Theorem 2.5 for different positions of the interface and the graph is obtained in Figure 2.6.

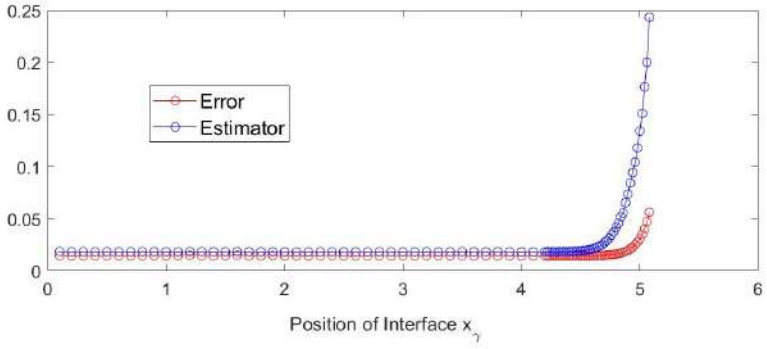

Figure 2.6.: Error on Ω and Estimator on $\tilde{\Omega}$ for Theorem 2.5 for mesh size $h = 0.02$

In Figure 2.5 and Figure 2.6, we see that the error and the estimator become much bigger as the interface becomes near to the corner and this is due to the dominance of the 2D affects in the corner. We must specify some tolerance in order to detect the suitable position of the interface. For this reason for a fixed mesh size, we want to see the variation between the reconstructed approximated flux σ_h^γ and the approximated flux $-\nabla\tilde{u}_h$ on the domain ω^γ i.e. $||\sigma_h^\gamma + (\nabla\tilde{u}_h)\psi_h^\gamma||_{\omega^\gamma}$with respect to different positions of the interface where ω^γ is showed in the Figure 2.3.
Let us take the mesh size $h \approx 0.08$ and plot $||\sigma_h^\gamma + (\nabla\tilde{u}_h)\psi_h^\gamma||_{\omega^\gamma}$with respect to different positions of the interface in the Figure 2.7 below with base-10 logarithmic scale on the y-axis. Now, let us fix the position of the interface at $x_\gamma = 4$. We plot in Figure 2.8 the estimator on ω^γ with respect to different mesh sizes. We find that $||\sigma_h^\gamma + (\nabla\tilde{u}_h)\psi_h^\gamma||_{\omega^\gamma}$ takes the values between 1.2×10^{-4} and 4.5×10^{-4} for different mesh sizes which is approximately of the same tolerance 10^{-4} (but not constant). Finally, $||\sigma_h^\gamma + (\nabla\tilde{u}_h)\psi_h^\gamma||_{\omega^\gamma}$ can be taken as an estimator for the position of the interface but it can be improved to be constant for different mesh sizes when we fix the position of the interface x_γ. This improvement is done if we introduce a new definition of reconstructing the flux which will be studied in the following section.

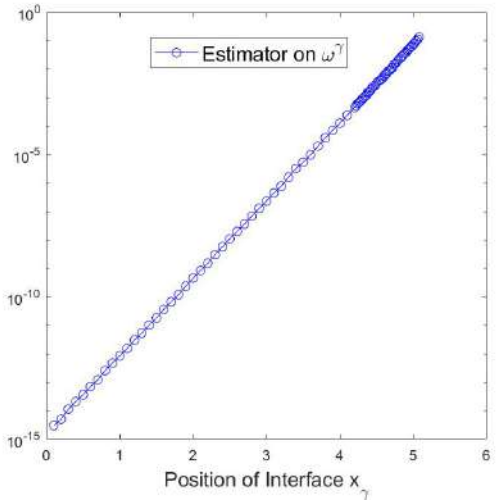

Figure 2.7.: $||\sigma_h^\gamma + (\nabla \tilde{u}_h)\psi_h^\gamma||_{\omega^\gamma}$ w.r.t. different positions of x_γ for mesh size $h \approx 0.08$

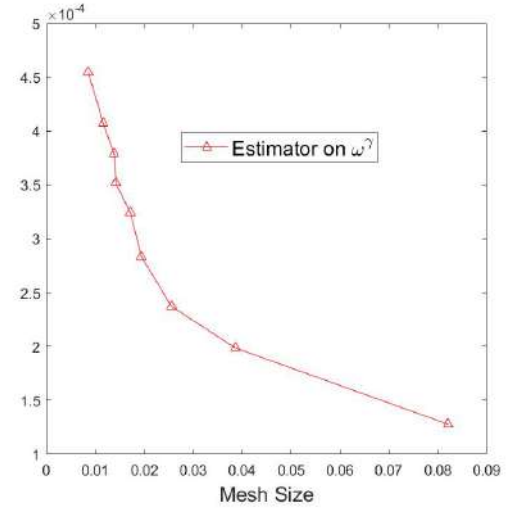

Figure 2.8.: $||\sigma_h^\gamma + (\nabla \tilde{u}_h)\psi_h^\gamma||_{\omega^\gamma}$ w.r.t. different mesh sizes for a fixed interface at $x_\gamma = 4$

The drawbacks of this definition of the flux are the following

- We can not prove the efficiency (lower bound).
- For fixed position of the interface, we find that $||\sigma_h^\gamma + (\nabla \tilde{u}_h)\psi_h^\gamma||_{\omega^\gamma}$ vary **a little bit** for different mesh sizes.

These drawbacks will be solved in the following section by introducing the new definition of the flux reconstruction.

2.2. A posteriori estimator with guaranteed upper and lower (efficiency) bounds

In this section we will make a new partition of unity of Ω and we will introduce *a posteriori* error indicator with guaranteed reliability and provable efficiency. We will make a new definition of the flux reconstruction in a way that we can prove the reliability and the efficiency of *a posteriori* error estimator. We have to introduce two lemmas in order to be able to prove the global efficiency. We note that this approach is more expensive but more accurate.

2.2.1. A posteriori error indicator

We now introduce the a posteriori error indicator with guaranteed reliability and provable efficiency. Let the position of the interface $x_\gamma \in [0.1, L_1 - R]$. To this end, consider the continuous function on Ω, named ψ^γ, defined on rectangular portion $[0, x_\gamma + R] \times [0, R]$ of the channel by

$$\psi^\gamma(x) = \begin{cases} 1, & \text{for} \quad x < x_\gamma \\ \frac{x_\gamma + R - x}{R}, & \text{for} \quad x \in [x_\gamma, x_\gamma + R] \\ 0, & \text{for} \quad x > x_\gamma + R \end{cases} \tag{2.14}$$

and extended by 0 everywhere else. Here, x_γ is the x-coordinate of the interface γ and we assume that $x_\gamma + R$ is still in the rectangular portion of the channel. We also introduce a piecewise affine (on mesh $\tilde{\mathcal{T}}_h$) version of ψ^γ:

$$\psi_h^\gamma(x) = \sum_{a:\text{all the nodes of } \tilde{\mathcal{T}}_h} \psi^\gamma(a)\psi^a(x) \quad \text{for x} \in \tilde{\Omega} \tag{2.15}$$

and $\psi_h^\gamma = 1$ on Ω', where ψ^a is a hat function i.e. a polynomial of degree 1 that takes the value 1 at the node a and 0 on the other nodes different from a. Note the partition of unity on Ω

$$1 = \psi_h^\gamma + \sum_{a \in \mathcal{V}_h^*} (1 - \psi^\gamma(a))\psi^a. \tag{2.16}$$

Recalling that $\mathcal{V}_h^*$ represents all vertices that belongs to $\tilde{\Omega} \backslash \gamma$ i.e $\mathcal{V}_h^* = \mathcal{V}_h \backslash \mathcal{V}_h^\gamma$ where $\mathcal{V}_h^\gamma$ represents the vertices located at γ, we define then the flux on whole $\Omega = \tilde{\Omega} \cup \Omega' \cup \gamma$ as

$$\sigma_h = \sigma_h^\gamma + \sum_{a \in \mathcal{V}_h^*} (1 - \psi^\gamma(a))\sigma_h^a + (-\nabla u')\mathbb{1}_{\Omega'}. \tag{2.17}$$

We will divide the flux into two fluxes. The first flux is defined on Ω' by

$$\sigma' = -\nabla u' \tag{2.18}$$

and the second flux is defined on $\tilde{\Omega}$ by

$$\tilde{\sigma}_h = \sigma_h^\gamma + \sum_{a \in \mathcal{V}_h^*} (1 - \psi^\gamma(a))\sigma_h^a, \tag{2.19}$$

where σ_h^a is defined on all patches $\omega^a = \text{supp}(\psi_h^a) \cap \tilde{\Omega}$ for all nodes $a \in \mathcal{V}_h^*$ as follows: $\sigma_h^a \in \Sigma_h^a$ and $p_h^a \in Q_h^a$ such that for all $\tau_h \in \Sigma_h^a$ and $q_h \in Q_h^a$

$$\int_{\omega^a} \sigma_h^a \cdot \tau_h - \int_{\omega^a} p_h^a \text{div} \tau_h = -\int_{\omega^a} (\nabla \tilde{u}_h)\psi^a \cdot \tau_h, \tag{2.20}$$

$$\int_{\omega^a} q_h \mathrm{div}\sigma_h^a = \int_{\omega^a} (f\psi^a - \nabla\tilde{u}_h \cdot \nabla\psi^a) q_h. \tag{2.21}$$

Similarly, σ_h^γ is defined on the patch $\omega^\gamma = \mathrm{supp}(\psi_h^\gamma) \cap \tilde{\Omega}$ as follows: $\sigma_h^\gamma \in \Sigma_h^\gamma$ and $p_h^\gamma \in Q_h^\gamma$ such that for all $\tau_h \in \Sigma_h^\gamma$ and $q_h \in Q_h^\gamma$

$$\int_{\omega^\gamma} \sigma_h^\gamma \cdot \tau_h - \int_{\omega^\gamma} p_h^\gamma \mathrm{div}\tau_h = -\int_{\omega^\gamma} (\nabla\tilde{u}_h)\psi_h^\gamma \cdot \tau_h, \tag{2.22}$$

$$\int_{\omega^\gamma} q_h \mathrm{div}\sigma_h^\gamma = \int_{\omega^\gamma} (f\psi_h^\gamma - \nabla\tilde{u}_h \cdot \nabla\psi_h^\gamma) q_h. \tag{2.23}$$

Where,

Case 1: a in an internal node of $\tilde{\Omega}$

$\Sigma_h^a := \{\sigma_h \in RT_k(\omega^a), \sigma_h \cdot n = 0 \quad \text{on} \quad \partial\omega^a\}$
$Q_h^a := \{q_h \in L^2(\omega^a), q_{h|_K} \in \mathbb{P}_k(K), \forall K \in \omega^a, \int_{\omega^a} q_h = 0\}$

Case 2: a on the wall of $\tilde{\Omega}\backslash\gamma$

$\Sigma_h^a := \{\sigma_h \in RT_k(\omega^a), \sigma_h \cdot n = 0 \quad \text{on} \quad \partial\omega^a\backslash\partial\tilde{\Omega}\}$
$Q_h^a := \{q_h \in L^2(\omega^a), q_{h|_K} \in \mathbb{P}_k(K), \forall K \in \omega^a\}$

Case 3: on the wall γ

$\Sigma_h^\gamma := \{\sigma_h \in RT_k(\omega^\gamma), \sigma_h \cdot n = 0 \quad \text{on} \quad \tilde{\gamma} \quad \text{and} \quad \sigma_h \cdot n = (-\nabla u') \cdot n = 0 \quad \text{on} \quad \gamma\}$
$Q_h^\gamma := \{q_h \in L^2(\omega^\gamma), q_h|_K \in \mathbb{P}_k(K), \forall K \in \omega^\gamma\}$
with $\tilde{\gamma} := \partial\omega^\gamma\backslash\partial\tilde{\Omega} = \partial\omega^\gamma \cap \tilde{\Omega}$.

Proposition 2.11. *We have $\tilde{\sigma}_h := \sigma_h^\gamma + \sum_{a\in\mathcal{V}_h^*}(1-\psi^\gamma(a))\sigma_h^a$ on $\tilde{\Omega}$, then $\nabla\cdot\tilde{\sigma}_h = \Pi_{Q_h}(f) = f$ on $\tilde{\Omega}$ and consequently $\nabla\cdot\sigma_h = f$ on Ω, where $Q_h = \mathbb{P}_k(\tilde{\mathcal{T}}_h)$.*

Proof. $\tilde{\sigma}_h \in H(\mathrm{div}, \tilde{\Omega})$ as all the individual components σ_h^γ and σ_h^a belong to $H(\mathrm{div}, \tilde{\Omega})$ for all vertices $a \in \tilde{\Omega}\backslash\gamma$, since by extension we can go from $H(\mathrm{div}, \omega^\gamma)$ and $H(\mathrm{div}, \omega^a)$ to $H(\mathrm{div}, \tilde{\Omega})$, and $\tilde{\sigma}_h$ is the sum of all these components. We will deal with the following three cases.

Case 1: a is internal node of $\tilde{\Omega}$.

We have $(\nabla\cdot\sigma_h^a, q_h)_{\omega^a} = (f\psi^a - \nabla\psi^a\cdot\nabla\tilde{u}_h, q_h)_{\omega^a}$ for all $q_h \in Q_h^a$, then we have $\int_{\omega^a} q_h = 0$ and we have $(\nabla\cdot\sigma_h^a, 1)_{\omega^a} = 0$ as $\sigma_h^a \cdot n = 0$ on $\partial\omega^a$ and using the divergence theorem. But from weak formulation (1.12), $(\nabla\tilde{u}_h, \nabla\tilde{v}_h)_{\tilde{\Omega}} = (f, \tilde{v}_h)_{\tilde{\Omega}}$ for all $\tilde{v}_h \in V_h, \tilde{v}_h = 0$ on $\partial\tilde{\Omega}$ so, let us take $\tilde{v}_h = \psi^a$ as a test function, then $(\nabla\tilde{u}_h \cdot \nabla\psi^a, 1)_{\tilde{\Omega}} = (f\psi^a, 1)_{\tilde{\Omega}}$. So, for all internal nodes a, we have $(\nabla\cdot\sigma_h^a, q_h)_{\omega^a} = (\psi^a f - \nabla\tilde{u}_h\cdot\nabla\psi^a, q_h)_{\omega^a}$ for all $q_h \in Q_h^a$ and not only for the vector-valued function with zero mean value. So we can redefine $Q_h^a := \{q_h \in L^2(\omega^a); q_h \in \mathbb{P}_k(K) \quad \forall K \in \omega^a\}$

Case 2: a is on wall of $\tilde{\Omega}\backslash\Gamma$:

We have $(\nabla\cdot\sigma_h^a, q_h)_{\omega^a} = (\psi^a f - \nabla\psi^a\cdot\nabla\tilde{u}_h, q_h)_{\omega^a}$ for all $q_h \in Q_h^a = Q_h(\omega^a)$.

Case 3: on wall γ:

We have $(\nabla\cdot\sigma_h^\gamma, q_h)_{\omega^\gamma} = (\psi_h^\gamma f - \nabla\psi_h^\gamma\cdot\nabla\tilde{u}_h, q_h)_{\omega^\gamma}$ for all $q_h \in Q_h^\gamma = Q_h(\omega^\gamma)$.

Let now $\tilde{q}_h \in Q_h = \mathbb{P}_k(\tilde{\mathcal{T}}_h)$ then,

$$\begin{aligned}
\big(\nabla\cdot\tilde{\sigma}_h,\tilde{q}_h\big)_{\tilde{\Omega}} &= \big(\nabla\cdot\sigma_h^\gamma,\tilde{q}_h\big)_{\tilde{\Omega}} + \sum_{a\in\mathcal{V}_h^*}(1-\psi^\gamma(a))\big(\nabla\cdot\sigma_h^a,\tilde{q}_h\big)_{\tilde{\Omega}}\\
&= \big(f\psi_h^\gamma - \nabla\psi_h^\gamma\cdot\nabla\tilde{u}_h,\tilde{q}_h\big)_{\tilde{\Omega}} + \sum_{a\in\mathcal{V}_h^*}(1-\psi^\gamma(a))\big(\psi^a f - \nabla\psi^a\cdot\nabla\tilde{u}_h,\tilde{q}_h\big)_{\tilde{\Omega}}\\
&= \Big(f\big(\psi_h^\gamma + \sum_{a\in\mathcal{V}_h^*}(1-\psi^\gamma(a))\psi^a\big) - \nabla\tilde{u}_h\cdot\nabla(\psi_h^\gamma + \sum_{a\in\mathcal{V}_h^*}(1-\psi^\gamma(a))\psi^a),\tilde{q}_h\Big)_{\tilde{\Omega}}\\
&= \big(f\mathbb{1}_{\tilde{\Omega}} - \nabla\tilde{u}_h\cdot\nabla(\mathbb{1}_{\tilde{\Omega}}),\tilde{q}_h\big)_{\tilde{\Omega}}\\
&= (f,\tilde{q}_h)_{\tilde{\Omega}}.
\end{aligned}$$

Since $\nabla\cdot(RT_k(K)) = Q_h(K) = \mathbb{P}_k(K)$ for all $K\in\tilde{\mathcal{T}}_h$, we get $\nabla\cdot\tilde{\sigma}_h = \Pi_{Q_h}(f) = f$ where, Π_{Q_h} is the $L^2(\tilde{\Omega})$-orthogonal projection onto Q_h and finally, we get

$$\nabla\cdot\tilde{\sigma}_h = f \qquad \text{on} \quad \tilde{\Omega}.$$

■

2.2.2. Main theorem and the proof

Theorem 2.12. *Let u be the weak solution defined by system (1.4). Let u_h^s and σ_h defined as in (1.12)–(1.13) and (2.17) respectively, then we have the upper bound with constant 1*

$$\|\nabla u - \nabla u_h^s\|_\Omega \leqslant \|\sigma_h + \nabla u_h^s\|_\Omega \tag{2.24}$$

and the lower bound

$$\|\sigma_h + \nabla u_h^s\|_\Omega \leqslant C\|\nabla u - \nabla u_h^s\|_\Omega \tag{2.25}$$

with a constant C depending only on the mesh regularity.

Proof. The proof of (2.24) is completely standard. We verify indeed that $\sigma_h \in H(\mathrm{div},\Omega)$, $\mathrm{div}\sigma_h = f$ on Ω, set $e = u - u_h^s$, observe $e\in H_0^1(\Omega)$ and do the usual calculation

$$\|\nabla u - \nabla u_h^s\|_\Omega^2 = (\nabla u - \nabla u_h^s,\nabla e)_\Omega = (f,e)_\Omega - (\nabla u_h^s,\nabla e)_\Omega = (\mathrm{div}\sigma_h,e)_\Omega - (\nabla u_h^s,\nabla e)_\Omega$$

$$= (-\sigma_h - \nabla u_h^s,\nabla e)_\Omega \leqslant \|\sigma_h + \nabla u_h\|_\Omega\|\nabla e\|_\Omega$$

hence (2.24). The proof of (2.25) is organized in several steps.

Step 1: error caused by the interface, prior to discretization. Let us begin with a "continuous " version of our "simplified " problem: we search for $\tilde{u}$ on $\tilde{\Omega}$ such that

$$-\Delta\tilde{u} = f \text{ in } \tilde{\Omega}\,, \tag{2.26a}$$

$$\tilde{u} = \begin{cases} u' & \text{on } \gamma\,,\\ 0 & \text{on } \Gamma_{wall}\,,\\ u_{out} & \text{on } \Gamma_{out}\,, \end{cases} \tag{2.26b}$$

and set

$$u^s = \begin{cases} u' \text{ on } \Omega', \\ \tilde{u} \text{ on } \tilde{\Omega}. \end{cases}$$

We want to study $\|\nabla u - \nabla u^s\|_\Omega$ which is the error introduced by the interface itself, without discretizing the problem on $\tilde{\Omega}$. More precisely, we want to relate it to the continuous version of $\|\sigma_h^\gamma + (\nabla \tilde{u}_h)\psi_h^\gamma\|_{\omega^\gamma}$. We thus introduce the continuous version of σ_h^γ: find $\sigma^\gamma \in H_\gamma(\mathrm{div}, \omega^\gamma), p^\gamma \in L^2(\omega^\gamma)$ with $H_\gamma(\mathrm{div}, \omega^\gamma) := \{\tau \in H(\mathrm{div}, \omega^\gamma) : \tau \cdot n = 0 \text{ on } \gamma\}$ such that

$$\int_{\omega^\gamma} \sigma^\gamma \cdot \tau^\gamma - \int_{\omega^\gamma} p^\gamma \mathrm{div}\tau^\gamma = -\int_{\omega^\gamma} (\nabla \tilde{u}) \cdot \tau^\gamma \qquad \forall \tau^\gamma \in H_\gamma(\mathrm{div}, \omega^\gamma) \tag{2.27a}$$

$$\int_{\omega^\gamma} q^\gamma \mathrm{div}\sigma^\gamma = \int_{\omega^\gamma} f q^\gamma \qquad \forall q^\gamma \in L^2(\omega^\gamma) \tag{2.27b}$$

Let us prove

$$\|\sigma^\gamma + \nabla \tilde{u}\|_{\omega^\gamma} \leq C \|\nabla u - \nabla u^s\|_\Omega . \tag{2.28}$$

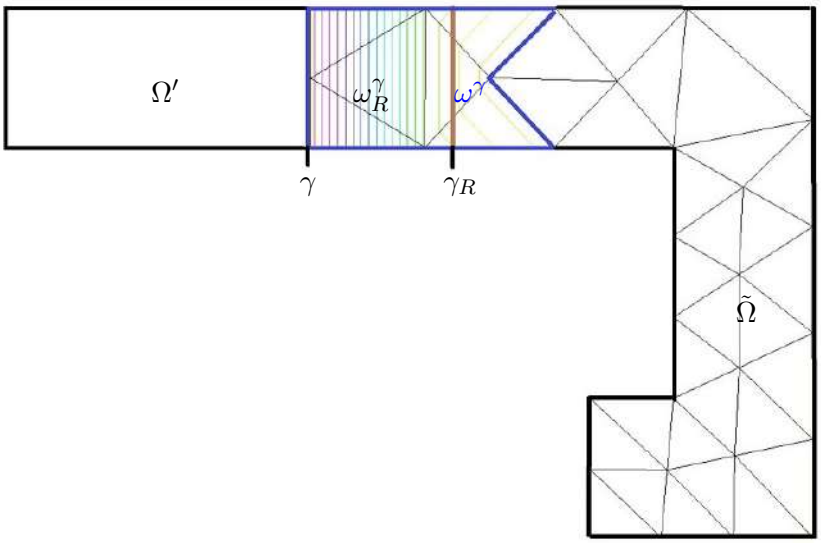

Figure 2.9.: Description of ω^γ and ω_R^γ

Let $\omega_R^\gamma = \mathrm{supp}(\psi^\gamma) \cap \tilde{\Omega}$ with $\gamma_R = \partial\omega_R^\gamma \cap \{x = x_\gamma + R\}$(In Figure 2.9, ω_R^γ is the square region where its boundary is composed of the interface γ, γ_R and the wall of $\tilde{\Omega}$). In Lemma 2.13 below we show that there exists $\theta \in H^1(\omega_R^\gamma)$ such that

$$\Delta\theta = 0 \text{ in } \omega_R^\gamma$$

$$\nabla\theta \cdot n = -\nabla\tilde{u} \cdot n \text{ on } \gamma$$

$$\nabla\theta \cdot n = 0 \text{ on } \gamma_R$$

$$\theta = 0 \quad \text{on } \tilde{\Gamma} \cap \partial\omega_R^\gamma$$

We have then

$$\|\nabla\theta\|_{\omega_R^\gamma} \leqslant C_1 \|\nabla\tilde{u} \cdot n\|_{-1/2,\gamma}$$

with $C_1 > 0$ which does not depend on R, as proved in Lemma 2.13. The norm $\|\cdot\|_{-1/2,\gamma}$ is defined in the same Lemma. Recalling that $f = -\mathrm{div}(\nabla\tilde{u})$, we see that (2.27b) implies $\mathrm{div}(\sigma^\gamma + \nabla\tilde{u}) = 0$ a.e. on ω^γ. Let $\tau^c \in H(\mathrm{div}, \omega^\gamma)$ defined by $\tau^c = \nabla\theta$ on ω_R^γ and $\tau^c = 0$ on $\omega^\gamma \setminus \omega_R^\gamma$ (note that $\omega_R^\gamma \subset \omega^\gamma$, where the patch ω^γ is described in Figure 2.9 as a patch with the blue boundary) so that $\mathrm{div}\tau^c = 0$ on ω^γ. Now set $\tau^\gamma = \sigma^\gamma + \nabla\tilde{u} + \tau^c$ and observe that $\mathrm{div}\tau^\gamma = 0$ a.e. on ω^γ and $\tau^\gamma \cdot n = 0$ on γ since $\sigma^\gamma \cdot n = 0$ and $\tau^c \cdot n = \nabla\tilde{u} \cdot n$ on γ. We can thus use this τ^γ as the test function in (2.27) and since $\int_{\omega^\gamma} p^\gamma \mathrm{div}\tau^\gamma = 0$, we get

$$\int_{\omega^\gamma} (\sigma^\gamma + \nabla\tilde{u}) \cdot (\sigma^\gamma + \nabla\tilde{u} + \tau^c) = 0.$$

Hence, by Cauchy-Schwartz,

$$\|\sigma^\gamma + \nabla\tilde{u}\|_{\omega^\gamma} \leqslant \|\tau^c\|_{\omega^\gamma} = \|\nabla\theta\|_{\omega_R^\gamma}.$$

Thus,

$$\|\sigma^\gamma + \nabla\tilde{u}\|_{\omega^\gamma} \leqslant C_1 \|\nabla\tilde{u} \cdot n\|_{-1/2,\gamma}. \tag{2.29}$$

Now, we return to bound the error $\|\nabla u - \nabla u^s\|_\Omega$ from below. Denoting by $[.]$ the jump on γ, we have the jump $[\nabla(u-u^s)\cdot n] = \nabla\tilde{u}\cdot n$ on γ as $\nabla u' \cdot n = 0$ on γ, then for all $v \in H_0^1(\Omega)$

$$\int_\Omega \nabla(u - u^s) \cdot \nabla v = \int_\gamma [\nabla(u - u^s) \cdot n] v = \int_\gamma \nabla\tilde{u} \cdot n v.$$

Since $\Omega = \tilde{\Omega} \cup \Omega' \cup \gamma$, $\Delta(u - u^s) = 0$ on Ω, $v = 0$ on $\partial\Omega$ and by integration by parts

$$\begin{aligned}
0 &= \int_\Omega \Delta(u - u^s) v \\
&= \int_{\tilde{\Omega}} \Delta(u - \tilde{u}) v + \int_{\Omega'} \Delta(u - u') v \\
&= \int_{\tilde{\Omega}} \nabla(u - \tilde{u}) \cdot \nabla v - \int_{\partial\tilde{\Omega}} \frac{\partial(u - \tilde{u})}{\partial n} v \, ds + \int_{\Omega'} \nabla(u - u') \cdot \nabla v - \int_{\partial\Omega'} \frac{\partial(u - u')}{\partial n} v \, ds \\
&= \int_{\tilde{\Omega}} \nabla(u - \tilde{u}) \cdot \nabla v - \int_{\partial\tilde{\Omega}} \nabla(u - \tilde{u}) \cdot n v \, ds + \int_{\Omega'} \nabla(u - u') \cdot \nabla v - \int_{\partial\Omega'} \nabla(u - u') \cdot n v \, ds \\
&= \int_\Omega \nabla(u - u^s) \cdot \nabla v - \int_\gamma [\nabla(u - u^s) \cdot n] v.
\end{aligned}$$

Now, from Lemma 2.14 below we know that $\forall \eta \in H^{1/2}(\gamma)$ $\exists v \in H^1(\Omega)$ vanishing on $\partial\Omega$ i.e. $v \in H_0^1(\Omega)$ such that $v_{|_\gamma} = \eta$ and such that

$$\|\nabla v\|_\Omega \leqslant C_2 \|\eta\|_{1/2,\gamma}$$

with C_2 independent of geometrical parameters. We can take $v = \theta$ in ω_R^γ, with θ the solution of Lemma 2.14 and extend it to all the domain e.g. defining v as the mirror image of θ to the left of γ in Ω'. We have thus $\forall \eta \in H^{1/2}(\gamma)$

$$\int_\gamma \nabla\tilde{u} \cdot n \eta = \int_\Omega \nabla(u - u^s) \cdot \nabla v \leqslant \|\nabla(u - u^s)\|_\Omega \|\nabla v\|_\Omega \leqslant C_2 \|\eta\|_{1/2,\gamma} \|\nabla(u - u^s)\|_\Omega$$

that implies

$$\|\nabla\tilde{u} \cdot n\|_{-1/2,\gamma} \leqslant C_2 \|\nabla u - \nabla u^s\|_\Omega.$$

Coming back to (2.29) and using this latter inequality, we get the desired estimate (2.28) with $C = C_1 C_2$.

Step 2: error caused by the interface, adding the discretization in $\tilde{\Omega}$. Here we prove that

$$\left\|\sigma_h^\gamma + (\nabla \tilde{u}_h)\psi_h^\gamma\right\|_{\omega^\gamma} \leq C(\|\nabla(\tilde{u} - \tilde{u}_h)\|_{\omega^\gamma} + \|\nabla(u - u^s)\|_\Omega \,. \tag{2.30}$$

This can be viewed as a discrete analogue of (2.28). The proof is based on Theorem 1.2 of [37], but the latter cannot be applied directly due to a mismatch in boundary conditions: σ_h^γ is required to vanish on both γ and $\tilde{\gamma}$, while ψ_h^γ vanishes only on $\tilde{\gamma}$. To circumvent this difficulty, we enlarge ω^γ to $\omega^{\gamma,m}$ by adding to ω^γ its mirror image with respect to γ. Similarly, we extend $\psi_h^\gamma, \tilde{u}_h, \sigma_h^\gamma$ from ω^γ to $\psi_h^{\gamma,m}, \tilde{u}_h^m, \sigma_h^{\gamma,m}$ on $\omega^{\gamma,m}$ as functions symmetric with respect to γ. Let $\tilde{\gamma}^m$ denote the mirror image of $\tilde{\gamma}$. Theorem 1.2 of [37] can be formulated on $\omega^{\gamma,m}$ as

$$\min_{\substack{\mathbf{v}_h \in H(\mathrm{div},\omega^{\gamma,m}) \cap \mathrm{RT}_k \\ \mathrm{div}\,\mathbf{v}_h = \psi_h^{\gamma,m} f - \nabla\psi_h^{\gamma,m}\cdot\nabla\tilde{u}_h^m \\ \mathbf{v}_h\cdot n = 0 \,\mathrm{on}\, \tilde{\gamma}\cup\tilde{\gamma}^m}} \left\|\mathbf{v}_h + \psi_h^{\gamma,m}\nabla\tilde{u}_h^m\right\|_{\omega^{\gamma,m}} \leqslant C(\omega^{\gamma,m},\psi_h^{\gamma,m}) \min_{\substack{\mathbf{v}\in H(\mathrm{div},\omega^{\gamma,m}) \\ \mathrm{div}\,\mathbf{v} = f}} \|\mathbf{v} + \nabla\tilde{u}_h^m\|_{\omega^{\gamma,m}} \tag{2.31}$$

where $C(\omega^{\gamma,m},\psi_h^{\gamma,m}) \leqslant C(\|\psi_h^{\gamma,m}\|_\infty + C_P\|\nabla\psi_h^{\gamma,m}\|_\infty)$ with C_P the Poincaré constant of the space $H^1(\omega^{\gamma,m})$ under the constraint of functions vanishing on $\tilde{\gamma}\cup\tilde{\gamma}^m$, i.e. $\|v\|_{\omega^{\gamma,m}} \leqslant C_P\|\nabla v\|_{\omega^{\gamma,m}}$ for all $v \in H^1(\omega^{\gamma,m})$ with $v = 0$ on $\tilde{\gamma}\cup\tilde{\gamma}^m$ (note that these constraints are imposed on the part of $\partial\omega^{\gamma,m}$ where $\psi_h^{\gamma,m}$ vanishes). By our geometrical assumptions, C_P is of order R and $\|\nabla\psi_h^\gamma\|_\infty \leqslant \frac{C}{R}$ so that $C(\omega^{\gamma,m},\psi_h^{\gamma,m}) \leqslant C$. Comparing with the definition of σ_h^γ we see that the minimum on the left-hand side of (2.31) is attained on $\sigma_h^{\gamma,m}$ (note in particular that $\sigma_h^{\gamma,m}\cdot n = 0$ on γ by symmetry). In order to identify the minimum on the other side, we introduce $\hat{\sigma}^\gamma \in H_\gamma(\mathrm{div},\omega^\gamma)$, $\hat{p}^\gamma \in L^2(\omega^\gamma)$ such that

$$\int_{\omega^\gamma} \hat{\sigma}^\gamma\cdot\tau^\gamma + \int_{\omega^\gamma}\hat{p}^\gamma\,\mathrm{div}\,\tau^\gamma = -\int_{\omega^\gamma}\nabla\tilde{u}_h\cdot\tau^\gamma \qquad \forall\tau^\gamma \in H_\gamma(\mathrm{div},\omega^\gamma)\,, \tag{2.32a}$$

$$\int_{\omega^\gamma} q^\gamma\,\mathrm{div}\,\hat{\sigma}^\gamma = \int_{\omega^\gamma} f q^\gamma \qquad \forall q^\gamma \in L^2(\omega^\gamma)\,. \tag{2.32b}$$

We see then that the minimum on the right-hand side of (2.31) is attained on $\hat{\sigma}^{\gamma,m}$, which is the mirror extension of $\hat{\sigma}^\gamma$ to $\omega^{\gamma,m}$. Going back in (2.31) to the subdomain ω^γ of $\omega^{\gamma,m}$ and using the symmetry gives

$$\left\|\sigma_h^\gamma + (\nabla\tilde{u}_h)\psi_h^\gamma\right\|_{\omega^\gamma} \leqslant C\,\|\hat{\sigma}^\gamma + \nabla\tilde{u}_h\|_{\omega^\gamma}\,.$$

This entails by the triangle inequality

$$\left\|\sigma_h^\gamma + (\nabla\tilde{u}_h)\psi_h^\gamma\right\|_{\omega^\gamma} \leqslant C(\|\hat{\sigma}^\gamma - \sigma^\gamma\|_{\omega^\gamma} + \|\sigma^\gamma + \nabla\tilde{u}\|_{\omega^\gamma} + \|-\nabla\tilde{u} + \nabla\tilde{u}_h\|_{\omega^\gamma}). \tag{2.33}$$

To bound the first term in the right hand side of (2.33), we take the difference between (2.27) and (2.32) setting $\tau^\gamma = \sigma^\gamma - \hat{\sigma}^\gamma$. Noting that $\mathrm{div}\,\tau^\gamma = 0$, this yields

$$\|\sigma^\gamma - \hat{\sigma}^\gamma\|_{\omega^\gamma} \leq C\,\|\nabla\tilde{u} - \nabla\tilde{u}_h\|_{\omega^\gamma}\,. \tag{2.34}$$

The second term in the right side of (2.33) is bounded by (2.28). Finally, (2.33) gives (2.30).

Step 3: discretization error inside $\tilde{\Omega}$. We have at all the nodes a of the mesh $\tilde{\mathcal{T}}_h$

$$\|\sigma_h^a + (\nabla\tilde{u}_h)\psi^a\|_{\omega^a} \leqslant C\|\nabla\tilde{u} - \nabla\tilde{u}_h\|_{\omega^a} \tag{2.35}$$

This well known estimate follows, for example, from Theorem 1.2 of [39] applied on each patch ω^a.

Step 4: putting everything together. From definition of σ_h, see (2.17), (2.18) and the partition of unity (2.16) we obtain on every mesh element $K \in \tilde{\mathcal{T}}_h$

$$\|\tilde{\sigma}_h + \nabla \tilde{u}_h\|_K \leq \left\|\sigma_h^\gamma + (\nabla \tilde{u}_h)\psi_h^\gamma\right\|_K + \sum_{a \in \mathcal{V}_h^*} (1 - \psi^\gamma(a)) \left\|\sigma_h^a + (\nabla \tilde{u}_h)\psi^a\right\|_K$$

where σ_h^γ and σ_h^a are extended by 0 outside of their domains of definitions ω^γ and ω^a respectively. The number of non-zero terms in the sum above is thus uniformly bounded by a constant that depends only on the regularity of the mesh. Taking the squares on both sides of the inequality above leads to

$$\|\tilde{\sigma}_h + \nabla \tilde{u}_h\|_K^2 \leq C \left(\left\|\sigma_h^\gamma + (\nabla \tilde{u}_h)\psi_h^\gamma\right\|_K^2 + \sum_{a \in \mathcal{V}_h^*} \left\|\sigma_h^a + (\nabla \tilde{u}_h)\psi^a\right\|_K^2 \right) .$$

Taking the sum over $K \in \tilde{\mathcal{T}}_h$, noting $\sigma' + \nabla u' = 0$ on Ω', and then using the bounds (2.30), (2.35) leads to

$$\begin{aligned}
\|\sigma_h + \nabla u_h^s\|_\Omega^2 &\leq C \left(\left\|\sigma_h^\gamma + (\nabla \tilde{u}_h)\psi_h^\gamma\right\|_{\omega^\gamma}^2 + \sum_{a \in \mathcal{V}_h^*} \left\|\sigma_h^a + (\nabla \tilde{u}_h)\psi^a\right\|_{\omega^a}^2 \right) \\
&\leq C \left(\|\nabla(u - u^s)\|_\Omega^2 + \|\nabla \tilde{u} - \nabla \tilde{u}_h\|_{\omega^\gamma}^2 + \sum_{a \in \mathcal{V}_h^*} \|\nabla \tilde{u} - \nabla \tilde{u}_h\|_{\omega^a}^2 \right) \\
&\leq C \left(\|\nabla(u - u^s)\|_\Omega^2 + \|\nabla \tilde{u} - \nabla \tilde{u}_h\|_{\tilde{\Omega}}^2 \right)
\end{aligned}$$

since the number of possible overlaps between the different patches ω^γ and ω^a is uniformly bounded. By integration by parts,

$$\int_{\tilde{\Omega}} (\nabla u - \nabla \tilde{u}) \cdot (\nabla \tilde{u} - \nabla \tilde{u}_h) = - \int_{\tilde{\Omega}} (\Delta u - \Delta \tilde{u})(\tilde{u} - \tilde{u}_h) + \int_{\partial \tilde{\Omega}} (\nabla u - \nabla \tilde{u}) \cdot n (\tilde{u} - \tilde{u}_h) = 0 .$$

Hence

$$\|\nabla(u - u_h^s)\|_\Omega^2 = \left\|\nabla(u - u')\right\|_{\Omega'}^2 + \|\nabla(u - \tilde{u}) + \nabla(\tilde{u} - \tilde{u}_h)\|_{\tilde{\Omega}}^2 = \|\nabla(u - u^s)\|_\Omega^2 + \|\nabla \tilde{u} - \nabla \tilde{u}_h\|_{\tilde{\Omega}}^2 ,$$

so that

$$\|\sigma_h + \nabla u_h^s\|_\Omega^2 \leq C \|\nabla(u - u_h^s)\|_\Omega ,$$

i.e. (2.25).

■

Lemmas for principal theorem.

We recall here two well-known lemmas, needed for the proof of Theorem 2.12, and give their proofs for completeness of exposition. Let $H_{00}^s(\gamma)$, with $s \in \{-\frac{1}{2}, \frac{1}{2}\}$ be the spaces of functions (distributions) on γ of the form

$$\eta = \sum_{k \geqslant 1} \eta_k \sin\left(\frac{k\pi}{R} y\right) , \tag{2.36}$$

with the norm

$$\|\eta\|_{s,\gamma} = \left(\sum_{k \geqslant 1} \frac{R}{2} \eta_k^2 \left(\frac{k\pi}{R} \right)^{2s} \right)^{1/2}. \tag{2.37}$$

Lemma 2.13. *For any $\eta \in H_{00}^{-1/2}(\gamma)$, let θ be the solution to*

$$\Delta\theta = 0 \text{ on } \omega_R^\gamma$$

$$\nabla\theta \cdot n = \eta \text{ on } \gamma$$

$$\nabla\theta \cdot n = 0 \text{ on } \gamma_R$$

$$\theta = 0 \text{ on } \tilde{\Gamma}_{wall} \cap \partial\omega_R^\gamma$$

Then,

$$\|\nabla\theta\|_{\omega_R^\gamma} \leqslant C_1 \|\eta\|_{-1/2,\gamma}$$

with $C_1 > 0$ which does not depend on R and $\|\eta\|_{-1/2,\gamma}$ is defined in (2.37).

Proof. For any $\eta \in H_{00}^{-1/2}(\gamma)$ written as (2.36), the solution θ is given by

$$\theta = \sum_{k \geqslant 1} \eta_k \sin\left(\frac{k\pi}{R} y \right) \frac{\cosh\left(\frac{k\pi}{R}(x - x_\gamma - R) \right)}{\frac{k\pi}{R} \sinh(k\pi)}$$

The result follows by direct calculations. We have

$$\|\eta\|_{-1/2,\gamma} = \left(\sum_{k \geqslant 1} \eta_k^2 \frac{R^2}{2k\pi} \right)^{1/2}$$

and want to prove that

$$\|\nabla\theta\|_{\omega_R^\gamma} \leqslant C_1 \|\eta\|_{-1/2,\gamma}.$$

Let us begin with the calculation of $\|\nabla\theta\|_{\omega_R^\gamma}$:

$$\frac{\partial\theta}{\partial x} = \sum_{k \geqslant 1} \eta_k \frac{\sin\left(\frac{k\pi}{R} y \right)}{\sinh(k\pi)} \sinh\left(\frac{k\pi}{R}(x - x_\gamma - R) \right)$$

and

$$\frac{\partial\theta}{\partial y} = \sum_{k \geqslant 1} \eta_k \frac{\cos\left(\frac{k\pi}{R} y \right)}{\sinh(k\pi)} \cosh\left(\frac{k\pi}{R}(x - x_\gamma - R) \right).$$

Then, we have $\|\nabla\theta\|^2_{\omega_R^\gamma} = \left\| \frac{\partial\theta}{\partial x} \right\|^2_{\omega_R^\gamma} + \left\| \frac{\partial\theta}{\partial y} \right\|^2_{\omega_R^\gamma} = \sum_{k \geq 1} (A) \times (B)$, where

$$A = \left(\frac{\eta_k}{\sinh(k\pi)} \right)^2$$

and

$$(B) = \left\|\sin\left(\frac{k\pi}{R}y\right)\sinh\left(\frac{k\pi}{R}(x-x_\gamma-R)\right)\right\|^2_{\omega_R^\gamma} + \left\|\cos\left(\frac{k\pi}{R}y\right)\cosh\left(\frac{k\pi}{R}(x-x_\gamma-R)\right)\right\|^2_{\omega_R^\gamma}.$$

Let us begin the calculation with (B):

$$\begin{aligned}
(B) &= \left\|\sin\left(\frac{k\pi}{R}y\right)\sinh\left(\frac{k\pi}{R}(x-x_\gamma-R)\right)\right\|^2_{\omega_R^\gamma} + \left\|\cos\left(\frac{k\pi}{R}y\right)\cosh\left(\frac{k\pi}{R}(x-x_\gamma-R)\right)\right\|^2_{\omega_R^\gamma} \\
&= \int_0^R \int_{x_\gamma}^{x_\gamma+R} \sin^2\left(\frac{k\pi}{R}y\right)\sinh^2\left(\frac{k\pi}{R}(x-x_\gamma-R)\right) + \cos^2\left(\frac{k\pi}{R}y\right)\cosh^2\left(\frac{k\pi}{R}(x-x_\gamma-R)\right)dxdy \\
&= \int_0^R \sin^2\left(\frac{k\pi}{R}y\right)dy \int_{x_\gamma}^{x_\gamma+R} \sinh^2\left(\frac{k\pi}{R}(x-x_\gamma-R)\right)dx \\
&\quad + \int_0^R \cos^2\left(\frac{k\pi}{R}y\right)dy \int_{x_\gamma}^{x_\gamma+R} \cosh^2\left(\frac{k\pi}{R}(x-x_\gamma-R)\right)dx
\end{aligned}$$

Now, we will use that $\cosh^2 - \sinh^2 = 1$, then

$$\begin{aligned}
(B) &= \int_0^R \sin^2\left(\frac{k\pi}{R}y\right)dy \int_{x_\gamma}^{x_\gamma+R} \sinh^2\left(\frac{k\pi}{R}(x-x_\gamma-R)\right)dx \\
&\quad + \int_0^R \cos^2\left(\frac{k\pi}{R}y\right)dy \int_{x_\gamma}^{x_\gamma+R} 1+\sinh^2\left(\frac{k\pi}{R}(x-x_\gamma-R)\right)dx \\
&= R\int_0^R \cos^2\left(\frac{k\pi}{R}y\right)dy \\
&\quad + \int_{x_\gamma}^{x_\gamma+R} \sinh^2\left(\frac{k\pi}{R}(x-x_\gamma-R)\right)dx \int_0^R \sin^2\left(\frac{k\pi}{R}y\right) + \cos^2\left(\frac{k\pi}{R}y\right)dy \\
&= R\int_0^R (1-\sin^2\left(\frac{k\pi}{R}y\right))dy + R\int_{x_\gamma}^{x_\gamma+R} \sinh^2\left(\frac{k\pi}{R}(x-x_\gamma-R)\right)dx \\
&= R\frac{R}{2} + R\left(-\frac{R}{2} + \frac{R}{4k\pi}\sinh(2k\pi)\right).
\end{aligned}$$

Let us see that $\int_0^R \sin^2\left(\frac{k\pi}{R}y\right)dy = \frac{R}{2}$ and $\int_{x_\gamma}^{x_\gamma+R} \sinh^2\left(\frac{k\pi}{R}(x_\gamma+R-x)\right)dx = -\frac{R}{2} + \frac{R}{4k\pi}\sinh(2k\pi)$:

$$\begin{aligned}
\int_0^R \sin^2\left(\frac{k\pi}{R}y\right)dy &= \int_0^R \frac{1-\cos\left(\frac{2k\pi}{R}y\right)}{2} \\
&= \frac{R}{2} - \frac{1}{2}\left[\frac{R}{2k\pi}\sin\left(\frac{2k\pi}{R}y\right)\right]_0^R = \frac{R}{2},
\end{aligned}$$

where we have used that $\sin(2k\pi) = 0$, and for the other integral we have:

$$\begin{aligned}
&\int_{x_\gamma}^{x_\gamma+R} \sinh^2\left(\frac{k\pi}{R}(x-x_\gamma-R)\right)dx = \int_{x_\gamma}^{x_\gamma+R} \frac{1}{2}\left(\cosh\left(\frac{2k\pi}{R}(x-x_\gamma-R)\right)-1\right)dx \\
&= \frac{1}{2}\left[\frac{R}{2k\pi}\sinh\left(\frac{2k\pi}{R}(x-x_\gamma-R)\right)\right]_{x_\gamma}^{x_\gamma+R} - \frac{R}{2} = \frac{R}{4k\pi}\left(\sinh(0)-\sinh(-2k\pi)\right) - \frac{R}{2} \\
&= -\frac{R}{2} + \frac{R}{4k\pi}\sinh(2k\pi).
\end{aligned}$$

Then,

$$(B) = \frac{R^2}{4k\pi}\sinh(2k\pi)$$

and finally

$$\|\nabla\theta\|^2_{\omega_R^\gamma} = \sum_{k\geqslant 1}(A)\times(B) = \sum_{k\geqslant 1}\left(\frac{\eta_k}{\sinh(k\pi)}\right)^2\frac{R^2}{4k\pi}\sinh(2k\pi) = \sum_{k\geqslant 1}\eta_k^2\frac{R^2}{2k\pi\tanh(k\pi)}$$
$$\leqslant \frac{1}{\tanh(\pi)}\sum_{k\geqslant 1}\eta_k^2\frac{R^2}{2k\pi} := C_1^2\|\eta\|^2_{-1/2,\gamma}.$$

■

Lemma 2.14. *Introduce the space $H^s_{00}(\gamma)$ as in the preceding lemma. For any $\eta \in H^{1/2}_{00}(\gamma)$, let θ be the solution to*

$$\Delta\theta = 0 \text{ on } \omega_R^\gamma$$

$$\theta = \eta \text{ on } \gamma$$

$$\theta = 0 \text{ on } \gamma_R \text{ and } \text{ on } \partial\omega_R^\gamma \cap \tilde{\Gamma}_{wall}$$

Then,

$$\|\nabla\theta\|_{\omega_R^\gamma} \leqslant C_2\|\eta\|_{1/2,\gamma}$$

with $C_2 > 0$ which does not depend on R.

Proof. For any $\eta \in H^{1/2}_{00}(\gamma)$ written as (2.36), by direct calculation the solution θ is given by

$$\theta = \sum_{k\geqslant 1}\eta_k\sin\left(\frac{k\pi}{R}y\right)\frac{\sinh\left(\frac{k\pi}{R}(x_\gamma + R - x)\right)}{\sinh(k\pi)}.$$

In this case we recall that the norm is

$$\|\eta\|_{1/2,\gamma} = \left(\sum_{k\geqslant 1}\eta_k^2\left(\frac{k\pi}{2}\right)\right)^{1/2}$$

and that we want to prove

$$\|\nabla\theta\|_{\omega_R^\gamma} \leqslant C_2\|\eta\|_{1/2,\gamma}.$$

Let us begin with the calculation of $\|\nabla\theta\|_{\omega_R^\gamma}$:

$$\frac{\partial\theta}{\partial x} = \sum_{k\geqslant 1}\eta_k\frac{-k\pi}{R}\frac{\sin\left(\frac{k\pi}{R}y\right)}{\sinh(k\pi)}\cosh\left(\frac{k\pi}{R}(x_\gamma + R - x)\right)$$

and

$$\frac{\partial\theta}{\partial y} = \sum_{k\geqslant 1}\eta_k\frac{k\pi}{R}\frac{\cos\left(\frac{k\pi}{R}y\right)}{\sinh(k\pi)}\sinh\left(\frac{k\pi}{R}(x_\gamma + R - x)\right).$$

Then, we have $\|\nabla\theta\|^2_{\omega_R^\gamma} = \left\|\frac{\partial\theta}{\partial x}\right\|^2_{\omega_R^\gamma} + \left\|\frac{\partial\theta}{\partial y}\right\|^2_{\omega_R^\gamma} = \sum_{k\geqslant 1}(A)\times(B)$, where

$$(A) = \left(\frac{\eta_k \frac{k\pi}{R}}{\sinh(k\pi)}\right)^2$$

and

$$(B) = \left\|\sin\left(\frac{k\pi}{R}y\right)\cosh\left(\frac{k\pi}{R}(x_\gamma+R-x)\right)\right\|^2_{\omega_R^\gamma} + \left\|\cos\left(\frac{k\pi}{R}y\right)\sinh\left(\frac{k\pi}{R}(x_\gamma+R-x)\right)\right\|^2_{\omega_R^\gamma}.$$

Let us begin the calculation with (B):

$$\begin{aligned}
(B) &= \left\|\sin\left(\frac{k\pi}{R}y\right)\cosh\left(\frac{k\pi}{R}(x_\gamma+R-x)\right)\right\|^2_{\omega_R^\gamma} + \left\|\cos\left(\frac{k\pi}{R}y\right)\sinh\left(\frac{k\pi}{R}(x_\gamma+R-x)\right)\right\|^2_{\omega_R^\gamma} \\
&= \int_0^R\int_{x_\gamma}^{x_\gamma+R} \sin^2\left(\frac{k\pi}{R}y\right)\cosh^2\left(\frac{k\pi}{R}(x_\gamma+R-x)\right) + \cos^2\left(\frac{k\pi}{R}y\right)\sinh^2\left(\frac{k\pi}{R}(x_\gamma+R-x)\right)dxdy \\
&= \int_0^R \sin^2\left(\frac{k\pi}{R}y\right)dy\int_{x_\gamma}^{x_\gamma+R}\cosh^2\left(\frac{k\pi}{R}(x_\gamma+R-x)\right)dx \\
&\quad + \int_0^R \cos^2\left(\frac{k\pi}{R}y\right)dy\int_{x_\gamma}^{x_\gamma+R}\sinh^2\left(\frac{k\pi}{R}(x_\gamma+R-x)\right)dx
\end{aligned}$$

Now, we will use $\cosh^2-\sinh^2=1$, then

$$\begin{aligned}
(B) &= \int_0^R \sin^2\left(\frac{k\pi}{R}y\right)dy\int_{x_\gamma}^{x_\gamma+R} 1+\sinh^2\left(\frac{k\pi}{R}(x_\gamma+R-x)\right)dx \\
&\quad + \int_0^R \cos^2\left(\frac{k\pi}{R}y\right)dy\int_{x_\gamma}^{x_\gamma+R}\sinh^2\left(\frac{k\pi}{R}(x_\gamma+R-x)\right)dx \\
&= R\int_0^R \sin^2\left(\frac{k\pi}{R}y\right)dy + \int_{x_\gamma}^{x_\gamma+R}\sinh^2\left(\frac{k\pi}{R}(x_\gamma+R-x)\right)dx\int_0^R \sin^2\left(\frac{k\pi}{R}y\right)+\cos^2\left(\frac{k\pi}{R}y\right)dy \\
&= R\int_0^R \sin^2\left(\frac{k\pi}{R}y\right)dy + R\int_{x_\gamma}^{x_\gamma+R}\sinh^2\left(\frac{k\pi}{R}(x_\gamma+R-x)\right)dx \\
&= R\frac{R}{2} + R\left(-\frac{R}{2}+\frac{R}{4k\pi}\sinh(2k\pi)\right).
\end{aligned}$$

Since, we have $\int_0^R \sin^2\left(\frac{k\pi}{R}y\right)dy = \frac{R}{2}$ (same calculation as before) and

$$\begin{aligned}
&\int_{x_\gamma}^{x_\gamma+R}\sinh^2\left(\frac{k\pi}{R}(x_\gamma+R-x)\right)dx = \int_{x_\gamma}^{x_\gamma+R}\frac{1}{2}\left(\cosh\left(\frac{2k\pi}{R}(x_\gamma+R-x)\right)-1\right)dx \\
&= \frac{1}{2}\left[\frac{-R}{2k\pi}\sinh\left(\frac{2k\pi}{R}(x_\gamma+R-x)\right)\right]_{x_\gamma}^{x_\gamma+R} - \frac{R}{2} = \frac{-R}{4k\pi}\left(\sinh(0)-\sinh(2k\pi)\right) - \frac{R}{2} = -\frac{R}{2}+\frac{R}{4k\pi}\sinh(2k\pi),
\end{aligned}$$

then,

$$(B) = \frac{R^2}{4k\pi}\sinh(2k\pi).$$

and finally,

$$\|\nabla\theta\|^2_{\omega_R^\Gamma} = \sum_{k\geqslant 1}(A)\times(B) = \sum_{k\geqslant 1}\left(\frac{\eta_k\frac{k\pi}{R}}{\sinh(k\pi)}\right)^2 \frac{R^2}{4k\pi}\sinh(2k\pi) = \frac{1}{2}\sum_{k\geqslant 1}\eta_k^2\frac{k\pi}{\tanh(k\pi)}$$
$$\leqslant \frac{1}{\tanh(\pi)}\sum_{k\geqslant 1}\eta_k^2\frac{k\pi}{2} := C_2^2\|\eta\|^2_{1/2,\gamma}.$$

■

2.2.3. Numerical results using the flux reconstruction (2.17)

We have a 0D/2D model for the Poisson equation and in the following we want to define a suitable interface estimator η^γ for the interface to be able to detect the suitable position of the interface γ according to this estimator. We will see that this estimator η^γ is depending only on the position of the interface and independent of the mesh size of the mesh. We will see that more the tolerance of η^γ is small, more the interface will be placed toward the inlet. For this purpose we will begin with the uniform refinement. We will take in this section $RT_k = RT_2$ and $\mathbb{P}_k = \mathbb{P}_2$.

Uniform Refinement and Estimator of the Interface

First of all, we fix the mesh size, then we change the position of the interface to obtain the graphs of the error $\|\nabla u - \nabla u_h^s\|_\Omega$ and estimator $\|\sigma_h + \nabla u_h^s\|_\Omega$ in (2.24) with respect to different positions of interface in Figure 2.10. We take the mesh sizes $h \approx 0.08$, $h \approx 0.04$ and $h \approx 0.02$ by making a quasi-uniform mesh refinement. In the proofs we suppose that the position x_γ of the interface must be located in the interval $x_\gamma \in [0.1, L_1 - R]$ and here $L_1 - R = 4.6$, see Figure 1.4, but in order to see what happens also after the upper bound for the interface position, that is $L_1 - R$, we take $x_\gamma \in [0, L_1 - 0.02]$. So we conclude from Figure 2.10 that as x_γ becomes near the corner as the estimator and error become bigger.
For a fixed mesh size $h \approx 0.08$, we want to see the variation between the reconstructed approximated flux σ_h^γ and the approximated flux $-\nabla\tilde{u}_h$ on the domain ω^γ i.e. $\eta^\gamma := ||\sigma_h^\gamma + (\nabla\tilde{u}_h)\psi_h^\gamma||_{\omega^\gamma}$ with respect to different positions of the interface where ω^γ is defined in Figure 2.11a. We plot $\eta^\gamma = ||\sigma_h^\gamma + (\nabla\tilde{u}_h)\psi_h^\gamma||_{\omega^\gamma}$ with respect to different positions of the interface in the Figure 2.11b below with base-10 logarithmic scale on the y-axis and for fixed mesh size $h \approx 0.08$.
For fixed position of interface at $x_\gamma = 4$, we plot in Figure 2.11c the estimator on ω^γ w.r.t. different mesh sizes to find that $\eta^\gamma = ||\sigma_h^\gamma + (\nabla\tilde{u}_h)\psi_h^\gamma||_{\omega^\gamma}$ is about 6.6×10^{-5} for all different mesh sizes which is constant and, consequently, this flux is better than previous flux since in the previous flux we don't have that $\eta^\gamma = ||\sigma_h^\gamma + (\nabla\tilde{u}_h)\psi_h^\gamma||_{\omega^\gamma}$ is constant for different mesh sizes. Finally, let us define $\eta^\gamma := ||\sigma_h^\gamma + (\nabla\tilde{u}_h)\psi_h^\gamma||_{\omega^\gamma}$ as an estimator for the position of the interface which depends only on the position of the interface.
For a fixed mesh size $h \approx 0.08$, we want to compare the above estimator **Estimator1** $:= \eta^\gamma = ||\sigma_h^\gamma + (\nabla\tilde{u}_h)\psi_h^\gamma||_{\omega^\gamma}$ with another proposed estimator for the interface **Indicator2** $:= ||\nabla(\tilde{u}_h - u')\psi_h^\gamma||_{\omega^\gamma}$ by plotting them with respect to different positions of the interface in Figure 2.12a below where now $x_\gamma \in [0.1, L_1 - 0.02]$, see Figure 1.4, then we see that they are approximately the same and this verified our choice of **Estimator1** to be a good estimator for the position of the interface. Now, if we fix the interface at $x_\gamma = 4$, after making uniform refinement we see that the error distribution in Figure 2.12b and the estimator

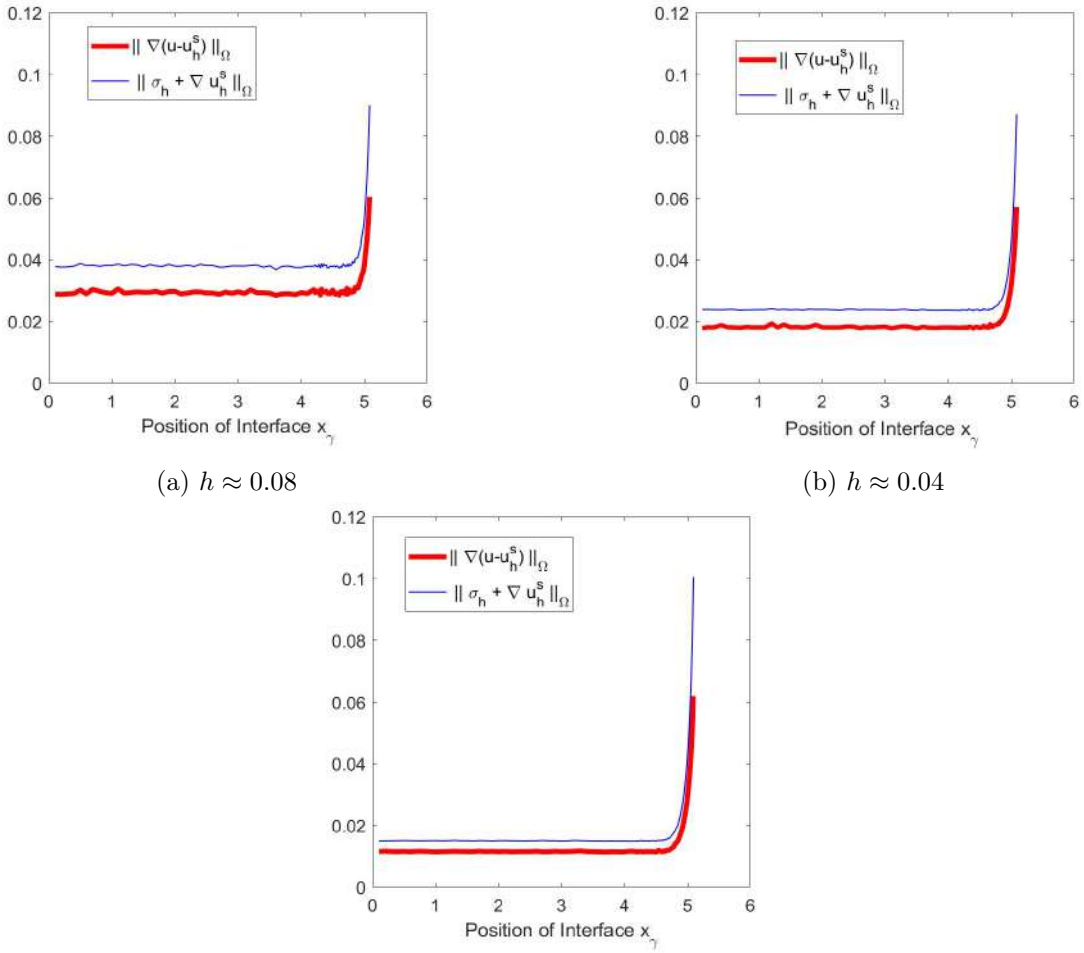

(a) $h \approx 0.08$

(b) $h \approx 0.04$

(c) $h \approx 0.02$

Figure 2.10.: Error and Estimator w.r.t. different positions of the interface for different mesh sizes h

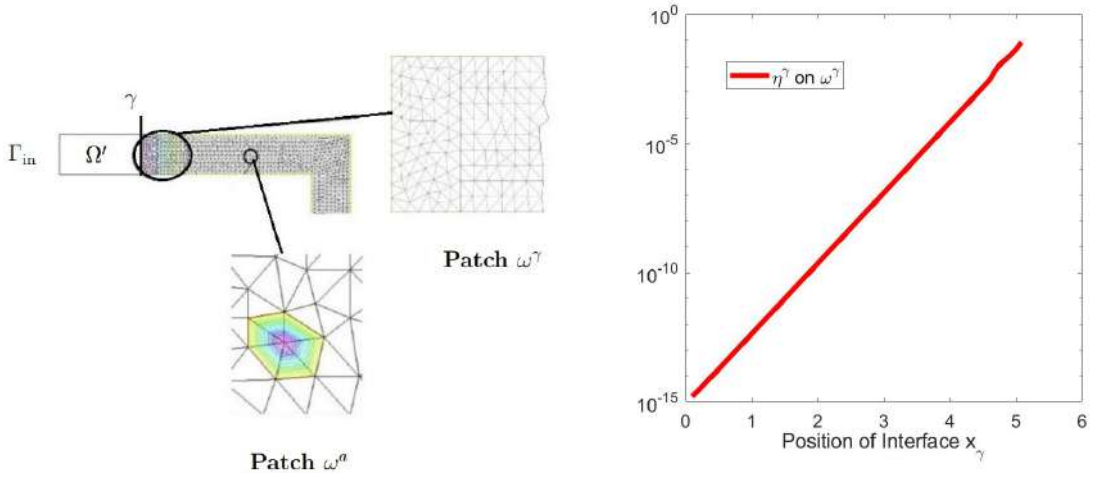

(a) Local Patches

(b) $h \approx 0.08$

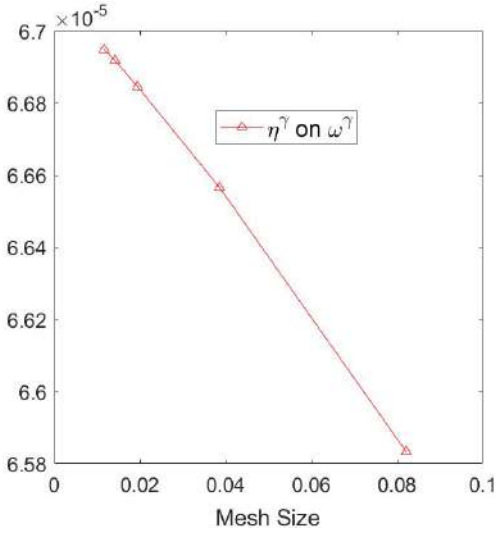

(c) $x_\gamma = 4$

Figure 2.11.: Estimator on ω^γ w.r.t the interface position x_γ and w.r.t mesh sizes h

distribution in Figure 2.12c are of biggest value near the corners and this is due to the singularities in the corners. The mesh should be thus refined there. In the next section, we will propose an adaptive algorithm both for the interface placement and for the mesh refinement.

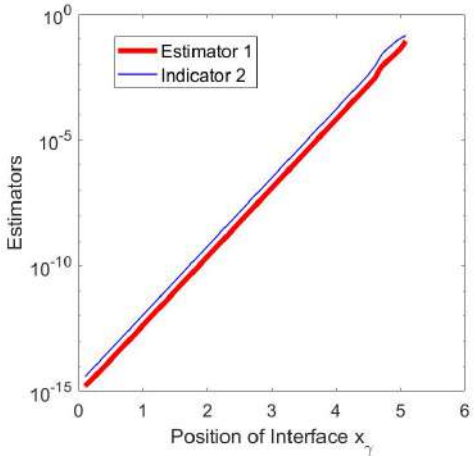

(a) Estimator and indicator on ω^γ w.r.t x_γ

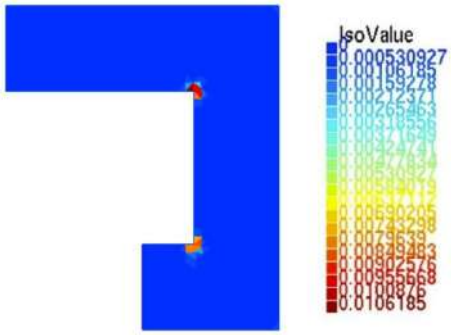

(b) Distribution of error with mesh size h=0.08 for $x_\gamma = 4$

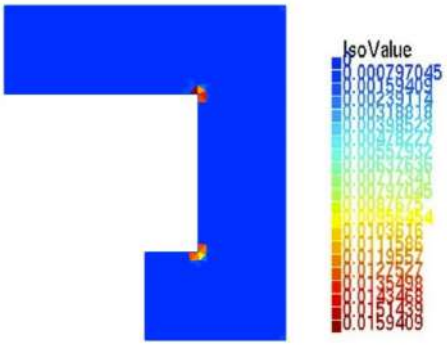

(c) Distribution of estimator with mesh size h=0.08 for $x_\gamma = 4$

Figure 2.12.: estimators on ω^γ and distribution of estimator and error on Ω

Let us define on Ω the error $e := \|\nabla(u - u_h^s)\|_\Omega$, the estimator $\eta := \|\sigma_h + \nabla u_h^s\|$ and the index of efficiency $I := \frac{e}{\eta}$. If we fix the interface position $x_\gamma = 4$ (e.g.) and make a quasi-uniform refinement, we find the order of convergence is about 0.7 as in the Table 2.1. We see that the convergence is not optimal and it is normal since $u \notin H^2(\Omega)$ (we have a singular solution). One strategy to try to improve the rate of convergence is to make a local mesh refinement as Section 2.3.

2.2.4. Numerical comparison between the two fluxes

In this section we are going to make a comparison between the two estimators developed in this chapter. The first flux which is defined in (2.2) will be denoted by $\sigma_h^{\mathrm{F}_1} = \tilde{\sigma}_h^{\mathrm{F}_1} + \sigma'$ and consequently the first estimator will be denoted by $\eta^{\mathrm{F}_1} := \sum_{K \in \tilde{\mathcal{T}}_h} \eta^2_{\mathrm{F}_1,K}$ where $\eta_{\mathrm{F}_1,K} := ||\nabla \tilde{u}_h + \tilde{\sigma}_h^{\mathrm{F}_1}||_K$. The second flux which is defined in (2.17) will be denoted by $\sigma_h^{F_2} = \tilde{\sigma}_h^{\mathrm{F}_2} + \sigma'$

h	e	η	I	order of convergence
0.0760918	0.0288059	0.037627	1.30623	-
0.0400266	0.018209	0.0236558	1.29913	0.713991
0.0223199	0.0115984	0.0148648	1.28162	0.772254

Table 2.1.: Order of convergence.

and consequently the second estimator will be denoted by $\eta^{\mathrm{F}_2} := \sum_{K\in\tilde{\mathcal{T}}_h} \eta^2_{\mathrm{F}_2,K}$ where $\eta_{\mathrm{F}_2,K} := ||\nabla\tilde{u}_h + \tilde{\sigma}_h^{\mathrm{F}_2}||_K$. First of all, the estimator η^{F_1} does not guarantee the efficiency (lower bound) while the second one η^{F_2} guarantee the efficiency. Now, let us make a uniform mesh refinement and plot the two estimators η^{F_1} and η^{F_2} and the error $\|\nabla u - \nabla u_h^s\|_\Omega$ with respect to different positions x_γ of the interface γ and for mesh size $h \approx 0.08$ as shown in Figure 2.13. Here we consider that $x_\gamma \in [0, L_1 - 0.02]$ to be able to see the better estimator although that we suppose $x_\gamma \in [0, L_1 - R]$, with $R = 0.5$, to be able to define the flux since if x_γ exceeds $L_1 - R = 4.6$ position, then the flux will not belong to $H(\mathrm{div}, \Omega)$. We observe that the estimators η^{F_1} and η^{F_2} are equivalent until the position $x_\gamma = 4$ of the interface γ. To see more what happen between $x_\gamma = 4$ and $x_\gamma = L_1 - 0.02$ we have introduced Figure 2.14. In Figure 2.14 we see that the estimators η^{F_1} and η^{F_2} are equivalent until the position $x_\gamma = 4.6$ (this is the point where we must not exceed it when we consider the second flux $\sigma_h^{\mathrm{F}_2}$ where we have guaranteed efficiency) and for this reason we will make the comparison between the local estimators $\eta^{\mathrm{F}_1,\gamma} := ||\sigma_h^{\mathrm{F}_1,\gamma} + (\nabla\tilde{u}_h)\psi_h^{\mathrm{F}_1,\gamma}||_{\omega^\gamma}$ and $\eta^{\mathrm{F}_2,\gamma} := ||\sigma_h^{\mathrm{F}_2,\gamma} + (\nabla\tilde{u}_h)\psi_h^{\mathrm{F}_2,\gamma}||_{\omega^\gamma}$ on the interface patch ω^γ for the two fluxes. For this purpose let us fix $x_\gamma = 4$ and plot in Figure 2.15 the variation of η^{F_1} and η^{F_1} with respect to different mesh sizes.

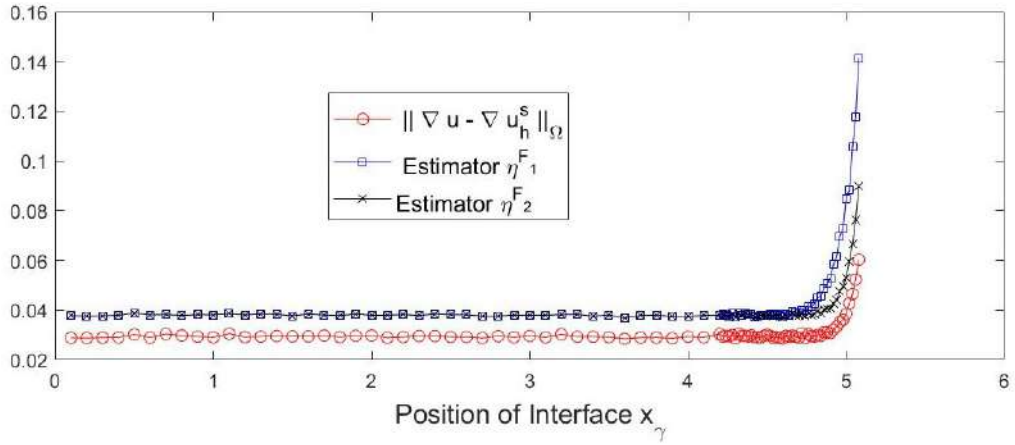

Figure 2.13.: Error and estimators η^{F_1} and η^{F_2} w.r.t different interface positions x_γ

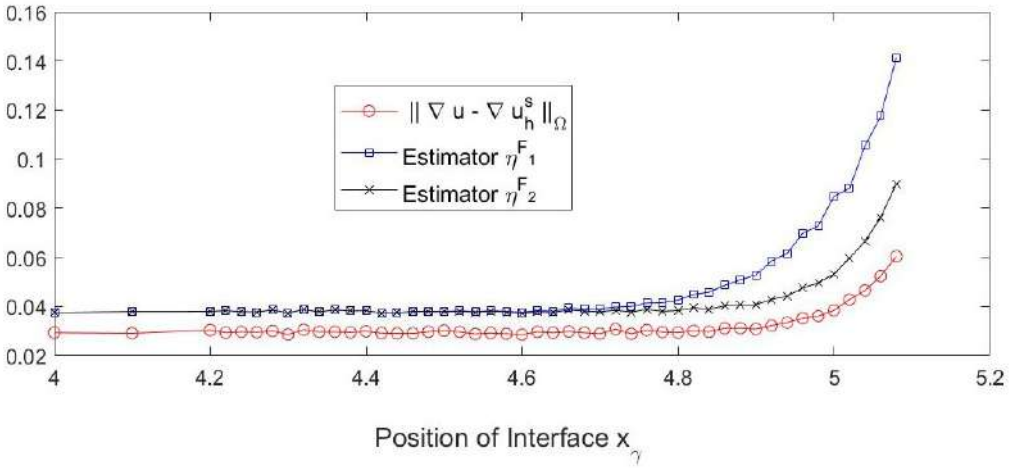

Figure 2.14.: Error and estimators η^{F_1} and η^{F_2} w.r.t different interface positions x_γ

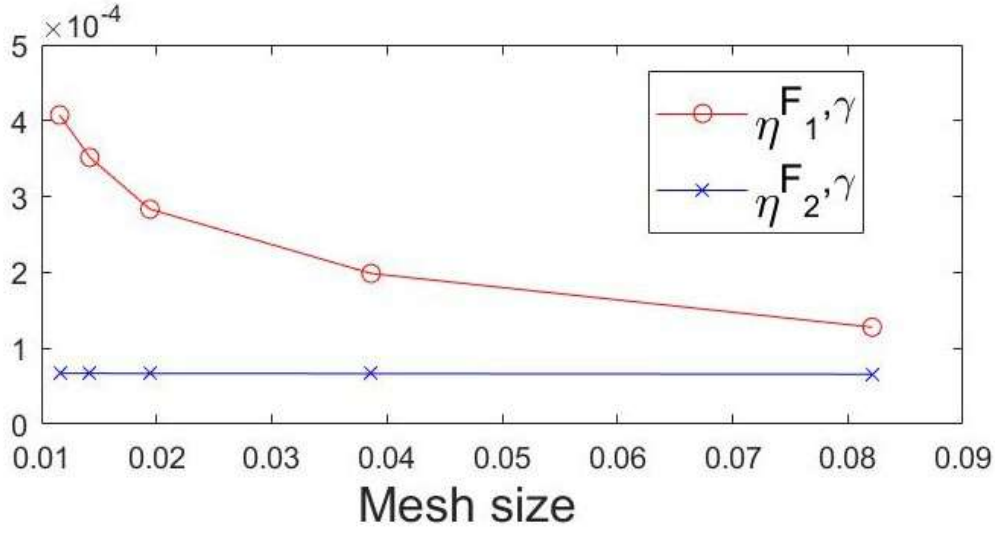

Figure 2.15.: Comparison between the two local estimators $\eta^{\mathrm{F}_1,\gamma}$ and $\eta^{\mathrm{F}_2,\gamma}$ with respect to different mesh sizes

From Figure 2.15 we deduce that the estimator $\eta^{\mathrm{F}_1,\gamma}$ is greater than $\eta^{\mathrm{F}_2,\gamma}$ and $\eta^{\mathrm{F}_2,\gamma}$ is constant with respect to different mesh sizes which is very important to take it as the estimator for detecting the position of interface γ since it is independent from the mesh size and it depends only on the position of the interface as showed in Figure 2.11b. The fact that the efficiency is guaranteed when we take $\sigma_h^{\mathrm{F}_2}$ defined in (2.17) and all the above numerical results about the comparison between the two fluxes detect that the best choice of the definition of the flux is $\sigma_h^{\mathrm{F}_2}$ that is defined in (2.17).

2.3. Adaptive algorithms

2.3.1. Adaptive mesh refinement: "hopt" strategy

It is classical to use the *a posteriori* error estimate to refine the mesh, by marking certain mesh elements as contributing the most to the error, and then splitting them into smaller elements. However, we do all our numerical experiments in the FreeFEM software [49] which does not provide the possibility to produce a new regular mesh by refining some marked elements of the old mesh. Instead, FreeFEM provides a function `adapmesh` that produces a new mesh of the entire domain which respects (approximately) the given distribution of the local element sizes. We thus need to design a mesh refinement algorithm compatible with the FreeFEM meshing capabilities.

To introduce our mesh adaptive algorithm, referred to as "hopt",[1] let us characterize the mesh $\tilde{\mathcal{T}}_h$ of $\tilde{\Omega}$ by the mesh size distrubution $h(x)$ such that $h(x)$ at a point x inside a triangle $K \in \tilde{\mathcal{T}}_h$ is approximately equal to h_K. Moreover, we have the simplified error on $\Omega = \tilde{\Omega} \cup \Omega' \cup \gamma$ which is defined in (1.14) by

$$|u - u_h^s|_{1,\Omega}^2 \approx |u - \tilde{u}_h|_{1,\tilde{\Omega}}^2 \approx \int_{\tilde{\Omega}} h^{2\delta}(x) c^2(x) \,\mathrm{dx} \tag{2.38}$$

where u_h^s is the approximated solution of the coupled 0D/2D model which is defined in (1.13), some *a priori* unknown $c(x)$ and the order parameter δ chosen once for all. This is reasonable for example for $\mathbb{P}_1$ FEM with $\delta = 1$, $c(x) \sim |D^2 u|(x)$, i.e. the norm of the second order derivatives at x, provided u is sufficiently smooth. Note also that the number of DOFs is approximately given in 2D case by

$$N_{\mathrm{DOF}} \sim \int_{\tilde{\Omega}} \frac{\mathrm{dx}}{h^2(x)}$$

since a triangle of size $h(x)$ occupies the area of order $h^2(x)$. Let us imagine first that we know $c(x)$ and we want to construct an optimal mesh (with the minimal possible N_{DOF}) to achieve a given error tolerance, i.e. $|u - \tilde{u}_h|_{1,\tilde{\Omega}} = \mathrm{tol}$. This is a constrained minimization problem for the mesh size distribution $h(x)$:

$$\min_{\substack{h \,\in\, L^2(\tilde{\Omega}) \\ \int_{\tilde{\Omega}} h^{2\delta}(x) c^2(x) \,\mathrm{dx} \,=\, \mathrm{tol}^2}} \quad \int_{\tilde{\Omega}} \frac{\mathrm{dx}}{h^2(x)}.$$

The minimum is achieved on a stationary point of the Lagrangian

$$L(h, \lambda) = \int_{\tilde{\Omega}} \frac{\mathrm{dx}}{h^2(x)} + \lambda \left(\int_{\tilde{\Omega}} h^{2\delta}(x) c^2(x) \,\mathrm{dx} - \mathrm{tol}^2 \right)$$

with $h \in L^2(\tilde{\Omega})$ and $\lambda \in \mathbb{R}$. Taking the variations yields

$$-\int_{\tilde{\Omega}} \frac{2v(x) \,\mathrm{dx}}{h^3(x)} + \lambda \int_{\tilde{\Omega}} 2\delta h^{2\delta - 1}(x) v(x) c^2(x) \,\mathrm{dx} = 0, \quad \forall v = v(x)$$

so that the optimal mesh size distribution is

$$h_{\mathrm{opt}}(x) = \frac{\mathrm{tol}^{1/\delta}}{\left(\int_{\tilde{\Omega}} c^{2/(\delta+1)}(x) \,\mathrm{dx} \right)^{1/(2\delta)}} \frac{1}{(c(x))^{1/(\delta+1)}}.$$

[1] Another mesh adaptive algorithm is proposed in Appendix A.

Of course, $c(x)$ is not known in practice. But, on a given mesh $\tilde{\mathcal{T}}_h$, we have a posteriori error estimates with provable upper bound (2.24) and lower bound (2.25) and thus $\|\nabla u - \nabla u_h^s\|_\Omega^2 \approx \sum_{K\in\tilde{\mathcal{T}}_h} \eta_K^2$ where the total estimator η is defined by $\eta^2 := \|\sigma_h + \nabla u_h^s\|_\Omega^2 = \|\tilde{\sigma}_h + \nabla \tilde{u}_h\|_{\tilde{\Omega}}^2 = \sum_{K\in\tilde{\mathcal{T}}_h} \eta_K^2$ and let us reinterpret this in the form (2.38),

$$\sum_{K\in\tilde{\mathcal{T}}_h} \int_K h^{2\delta}(x) c^2(x)\,\mathrm{dx} \sim \sum_{K\in\tilde{\mathcal{T}}_h} \eta_K^2.$$

This suggests to approximate $c(x)$ on any triangle $K \in \tilde{\mathcal{T}}_h$ by

$$c(x) \approx \frac{\eta_K}{h_K^\delta \sqrt{|K|}} \quad \text{for } x \in K.$$

This gives

$$h_{\mathrm{opt}}(x) = \frac{\mathrm{tol}^{1/\delta}}{\left(\sum_{K\in T_h} \eta_K^{2/(\delta+1)} h_K^{-2\delta/(\delta+1)} |K|^{\delta/(\delta+1)}\right)^{1/(2\delta)}} \frac{h_K^{\delta/(\delta+1)} |K|^{1/(2\delta+2)}}{\eta_K^{1/(\delta+1)}} \quad \text{for } x \in K. \tag{2.39}$$

Now, rather then trying to achieve the target tolerance, let us adapt the mesh by aiming to diminish the current error estimate R_{tol} times (i.e. set $\mathrm{tol} = \mathrm{Est}\,/R_{\mathrm{tol}}$) with given $R_{\mathrm{tol}} > 1$ on each iteration of the algorithm. So, the "hopt" algorithm is

1. Choose δ and R_{tol}
2. Given the mesh $\tilde{\mathcal{T}}_h$ and the estimator η, set current desired tolerance to
$$\mathrm{tol} = \frac{1}{R_{\mathrm{tol}}} \left(\sum_{K\in\mathcal{T}_h} \eta_K^2 \right)^{1/2}$$
3. Set h_{new} as the $\mathbb{P}_0$-FE function on the current mesh by $h_{\mathrm{new}} = h_{\mathrm{opt}}$ using (2.39)
4. Generate the new mesh through the FreeFEM function `adaptmesh` with parameters h_{new} and `IsMetric=1`

Note: We make mesh adaptation "hopt" ($\delta = 1$ and $R_{\mathrm{tol}} = 4$) to obtain the new total estimator η. We have chosen $\delta = 1$ and $R_{\mathrm{tol}} = 4$ since it is the best choice and you can see the explanation in Appendix A at the end of the thesis's report.

Let us see in the next subsection how we couple this mesh refinement with a suitable choice of interface γ.

2.3.2. Algorithms for the interface placement and the 2D model mesh optimization

In this section we will choose a suitable interface position and make an adaptive refinement to achieve the optimal convergence. We deal with the following Steps.

Step 0: Choices of parameters

Fix the tolerances tol(η) and tol(η^γ) for the total estimator $\eta = \|\sigma_h + \nabla u_h^s\|_\Omega$ on Ω and for the interface estimator $\eta^\gamma := ||\sigma_h^\gamma + \nabla\tilde{u}_h\psi_h^\gamma||_{\omega^\gamma}$ on ω^γ respectively in order to control the number of times of adapting the mesh until we achieve that the total estimator $\eta \leqslant \text{tol}(\eta)$ and to detect the suitable interface position in a way to get $\eta^\gamma \leqslant \text{tol}(\eta^\gamma)$.

Step 1: Detection of the Interface
Fix the position of the interface γ at abscissa $x_\gamma = L_1 - R$ (since the corner is located at $x = L_1$, see Figure 1.4) and we solve the 0D/2D problem with very coarse mesh to save the computational time cost as the detection of the position of the interface is independent from the discretization. Then we denote u_h^s the 0D/2D solution and we compute the flux σ_h^γ on ω^γ and the estimator $\eta^\gamma = ||\sigma_h^\gamma + \nabla\tilde{u}_h\psi_h^\gamma||_{\omega^\gamma}$ on ω^γ. If $\eta^\gamma > \text{tol}(\eta)$ then we redefine the abscissa x_γ as $x_\gamma = x_\gamma - \delta x$, with $\delta x = 0.1$ and we restart **Step 1** until $\eta^\gamma \leq \text{tol}(\eta^\gamma)$.

Step 2: Adapting the mesh
Once the suitable interface γ is placed (see **Step 1**), we make mesh adaptivity as in **Algorithm 1** until we obtain $\eta \leq \text{tol}(\eta)$. If we reach a MaxLevelRef of refinement, we stop adaptation even if $\eta > \text{tol}(\eta)$.

This approach is summarized as **Algorithm 1**, page 78. Using this algorithm we notice that the mesh adaptation following the global estimator η, in line 13 of **Algorithm 1**, produces a refinement near the interface also. The rate of convergence is not optimal, so that we change the strategy to perform the mesh adaptivity: for adaptivity (once the interface is placed), we take the standard equilibrated estimator in $\tilde{\Omega}$ as in [39], that is defined by $\eta^V := \left\|\sigma_h^V + \nabla\tilde{u}_h\right\|_{\tilde{\Omega}}$ where $\sigma_h^V = \sum_{a\in\mathcal{V}_h}\sigma_h^a$, recalling that $\mathcal{V}_h$ represents the set of all vertices on the mesh of the domain $\tilde{\Omega}$.

1: Fix a tolerance for the global estimator in the meshed domain $\tilde{\Omega}$, named tol(η)
2: Fix a tolerance for the estimator of the interface position, named tol(η^γ) := αtol(η) for some $\alpha \in]0, 1[$.
3: Fix a step for moving the interface position, named $\delta x > 0$
4: Fix a maximum level of refinements for the "hopt" algorithm named MaxLevelRef
5: Fix the interface position near the corner at coordinate $x_\gamma = L - R$, see Figure 1.4
6: Fix a coarse mesh in $\tilde{\Omega}$ and compute the coupled solution and η^γ.
7: **while** $\eta^\gamma > \text{tol}(\eta^\gamma)$ and $x_\gamma > 0$ **do**
8: Redefine $x_\gamma = x_\gamma - \delta x$
9: Compute the coupled solution and η^γ
10: **end while**
11: Compute η, set Level=0
12: **while** $\eta > \text{tol}(\eta)$ and Level$\leq$ MaxLevelRef **do**
13: Make adaptive refinement following "hopt" on $\tilde{\Omega}$ using η^V
14: Update Level+=1
15: Compute the coupled solution, the error and η on the new mesh
16: **end while**
17: **return** Coupled solution and x_γ

Algorithm 1: Detect the interface position and adapt the mesh.

An alternative way to make adaptivity (once the interface is placed) is to try to use a

reasonable part of our estimator of Theorem 2.12. Indeed, our estimator is defined by

$$\eta = \|\tilde{\sigma}_h + \nabla\tilde{u}_h\|_{\tilde{\Omega}} = \left\| \sigma_h^\gamma + \sum_{a\in\mathcal{V}_h\setminus\mathcal{V}_h^\gamma} (1-\psi^\Gamma(a))\sigma_h^a + \nabla\tilde{u}_h \underbrace{\left(\psi_h^\gamma + \sum_{a\in\mathcal{V}_h\setminus\mathcal{V}_h^\gamma}(1-\psi^\gamma(a))\psi^a\right)}_{=1} \right\|_{\tilde{\Omega}}$$

$$= \left\| \sigma_h^\gamma + \nabla\tilde{u}_h\psi_h^\gamma + \underbrace{\sum_{\mathcal{V}_h\setminus\mathcal{V}_h^\gamma}(1-\psi^\gamma(a))\sigma_h^a}_{\sigma_h^{\mathrm{D}}:=} + \nabla\tilde{u}_h \underbrace{\left(\sum_{\mathcal{V}_h\setminus\mathcal{V}_h^\gamma}(1-\psi^\Gamma(a))\psi^a\right)}_{1-\psi_h^\gamma} \right\|_{\tilde{\Omega}},$$

So we can split the estimators of the coupled model into two types: the first one related to the interface position, that is

$$\eta^\gamma := \left\|\sigma_h^\gamma + \nabla\tilde{u}_h\psi_h^\gamma\right\|_{\omega^\gamma},$$

and the second one related to the mesh refinement, that is

$$\eta^{\mathrm{D}} := \left\|\sigma_h^{\mathrm{D}} + \nabla\tilde{u}_h(1-\psi_h^\gamma)\right\|_{\tilde{\Omega}}. \tag{2.40}$$

The algorithm will be the same as **Algorithm 1** but we use η^D instead of η^V. Let's call this algorithm **Algorithm 2**

2.3.3. Numerical results with Algorithm 1 and Algorithm 2

In this section we make a numerical comparison between the two algorithms presented in the previous section, named **Algorithm 1** and **Algorithm 2**. The fixed parameters for all the simulations are: $\delta x = 0.1$, $MaxLevelRef = 20$. We consider three different tests: test 1 where we choose $tol(\eta) = 1e-2$, test 2 where we choose $tol(\eta) = 1e-3$ and test 3 where we choose $tol(\eta) = 1e-4$.

Test 1: $\mathrm{tol}(\eta) = 10^{-2}$**:**
We run the two algorithms for different values of $\alpha = 0.1, 0.25, 0.5$, the idea is that we want to achieve a reasonable tolerance for η^γ such that this contribution will be a smaller order or at most the same order of the local contributions of η^{V} (for Algorithm 1) or of η^{D} (for Algorithm2) for the last level of refinement giving the desired final accuracy.

Let us take $\alpha = 0.1$. In Table 2.2 we see the convergence of the error e and the estimator η with respect to the dof obtained from the adaptive refined mesh. Let us notice that the interface position is $x^\gamma = 4.4$. We show also the index of efficiency $\frac{\eta}{e}$, named Index, and the convergence rate, named Rate, in Table 2.2. In the Table 2.2a we see the results for **Algorithm 1** and in Table 2.2b for **Algorithm 2**. The two adaptations are very similar and give quite same results: the optimal rate of convergence is restored and the given accuracy for η reached.
Concerning Algorithm1, in Figure 2.16 we plot the initial mesh (Figure 2.16a) correspond-

Dof	e	η	Index	Rate
84	0.149679	0.170874	1.1416	-
302	0.0516935	0.0654847	1.26679	0.830
417	0.0295903	0.0358232	1.21064	1.72
814	0.0132612	0.0156466	1.17988	1.19
2395	0.00479483	0.00567086	1.1827	0.94

(a) Results using **Algorithm 1**

Dof	Error	η	Index	Rate
84	0.149679	0.170874	1.1416	-
302	0.0511889	0.0647278	1.26449	0.838
436	0.0258347	0.0309826	1.19926	1.86
1141	0.010464	0.0126444	1.20837	1.03
2942	0.00394587	0.00466495	1.18224	1.02

(b) Results using **Algorithm 2**

Table 2.2.: Error e and estimator η w.r.t. degrees of freedom Dof for $\alpha = 0.1$

ing to 84 Dof, the distributions of the error e, estimator η and the standard equilibrated estimator η^{V} (respectively in figure 2.16b, 2.16c and 2.16d).
In Figure 2.17 we plot the mesh coming from the first refinement level (with 302 Dof) with the distributions of e, η and η^{V} and in Figure 2.18 we plot the mesh coming from the last refinement level (that is a 4 refinement level with 2395 Dof) and the usual distributions. For this latter refinement Figure 2.19 shows a zoom in one of the two corners where the most important refinement is performed.

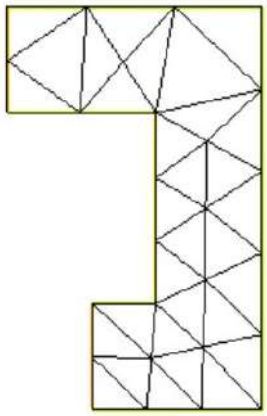

(a) Mesh $\tilde{\mathcal{T}}_h^{(0)}$ as an initial mesh before adapting.

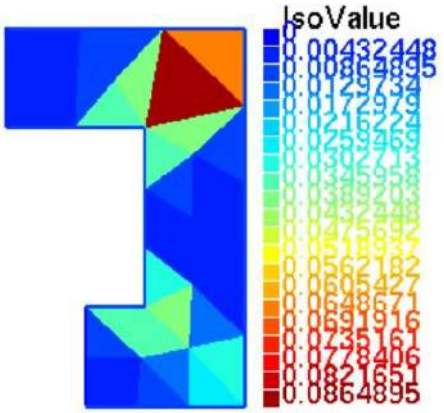

(b) Distribution of error on the mesh $\tilde{\mathcal{T}}_h^{(0)}$

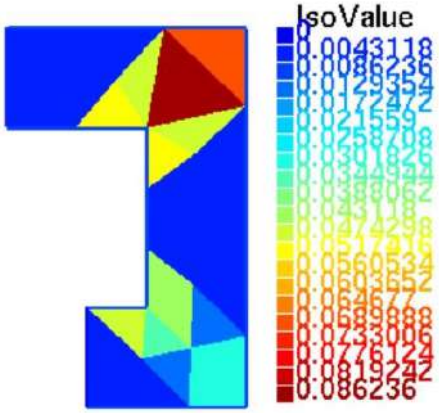

(c) Distribution of estimator on the mesh $\tilde{\mathcal{T}}_h^{(0)}$

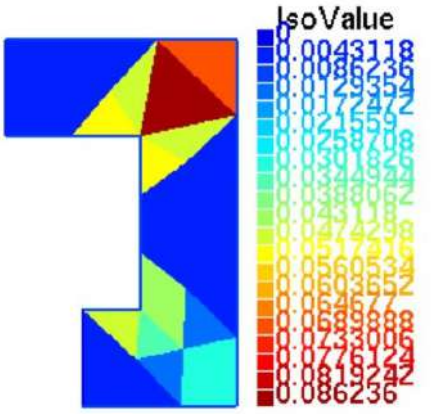

(d) Distribution of standard non-coupled equilibrated estimator η^{V} on mesh $\tilde{\mathcal{T}}_h^{(0)}$

Figure 2.16.: Distribution of coupled error and estimator on the mesh $\tilde{\mathcal{T}}_h^{(0)}$ of $\tilde{\Omega}$ with Dofs=84 using **Algorithm 1** where, $\mathrm{tol}(\eta) = 10^{-2}$ and $\alpha = 0.1$

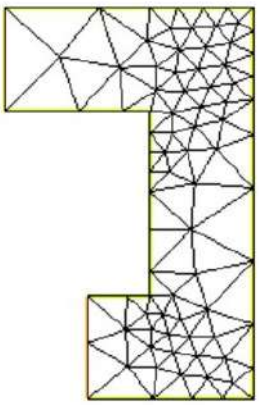

(a) Mesh $\tilde{\mathcal{T}}_h^{(1)}$ for the first adapting.

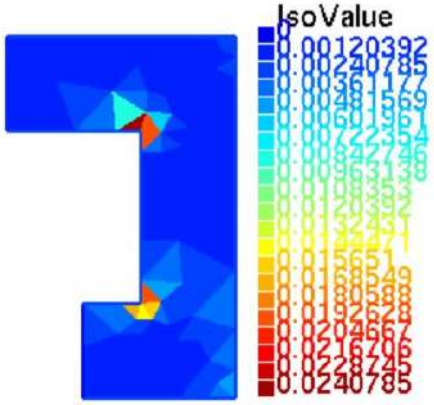

(b) Distribution of error on the mesh $\tilde{\mathcal{T}}_h^{(1)}$

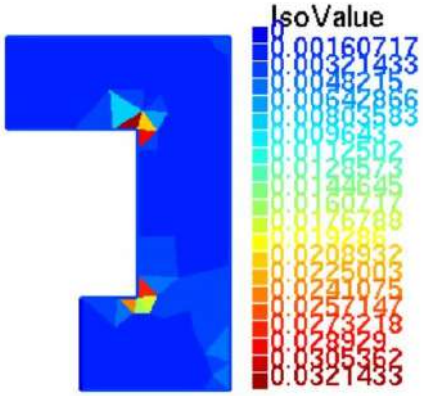

(c) Distribution of estimator on the mesh $\tilde{\mathcal{T}}_h^{(1)}$

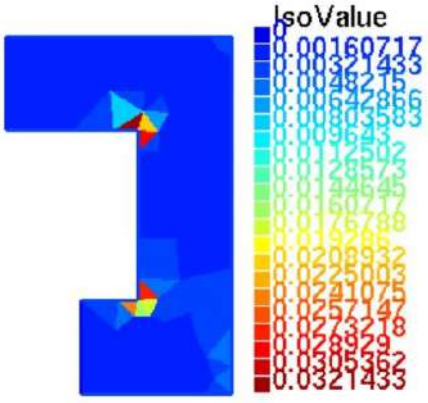

(d) Distribution of usual non-coupled estimator on the mesh $\tilde{\mathcal{T}}_h^{(1)}$

Figure 2.17.: Distribution of coupled error and estimator on the mesh $\tilde{\mathcal{T}}_h^{(1)}$ of $\tilde{\Omega}$ with Dofs=302 using **Algorithm 1** where, $\text{tol}(\eta) = 10^{-2}$ and $\alpha = 0.1$

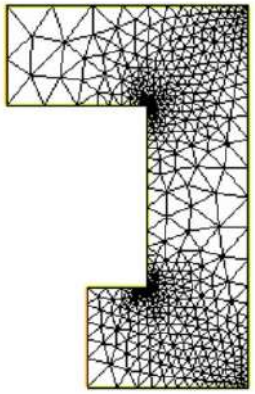

(a) Mesh $\tilde{\mathcal{T}}_h^{(4)}$ for the fourth adapting.

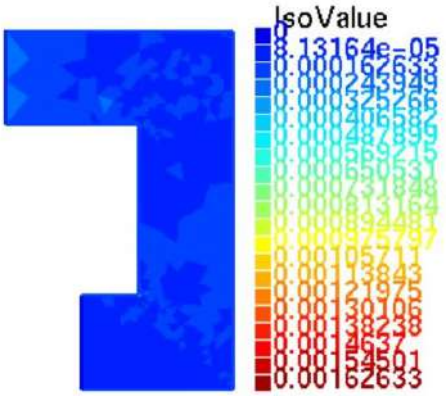

(b) Distribution of error on the mesh $\tilde{\mathcal{T}}_h^{(4)}$

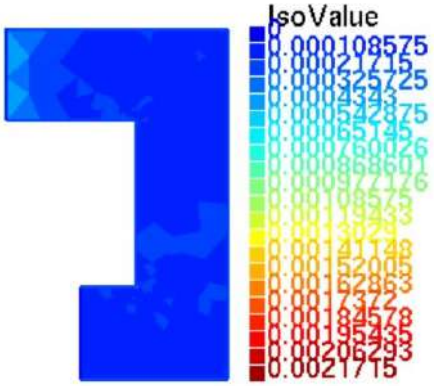

(c) Distribution of estimator on the mesh $\tilde{\mathcal{T}}_h^{(4)}$

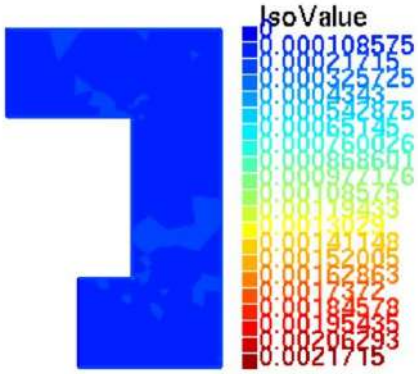

(d) Distribution of usual non-coupled estimator on the mesh $\tilde{\mathcal{T}}_h^{(4)}$

Figure 2.18.: Distribution of coupled error and estimator on the mesh $\tilde{\mathcal{T}}_h^{(4)}$ of $\tilde{\Omega}$ with Dofs=2395 using **Algorithm 1** where, $\text{tol}(\eta) = 10^{-2}$ and $\alpha = 0.1$

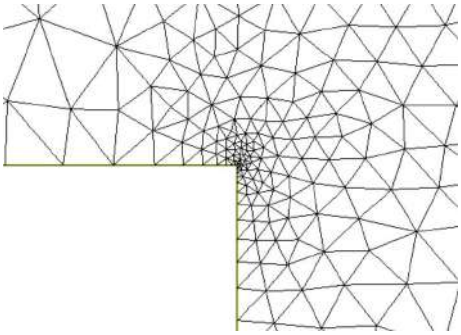

(a) Corner of the mesh $\tilde{\mathcal{T}}_h^{(4)}$

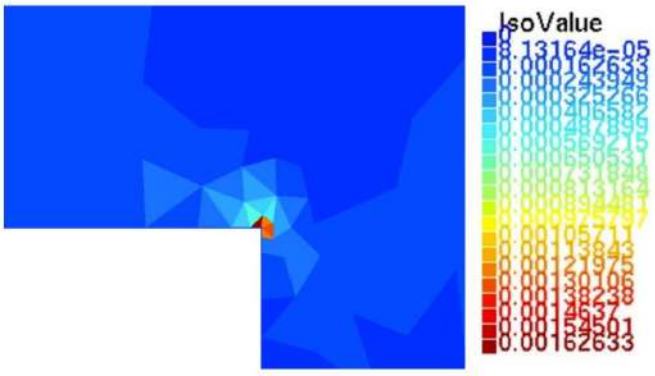

(b) Distribution of error on the corner of the mesh $\tilde{\mathcal{T}}_h^{(4)}$

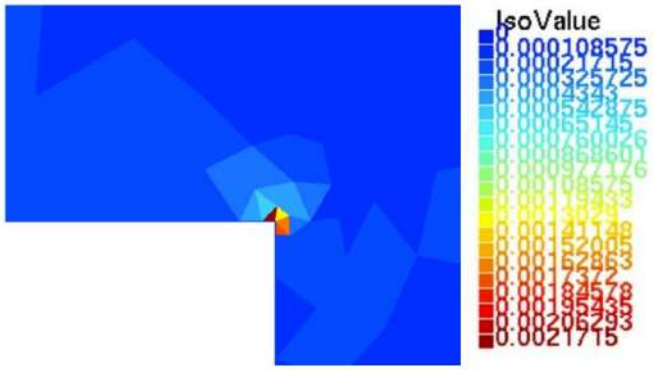

(c) Distribution of estimator on the corner of the mesh $\tilde{\mathcal{T}}_h^{(4)}$

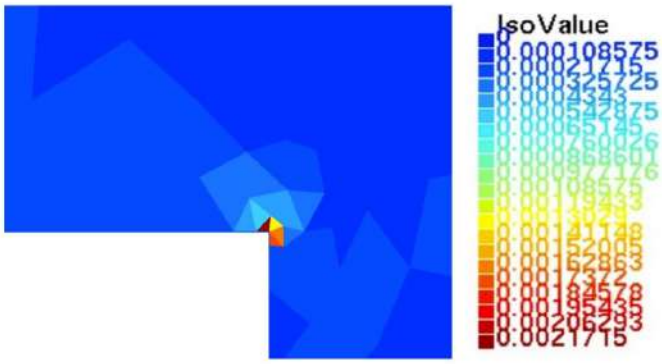

(d) Distribution of usual non-coupled estimator on the corner of the mesh $\tilde{\mathcal{T}}_h^{(4)}$

Figure 2.19.: Distribution of coupled error and estimator on the corner of the mesh $\tilde{\mathcal{T}}_h^{(4)}$ of $\tilde{\Omega}$ with Dofs=2395 using **Algorithm 1** where, $\text{tol}(\eta) = 10^{-2}$ and $\alpha = 0.1$

We do the same plots for **Algorithm 2** : see Figure 2.20 for the initial mesh and distributions for e, η and η^D, see Figure 2.21 for the first refinement level, Figure 2.22 for the last level of refinement and Figure 2.23 for the zoom in the corner.

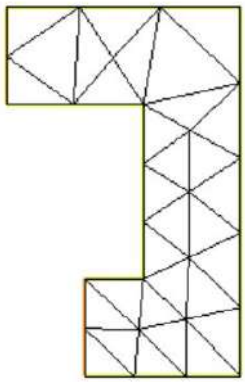

(a) Mesh $\tilde{\mathcal{T}}_h^{(0)}$ as an initial mesh before adapting.

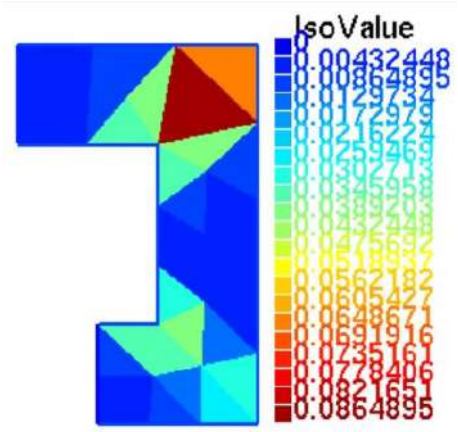

(b) Distribution of error on the mesh $\tilde{\mathcal{T}}_h^{(0)}$

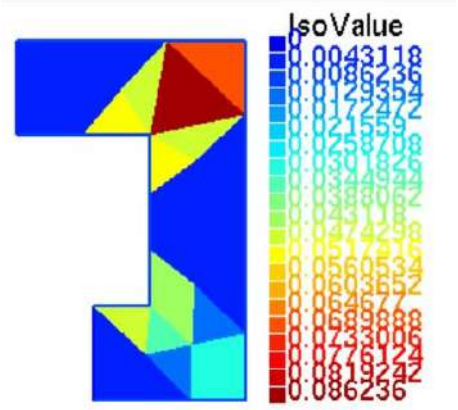

(c) Distribution of estimator on the mesh $\tilde{\mathcal{T}}_h^{(0)}$

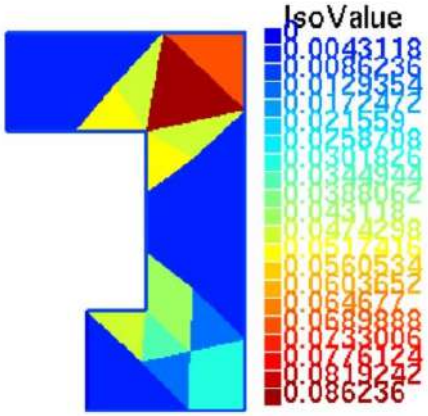

(d) Distribution of the estimator η^D for mesh $\tilde{\mathcal{T}}_h^{(0)}$

Figure 2.20.: Distribution of coupled error and estimator on the mesh $\tilde{\mathcal{T}}_h^{(0)}$ of $\tilde{\Omega}$ with Dofs=84 using **Algorithm 2** where, $\text{tol}(\eta) = 10^{-2}$ and $\alpha = 0.1$

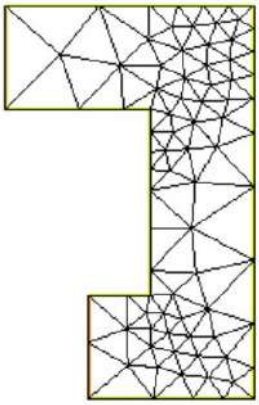

(a) Mesh $\tilde{\mathcal{T}}_h^{(1)}$ for the first adapting.

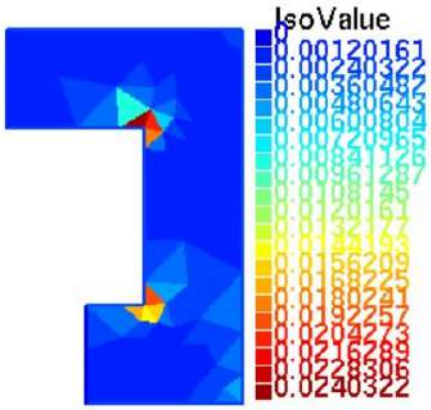

(b) Distribution of error on the mesh $\tilde{\mathcal{T}}_h^{(1)}$

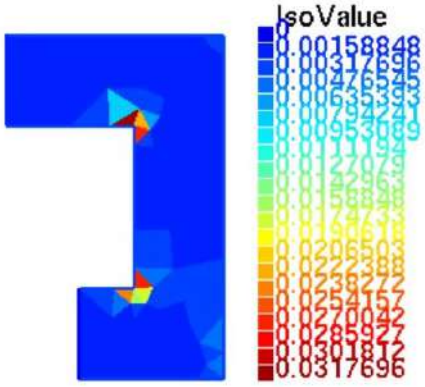

(c) Distribution of estimator on the mesh $\tilde{\mathcal{T}}_h^{(1)}$

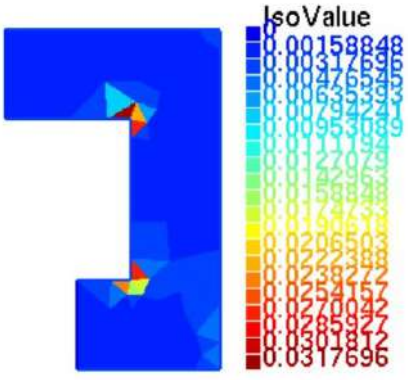

(d) Distribution of the estimator η^D for mesh $\tilde{\mathcal{T}}_h^{(1)}$

Figure 2.21.: Distribution of coupled error and estimator on the mesh $\tilde{\mathcal{T}}_h^{(1)}$ of $\tilde{\Omega}$ with Dofs=302 using **Algorithm 2** where, $\text{tol}(\eta) = 10^{-2}$ and $\alpha = 0.1$

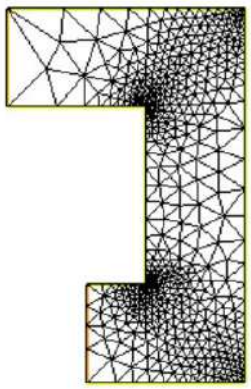

(a) Mesh $\tilde{\mathcal{T}}_h^{(4)}$ for the fourth adapting.

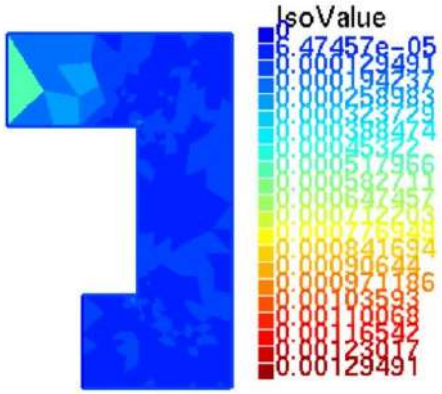

(b) Distribution of error on the mesh $\tilde{\mathcal{T}}_h^{(4)}$

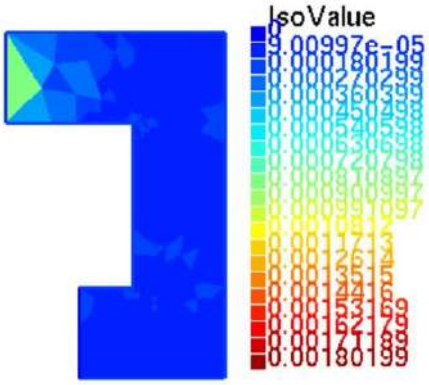

(c) Distribution of estimator on the mesh $\tilde{\mathcal{T}}_h^{(4)}$

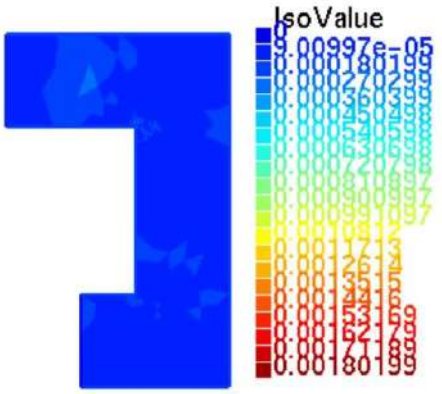

(d) Distribution of the estimator η^D on the mesh $\tilde{\mathcal{T}}_h^{(4)}$

Figure 2.22.: Distribution of coupled error and estimator on the mesh $\tilde{\mathcal{T}}_h^{(4)}$ of $\tilde{\Omega}$ with Dofs=2942 using **Algorithm 2** where, $\text{tol}(\eta) = 10^{-2}$ and $\alpha = 0.1$

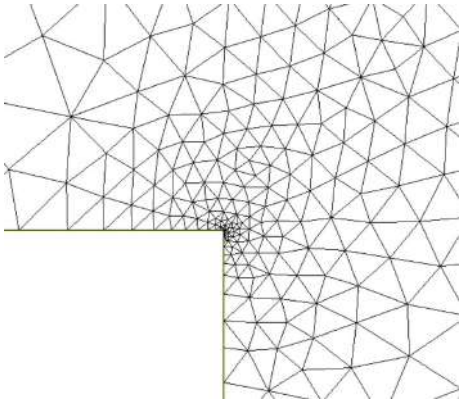

(a) Corner of the mesh $\tilde{\mathcal{T}}_h^{(4)}$

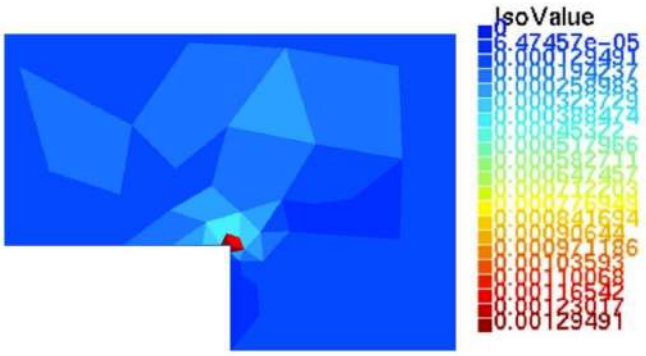

(b) Distribution of error on the corner of the mesh $\tilde{\mathcal{T}}_h^{(4)}$

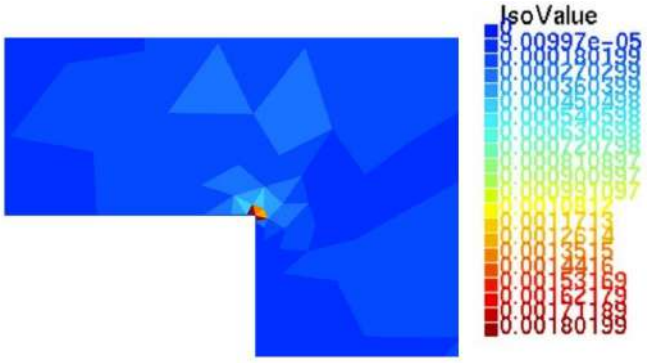

(c) Distribution of estimator on the corner of the mesh $\tilde{\mathcal{T}}_h^{(4)}$

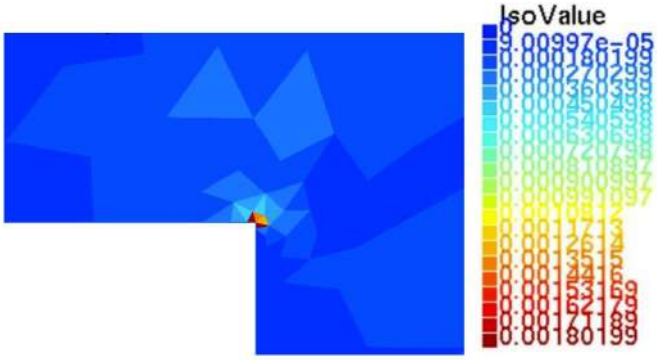

(d) Distribution of η^D on the corner of the mesh $\tilde{\mathcal{T}}_h^{(4)}$

Figure 2.23.: Distribution of coupled error and estimator on the corner of the mesh $\tilde{\mathcal{T}}_h^{(4)}$ of $\tilde{\Omega}$ with Dofs=2942 using **Algorithm 2** where, $\text{tol}(\eta) = 10^{-2}$ and $\alpha = 0.1$

For both cases the conclusions are the same : in general the distribution of the error e and the estimator η are locally almost the same, and after refining we see local contributions of e and η that appear also near the interface, meanwhile both distributions of η^{V} and ηD do not detect error near the interface but moreover an important error in the corners where we have singularity. Making refinements following η^{V} and ηD we verify a real decreasing of the error and the desired rate of convergence expected for a smooth test case.

In Table 2.3 and 2.4 one can see the convergence for the cases respectively with $\alpha = 0.25$ and $\alpha = 0.5$. The behaviors of both algorithms are practically the same, the difference is that the interface position chosen is $x^{\gamma} = 4.5$ and $x^{\gamma} = 4.6$ respectively.

Dof	e	η	Index	Rate
88	0.126743	0.147801	1.16615	-
301	0.0486227	0.0606712	1.2478	0.779
542	0.023844	0.0285502	1.19737	1.211
1272	0.00927946	0.0113015	1.21791	1.106
3462	0.0033839	0.00412536	1.21911	1.007

(a) Results using **Algorithm 1**

Dof	Error	η	Index	Rate
88	0.126743	0.147801	1.16615	-
297	0.0474781	0.0590356	1.24343	0.807
451	0.0243649	0.0299052	1.22739	1.597
1143	0.0102187	0.0123655	1.21009	0.934
2973	0.00369422	0.00444173	1.20235	1.079

(b) Results using **Algorithm 2**

Table 2.3.: Error e and estimator η w.r.t. degrees of freedom Dof for $\alpha = 0.25$

Dof	e	η	Index	Rate
88	0.117868	0.13842	1.17436	-
360	0.0452827	0.057106	1.2611	0.679
616	0.0234623	0.028229	1.20317	1.224
1117	0.0103151	0.0123804	1.20022	1.38
2986	0.00412791	0.00512294	1.24105	0.93

(a) Results using **Algorithm 1**

Dof	Error	η	Index	Rate
88	0.117868	0.13842	1.17436	-
360	0.0452499	0.057064	1.26108	0.679
490	0.024088	0.0287519	1.19362	2.045
1308	0.0095169	0.0113945	1.19729	0.945
3142	0.00378678	0.00472758	1.24844	1.051

(b) Results using **Algorithm 2**

Table 2.4.: Error e and estimator η w.r.t. degrees of freedom Dof for $\alpha = 0.5$

Test 2: $\text{tol}(\eta) = 10^{-3}$**:**
We run the two algorithms for $\alpha = 0.1$, the idea is that we want to achieve a reasonable tolerance for η^γ such that this contribution will be a smaller order or at most the same order of the local contributions of η^{V} (for Algorithm1) or of η^{D} (for Algorithm2) for the last level of refinement giving the desired final accuracy.
In Table 2.5 we see the convergence of the error e and the estimator η with respect to the dof obtained from the adaptive refined mesh. Let us notice that the interface position is $x^\gamma = 4.2$. We show also the index of efficiency $\frac{\eta}{e}$, named Index, and the convergence rate, named Rate, in Table 2.5. In the Table 2.5a we see the results for **Algorithm 1** and in Table 2.5b for **Algorithm 2**. The two adaptations are very similar and give quite same results: the optimal rate of convergence is restored and the given accuracy for η reached.
Concerning Algorithm1, in Figure 2.24 we plot the initial mesh (Figure 2.24a) corresponding to 84 Dof, the distributions of the error e, estimator η and the standard equilibrated estimator η^{V} (respectively in figure 2.24b, 2.24c and 2.24d).
In Figure 2.25 we plot the mesh coming from the first refinement level (with 282 Dof) with the distributions of e, η and η^{V} and in Figure 2.26 we plot the mesh coming from the last refinement level (that is a 6 refinement level with 25474 Dof) and the usual distributions.

Dof	e	η	Index	Rate
84	0.162116	0.183071	1.12926	-
282	0.0548775	0.0700119	1.27579	0.894
595	0.0269704	0.0325629	1.20735	0.951
1018	0.0112737	0.0133638	1.18539	1.168
2857	0.00395291	0.00473887	1.19883	1.015
7321	0.00134209	0.00157586	1.17418	1.147
25474	0.000394305	0.000478341	1.21312	0.982

(a) Results using **Algorithm 1**

Dof	Error	η	Index	Rate
84	0.162116	0.183071	1.12926	-
282	0.0548775	0.070012	1.27579	0.8944
529	0.0282411	0.0342134	1.21148	1.0560
986	0.0123483	0.0148866	1.20556	1.328
2177	0.00502207	0.00596826	1.18841	1.135
5992	0.00162056	0.00188328	1.16212	1.117
21726	0.000457287	0.000550204	1.20319	0.98

(b) Results using **Algorithm 2**

Table 2.5.: Error e and estimator η w.r.t. degrees of freedom Dof for $\alpha = 0.1$

We do the same plots for **Algorithm 2** : see Figure 2.27 for the initial mesh and distributions for e, η and η^D, see Figure 2.28 for the first refinement level, Figure 2.29 for the last level of refinement

For both cases the conclusions are the same as before : in general the distribution of the error e and the estimator η are locally almost the same, and after refining we see local contributions of e and η that appear also near the interface, meanwhile both distributions of η^{V} and η^{D} do not detect error near the interface but moreover an important error in the corners where we have singularity. Making refinements following η^{V} and η^{D} we verify a real decreasing of the error and the desired rate of convergence expected for a smooth test case.

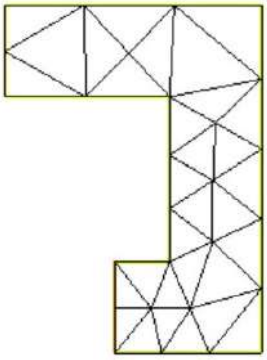

(a) Mesh $\tilde{\mathcal{T}}_h^{(0)}$ as an initial mesh before adapting.

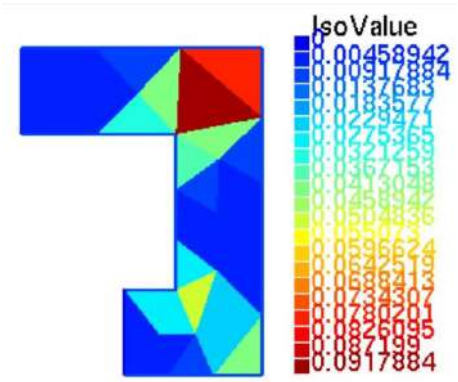

(b) Distribution of error on the mesh $\tilde{\mathcal{T}}_h^{(0)}$

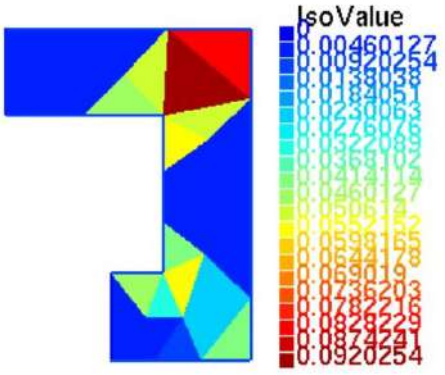

(c) Distribution of estimator on the mesh $\tilde{\mathcal{T}}_h^{(0)}$

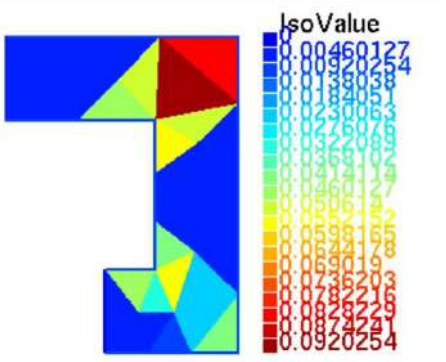

(d) Distribution of usual non-coupled estimator on the mesh $\tilde{\mathcal{T}}_h^{(0)}$

Figure 2.24.: Distribution of coupled error and estimator on the mesh $\tilde{\mathcal{T}}_h^{(0)}$ of $\tilde{\Omega}$ with Dofs=84 using **Algorithm 1** where, $\text{tol}(\eta) = 10^{-3}$ and $\alpha = 0.1$

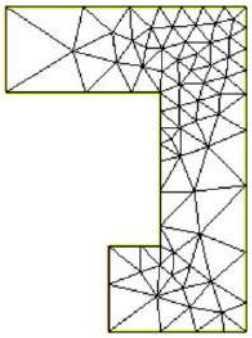

(a) Mesh $\tilde{\mathcal{T}}_h^{(1)}$ for the first adapting.

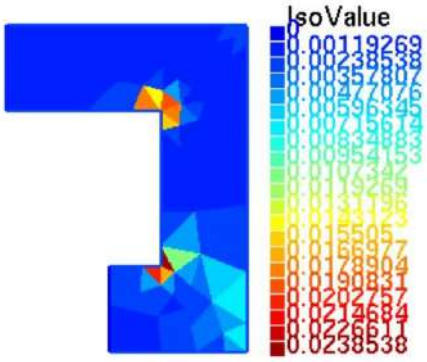

(b) Distribution of error on the mesh $\tilde{\mathcal{T}}_h^{(1)}$

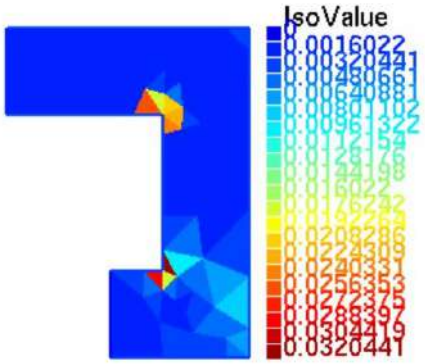

(c) Distribution of estimator on the mesh $\tilde{\mathcal{T}}_h^{(1)}$

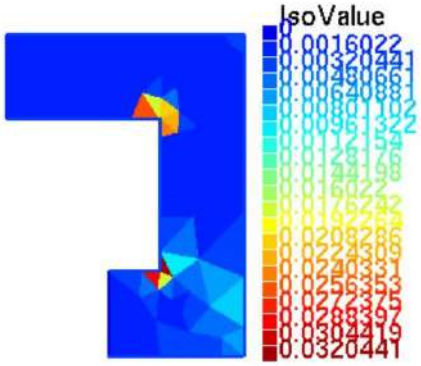

(d) Distribution of usual non-coupled estimator on the mesh $\tilde{\mathcal{T}}_h^{(1)}$

Figure 2.25.: Distribution of coupled error and estimator on the mesh $\tilde{\mathcal{T}}_h^{(1)}$ of $\tilde{\Omega}$ with Dofs=282 using **Algorithm 1** where, $\text{tol}(\eta) = 10^{-3}$ and $\alpha = 0.1$

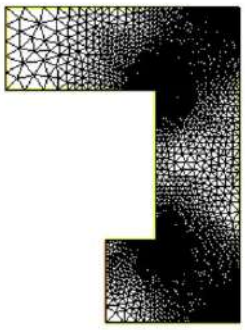

(a) Mesh $\tilde{\mathcal{T}}_h^{(6)}$ for the first adapting.

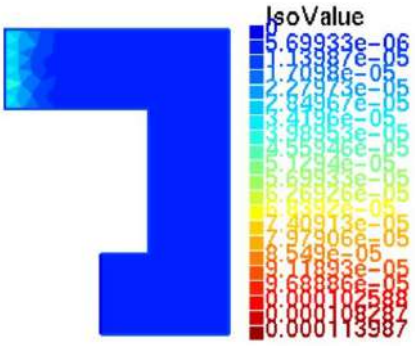

(b) Distribution of error on the mesh $\tilde{\mathcal{T}}_h^{(6)}$

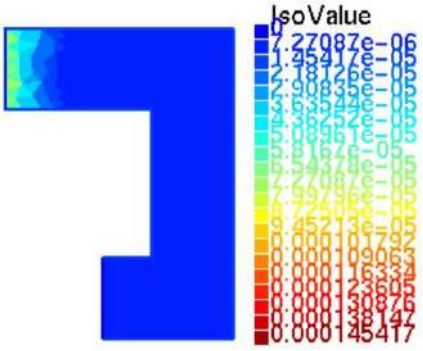

(c) Distribution of estimator on the mesh $\tilde{\mathcal{T}}_h^{(6)}$

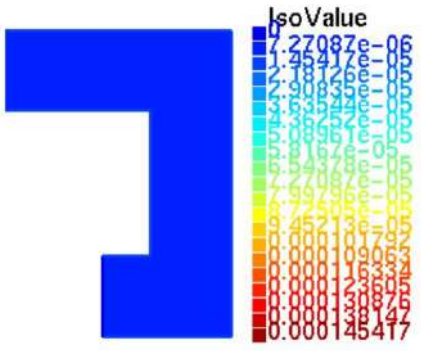

(d) Distribution of usual non-coupled estimator on the mesh $\tilde{\mathcal{T}}_h^{(6)}$

Figure 2.26.: Distribution of coupled error and estimator on the mesh $\tilde{\mathcal{T}}_h^{(6)}$ of $\tilde{\Omega}$ with Dofs=25474 using **Algorithm 1** where, $\text{tol}(\eta) = 10^{-3}$ and $\alpha = 0.1$

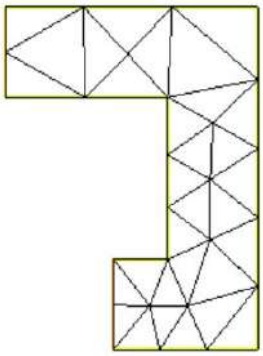

(a) Mesh $\tilde{\mathcal{T}}_h^{(0)}$ as an initial mesh before adapting.

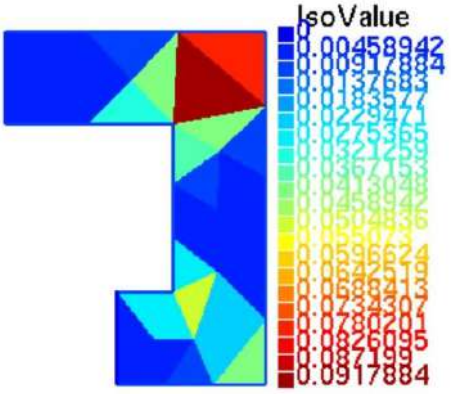

(b) Distribution of error on the mesh $\tilde{\mathcal{T}}_h^{(0)}$

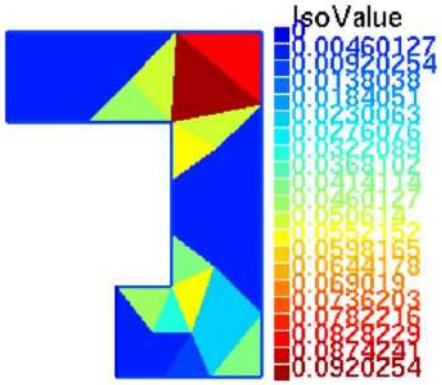

(c) Distribution of estimator on the mesh $\tilde{\mathcal{T}}_h^{(0)}$

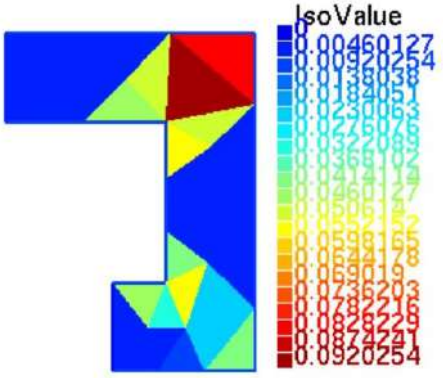

(d) Distribution of the estimator η^D on the mesh $\tilde{\mathcal{T}}_h^{(0)}$

Figure 2.27.: Distribution of coupled error and estimator on the mesh $\tilde{\mathcal{T}}_h^{(0)}$ of $\tilde{\Omega}$ with Dofs=84 using **Algorithm 2** where, $\text{tol}(\eta) = 10^{-3}$ and $\alpha = 0.1$

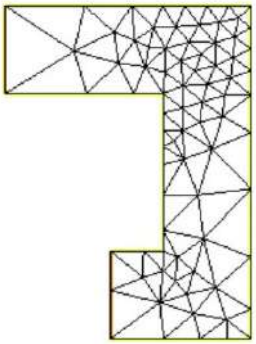

(a) Mesh $\tilde{\mathcal{T}}_h^{(1)}$ as an initial mesh before adapting.

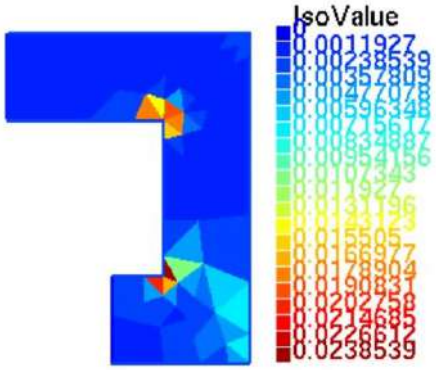

(b) Distribution of error on the mesh $\tilde{\mathcal{T}}_h^{(1)}$

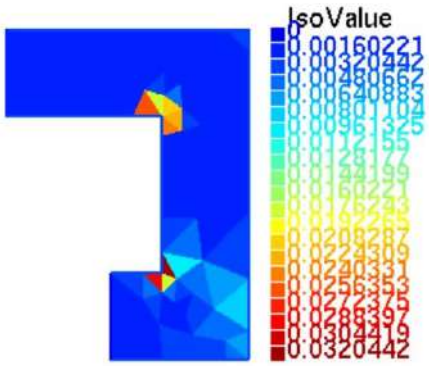

(c) Distribution of estimator on the mesh $\tilde{\mathcal{T}}_h^{(1)}$

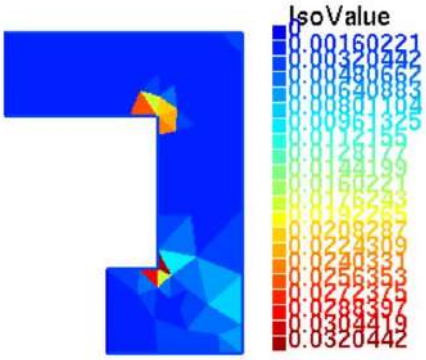

(d) Distribution of the estimator η^D on the mesh $\tilde{\mathcal{T}}_h^{(1)}$

Figure 2.28.: Distribution of coupled error and estimator on the mesh $\tilde{\mathcal{T}}_h^{(1)}$ of $\tilde{\Omega}$ with Dofs=282 using **Algorithm 2** where, $\text{tol}(\eta) = 10^{-3}$ and $\alpha = 0.1$

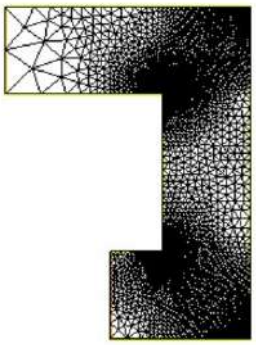

(a) Mesh $\tilde{\mathcal{T}}_h^{(6)}$ for the fourth adapting.

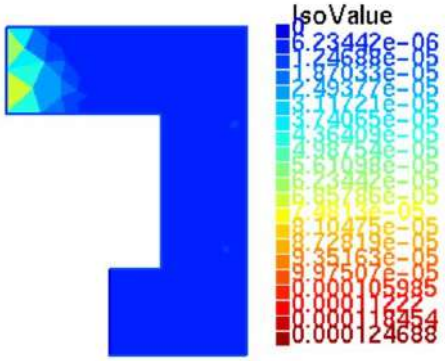

(b) Distribution of error on the mesh $\tilde{\mathcal{T}}_h^{(6)}$

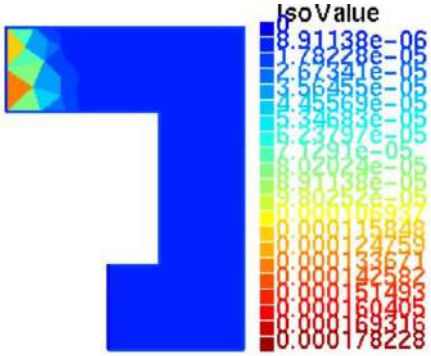

(c) Distribution of estimator on the mesh $\tilde{\mathcal{T}}_h^{(6)}$

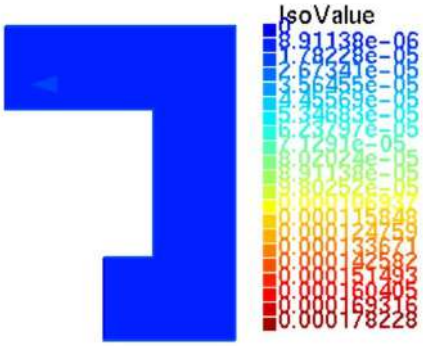

(d) Distribution of the estimator η^D on the mesh $\tilde{\mathcal{T}}_h^{(6)}$

Figure 2.29.: Distribution of coupled error and estimator on the mesh $\tilde{\mathcal{T}}_h^{(6)}$ of $\tilde{\Omega}$ with Dofs=21726 using **Algorithm 2** where, $\text{tol}(\eta) = 10^{-3}$ and $\alpha = 0.1$

Test 3: $\text{tol}(\eta) = 10^{-4}$**:**
We run the two algorithms for $\alpha = 0.1$, the idea is that we want to achieve a reasonable tolerance for η^γ such that this contribution will be a smaller order or at most the same order of the local contributions of η^{V} (for Algorithm1) or of η^{D} (for Algorithm2) for the last level of refinement giving the desired final accuracy.
In Table 2.6 we see the convergence of the error e and the estimator η with respect to the dof obtained from the adaptive refined mesh. Let us notice that the interface position is $x^\gamma = 3.8$. We show also the index of efficiency $\frac{\eta}{e}$, named Index, and the convergence rate, named Rate, in Table 2.6. In the Table 2.6a we see the results for **Algorithm 1** and in Table 2.6b for **Algorithm 2**. The two adaptations are very similar and give quite same results: the optimal rate of convergence is restored and the given accuracy for η reached.

Dof	e	η	Index	Rate
98	0.154895	0.176161	1.13729	-
347	0.0532323	0.0667582	1.25409	0.844
512	0.0260445	0.0315484	1.21133	1.837
1269	0.0104203	0.0126315	1.2122	1.009
2721	0.00384351	0.00457943	1.19147	1.307
8388	0.00120907	0.0014192	1.17379	1.0272
27531	0.000331174	0.000390075	1.17786	1.0895
106473	8.18902e-05	9.98675e-05	1.21953	1.033

(a) Results using **Algorithm 1**

Dof	Error	η	Index	Rate
98	0.154895	0.176161	1.13729	-
347	0.0532323	0.0667582	1.25409	0.8447
520	0.0255367	0.030641	1.19988	1.815
1495	0.00976458	0.0119389	1.22268	0.9103
3114	0.00359059	0.00425519	1.1851	1.3634
9427	0.0010187	0.00118431	1.16257	1.1373
34872	0.000254918	0.000299412	1.17454	1.0590
142309	5.95169e-05	7.7972e-05	1.31008	1.0343

(b) Results using **Algorithm 2**

Table 2.6.: Error e and estimator η w.r.t. degrees of freedom Dof for $\alpha = 0.1$

Concerning Algorithm 1, in Figure 2.30 we plot the initial mesh (Figure 2.30a) corresponding to 98 Dof, the distributions of the error e, estimator η and the standard equilibrated estimator η^{V} (respectively in figure 2.30b, 2.30c and 2.30d).
In Figure 2.31 we plot the mesh coming from the first refinement level (with 347 Dof) with the distributions of e, η and η^{V} and in Figure 2.32 we plot the mesh coming from the last refinement level (that is a 7 refinement level with 106473 Dof) and the usual distributions.

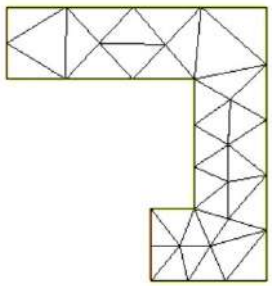

(a) Mesh $\tilde{\mathcal{T}}_h^{(0)}$ as an initial mesh before adapting.

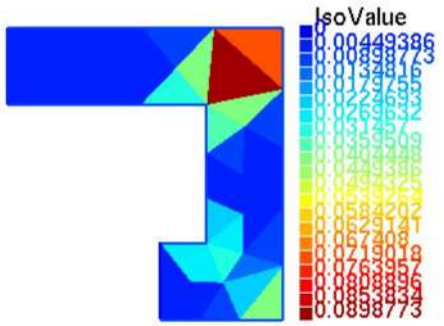

(b) Distribution of error on the mesh $\tilde{\mathcal{T}}_h^{(0)}$

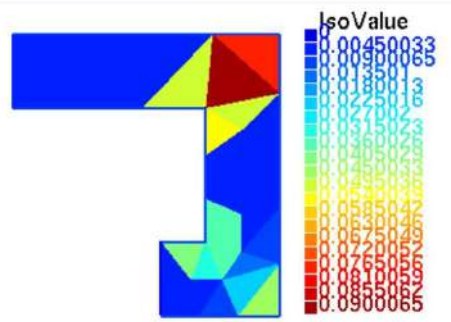

(c) Distribution of estimator on the mesh $\tilde{\mathcal{T}}_h^{(0)}$

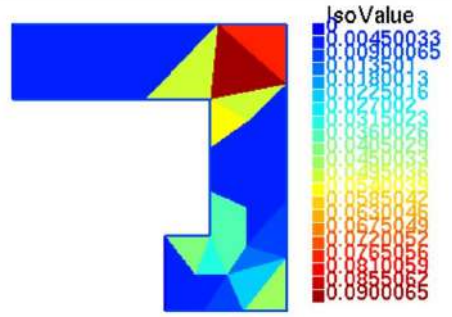

(d) Distribution of usual non-coupled estimator on the mesh $\tilde{\mathcal{T}}_h^{(0)}$

Figure 2.30.: Distribution of coupled error and estimator on the mesh $\tilde{\mathcal{T}}_h^{(0)}$ of $\tilde{\Omega}$ with Dofs=98 using **Algorithm 1** where, $\text{tol}(\eta) = 10^{-4}$ and $\alpha = 0.1$

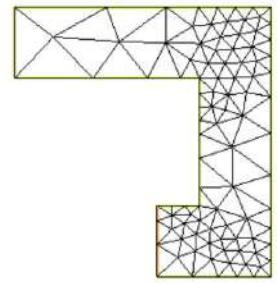

(a) Mesh $\tilde{\mathcal{T}}_h^{(1)}$ for the first adapting.

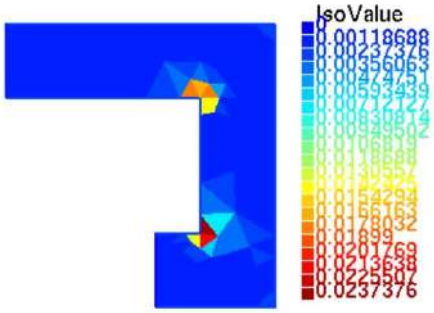

(b) Distribution of error on the mesh $\tilde{\mathcal{T}}_h^{(1)}$

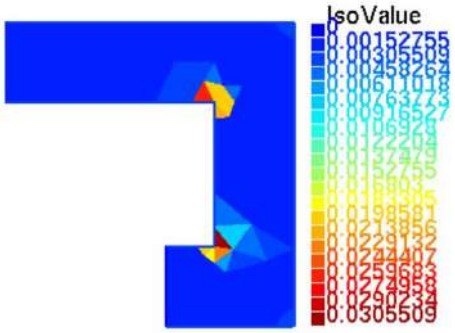

(c) Distribution of estimator on the mesh $\tilde{\mathcal{T}}_h^{(1)}$

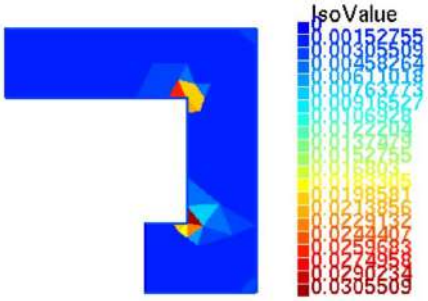

(d) Distribution of usual non-coupled estimator on the mesh $\tilde{\mathcal{T}}_h^{(1)}$

Figure 2.31.: Distribution of coupled error and estimator on the mesh $\tilde{\mathcal{T}}_h^{(1)}$ of $\tilde{\Omega}$ with Dofs=347 using **Algorithm 1** where, $\text{tol}(\eta) = 10^{-4}$ and $\alpha = 0.1$

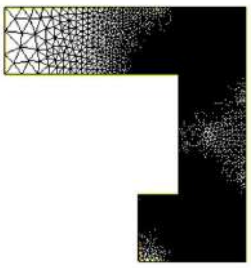

(a) Mesh $\tilde{\mathcal{T}}_h^{(7)}$ for the seven adapting.

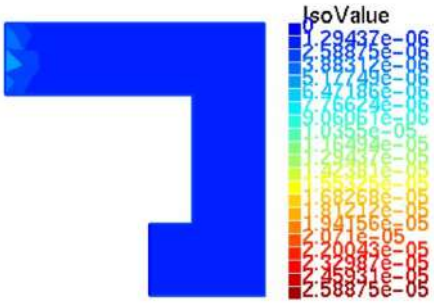

(b) Distribution of error on the mesh $\tilde{\mathcal{T}}_h^{(7)}$

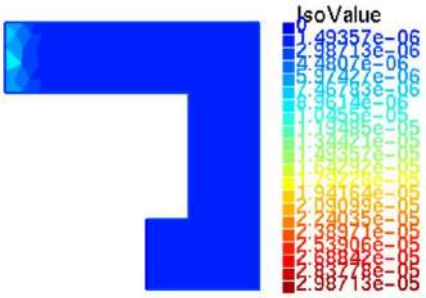

(c) Distribution of estimator on the mesh $\tilde{\mathcal{T}}_h^{(7)}$

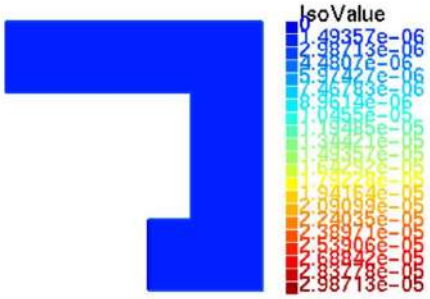

(d) Distribution of usual non-coupled estimator on the mesh $\tilde{\mathcal{T}}_h^{(7)}$

Figure 2.32.: Distribution of coupled error and estimator on the mesh $\tilde{\mathcal{T}}_h^{(7)}$ of $\tilde{\Omega}$ with Dofs=106473 using **Algorithm 1** where, $\text{tol}(\eta) = 10^{-4}$ and $\alpha = 0.1$

We do the same plots for **Algorithm 2** : see Figure 2.33 for the initial mesh and distributions for e, η and η^D, see Figure 2.34 for the first refinement level, Figure 2.35 for the last level of refinement

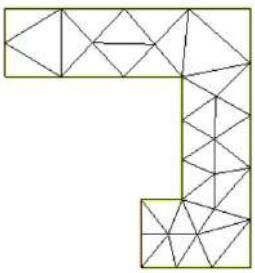

(a) Mesh $\tilde{\mathcal{T}}_h^{(0)}$ as an initial mesh before adapting.

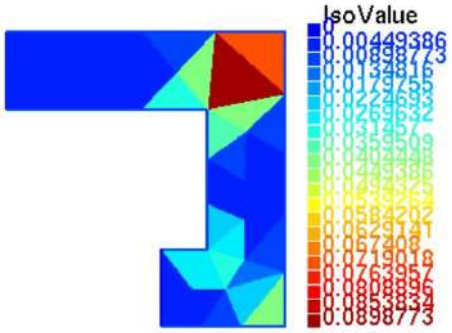

(b) Distribution of error on the mesh $\tilde{\mathcal{T}}_h^{(0)}$

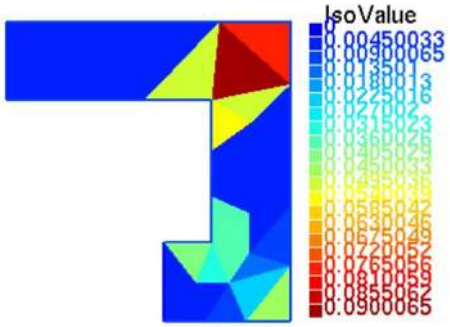

(c) Distribution of estimator on the mesh $\tilde{\mathcal{T}}_h^{(0)}$

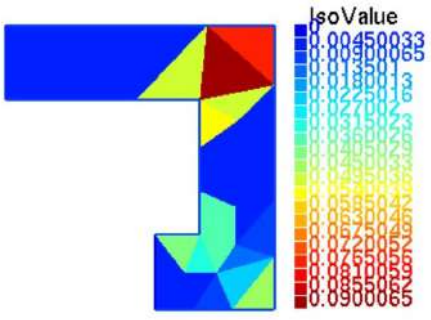

(d) Distribution of usual non-coupled estimator on the mesh $\tilde{\mathcal{T}}_h^{(0)}$

Figure 2.33.: Distribution of coupled error and estimator on the mesh $\tilde{\mathcal{T}}_h^{(0)}$ of $\tilde{\Omega}$ with Dofs=98 using **Algorithm 2** where, $\text{tol}(\eta) = 10^{-4}$ and $\alpha = 0.1$

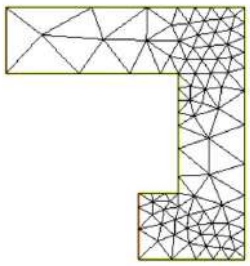

(a) Mesh $\tilde{\mathcal{T}}_h^{(1)}$ as an initial mesh before adapting.

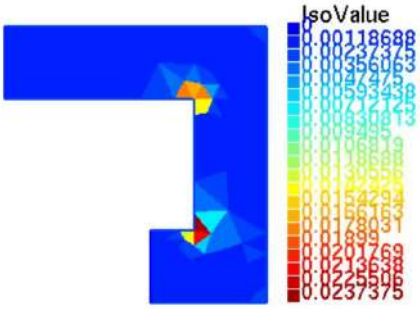

(b) Distribution of error on the mesh $\tilde{\mathcal{T}}_h^{(1)}$

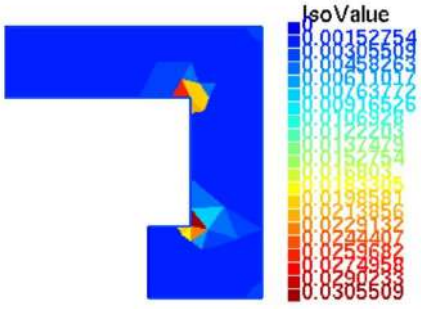

(c) Distribution of estimator on the mesh $\tilde{\mathcal{T}}_h^{(1)}$

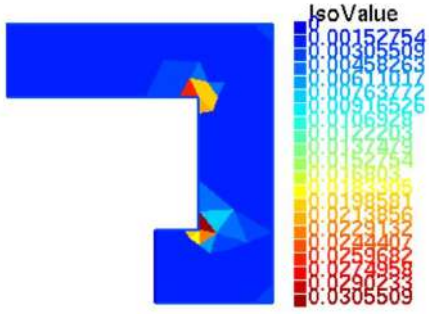

(d) Distribution of usual non-coupled estimator on the mesh $\tilde{\mathcal{T}}_h^{(1)}$

Figure 2.34.: Distribution of coupled error and estimator on the mesh $\tilde{\mathcal{T}}_h^{(1)}$ of $\tilde{\Omega}$ with Dofs=347 using **Algorithm 2** where, $\text{tol}(\eta) = 10^{-4}$ and $\alpha = 0.1$

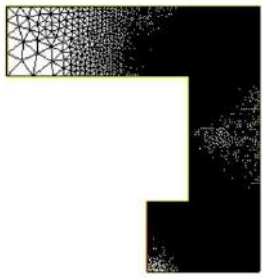

(a) Mesh $\tilde{\mathcal{T}}_h^{(7)}$ as an initial mesh before adapting.

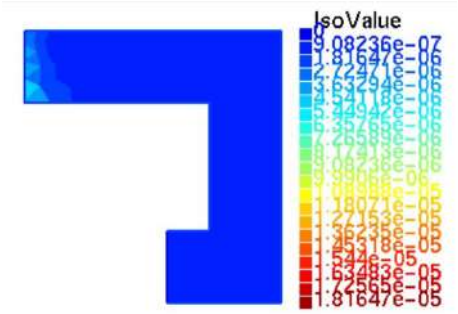

(b) Distribution of error on the mesh $\tilde{\mathcal{T}}_h^{(7)}$

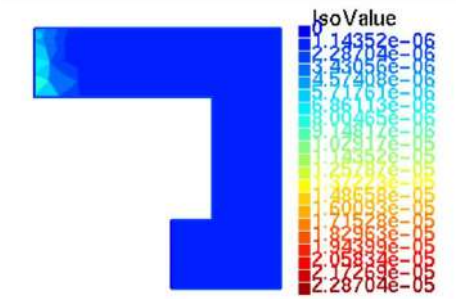

(c) Distribution of estimator on the mesh $\tilde{\mathcal{T}}_h^{(7)}$

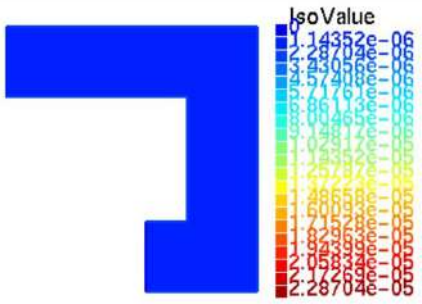

(d) Distribution of usual non-coupled estimator on the mesh $\tilde{\mathcal{T}}_h^{(7)}$

Figure 2.35.: Distribution of coupled error and estimator on the mesh $\tilde{\mathcal{T}}_h^{(7)}$ of $\tilde{\Omega}$ with Dofs=142309 using **Algorithm 2** where, $\text{tol}(\eta) = 10^{-4}$ and $\alpha = 0.1$

For both cases the conclusions are the same as before : in general the distribution of the error e and the estimator η are locally almost the same, and after refining we see local contributions of e and η that appear also near the interface, meanwhile both distributions of η^{V} and η^{D} do not detect error near the interface but moreover an important error in the corners where we have singularity. Making refinements following η^{V} and η^{D} we verify a real decreasing of the error and the desired rate of convergence expected for a smooth test case.

2.4. Poisson problem on a channels with several straight sections

In this section we will introduce more channels with more corners to generalize the previous study about coupling 0D/2D and determine the suitable positions of the interfaces for the whole channel and study a posteriori error for the whole domain Ω.
Let us now consider the whole domain Ω with more channels as in Figure 2.36.

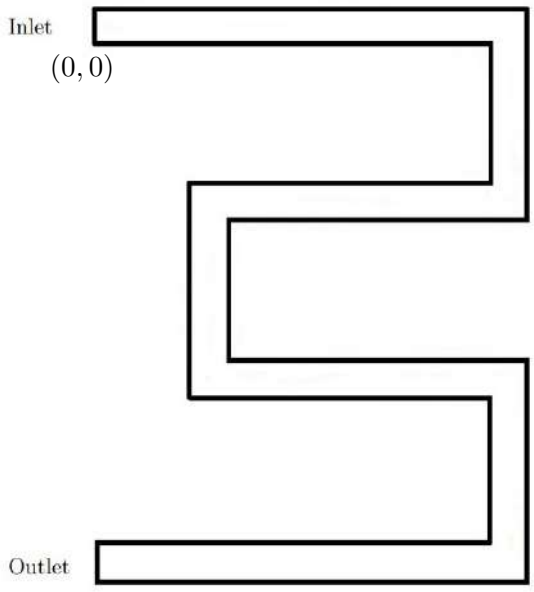

Figure 2.36.: New Domain Ω with more channels

As before we will take a very simple Poisson equation on the whole domain Ω. Let us recall it:

$$-\Delta u = f, \qquad \text{in} \quad \Omega, \tag{2.41a}$$
$$u = u_{\text{in}}, \qquad \text{on} \quad \Gamma_{\text{in}}, \tag{2.41b}$$
$$u = u_{\text{out}}, \qquad \text{on} \quad \Gamma_{\text{out}}, \tag{2.41c}$$
$$u = 0, \qquad \text{on} \quad \Gamma_{\text{wall}}, \tag{2.41d}$$

where, $f = \frac{12u_{av}}{R^2}$, $u_{\text{in}} = \frac{6u_{av}}{R^2}(R-y)y$ and $u_{\text{out}} = -\frac{6u_{av}}{R^2}\big(y+3W+3R\big)\big(y+3W+2R\big)$.
The weak formulation of system (2.41) is: Find $u \in H^1_g(\Omega)$ such that:

$$(\nabla u, \nabla v)_\Omega = (f, v)_\Omega \quad \forall v \in H_0^1(\Omega), \tag{2.42}$$

where,

$$H_0^1(\Omega) := \{u \in H^1(\Omega); \quad u = 0 \quad \text{on} \quad \partial\Omega\},$$
$$H_g^1(\Omega) := \{u \in H^1(\Omega); \quad u = u_g \quad \text{on} \quad \partial\Omega\}$$

and

$$u_g = \begin{cases} u = u_{in} & \text{on} \quad \Gamma_{\text{in}}, \\ u = u_{out} & \text{on} \quad \Gamma_{\text{out}}, \\ u = 0 & \text{on} \quad \Gamma. \end{cases}$$

2.4.1. Coupled System

Let us introduce the simplified model as simplified 0D models in $D_1^{(i)}$ domains and the non simplified 2D models in $D_2^{(i)}$ domains such that $\Omega = \left(\cup_{i=1}^{7} D_1^{(i)}\right) \cup \left(\cup_{i=1}^{6} D_2^{(i)}\right)$ as in Figure 2.37. Let $\gamma_1^{(i)}$ and $\gamma_2^{(i)}$ be the inlet and outlet interfaces of $D_2^{(i)}$ domains respectively and let $\Gamma^{(i)}$ be the wall of $D_2^{(i)}$ domains. Let $D_2 = \cup_{i=1}^{6} D_2^{(i)}$ which is the collection of regions where have 2D models are dominance and $D_1 = \cup_{i=1}^{7} D_1^{(i)}$ be collection of regions where we have 0D models as in Figure 2.37.

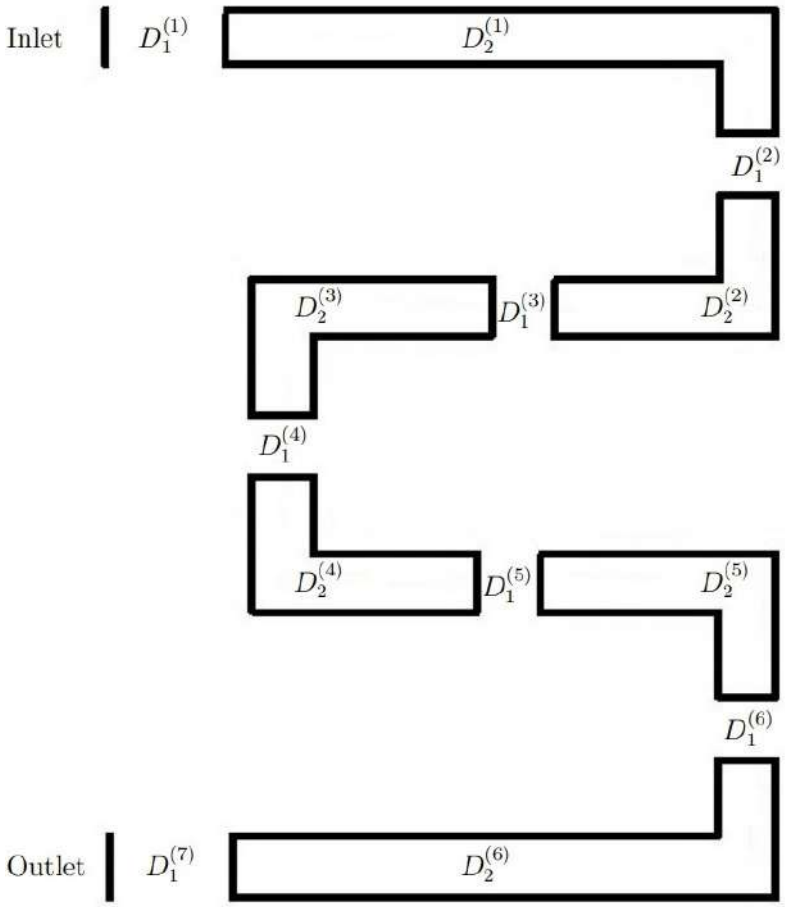

Figure 2.37.: Coupled 0D/2D model in the whole domain Ω

The simplified 0D models $u_1^{(i)}$ are defined on each domain $D_1^{(i)}$ by:

$$u_1^{(i)} = Poiseuille(i) \quad \text{in} \quad D_1^{(i)}. \tag{2.43}$$

The non simplified models in each $D_2^{(i)}$ consists to find $\tilde{u}^{(i)}$ in $D_2^{(i)}$ such that:

$$\begin{cases} -\Delta\tilde{u}^{(i)} = \frac{12u_{av}}{R^2}, & \text{in} \quad D_2^{(i)}, \\ \tilde{u}^{(i)} = u_{in}^{(i)} = u_1^{(i)}, & \text{on} \quad \gamma_1^{(i)}, \\ \tilde{u}^{(i)} = u_{out}^{(i)} = u_1^{(i+1)}, & \text{on} \quad \gamma_2^{(i)}, \\ \tilde{u}^{(i)} = 0, & \text{on} \quad \Gamma^{(i)}, \end{cases} \tag{2.44}$$

where, $u_{in}^{(i)}$ and $u_{out}^{(i)}$ are the inlet and the outlet respectively in the domains $D_2^{(i)}$.
We have the continuity coupled conditions on the inlet $\gamma_1^{(i)}$ of the domain $D_2^{(i)}$:

$$\tilde{u}^{(i)} = u_1^{(i)} \quad \text{on} \quad \gamma_1^{(i)}. \tag{2.45}$$

We have the continuity coupled conditions on the outlet $\gamma_2^{(i)}$ of the domain $D_2^{(i)}$:

$$\tilde{u}^{(i)} = u_1^{(i+1)} \quad \text{on} \quad \gamma_2^{(i)}. \tag{2.46}$$

Let us consider the variational formulation of system (2.44): Find $\tilde{u}^{(i)} \in H_g^1(D_2^{(i)})$ such that:

$$(\nabla\tilde{u}^{(i)}, \nabla\tilde{v}^{(i)})_{D_2^{(i)}} = (f, \tilde{v}^{(i)})_{D_2^{(i)}} \qquad \forall\tilde{v}^{(i)} \in H_0^1(D_2^{(i)}) \tag{2.47}$$

where,

$$H_g^1(D_2^{(i)}) := \{\tilde{u}^{(i)} \in H^1(D_2^{(i)}); \quad \tilde{u}^{(i)} = \tilde{u}_g^{(i)} \quad \text{on} \quad \partial(D_2^{(i)})\}$$

and

$$\tilde{u}_g^{(i)} = \begin{cases} \tilde{u}^{(i)} = u_{in}^{(i)} = u_1^{(i)} & \text{on} \quad \gamma_1^{(i)}, \\ \tilde{u}^{(i)} = u_{out}^{(i)} = u_1^{(i+1)} & \text{on} \quad \gamma_2^{(i)}, \\ \tilde{u}^{(i)} = 0 & \text{on} \quad \Gamma^{(i)}. \end{cases}$$

Let $\tilde{\mathcal{T}}_h^{(i)}$ be a regular triangular mesh on $D_2^{(i)}$. Introduce the FE spaces

- $\tilde{V}_h^{(i)} := \{\tilde{v}_h^{(i)} \quad \text{continuous on} \quad D_2^{(i)} \quad \text{such that:} \quad \tilde{v}_h^{(i)}|_{D_2^{(i)}} \in \mathbb{P}_k(\tilde{\mathcal{T}}_h^{(i)})\}$,
- $\tilde{V}_{h,g}^{(i)} := \{\tilde{v}_h^{(i)} \in \tilde{V}_h^{(i)} \quad \text{such that:} \quad \tilde{v}_h^{(i)}|_{\partial(D_2^{(i)})} = \tilde{u}_g^{(i)}\}$,
- $\tilde{V}_{h,0}^{(i)} := \{\tilde{v}_h^{(i)} \in \tilde{V}_h^{(i)} \quad \text{such that:} \quad \tilde{v}_h^{(i)}|_{\partial(D_2^{(i)})} = 0\}$.

Now, we discretize the problem of system (2.47) above as: find $\tilde{u}_h^{(i)} \in \tilde{V}_{h,g}^{(i)}$, such that

$$(\nabla\tilde{u}_h^{(i)}, \nabla\tilde{v}_h^{(i)})_{D_2^{(i)}} = (f, \tilde{v}_h^{(i)})_{D_2^{(i)}} \quad \forall\tilde{v}_h^{(i)} \in \tilde{V}_{h,0}^{(i)}. \tag{2.48}$$

Then the approximate solution on the whole Ω is reconstructed as

$$u_h^s = \begin{cases} u_1^{(i)} \text{ in } D_1^{(i)} \\ \tilde{u}_h^{(i)} \text{ in } D_2^{(i)} \end{cases}. \tag{2.49}$$

2.4.2. *A posteriori* error estimates

In this section we are going to study *a posteriori* error estimator for whole domain Ω i.e. Ω will be as in Figure 2.36. We will introduce the flux reconstruction for all the coupled 0D/2D model in the whole domain Ω as in Figure 2.37. We will detect the positions of all these interfaces in Figure 2.37 by introducing the interfaces estimators η^γ for all interfaces γ as we did in Section 2.2

Definition 2.15 (Flux σ)**.** *Let u be the solution of system (2.42) then, we denote the flux by: $\sigma := -\nabla u$.*

Proposition 2.16 (Properties of weak solution of system (2.42))**.** *Let u be solution of system (2.42) and let σ be defined as in Defonition 2.15. Then, $u \in H^1_g(\Omega)$, $\sigma \in H(\mathrm{div}, \Omega)$ and $\nabla \cdot \sigma = f$.*

Proposition 2.17 (Properties of approximate solution u_h^s))**.** *Let u_h^s be the approximate solution defined by (2.48)–(2.49). Then $u_h^s \in H^1_g(\Omega)$, $-\nabla u_h^s \notin H(\mathrm{div}, \Omega)$ and $\nabla\cdot(-\nabla u_h^s) \neq f$ in general.*

Stress Reconstruction

Let u_h^s be the approximate solution defined by (2.48)–(2.49). We look for stress $\sigma_h \in \Sigma_h \subset H(\mathrm{div}, \Omega)$ such that:

$$\sigma_h^{\text{ideal}} := \underset{\substack{v_h \in \Sigma_h, \\ \mathrm{div}\, v_h = \Pi_{Q_h}(f) = f \text{on } \Omega}}{\arg\min} ||\nabla u_h^s + v_h||_{L^2(\Omega)}. \tag{2.50}$$

In practice, Σ_h will be RT_k on $D_2^{(i)}$ and $H(\mathrm{div}, D_1^{(i)})$ on $D_1^{(i)}$ and Q_h will be $\mathbb{P}_k(\tilde{\mathcal{T}}_h^{(i)})$ on $D_2^{(i)}$ and $L^2(D_1^{(i)})$ on $D_1^{(i)}$. Computing σ_h as the solution of (2.50): σ_h^{ideal} would be too costly, so we localize this minimization. For each vertex $a \in D_2^{(i)} \backslash (\gamma_1^{(i)} \cup \gamma_2^{(i)})$ we consider a patch $\omega_a^{(i)}$ to be the collection of all triangles that share this vertex a i.e. $\omega_a^{(i)} = \mathrm{supp}(\psi_a^{(i)})$, where $\psi_a^{(i)}$ is a hat function i.e. a polynomial of degree 1 that takes the value 1 at the node a and 0 on the other nodes different from a in the mesh $\tilde{\mathcal{T}}_h^{(i)}$ of the domain $D_2^{(i)}$. Let $\mathcal{V}_{h,*}^{(i)}$ be the vertices of $D_2^{(i)} \backslash (\gamma_1^{(i)} \cup \gamma_2^{(i)})$. Let $\omega_{\gamma_1}^{(i)} = \mathrm{supp}(\psi_{h,\gamma_1}^{(i)})$ and $\omega_{\gamma_2}^{(i)} = \mathrm{supp}(\psi_{h,\gamma_2}^{(i)})$ where $\psi_{h,\gamma_1}^{(i)}$ and $\psi_{h,\gamma_2}^{(i)}$ are *a posteriori* error indicators for the two interfaces $\gamma_1^{(i)}$ and $\gamma_2^{(i)}$ respectively, they are a piecewise affine (on mesh $\tilde{\mathcal{T}}_h^{(i)}$) version of $\psi_{\gamma_1}^{(i)}$ and $\psi_{\gamma_2}^{(i)}$ respectively and they are defined in a similar way of *a posteriori* error indicator in (2.15). For example, if we take the domain $D_2^{(1)}$ in Figure 2.37 then, our notations are shown in Figure 2.38. The inlet and outlet interfaces $\gamma_1^{(1)}$ and $\gamma_2^{(1)}$ of $D_2^{(1)}$ are located at $x = x_{\gamma_1}^{(1)}$ and $y = y_{\gamma_2}^{(1)}$ respectively. We can now define *a posteriori* error indicators $\psi_{h,\gamma_1}^{(1)}$ and $\psi_{h,\gamma_2}^{(1)}$ by:

$$\psi_{h,\gamma_1}^{(1)}(x,y) = \begin{cases} \sum_{a:\text{all the nodes of } \tilde{\mathcal{T}}_h^{(1)}} \psi_{\gamma_1}^{(1)}(a)\psi_a^{(1)}(x,y) & \text{for (x,y)} \in D_2^{(1)}, \\ 1 & \text{for (x,y)} \in D_1^{(1)}, \end{cases}$$

where, $\psi_a^{(1)}$ is a hat function associated to the node a and

$$\psi_{\gamma_1}^{(1)}(x,y) = \begin{cases} 1, & \text{for} \quad x < x_{\gamma_1}^{(1)}, \\ \frac{x_{\gamma_1}^{(1)}+R-x}{R}, & \text{for} \quad x \in [x_{\gamma_1}^{(1)}, x_{\gamma_1}^{(1)}+R], \\ 0, & \text{for} \quad x > x_{\gamma_1}^{(1)}+R. \end{cases}$$

Similarly,

$$\psi_{h,\gamma_2}^{(1)}(x,y) = \begin{cases} \sum_{a:\text{all the nodes of } \tilde{\mathcal{T}}_h^{(1)}} \psi_{\gamma_2}^{(1)}(a)\psi_a^{(1)}(x,y) & \text{for (x,y)} \in D_2^{(1)}, \\ 1 & \text{for (x,y)} \in D_1^{(2)}, \end{cases}$$

where

$$\psi_{\gamma_2}^{(1)}(x,y) = \begin{cases} 1, & \text{for} \quad y < y_{\gamma_2}^{(1)}, \\ \frac{y_{\gamma_2}^{(1)}+R-y}{R}, & \text{for} \quad y \in [y_{\gamma_2}^{(1)}, y_{\gamma_2}^{(1)}+R], \\ 0, & \text{for} \quad y > y_{\gamma_2}^{(1)}+R. \end{cases}$$

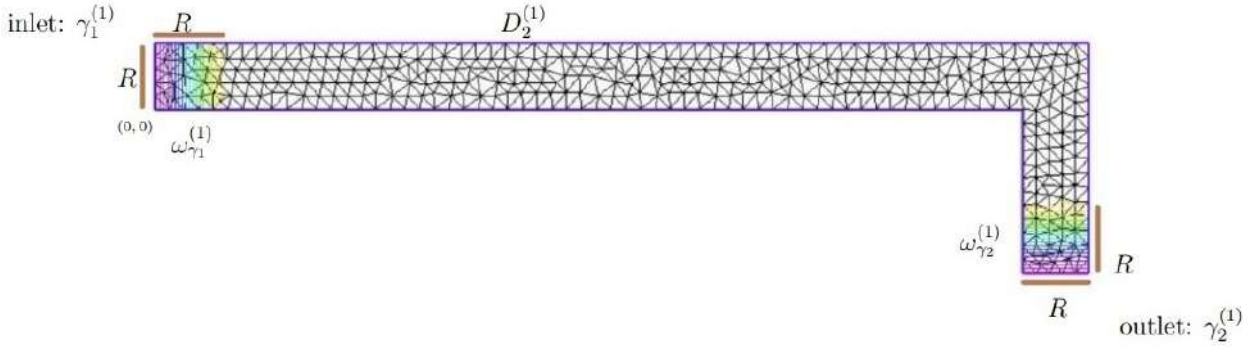

Figure 2.38.: Patches $\omega_{\gamma_1^{(1)}}$ in the inlet of $D_2^{(1)}$ on interface $\gamma_1^{(1)}$ and $\omega_{\gamma_2^{(1)}}$ in the outlet of $D_2^{(1)}$ on interface $\gamma_2^{(1)}$

Let N be the total number of 2D domains i.e. we have the 2D domains $D_2^{(i)}$ for $i = 1 \dots N$.
In a similar way we can introduce $\psi_{\gamma_1}^{(i)}$, $\psi_{\gamma_2}^{(i)}$, $\psi_{h,\gamma_1}^{(i)}$ and $\psi_{h,\gamma_2}^{(i)}$ for all $i = 1 \dots N$ then, we introduce the partition of unity:

$$\begin{aligned} \mathbb{1}_\Omega &= \sum_{i=1}^{N+1} \mathbb{1}_{D_1^{(i)}} + \sum_{i=1}^{N} \mathbb{1}_{D_2^{(i)}} \\ &= \sum_{i=1}^{N+1} \mathbb{1}_{D_1^{(i)}} + \sum_{i=1}^{N} \left(\psi_{h,\gamma_1}^{(i)} + \psi_{h,\gamma_2}^{(i)} + \sum_{a \,\in\, \mathcal{V}_{h,*}^{(i)}} \big(1 - \psi_{\gamma_1}^{(i)}(a) - \psi_{\gamma_2}^{(i)}(a)\big)\psi_a^{(i)} \right). \end{aligned}$$

Let us recall that $\psi_a^{(i)}$ is the hat function for any mesh node a in $D_2^{(i)}$ excluding those in $\gamma_1^{(i)}$ and $\gamma_2^{(i)}$ and $\mathcal{V}_{h,*}^{(i)}$ includes the vertices of $D_2^{(i)} \backslash (\gamma_1^{(i)} \cup \gamma_2^{(i)})$. Now, we replace σ_h^{ideal} in

(2.50) by:

$$\sigma_h = \underbrace{\sum_{i=1}^{N}\Big(\sigma_{h,\gamma_1}^{(i)} + \sigma_{h,\gamma_2}^{(i)} + \sum_{a\in\mathcal{V}_{h,*}^{(i)}}\big(1-\psi_{\gamma_1}^{(i)}(a)-\psi_{\gamma_2}^{(i)}(a)\big)\sigma_{h,a}^{(i)}\Big)\mathbb{1}_{D_2^{(i)}}}_{\sigma_h^{D_2}} + \underbrace{\sum_{i=1}^{N+1}\Big(-\nabla u_1^{(i)}\Big)\mathbb{1}_{D_1^{(i)}}}_{\sigma^{D_1}} \tag{2.51}$$

where for each $a \in \mathcal{V}_{h,*}^{(i)}$, we define $\sigma_{h,a}^{(i)} \in \Sigma_{h,a}^{(i)}$ by

$$\sigma_{h,a}^{(i)} := \underset{\substack{v_{h,a}^{(i)}\in\Sigma_{h,a}^{(i)},\\ \operatorname{div} v_{h,a}^{(i)}=\Pi_{Q_{h,a}^{(i)}}\left(\psi_a^{(i)}\cdot f-\nabla\psi_a^{(i)}\cdot\nabla\tilde{u}_h^{(i)}\right)}}{\arg\min} ||v_{h,a}^{(i)} + \psi_a^{(i)}\nabla\tilde{u}_h^{(i)}||_{L^2(\omega_a^{(i)})}$$

on the interface $\gamma_1^{(i)}$ we define $\sigma_{h,\gamma_1}^{(i)} \in \Sigma_{h,\gamma_1}^{(i)}$ by

$$\sigma_{h,\gamma_1}^{(i)} := \underset{\substack{v_{h,\gamma_1}^{(i)}\in\Sigma_{h,\gamma_1}^{(i)},\\ \operatorname{div} v_{h,\gamma_1}^{(i)}=\Pi_{Q_{h,\gamma_1}^{(i)}}\left(\psi_{h,\gamma_1}^{(i)}\cdot f-\nabla\psi_{h,\gamma_1}^{(i)}\cdot\nabla\tilde{u}_h^{(i)}\right)}}{\arg\min} ||v_{h,\gamma_1}^{(i)} + \psi_{h,\gamma_1}^{(i)}\nabla\tilde{u}_h^{(i)}||_{L^2(\omega_{\gamma_1}^{(i)})}$$

and on the interface $\gamma_2^{(i)}$ we define $\sigma_{h,\gamma_2}^{(i)} \in \Sigma_{h,\gamma_2}^{(i)}$ by

$$\sigma_{h,\gamma_2}^{(i)} := \underset{\substack{v_{h,\gamma_2}^{(i)}\in\Sigma_{h,\gamma_2}^{(i)},\\ \operatorname{div} v_{h,\gamma_2}^{(i)}=\Pi_{Q_{h,\gamma_2}^{(i)}}\left(\psi_{h,\gamma_2}^{(i)}\cdot f-\nabla\psi_{h,\gamma_2}^{(i)}\cdot\nabla\tilde{u}_h^{(i)}\right)}}{\arg\min} ||v_{h,\gamma_2}^{(i)} + \psi_{h,\gamma_2}^{(i)}\nabla\tilde{u}_h^{(i)}||_{L^2(\omega_{\gamma_2}^{(i)})}$$

where,

Case 1: a in an internal node of $D_2^{(i)}$

$\Sigma_{h,a}^{(i)} := \{\sigma_h \in RT_k(\omega_a^{(i)}), \sigma_h\cdot n = 0 \quad \text{on} \quad \partial\omega_a^{(i)}\}$,
$Q_{h,a}^{(i)} := \{q_h \in L^2(\omega_a^{(i)}), q_h|_K \in \mathbb{P}_k(K), \forall K \in \omega_a^{(i)}, \int_{\omega_a^{(i)}} q_h = 0\}$.

Case 2: a on the wall of $D_2^{(i)}\backslash(\gamma_1^{(i)} \cup \gamma_2^{(i)})$

$\Sigma_{h,a}^{(i)} := \{\sigma_h \in RT_k(\omega_a^{(i)}), \sigma_h\cdot n = 0 \quad \text{on} \quad \partial\omega_a^{(i)}\backslash\partial(D_2^{(i)})\}$,
$Q_{h,a}^{(i)} := \{q_h \in L^2(\omega_a^{(i)}), q_h|_K \in \mathbb{P}_k(K), \forall K \in \omega_a^{(i)}\}$.

Case 3: $a = \gamma_1^{(i)}$

$\Sigma_{h,\gamma_1}^{(i)} := \{\sigma_h \in RT_k(\omega_{\gamma_1}^{(i)}), \sigma_h\cdot n = 0 \quad \text{on} \quad \partial\omega_{\gamma_1}^{(i)}\backslash\partial(D_2^{(i)}) \quad \text{and} \quad \sigma_h\cdot n = (-\nabla u_1^{(i)})\cdot n = 0 \quad \text{on} \quad \gamma_1^{(i)}\}$,
$Q_{h,\gamma_1}^{(i)} := \{q_h \in L^2(\omega_{\gamma_1}^{(i)}), q_h|_K \in \mathbb{P}_k(K), \forall K \in \omega_{\gamma_1}^{(i)}\}$.

Case4: $a = \gamma_2^{(i)}$

$\Sigma_{h,\gamma_2}^{(i)} := \{\sigma_h \in RT_k(\omega_{\gamma_2}^{(i)}), \sigma_h\cdot n = 0 \quad \text{on} \quad \partial\omega_{\gamma_2}^{(i)}\backslash\partial(D_2^{(i)}) \quad \text{and} \quad \sigma_h\cdot n = (-\nabla u_1^{(i+1)})\cdot n = 0 \quad \text{on} \quad \gamma_2^{(i)}\}$,
$Q_{h,\gamma_2}^{(i)} := \{q_h \in L^2(\omega_{\gamma_2}^{(i)}), q_h|_K \in \mathbb{P}_k(K), \forall K \in \omega_{\gamma_2}^{(i)}\}$.

$\Pi_{Q_{h,a}^{(i)}}$ is the $L^2(\omega_a^{(i)})$-orthogonal projection, $\Pi_{Q_{h,\gamma_1}^{(i)}}$ is the $L^2(\omega_{\gamma_1}^{(i)})$-orthogonal projection and $\Pi_{Q_{h,\gamma_2}^{(i)}}$ is the $L^2(\omega_{\gamma_2}^{(i)})$-orthogonal projection. But $\sigma_{h,a}^{(i)}$, $\sigma_{h,\gamma_1}^{(i)}$ and $\sigma_{h,\gamma_2}^{(i)}$ defined above is equivalent to:
Find $\sigma_{h,\gamma_1}^{(i)} \in \Sigma_{h,\gamma_1}^{(i)}$ and $r_{h,\gamma_1}^{(i)} \in Q_{h,\gamma_1}^{(i)}$ such that:

$$\begin{cases} (\sigma_{h,\gamma_1}^{(i)}, v_h)_{\omega_{\gamma_1}^{(i)}} - (r_{h,\gamma_1}^{(i)}, \nabla \cdot v_h)_{\omega_{\gamma_1}^{(i)}} = (-\psi_{\gamma_1}^{(i)} \nabla \tilde{u}_h^{(i)}, v_h)_{\omega_{\gamma_1}^{(i)}} & \forall v_h \in \Sigma_{h,\gamma_1}^{(i)}, \\ (\nabla \cdot \sigma_{h,\gamma_1}^{(i)}, q_h)_{\omega_{\gamma_1}^{(i)}} = (\psi_{\gamma_1}^{(i)} f - \nabla \psi_{\gamma_1}^{(i)} \cdot \nabla \tilde{u}_h^{(i)}, q_h)_{\omega_{\gamma_1}^{(i)}} & \forall q_h \in Q_{h,\gamma_1}^{(i)}. \end{cases} \tag{2.52}$$

Find $\sigma_{h,\gamma_2}^{(i)} \in \Sigma_{h,\gamma_2}^{(i)}$ and $r_{h,\gamma_2}^{(i)} \in Q_{h,\gamma_2}^{(i)}$ such that:

$$\begin{cases} (\sigma_{h,\gamma_2}^{(i)}, v_h)_{\omega_{\gamma_2}^{(i)}} - (r_{h,\gamma_2}^{(i)}, \nabla \cdot v_h)_{\omega_{\gamma_2}^{(i)}} = (-\psi_{\gamma_2}^{(i)} \nabla \tilde{u}_h^{(i)}, v_h)_{\omega_{\gamma_2}^{(i)}} & \forall v_h \in \Sigma_{h,\gamma_2}^{(i)}, \\ (\nabla \cdot \sigma_{h,\gamma_2}^{(i)}, q_h)_{\omega_{\gamma_2}^{(i)}} = (\psi_{\gamma_2}^{(i)} f - \nabla \psi_{\gamma_2}^{(i)} \cdot \nabla \tilde{u}_h^{(i)}, q_h)_{\omega_{\gamma_2}^{(i)}} & \forall q_h \in Q_{h,\gamma_2}^{(i)}. \end{cases} \tag{2.53}$$

And for all vertices $a \in \mathcal{V}_{h,*}^{(i)}$, find $\sigma_{h,a}^{(i)} \in \Sigma_{h,a}^{(i)}$ and $r_{h,a}^{(i)} \in Q_{h,a}^{(i)}$ such that:

$$\begin{cases} (\sigma_{h,a}^{(i)}, v_h)_{\omega_a^{(i)}} - (r_{h,a}^{(i)}, \nabla \cdot v_h)_{\omega_a^{(i)}} = -(\psi_a^{(i)} \cdot \nabla \tilde{u}_h^{(i)}, v_h)_{\omega_a^{(i)}} & \forall v_h \in \Sigma_{h,a}^{(i)}, \\ (\nabla \cdot \sigma_{h,a}^{(i)}, q_h)_{\omega_a^{(i)}} = (\psi_a^{(i)} f - \nabla \psi_a^{(i)} \cdot \nabla \tilde{u}_h^{(i)}, q_h)_{\omega_a^{(i)}} & \forall q_h \in Q_{h,a}^{(i)}. \end{cases} \tag{2.54}$$

Proposition 2.18. *Let σ_h be defined by equation (2.51). We have on 2D domains:*

$$\sigma_h^{D_2} = \sum_{i=1}^{N} \left(\sigma_{h,\gamma_1}^{(i)} + \sigma_{h,\gamma_2}^{(i)} + \sum_{a \in \mathcal{V}_{h,*}^{(i)}} \big(1 - \psi_{\gamma_1}^{(i)}(a) - \psi_{\gamma_2}^{(i)}(a)\big) \sigma_{h,a}^{(i)} \right) \mathbb{1}_{D_2^{(i)}}$$

then

$$\nabla \cdot \sigma_h^{D_2} = f \mathbb{1}_{D_2}$$

and consequently $\nabla \cdot \sigma_h = f$ on Ω.

Proof. The proof is an adaptation of the proof in Proposition 2.11. ■

A general a posteriori error estimate

Theorem 2.19 (A general a posterior error estimate)**.** *Let u be the solution of (2.42). Let u_h^s be defined as in (2.48)–(2.49) and σ_h is reconstructed as in (2.51). We define*

$$\tilde{\sigma}_h^{(i)} = \sigma_h^{\gamma_1^{(i)}} + \sigma_h^{\gamma_2^{(i)}} + \sum_{a \in \mathcal{V}_{h,*}^{(i)}} \sigma_h^{a,i} \text{ on } D_2^{(i)} \ \forall i = 1 \dots N,$$

and the Flux estimator by: $\eta^{(i)} := ||\nabla \tilde{u}_h^{(i)} + \tilde{\sigma}_h^{(i)}||_{D_2^{(i)}}$. Then,

$$||\nabla(u - \tilde{u}_h^{(i)})||_{D_2^{(i)}} \leq \eta^{(i)} \quad \forall i = 1 \dots N, \tag{2.55}$$

$$\eta^{(i)} \leq C ||\nabla(u - \tilde{u}_h^{(i)})||_{D_2^{(i)}} \quad \forall i = 1 \dots N, \tag{2.56}$$

$$||\nabla(u-u_h^s)||_\Omega \leq \left(\sum_{i=1}^{N}\left(\eta^{(i)}\right)^2\right)^{\frac{1}{2}}, \tag{2.57}$$

and

$$\left(\sum_{i=1}^{N}\left(\eta^{(i)}\right)^2\right)^{\frac{1}{2}} \leq C'||\nabla(u-u_h^s)||_\Omega \tag{2.58}$$

with constants C and C' depending only on the mesh regularity.

Proof. The first two inequalities (the upper bound (2.55) and the lower bound (2.55)) are exactly of the same proof of Theorem 2.12. Now, let us begin with the third inequality (2.57) that represents the reliability of a posteriori error estimator. We will begin with the calculation of $||\nabla(u-u_h^s)||_\Omega$. First, $u-u_h^s \in H_0^1(\Omega)$, thus as $||\nabla v|| = \sup_{\phi\in H_0^1(\Omega):||\nabla\phi||=1} (\nabla v, \nabla\phi) \quad \forall v \in H_0^1(\Omega)$, then

$$||\nabla(u-u_h^s)||_\Omega = \sup_{\phi\in H_0^1(\Omega):||\nabla\phi||=1}(\nabla(u-u_h^s),\nabla\phi) \qquad \forall\phi\in H_0^1(\Omega).$$

Now, let $\phi \in H_0^1(\Omega)$ and $||\nabla\phi||_\Omega = 1$ be fixed. Then, by using the weak formulation (2.42), we get:

$$(\nabla(u-u_h^s),\nabla\phi)_\Omega = (f,\phi)_\Omega - (\nabla u_h^s,\nabla\phi)_\Omega.$$

Now, adding and subtracting $(\sigma_h,\nabla\phi)_\Omega$ we get:

$$\begin{aligned}
(\nabla(u-u_h^s),\nabla\phi)_\Omega &= (f,\phi)_\Omega - (\nabla u_h^s,\nabla\phi)_\Omega + (\sigma_h,\nabla\phi)_\Omega - (\sigma_h,\nabla\phi)_\Omega \\
&= (f,\phi)_\Omega - (\nabla u_h^s,\nabla\phi)_\Omega - (\nabla\cdot\sigma_h,\phi)_\Omega - (\sigma_h,\nabla\phi)_\Omega \\
&= (f-\nabla\cdot\sigma_h,\phi)_\Omega - (\nabla u_h^s+\sigma_h,\nabla\phi)_\Omega \\
&= -(\nabla u_h^s+\sigma_h,\nabla\phi)_\Omega \\
&\leq \|\nabla u_h^s+\sigma_h\|_\Omega\|\nabla\phi\|_\Omega = \|\nabla u_h^s+\sigma_h\|_\Omega, \text{ since we have } \|\nabla\phi\|_\Omega = 1.
\end{aligned}$$

Finally

$$\begin{aligned}
||\nabla(u-u_h^s)||_\Omega^2 &\leq \|\nabla u_h^s+\sigma_h\|_\Omega^2 \\
&= \sum_{i=1}^{N+1}\|\nabla u_1^{(i)} + (-\nabla u_1^{(i)})\|_{D_1^{(i)}}^2 + \sum_{i=1}^{N}\|\nabla\tilde{u}_h^{(i)}+\tilde{\sigma}_h^{(i)}\|_{D_2^{(i)}}^2 \\
&= \sum_{i=1}^{N}\|\nabla\tilde{u}_h^{(i)}+\tilde{\sigma}_h^{(i)}\|_{D_2^{(i)}}^2 = \sum_{i=1}^{N}\left(\eta^{(i)}\right)^2.
\end{aligned}$$

The proof of the last inequality (2.58) which represents the efficiency on the whole domain Ω can be done in a similar way of the proof of the lower bound (2.25) to get the result. ■

2.4.3. Numerical Results

In a similar way as in Section 2.2.3, we will introduce the interfaces estimator $\eta_{\gamma_1}^{(i)} := \|\sigma_{h,\gamma_1}^{(i)} + \nabla\tilde{u}_h^{(i)}\psi_{h,\gamma_1}^{(i)}\|_{\omega_{\gamma_1}^{(i)}}$ and $\eta_{\gamma_2}^{(i)} := \|\sigma_{h,\gamma_2}^{(i)} + \nabla\tilde{u}_h^{(i)}\psi_{h,\gamma_2}^{(i)}\|_{\omega_{\gamma_2}^{(i)}}$ to determine according to some tolerance $tolG$, the suitable positions of the interfaces $\gamma_1^{(i)}$ and $\gamma_2^{(i)}$ which represent the

inlet and the outlet of each $D_2^{(i)}$ domains for all $i = 1 \dots N$.
In order to determine the suitable positions of the interfaces we will have the following explanation about the steps that we will make them in the Algorithm. The steps are:

- **Step1**: We will fix some tolerance $tolG$ as a tolerance for the interfaces estimator $\eta_{\gamma_1}^{(i)}$ and $\eta_{\gamma_2}^{(i)}$ for all $i = 1 \dots N$ in order to detect the suitable positions of the interfaces $\gamma_1^{(i)}$ and $\gamma_1^{(i)}$ according to this tolerance $tolG$ in a way that we have $\eta_{\gamma_1}^{(i)} < tolG$ and $\eta_{\gamma_2}^{(i)} < tolG$.

- **Step2**: We will fix the first interface $\gamma_1^{(1)}$ and the last one $\gamma_2^{(N)}$ near to the inlet and outlet of the channel respectively as you see in the Figure 2.37 where $N = 6$ here and we will fix the other interfaces, $\gamma_1^{(i)}$ for $i = 2 \dots N$ and $\gamma_2^{(i)}$ for $i = 1 \dots N-1$, at the middle of each rod of the horizontal and vertical channels in a way that we keep a very small distance δ between each two interfaces $\gamma_2^{(i)}$ and $\gamma_1^{(i+1)}$ for $i = 1 \dots N-1$ as you see in the Figure 2.37 where $N = 6$.

- **Step3**: We will consider a very coarse mesh $\tilde{\mathcal{T}}_h^{(i)}$ for each domain $D_2^{(i)}$ and we will begin moving the interfaces towards the corners of the domain in a way that while $\eta_{\gamma_1}^{(i)} < tolG$, we move the first interface $\gamma_1^{(i)}$ towards the corner of $D_2^{(i)}$ and while $\eta_{\gamma_2}^{(i)} < tolG$, we move the second interface $\gamma_2^{(i)}$ towards the corner of $D_2^{(i)}$ in a way that we must keep in mind that the interfaces must be always away from the corner by distance R to be able to define the fluxes of the interfaces.

According to what we explained before, we will have the following algorithm.

- Fix a tolerance **tolG**.
- Fix $\gamma_1^{(1)}$ and $\gamma_2^{(N)}$ near the inlet and outlet.
- Fix $\gamma_1^{(i+1)}$ and $\gamma_2^{(i)}$ for $i = 1 \dots N-1$ at the middle of each rod with a small distance δ between them
- Consider a very coarse mesh $\tilde{\mathcal{T}}_h^{(i)}$ for each domain $D_2^{(i)}$.
- Calculate the local fluxes $\sigma_{h,\gamma_1}^{(i)}$ and $\sigma_{h,\gamma_2}^{(i)}$ and consequently the local estimators $\eta_{\gamma_1}^{(i)}$ and $\eta_{\gamma_2}^{(i)}$ on $\omega_{\gamma_1}^{(i)}$ and $\omega_{\gamma_2}^{(i)}$ respectively for $i = 1 \dots N$.

for *($i = 1 \dots N$)* **do**
  while *($\eta_{\gamma_1}^{(i)} < \frac{tolG}{3}$ or $\eta_{\gamma_2}^{(i)} < \frac{tolG}{3}$)* **do**
    1. Translate the positions of $\gamma_1^{(i)}$ and $\gamma_2^{(i)}$ toward same corner by step 0.01
    2. Calculate $\tilde{u}_h^{(i)}$, $\sigma_{h,\gamma_1}^{(i)}$, $\sigma_{h,\gamma_2}^{(i)}$, $\eta_{\gamma_1}^{(i)}$ and $\eta_{\gamma_2}^{(i)}$ on the new domain $D_2^{(i)}$
  end
end

Algorithm 2: Algorithm to fix the interfaces positions

Now, let us consider our non coupled domain Ω as in Figure 2.36. By applying the **Algorithm 2**, we want to detect the suitable positions of the interfaces of domains $D_2^{(i)}$ for $i = 1 \dots N$, where $N = 6$ as you see in Figure 2.37. The positions of the interfaces which are related to **tolG** are detected by applying the following tests.

Test1: **tolG** $= 10^{-4}$

Let us fix **tolG** $= 10^{-4}$, then according to **Algorithm 2**, we get the following results

Interface	Interface at x=	Interface at y=
$\gamma_1^{(1)}$	4.5	
$\gamma_2^{(1)}$		-0.955
$\gamma_1^{(2)}$		-1.045
$\gamma_2^{(2)}$	4.505	
$\gamma_1^{(3)}$	2.695	
$\gamma_2^{(3)}$		-3.355
$\gamma_1^{(4)}$		-3.445
$\gamma_2^{(4)}$	2.695	
$\gamma_1^{(5)}$	4.505	
$\gamma_2^{(5)}$		-5.755
$\gamma_1^{(6)}$		-5.845
$\gamma_2^{(6)}$	4.5	

The positions of the interfaces related to **tolG** $= 10^{-4}$ are located as in Figure 2.39.

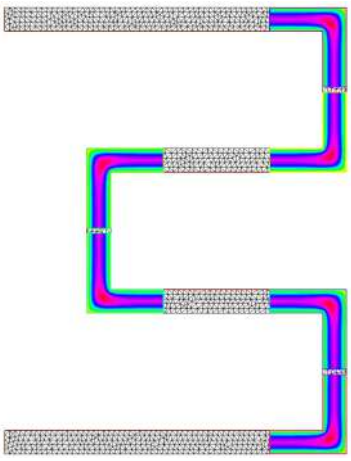

Figure 2.39.: Locations of 2D domains in coupled 0D/2D model in the whole domain Ω for **tolG** $= 10^{-4}$

After fixing the positions of the interfaces according to the **Algorithm 2**, we will begin making a uniform refinement of each mesh $\tilde{\mathcal{T}}_h^{(i)}$ and we are going to calculate $\|\nabla(u -$

$\tilde{u}_h^{(i)})\|_{D_2^{(i)}}$, $\eta^{(i)}$ and the indices $I_{eff}^{(i)} = \frac{\eta^{(i)}}{\|\nabla(u-\tilde{u}_h^{(i)})\|_{D_2^{(i)}}}$ in order to validate the reliability (2.55) of a posteriori error on each domain $D_2^{(i)}$ for all $i = 1 \dots N$ where $N = 6$. The results are in the following table. We conclude from the table below that the indices of efficiency on all 2D domains $D_2^{(i)}$ are approximately one. We have verified that the error and the estimator on each 2D domain $D_2^{(i)}$ converge for uniform refinement.

$D_2^{(i)}$	Mesh Size	$\|\nabla(u-\tilde{u}_h^{(i)})\|_{D_2^{(i)}}$	$\eta^{(i)}$	$I_{eff}^{(i)}$
$D_2^{(1)}$	0.128447	0.0348902	0.0441934	1.26664
	0.0657565	0.0219497	0.0286776	1.30652
	0.0350784	0.0134795	0.0177497	1.31679
$D_2^{(2)}$	0.128371	0.0351082	0.0454093	1.29341
	0.0672227	0.0242147	0.0305191	1.26035
	0.0339791	0.0139611	0.0182626	1.3081
$D_2^{(3)}$	0.130102	0.0351905	0.0453916	1.28988
	0.06679	0.0217905	0.0290811	1.33458
	0.0353895	0.0139509	0.017943	1.28616
$D_2^{(4)}$	0.131167	0.0348834	0.0452092	1.29601
	0.0671029	0.0220007	0.0292808	1.3309
	0.0358843	0.014183	0.0181425	1.27917
$D_2^{(5)}$	0.128371	0.0349467	0.045467	1.30104
	0.0676512	0.0219677	0.0288138	1.31165
	0.0353213	0.0143505	0.0181906	1.2676
$D_2^{(6)}$	0.131624	0.0338941	0.0440533	1.29973
	0.0645722	0.0211543	0.0281654	1.33143
	0.0323899	0.0139266	0.0178176	1.27939

Now, we are going to calculate $\|\nabla(u-u_h^s)\|_\Omega$, $\eta := \left(\sum_{i=1}^N \left(\eta^{(i)}\right)^2\right)^{\frac{1}{2}}$ and the indices $I_{eff} = \frac{\eta}{\|\nabla(u-u_h^s)\|_\Omega}$ in order to validate the reliability (2.57) of a posteriori error on the total domain Ω. We conclude from the table below that the total index of efficiency on the whole domain Ω is approximately one. We have verified that the error and the estimator on the whole domain Ω converge for uniform refinement.

Mesh Size	$\|\nabla(u-u_h^s)\|_\Omega$	η	I_{eff}
0.128447	0.085295	0.110124	1.29109
0.0657565	0.0543791	0.0712771	1.31074
0.0350784	0.0342387	0.0441366	1.28909
0.0178413	0.0208386	0.0279421	1.34088

We have made a uniform refinement for the mesh $\tilde{\mathcal{T}}_h^{(1)}$ of the domain $D_2^{(1)}$. We plot the distribution of the error and estimator on $D_2^{(1)}$ for different mesh sizes. For mesh size $h \approx 0.128447$ in Figure 2.40, for mesh size $h \approx 0.0657$ in Figure 2.41 and for mesh size $h \approx 0.03507$ in Figure 2.42. We deduce that the error and estimator take the greatest values at the corner and this is due to the singularity of the solution at the corner.

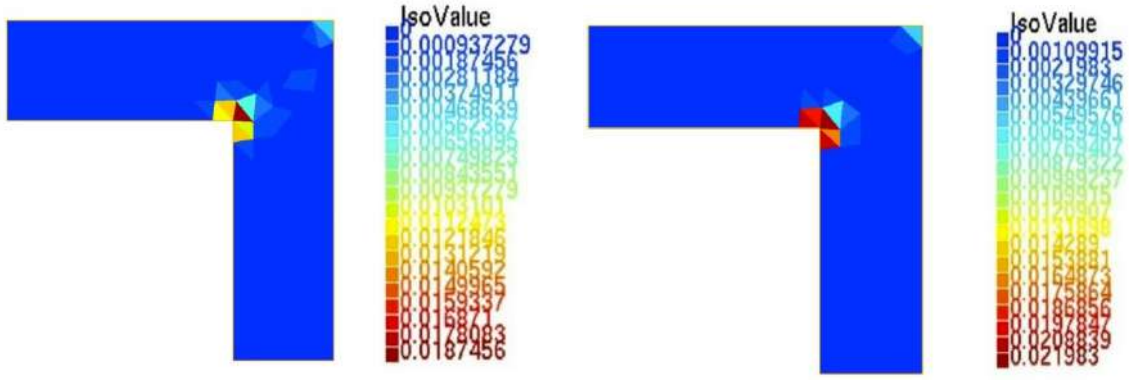

(a) Distribution of error (b) Distribution of estimator

Figure 2.40.: Distribution of error and estimator on $D_2^{(1)}$ for $h \approx 0.128$

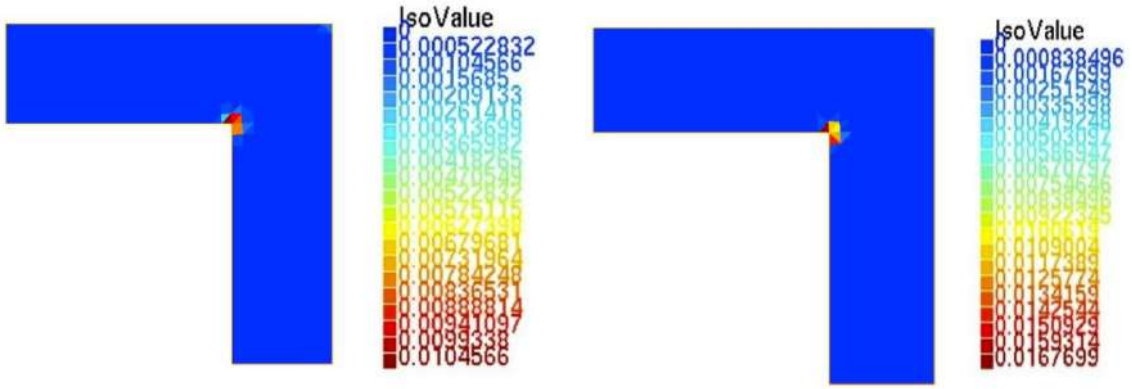

(a) Distribution of error (b) Distribution of estimator

Figure 2.41.: Distribution of error and estimator on $D_2^{(1)}$ for $h \approx 0.06$

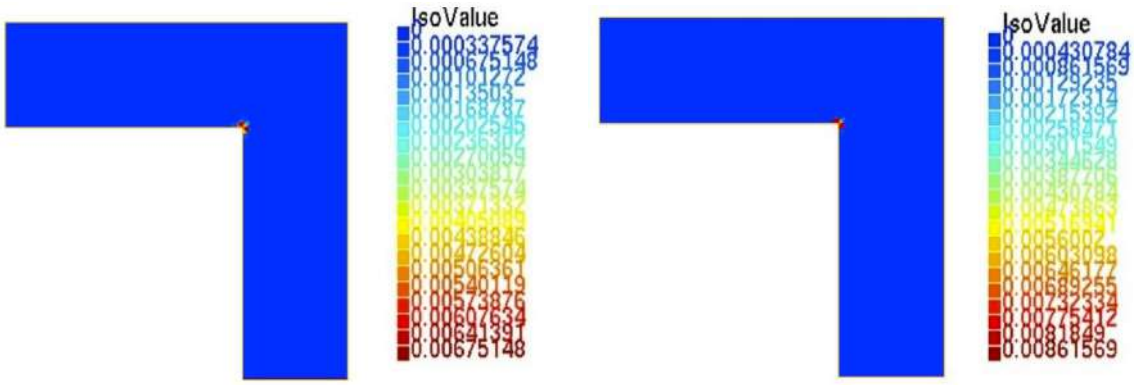

(a) Distribution of error (b) Distribution of estimator

Figure 2.42.: Distribution of error and estimator on $D_2^{(1)}$ for $h \approx 0.03$

Test2: $\mathbf{tolG} = 10^{-3}$

Now, let us fix $\mathbf{tolG} = 10^{-3}$, then according to **Algorithm 2**, we get the following results:

Interface	Interface at x=	Interface at y=
$\gamma_1^{(1)}$	4.8	
$\gamma_2^{(1)}$		-0.665
$\gamma_1^{(2)}$		-1.335
$\gamma_2^{(2)}$	4.805	
$\gamma_1^{(3)}$	2.395	
$\gamma_2^{(3)}$		-3.065
$\gamma_1^{(4)}$		-3.735
$\gamma_2^{(4)}$	2.395	
$\gamma_1^{(5)}$	4.805	
$\gamma_2^{(5)}$		-5.465
$\gamma_1^{(6)}$		-6.135
$\gamma_2^{(6)}$	4.8	

The positions of the interfaces related to $\mathbf{tolG} = 10^{-3}$ are located as in Figure 2.43

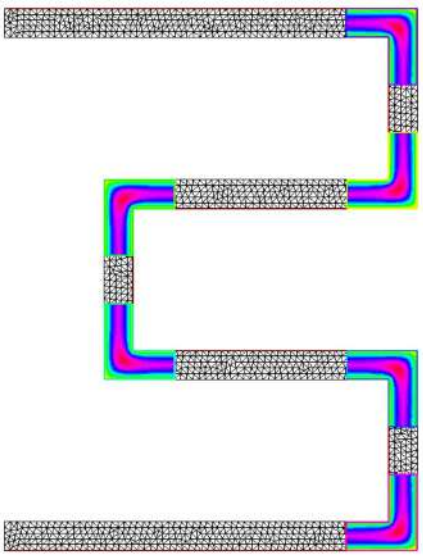

Figure 2.43.: Locations of 2D domains in coupled 0D/2D model in the whole domain Ω for $\mathbf{tolG} = 10^{-3}$

By compering Figure 2.39 when we take $\mathbf{tolG} = 10^{-4}$ and Figure 2.43 when we take $\mathbf{tolG} = 10^{-3}$, we observe that as the positions of the interfaces in Figure 2.43 are more near

to the corner than the interfaces in Figure 2.39 and thus as the tolerance **tolG** increases, the interfaces become closer to the corner.
After fixing the positions of the interfaces according to the **Algorithm 2**, we will begin making a uniform refinement of each mesh $\tilde{\mathcal{T}}_h^{(i)}$ and we are going to calculate $\|\nabla(u-\tilde{u}_h^{(i)})\|_{D_2^{(i)}}$, $\eta^{(i)}$ and the indices $I_{eff}^{(i)} = \frac{\eta^{(i)}}{\|\nabla(u-\tilde{u}_h^{(i)})\|_{D_2^{(i)}}}$ in order to validate the reliability (2.55) of a posteriori error on each domain $D_2^{(i)}$ for all $i = 1 \dots N$ where $N = 6$. The results are in the following table

$D_2^{(i)}$	Mesh Size	$\|\nabla(u-\tilde{u}_h^{(i)})\|_{D_2^{(i)}}$	$\eta^{(i)}$	$I_{eff}^{(i)}$
$D_2^{(1)}$	0.128288	0.0344023	0.0451638	1.31281
	0.0680391	0.0215762	0.0286248	1.32669
	0.0347673	0.0139428	0.0178793	1.28233
$D_2^{(2)}$	0.124877	0.0347746	0.0446278	1.28335
	0.0811391	0.021578	0.0283973	1.31603
	0.0355952	0.0136941	0.0177217	1.29411
$D_2^{(3)}$	0.127817	0.0346032	0.0439119	1.26901
	0.0811391	0.0216188	0.0285536	1.32078
	0.0332432	0.0138587	0.0177595	1.28146
$D_2^{(4)}$	0.128356	0.0349473	0.0441883	1.26442
	0.0680527	0.021489	0.0283898	1.32113
	0.0343932	0.0142785	0.0178729	1.25174
$D_2^{(5)}$	0.126115	0.0345202	0.0450778	1.30584
	0.0652866	0.0230787	0.0281297	1.21886
	0.0346837	0.0137955	0.0177264	1.28494
$D_2^{(6)}$	0.126088	0.034324	0.0440049	1.28205
	0.0667871	0.0213494	0.0281837	1.32011
	0.0370029	0.0138759	0.018034	1.29966

We conclude from the above table that, although we change the tolerance of the estimator of the interface i.e. **tolG**, we still have that the indices of efficiencies on all 2D domains $D_2^{(i)}$ are approximately one. We have verified that the error and the estimator on each 2D domain $D_2^{(i)}$ converge for uniform refinement. In order to obtain the optimal convergence we must make an adaptive refinements as we did in Section 2.3. for each 2D domain $D_2^{(i)}$.

Now, we are going to calculate $\|\nabla(u-u_h^s)\|_\Omega$, $\eta := \left(\sum_{i=1}^N \left(\eta^{(i)}\right)^2\right)^{\frac{1}{2}}$ and the indices $I_{eff} = \frac{\eta}{\|\nabla(u-u_h^s)\|_\Omega}$ in order to validate the reliability (2.57) of a posteriori error on the total domain Ω.

Mesh Size	$\|\nabla(u-u_h^s)\|_\Omega$	η	I_{eff}
0.128288	0.0847469	0.108999	1.28617
0.0680391	0.0533806	0.0695175	1.3023
0.0347673	0.0340807	0.0436809	1.28169

We have made a uniform refinement for the mesh $\tilde{\mathcal{T}}_h^{(1)}$ of the domain $D_2^{(1)}$. We plot the distribution of the error and estimator on $D_2^{(1)}$ for different mesh sizes. For mesh size

$h \approx 0.128447$ in Figure 2.44, for mesh size $h \approx 0.0657$ in Figure 2.45 and for mesh size $h \approx 0.03507$ in Figure 2.46. We deduce that the error and estimator take the greatest values at the corner and this is due to the singularity of the solution at the corner.

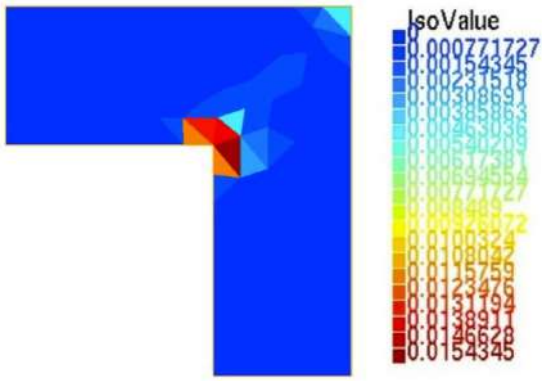

(a) Distribution of error

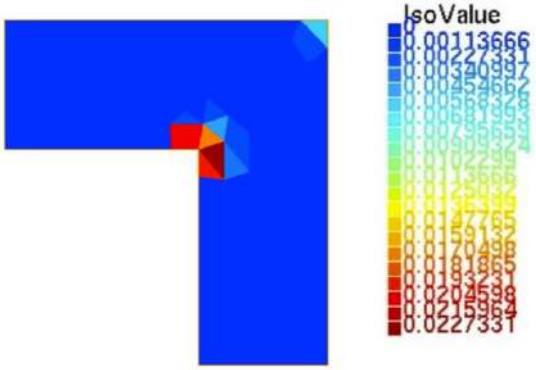

(b) Distribution of estimator

Figure 2.44.: Distribution of error and estimator on $D_2^{(1)}$ for $h \approx 0.128$

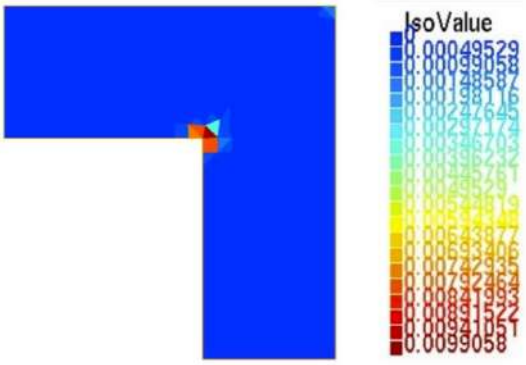

(a) Distribution of error

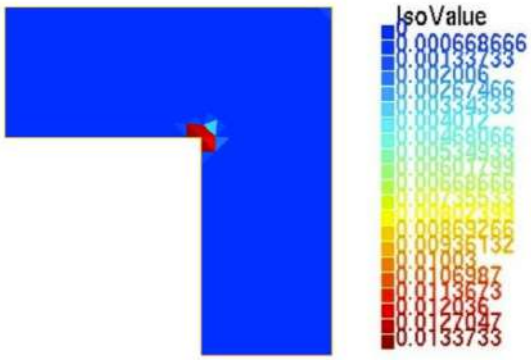

(b) Distribution of estimator

Figure 2.45.: Distribution of error and estimator on $D_2^{(1)}$ for $h \approx 0.06$

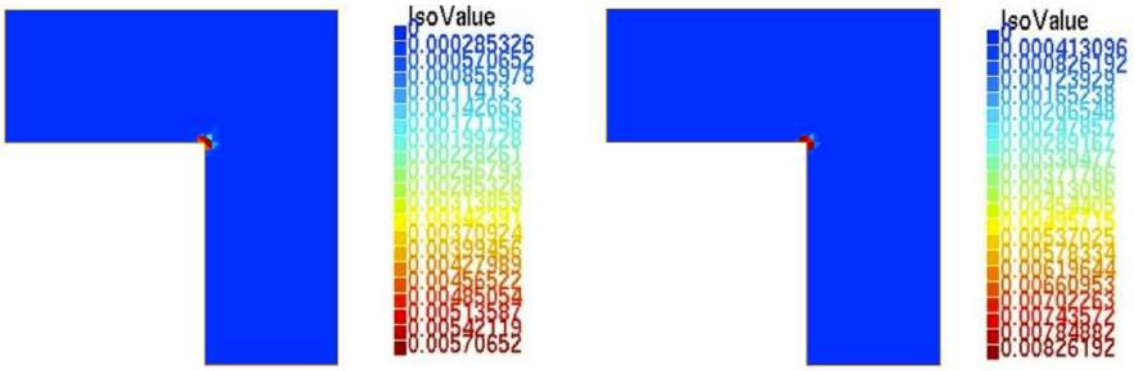

(a) Distribution of error (b) Distribution of estimator

Figure 2.46.: Distribution of error and estimator on $D_2^{(1)}$ for $h \approx 0.03$

3. A posteriori estimator for the coupled 0D/2D Stokes equation

In this chapter we are going to talk about *a posteriori* error estimation for the coupled 0D/2D model of the Stokes equation (1.15) on $\Omega = \Omega' \cup \gamma \cup \tilde{\Omega}$ which is represented in Figure 1.4. Recall that this coupled solution is denoted as (u_h^s, p_h^s) and defined by (1.40)-(1.41) in Section 1.2.4. We will introduce two possibilities of reconstructing the flux σ_h on Ω of the coupled 0D/2D model. In Section 3.1, we will construct the first attempt of defining the flux reconstruction where the upper bound is guaranteed (reliability of the estimator) while the lower bound (efficiency of the estimator) is not satisfied (or it is very difficult to be proved). In Section 3.2, we will make a new stress reconstruction where we proved the reliability of the estimator and efficiency of the estimator. In Section 3.3 we make a conclusion and perspectives.

We recall that the variational formulation of (1.15) is (1.17). Let us also list here some important definitions and properties.

Definition 3.1 (Stress σ)**.** *Let (u, p) be the solution of system (1.17) then, we denote the stress by: $\sigma := \nabla u - pI$.*

Remark 3.2 (Properties of weak solution of system (1.17))**.** *Let (u, p) be solution of system (1.17) and let σ be defined as in Definition 3.1. Then, $u \in [H_g^1(\Omega)]^2$, $\sigma \in [H(div, \Omega)]^2$ and $\nabla \cdot \sigma = 0$.*

Proof. The proof is quite standard, see [78, Theorem 7.1.3] ■

Proposition 3.3 (Properties of approximate solution (u_h^s, p_h^s))**.** *Let (u_h^s, p_h^s) be the approximate solution (1.40)–(1.41) then, $u_h^s \in [H_g^1(\Omega)]^2$, $\nabla u_h^s - p_h^s I \notin [H(\mathrm{div}, \Omega)]^2$ and $\nabla \cdot (\nabla u_h^s - p_h^s I) \neq 0$ in general.*

Now, our aim is to reconstruct a flux, $\sigma_h \in [H(\mathrm{div}, \Omega)]^2$, such that σ_h is close to $\nabla u_h^s - p_h^s I$ so that $\|\sigma_h - \nabla u_h^s + p_h^s I\|_\Omega$ is as small as possible and $\nabla \cdot \sigma_h = 0$.

3.1. A simple a posteriori estimator with guaranteed upper bound only

3.1.1. Sress Reconstruction

Let u_h^s and p_h^s be the approximate solution (1.40)–(1.41). We shall adapt to this approximation of the solution to Stokes equations the flux reconstruction presented in Section 2.1.1 in the context of the Poisson equation. We recall the definitions of patches of mesh elements introduced there: $\mathcal{V}_h^*$ for the set of vertices on $\overline{\tilde{\Omega}} \backslash \bar{\gamma}$, ω^a for the patch of mesh

elements around a node $a \in \mathcal{V}_h^*$, $\omega^\gamma = \bigcup_{a_i \in \gamma} \omega_{a_i}$ as in the Figure 2.2. We also recall the partition of unity

$$\mathbb{1}_\Omega = \mathbb{1}_{\Omega'} + \psi^\gamma + \sum_{a \,\in\, \mathcal{V}_h^*} \psi^a,$$

where ψ^a is the hat function for any mesh node excluding those in γ, and ψ^γ is 1 on γ, 0 on all nodes not on γ.

Now, we define the stress reconstruction as

$$\sigma_h = \sigma_h^\gamma + \sum_{a \in \mathcal{V}_h^*} \sigma_h^a + (\nabla u' - p' I)\mathbb{1}_{\Omega'} = \tilde{\sigma}_h + \sigma', \tag{3.1}$$

where, the simplified model (u', p') is defined on Ω' by (1.22) and $\tilde{\sigma}_h$ is defined by

$$\tilde{\sigma}_h := \sigma_h^\gamma + \sum_{a \in \mathcal{V}_h^*} \sigma_h^a, \tag{3.2}$$

where for each $a \in \mathcal{V}_h^*$

$$\sigma_h^a := \underset{\substack{v_h^a \in \Sigma_h^a, \\ \operatorname{div} v_h^a = \Pi_{Q_h^a}\left((\nabla \tilde{u}_h - \tilde{p}_h I)\cdot \nabla \psi_a\right)}}{\arg\min} ||v_h^a - \psi^a(\nabla \tilde{u}_h - \tilde{p}_h I)||_{L^2(\omega^a)}$$

and

$$\sigma_h^\gamma := \underset{\substack{v_h^\gamma \in \Sigma_h^\gamma, \\ \operatorname{div} v_h^\gamma = \Pi_{Q_h^\gamma}\left((\nabla \tilde{u}_h - \tilde{p}_h I)\cdot \nabla \psi^\gamma\right)}}{\arg\min} ||v_h^\gamma - \psi^\gamma(\nabla \tilde{u}_h - \tilde{p}_h I)||_{L^2(\omega^\gamma)}.$$

Here the spaces are chosen in the following cases.

Case 1: a is an internal node of $\tilde{\Omega}$

$\Sigma_h^a := \{\sigma_h \in RT_2(\omega^a), \sigma_h \cdot n = 0 \quad \text{on} \quad \partial\omega^a\}$

$Q_h^a := \{q_h \in [L^2(\omega^a)]^2, q_{h|_K} \in [\mathbb{P}_2(K)]^2, \forall K \in \omega^a, \int_{\omega^a} q_h = 0\}$

Case 2: a on the wall of $\tilde{\Omega}\backslash\gamma$

$\Sigma_h^a := \{\sigma_h \in RT_2(\omega^a), \sigma_h \cdot n = 0 \quad \text{on} \quad \partial\omega^a \backslash \partial\tilde{\Omega}\}$

$Q_h^a := \{q_h \in [L^2(\omega^a)]^2, q_{h|_K} \in [\mathbb{P}_2(K)]^2, \forall K \in \omega^a\}$

Case 3: $a = \gamma$

$\Sigma_h^\gamma := \{\sigma_h \in RT_2(\omega^\gamma), \sigma_h \cdot n = 0 \quad \text{on} \quad \partial\omega^\gamma \backslash \partial\tilde{\Omega} \quad \text{and} \quad \sigma_h \cdot n = (\nabla u' - p' I)n \quad \text{on} \quad \gamma\}$

$Q_h^\gamma := \{q_h \in [L^2(\omega^\gamma)]^2, q_{h|_K} \in [\mathbb{P}_2(K)]^2, \forall K \in \omega^\gamma\}$

$\Pi_{Q_h^a}$ is the $L^2(\omega^a)$-orthogonal projection and $\Pi_{Q_h^\gamma}$ is the $L^2(\omega^\gamma)$-orthogonal projection.

σ_h^γ and σ_h^a defined above is equivalent to: Find $\sigma_h^\gamma \in \Sigma_h^\gamma$ and $r_h^\gamma \in Q_h^\gamma$ such that:

$$\begin{cases} (\sigma_h^\gamma, v_h)_{\omega^\gamma} + (r_h^\gamma, \nabla \cdot v_h)_{\omega^\gamma} = (\psi^\gamma(\nabla \tilde{u}_h - \tilde{p}_h I), v_h)_{\omega^\gamma} & \forall v_h \in \Sigma_h^\gamma, \\ (\nabla \cdot \sigma_h^\gamma, q_h)_{\omega^\gamma} = ((\nabla \tilde{u}_h - \tilde{p}_h I)\cdot \nabla \psi^\gamma, q_h)_{\omega^\gamma} & \forall q_h \in Q_h^\gamma. \end{cases} \tag{3.3}$$

And for all vertices $a \in \mathcal{V}_h^*$, find $\sigma_h^a \in \Sigma_h^a$ and $r_h^a \in Q_h^a$ such that:

$$\begin{cases} (\sigma_h^a, v_h)_{\omega^a} + (r_h^a, \nabla \cdot v_h)_{\omega^a} = (\psi^a(\nabla \tilde{u}_h - \tilde{p}_h I), v_h)_{\omega^a} & \forall v_h \in \Sigma_h^a, \\ (\nabla \cdot \sigma_h^a, q_h)_{\omega^a} = ((\nabla \tilde{u}_h - \tilde{p}_h I)\cdot \nabla \psi^a, q_h)_{\omega^a} & \forall q_h \in Q_h^a. \end{cases} \tag{3.4}$$

Proposition 3.4. *Let σ_h be defined by equation (3.1). We have $\tilde{\sigma}_h = \sigma_h^\gamma + \sum_{a\in\mathcal{V}_h^*}\sigma_h^a$, then $\nabla\cdot\tilde{\sigma}_h = 0$ on $\tilde{\Omega}$ and consequently $\nabla\cdot\sigma_h = 0$ on Ω.*

Proof. $\tilde{\sigma}_h \in H(\mathrm{div},\tilde{\Omega})$ as all the individual components σ_h^γ and σ_h^a belong to $H(\mathrm{div},\tilde{\Omega})$ for all $a\in\mathcal{V}_h^*$, since by extension we can go from $H(\mathrm{div},\omega^\gamma)$ and $H(\mathrm{div},\omega^a)$ to $H(\mathrm{div},\tilde{\Omega})$, and $\tilde{\sigma}_h$ is the sum of all these components. We will deal with the following three cases:
Case 1: a is internal node of $\tilde{\Omega}$:
$\forall a\in\mathcal{V}_h^*$ we have: $(\nabla\cdot\sigma_h^a, q_h)_{\omega^a} = (\nabla(\tilde{u}_h - \tilde{p}_h I)\cdot\nabla\psi^a, q_h)_{\omega^a}$ for all $q_h\in Q_h^a$, then we have $\int_{\omega^a} q_h = 0$ and we have $(\nabla\cdot\sigma_h^a, e_i)_{\omega^a} = 0$ as $\sigma_h^a\cdot n = 0$ on $\partial\omega^a$ and using the divergence theorem. Now, from system (1.35), we have $(\nabla\tilde{u}_h - \tilde{p}_h I, \nabla v_h)_{\tilde{\Omega}} = 0$ for all $v_h\in\tilde{V}_h^0$ as $(\tilde{p}_h I,\nabla v_h)_{\tilde{\Omega}} = (\tilde{p}_h, \nabla\cdot v_h)_{\tilde{\Omega}}$ so, let us take two test functions:

- if we take $v_h^1 = \begin{pmatrix}\psi^a\\ 0\end{pmatrix}$, then $((\nabla\tilde{u}_h - \tilde{p}_h I)\cdot\nabla\psi^a, e_1) = 0$ since $v_h^1\in\tilde{V}_h^0$,
- if we take $v_h^2 = \begin{pmatrix}0\\ \psi^a\end{pmatrix}$, then $((\nabla\tilde{u}_h - \tilde{p}_h I)\cdot\nabla\psi^a, e_2) = 0$ since $v_h^2\in\tilde{V}_h^0$.

So, for all $a\in\mathcal{V}_h^*$ we have $(\nabla\cdot\sigma_h^a, q_h)_{\omega^a} = ((\nabla\tilde{u}_h - \tilde{p}_h I)\cdot\nabla\psi^a, q_h)_{\omega^a}$ for all $q_h\in Q_h(\omega^a)$ and not only for the vector-valued function with zero mean value, where, $Q_h(\omega^a) := \{q_h\in [L^2(\omega^a)]^2; q_h\in[\mathbb{P}_2(K)]^2 \quad \forall K\in\omega^a\}$.
Case 2: a is on wall of $\tilde{\Omega}\backslash\gamma$:
We have $(\nabla\cdot\sigma_h^a, q_h)_{\omega^a} = ((\nabla\tilde{u}_h - \tilde{p}_h I)\cdot\nabla\psi^a, q_h)_{\omega^a}$ for all $q_h\in Q_h^a = Q_h(\omega^a)$.
Case 3: $a=\gamma$:
We have $(\nabla\cdot\sigma_h^\gamma, q_h)_{\omega^\gamma} = ((\nabla\tilde{u}_h - \tilde{p}_h I)\cdot\nabla\psi^\gamma, q_h)_{\omega^\gamma}$ for all $q_h\in Q_h^\gamma = Q_h(\omega^\gamma)$.
Let now $\tilde{q}_h$ be in $Q_h = \mathbb{P}_2(\mathcal{T}_h)$, then

$$\begin{aligned}
(\nabla\cdot\tilde{\sigma}_h,\tilde{q}_h)_{\tilde{\Omega}} &= \left(\nabla\cdot\sigma_h^\gamma,\tilde{q}_h\right)_{\tilde{\Omega}} + \left(\nabla\cdot(\sum_{a\in\mathcal{V}_h^*}\sigma_h^a),\tilde{q}_h\right)_{\tilde{\Omega}}\\
&= \left((\nabla(\tilde{u}_h - \tilde{p}_h I)\cdot\nabla\psi^\gamma,\tilde{q}_h\right)_{\tilde{\Omega}} + \sum_{a\in\mathcal{V}_h^*}\left((\nabla\tilde{u}_h - \tilde{p}_h I)\cdot\nabla\psi^a,\tilde{q}_h\right)_{\tilde{\Omega}}\\
&= \left((\nabla\tilde{u}_h - \tilde{p}_h I)\cdot\nabla(\psi^\gamma + \sum_{a\in\mathcal{V}_h^*}\psi^a),\tilde{q}_h\right)_{\tilde{\Omega}}\\
&= \left((\nabla\tilde{u}_h - \tilde{p}_h I)\cdot\nabla(\mathbb{1}_{\tilde{\Omega}}),\tilde{q}_h\right)_{\tilde{\Omega}}\\
&= 0.
\end{aligned}$$

Since $\nabla\cdot(RT_2(K)) = Q_h(K) = \mathbb{P}_2(K)$ for all $K\in\tilde{\mathcal{T}}_h$, we get $\nabla\cdot\tilde{\sigma}_h = \Pi_{Q_h}(0) = 0$ where, Π_{Q_h} is the $L^2(\tilde{\Omega})$-orthogonal projection onto Q_h and finally, we get

$$\nabla\cdot\tilde{\sigma}_h = 0 \qquad \text{on} \quad \tilde{\Omega}.$$

■

3.1.2. Reliability of the a posteriori error estimate based on (3.1)

We can study now posterior error estimate. We will prove here the guaranteed upper bound. The lower bound is difficult to be proved and the reason is explained in Section 2.1.3 for the Poisson problem.

As in the previous section, we start from the coupled approximate solution $u_h^s \in H_g^1(\Omega)$, $p_h^s \in L_0^2(\Omega)$ defined by (1.40)–(1.41) and we reconstruct the stress σ_h as in (3.1)

Theorem 3.5 (A general *a posterior* error estimate)**.** *Let (u,p) be the weak solution defined by system (1.17). Let (u_h^s, p_h^s) and the stress σ_h defined as in the previous remark. Let $\tilde{\mathcal{T}}_h$ be the mesh of $\tilde{\Omega}$, then $\forall K \in \tilde{\mathcal{T}}_h$ define the stress estimator*

$$\eta_{F,K} := ||\nabla \tilde{u}_h - \tilde{p}_h I - \tilde{\sigma}_h||_K.$$

and the divergence estimator

$$\eta_{D,K} := \frac{||\nabla \cdot \tilde{u}_h||_K}{\beta}.$$

Then

$$||\nabla(u - u_h^s)||_\Omega^2 \leq \sum_{K\in\tilde{\mathcal{T}}_h} \eta_{F,K}^2 + \sum_{K\in\tilde{\mathcal{T}}_h} \eta_{D,K}^2$$

$$||p - p_h^s||_\Omega \leq \frac{1}{\beta}\left\{ \left(\sum_{K\in\tilde{\mathcal{T}}_h} \eta_{F,K}^2 \right)^{\frac{1}{2}} + \left(\sum_{K\in\tilde{\mathcal{T}}_h} \eta_{D,K}^2 \right)^{\frac{1}{2}} \right\}.$$

Proof. Let us start with $||\nabla(u - u_h^s)||$. Now let us introduce s defined by

$$\begin{cases} \text{Find} \quad s \in [H_g^1(\Omega)]^2 \quad \text{with} \quad \nabla \cdot s = 0 \quad \text{such that:} \\ (\nabla s, \nabla v)_\Omega = (\nabla u_h, \nabla v)_\Omega \quad \forall v \in [H_0^1(\Omega)]^2 \quad \text{with} \quad \nabla \cdot v = 0. \end{cases} \tag{3.5}$$

Then,

$||\nabla(u-u_h^s)||_\Omega^2 = ||\nabla(u-s+s-u_h^s)||_\Omega^2 = ||\nabla(u-s)||_\Omega^2 + ||\nabla(s-u_h^s)||_\Omega^2 + 2(\nabla(u-s), \nabla(s-u_h^s))_\Omega$,

but, $u - s \in [H_0^1(\Omega)]^2$, $\nabla \cdot u = 0$ and $\nabla \cdot s = 0$, then $\nabla \cdot (u - s) = 0$ so, substituting $v = u - s$ in system (3.5) we get $(\nabla(u - s), \nabla(s - u_h^s))_\Omega = 0$ and hence

$$||\nabla(u - u_h^s)||_\Omega^2 = ||\nabla(u - s + s - u_h^s)||_\Omega^2 = \underbrace{||\nabla(u - s)||_\Omega^2}_{=:A} + \underbrace{||\nabla(s - u_h^s)||_\Omega^2}_{=:B}.$$

Now, we begin with $A := ||\nabla(u - s)||_\Omega^2$. By definition we have:

$$||\nabla(u - s)||_\Omega = \sup_{\substack{\phi\in[H_0^1(\Omega)]^2 \\ \nabla\cdot\phi=0, \\ ||\nabla\phi||_\Omega=1}} (\nabla(u - s), \nabla\phi).$$

So, let $\phi \in [H_0^1(\Omega)]^2$, $\nabla \cdot \phi = 0$ and $||\nabla\phi||_\Omega = 1$ be fixed, then by system (1.17) and system (3.5), we get $(\nabla(u - s), \nabla\phi)_\Omega = -(\nabla u_h^s, \nabla\phi)_\Omega$. We also use $(p_h^s, \nabla \cdot \phi)_\Omega = 0$ and $(p_h^s I, \nabla\phi)_\Omega = (p_h^s, \nabla \cdot \phi) = 0$ since $\nabla \cdot \phi = 0$, then

$$\begin{aligned} (\nabla(u - s), \nabla\phi)_\Omega &= -(\nabla u_h^s, \nabla\phi)_\Omega \\ &= -(\nabla u_h^s, \nabla\phi)_\Omega + (p_h^s I, \nabla\phi)_\Omega + (\sigma_h, \nabla\phi)_\Omega - (\sigma_h, \nabla\phi)_\Omega \\ &= \underbrace{-(\sigma_h, \nabla\phi)_\Omega}_{=(*)} + \underbrace{-(\nabla u_h - p_h^s I - \sigma_h, \nabla\phi)_\Omega}_{=(**)} \end{aligned}$$

We observe that: $(*) = -(\sigma_h, \nabla\phi)_\Omega = -(\sigma', \nabla\phi)_{\Omega'} - (\tilde{\sigma}_h, \nabla\phi)_{\tilde{\Omega}}$

$$\begin{aligned} &= (\nabla \cdot \sigma', \phi)_{\Omega'} - \langle \sigma' \cdot n_{\Omega'}, \phi\rangle_{\partial\Omega'} + (\nabla \cdot \tilde{\sigma}_h, \phi)_{\tilde{\Omega}} - \langle \tilde{\sigma}_h \cdot n_{\tilde{\Omega}}, \phi\rangle_{\partial\tilde{\Omega}} \\ &= -\langle \sigma' \cdot n_{\Omega'}, \phi\rangle_{\partial\Omega'} + (\nabla \cdot \tilde{\sigma}_h, \phi)_{\tilde{\Omega}} - \langle \tilde{\sigma}_h \cdot n_{\tilde{\Omega}}, \phi\rangle_{\partial\tilde{\Omega}}, \end{aligned}$$

where $n_{\Omega'}$ and $n_{\tilde{\Omega}}$ are the outward unit normal to Ω' and $\tilde{\Omega}$ respectively. Since $\phi = 0$ on $\partial\Omega$, $\langle \tilde{\sigma}_h \cdot n_{\tilde{\Omega}}, \phi\rangle_{\partial\tilde{\Omega}} = \langle \tilde{\sigma}_h \cdot n_{\tilde{\Omega}}, \phi\rangle_\gamma = \langle \sigma_h^\gamma \cdot n_{\tilde{\Omega}}, \phi\rangle_\gamma$ and since $\sigma_h^\gamma \in \Sigma_h^\gamma$, $\sigma_h^\gamma \cdot n = (\nabla u' - p'I)n$ on γ so, $\langle \tilde{\sigma}_h \cdot n_{\tilde{\Omega}}, \phi\rangle_{\partial\tilde{\Omega}} = \langle (\nabla u' - p'I)n_{\tilde{\Omega}}, \phi\rangle_\gamma = -\langle \sigma' \cdot n_{\Omega'}, \phi\rangle_\gamma$ since $n_{\tilde{\Omega}} = -n_{\Omega'}$ on γ and $\langle \sigma' \cdot n_{\Omega'}, \phi\rangle_{\partial\Omega'} = \langle \sigma' \cdot n_{\Omega'}, \phi\rangle_\gamma$ as $\phi = 0$ on $\partial\Omega$. Using Proposition 3.4 we get
$(*) = -\langle \sigma^{'} \cdot n_{\Omega'}, \phi\rangle_\gamma + (\nabla \cdot \tilde{\sigma}_h, \phi)_{\tilde{\Omega}} + \langle \sigma^{'} \cdot n_{\Omega'}, \phi\rangle_\gamma = (\nabla \cdot \tilde{\sigma}_h, \phi)_{\tilde{\Omega}} = 0$. Moreover, we remark that:

$$
\begin{aligned}
(**) &= -(\nabla u_h^s - p_h^s I - \sigma_h, \nabla\phi)_\Omega \\
&= -(\nabla u^{'} - p^{'} I - \sigma^{'}, \nabla\phi)_{\Omega'} - (\nabla\tilde{u}_h - \tilde{p}_h I - \tilde{\sigma}_h, \nabla\phi)_{\tilde{\Omega}} \\
&= -(\nabla\tilde{u}_h - \tilde{p}_h I - \tilde{\sigma}_h, \nabla\phi)_{\tilde{\Omega}} \\
&= -\sum_{K\in\tilde{\mathcal{T}}_h} (\nabla\tilde{u}_h - \tilde{p}_h I - \tilde{\sigma}_h, \nabla\phi)_K \\
&\leq \sum_{K\in\tilde{\mathcal{T}}_h} ||\nabla\tilde{u}_h - \tilde{p}_h I - \tilde{\sigma}_h||_K ||\nabla\phi||_K \\
&\leq \sum_{K\in\tilde{\mathcal{T}}_h} \eta_{F,K} ||\nabla\phi||_K.
\end{aligned}
$$

In conclusion we have

$$
\begin{aligned}
(\nabla(u-s), \nabla\phi)_\Omega = (*) + (**) &\leq \sum_{K\in\tilde{\mathcal{T}}_h} \eta_{F,K} ||\nabla\phi||_K \\
&\leq \Big(\sum_{K\in\tilde{\mathcal{T}}_h} \eta_{F,K}^2\Big)^{\frac{1}{2}} \Big(\sum_{K\in\tilde{\mathcal{T}}_h} ||\nabla\phi||_K^2\Big)^{\frac{1}{2}} \leq \Big(\sum_{K\in\tilde{\mathcal{T}}_h} \eta_{F,K}^2\Big)^{\frac{1}{2}} ||\nabla\phi||_\Omega.
\end{aligned}
$$

Then,

$$
\begin{aligned}
||\nabla(u-s)||_\Omega = \sup_{\substack{\phi\in H_0^1(\Omega)\\ \nabla\cdot\phi=0,\\ ||\nabla\phi||_\Omega=1}} (\nabla(u-s), \nabla\phi)_\Omega &\leq \sup_{\substack{\phi\in H_0^1(\Omega)\\ \nabla\cdot\phi=0,\\ ||\nabla\phi||=1}} \Big(\sum_{K\in\tilde{\mathcal{T}}_h} \eta_{F,K}^2\Big)^{\frac{1}{2}} ||\nabla\phi||_\Omega \\
&= \Big(\sum_{K\in\tilde{\mathcal{T}}_h} \eta_{F,K}^2\Big)^{\frac{1}{2}}
\end{aligned}
$$

So, $A = ||\nabla(u-s)||_\Omega^2 \leq \sum_{K\in\tilde{\mathcal{T}}_h} \eta_{F,K}^2$.
Now, let us estimate $B := ||\nabla(s-u_h^s)||_\Omega^2$. We recall that, system (3.5) s is equivalent to:

$$
\begin{cases}
\text{Find} \quad (s,w) \in [H_g^1(\Omega)]^2 \times L_0^2(\Omega) \quad \text{such that:} \\
(\nabla s, \nabla v)_\Omega - (\nabla\cdot v, w)_\Omega = (\nabla u_h^s, \nabla v)_\Omega \quad \forall v \in [H_0^1(\Omega)]^2, \\
-(\nabla\cdot s, q)_\Omega = 0 \quad \forall q \in L_0^2(\Omega).
\end{cases}
$$

Since, $u_h^s \in [H_g^1(\Omega)]^2$ and $s \in [H_g^1(\Omega)]^2$, we have $s - u_h^s \in [H_0^1(\Omega)]^2$ and since $\nabla\cdot s = 0$ on Ω and $\nabla\cdot u_h^s = 0$ on $\Omega^{'}$, then

$$
\|\nabla(s-u_h^s)\|_\Omega^2 = (\nabla(s-u_h^s), \nabla(s-u_h^s))_\Omega = (\nabla\cdot(s-u_h^s), w)_\Omega = -(\nabla\cdot u_h^s, w)_\Omega \leq ||\nabla\cdot\tilde{u}_h||_{\tilde{\Omega}} ||w||_\Omega.
$$

Now, we will rely on the inf-sup condition to estimate $||w||_\Omega$:

$$\inf_{q\in L_0^2(\Omega)} \sup_{v\in[H_0^1(\Omega)]^2} \frac{(q,\nabla\cdot v)_\Omega}{||q||||\nabla v||} = \beta > 0$$

Since $w \in L_0^2(\Omega)$, $\beta \leq \sup_{v\in[H_0^1(\Omega)]^2} \frac{(w,\nabla\cdot v)_\Omega}{||w||||\nabla v||}$, so that:

$$||w||_\Omega \leq \frac{1}{\beta} \sup_{v\in[H_0^1(\Omega)]^2} \frac{(w,\nabla\cdot v)_\Omega}{||\nabla v||} = \frac{1}{\beta} \sup_{v\in[H_0^1(\Omega)]^2} \frac{(\nabla(s-u_h^s),\nabla v)_\Omega}{||\nabla v||} \leq \frac{1}{\beta}||\nabla(s-u_h^s)||_\Omega,$$

hence, $\|\nabla(s-u_h^s)\|_\Omega^2 \leq \frac{||\nabla\cdot\tilde{u}_h||_{\tilde{\Omega}}}{\beta}||\nabla(s-u_h^s)||_\Omega$,

Thus: $||\nabla(s-u_h^s)||_\Omega \leq \frac{||\nabla\cdot\tilde{u}_h||_{\tilde{\Omega}}}{\beta} = \left(\sum_{K\in\tilde{\mathcal{T}}_h} \frac{||\nabla\cdot\tilde{u}_h||_K^2}{\beta^2}\right)^{\frac{1}{2}}$.

It all together gives:

$$||\nabla(u-u_h^s)||_\Omega^2 = A + B \leq \sum_{K\in\tilde{\mathcal{T}}_h} \eta_{F,K}^2 + \sum_{K\in\tilde{\mathcal{T}}_h} \eta_{D,K}^2.$$

Now, we will deal with $||p-p_h^s||_\Omega$ through the inf-sup condition:

$$\inf_{q\in L_0^2(\Omega)} \sup_{v\in[H_0^1(\Omega)]^2} \frac{(q,\nabla\cdot v)_\Omega}{||q||||\nabla v||} = \beta > 0.$$

Since $p-p_h^s \in L_0^2(\Omega)$, we have $\beta \leq \sup_{v\in[H_0^1(\Omega)]^2} \frac{(p-p_h^s,\nabla\cdot v)_\Omega}{||p-p_h^s||||\nabla v||}$ and thus $||p-p_h^s|_\Omega \leq \frac{1}{\beta}\sup_{v\in[H_0^1(\Omega)]^2} \frac{(p-p_h^s,\nabla\cdot v)_\Omega}{||\nabla v||}$.

For $v\in[H_0^1(\Omega)]^2$, we have $||\nabla v||_\Omega$ is bounded since Ω is bounded, so let us take $\phi = \frac{v}{||\nabla v||}$, then

$$||p-p_h^s||_\Omega \leq \frac{1}{\beta} \sup_{\substack{\phi\in[H_0^1(\Omega)]^2 \\ ||\nabla\phi||_\Omega=1}} (p-p_h^s,\nabla\cdot\phi)_\Omega.$$

Now, fix $\phi\in[H_0^1(\Omega)]^2$ with $||\nabla\phi||_\Omega = 1$, then the weak solution in the first equation of system (1.17) gives:

$$(p,\nabla\cdot\phi)_\Omega = (\nabla u,\nabla\phi)_\Omega.$$

We have, $(p_h^s,\nabla\cdot\phi)_\Omega = (p_h^s I,\nabla\phi)_\Omega$ then, add and subtract $(\sigma_h,\nabla\phi)$ as well as $(\nabla u_h^s,\nabla\phi)$ and using Green theorem we get:

$$\begin{aligned}(p-p_h^s,\nabla\cdot\phi)_\Omega &= (\nabla u,\nabla\phi)_\Omega - (p_h^s,\nabla\cdot\phi)_\Omega - (\nabla u_h^s,\nabla\phi)_\Omega + (\nabla u_h^s,\nabla\phi)_\Omega - (\sigma_h,\nabla\phi)_\Omega + (\sigma_h,\nabla\phi)_\Omega \\ &= (\nabla(u-u_h^s),\nabla\phi)_\Omega + (\nabla u_h^s - p_h^s I - \sigma_h,\nabla\phi)_\Omega + (\sigma_h,\nabla\phi)_\Omega.\end{aligned}$$

Let us add and subtract s defined in system (3.5), we get

$$(\nabla(u-u_h^s),\nabla\phi)_\Omega = (\nabla(u-s),\nabla\phi)_\Omega + (\nabla(s-u_h^s),\nabla\phi)_\Omega.$$

Let us split ϕ in a divergence free contribution: $\phi = \phi_C + \phi_{NC}$, where ϕ_C is the solution of:

$$\begin{cases}\text{Find} \quad \phi_C\in[H_0^1(\Omega)]^2 \quad \text{with} \quad \nabla\cdot\phi_C = 0 \quad \text{such that:} \\ (\nabla\phi_C,\nabla v)_\Omega = (\nabla\phi,\nabla v)_\Omega \quad \forall v\in[H_0^1(\Omega)]^2 \quad \text{with} \quad \nabla\cdot v = 0.\end{cases}$$

Let $\phi_{NC} := \phi - \phi_C$, then $(\nabla\phi_{NC}, \nabla v) = 0$ for all $v \in [H_0^1(\Omega)]^2$ and $\nabla \cdot v = 0$, and, since $\phi_C \in [H_0^1(\Omega)]^2$ and $\nabla \cdot \phi_C = 0$, using $(\nabla\phi_{NC}, \nabla\phi_C)_\Omega = 0$, we have

$$\begin{aligned}||\nabla\phi||_\Omega^2 &= ||\nabla(\phi - \phi_c + \phi_c)||_\Omega^2 = ||\nabla(\phi_{NC} + \phi_c)||_\Omega^2 \\ &= ||\nabla\phi_{NC}||_\Omega^2 + ||\nabla\phi_c||_\Omega^2 + 2(\nabla\phi_{NC}, \nabla\phi_c)_\Omega = ||\nabla\phi_{NC}||_\Omega^2 + ||\nabla\phi_c||_\Omega^2.\end{aligned}$$

Now, we have

$$\begin{aligned}(p - p_h^s, \nabla\cdot\phi)_\Omega &= (p - p_h^s, \nabla\cdot\phi_{NC})_\Omega \\ &= \underbrace{(\nabla(u - u_h^s), \nabla\phi_{NC})_\Omega}_{Z_1} + \underbrace{(\nabla u_h - p_h^s I - \sigma_h, \nabla\phi_{NC})_\Omega}_{Z_2} + \underbrace{(\sigma_h, \nabla\phi_{NC})_\Omega}_{Z_3}\end{aligned}$$

Let us estimate Z_1:
$Z_1 = (\nabla(u-u_h^s), \nabla\phi_{NC})_\Omega = (\nabla(u-s), \nabla\phi_{NC})_\Omega + (\nabla(s-u_h^s), \nabla\phi_{NC})_\Omega$, but $u-s \in [H_0^1(\Omega)]^2$ and $\nabla\cdot(u-s) = 0$, then by the definition of ϕ_{NC} we gain, $(\nabla(u-s), \nabla\phi_{NC})_\Omega = 0$ and hence

$$\begin{aligned}Z_1 &= (\nabla(s - u_h^s), \nabla\phi_{NC})_\Omega \le ||\nabla(s - u_h^s)||_\Omega ||\nabla\phi_{NC}||_\Omega \\ &\le ||\nabla(s - u_h^s)||_\Omega ||\nabla\phi||_\Omega = ||\nabla(s - u_h^s)||_\Omega \le \frac{||\nabla\cdot\tilde{u}_h||_{\tilde{\Omega}}}{\beta} = \left(\sum_{K\in\tilde{\mathcal{T}}_h} \eta_{D,K}^2\right)^{\frac{1}{2}}.\end{aligned}$$

Then,

$$Z_1 \le \left(\sum_{K\in\tilde{\mathcal{T}}_h} \eta_{D,K}^2\right)^{\frac{1}{2}}.$$

Let us estimate Z_2:

$$\begin{aligned}Z_2 &= (\nabla u_h^s - p_h^s I - \sigma_h, \nabla\phi_{NC})_\Omega \le \sum_{K\in\tilde{\mathcal{T}}_h} ||\nabla\tilde{u}_h - \tilde{p}_h I - \tilde{\sigma}_h||_K ||\nabla\phi_{NC}||_K = \sum_{K\in\tilde{\mathcal{T}}_h} \eta_{F,K} ||\nabla\phi_{NC}||_K \\ &\le \left(\sum_{K\in\tilde{\mathcal{T}}_h} \eta_{F,K}^2\right)^{\frac{1}{2}} ||\nabla\phi_{NC}||_{\tilde{\Omega}} \le \left(\sum_{K\in\tilde{\mathcal{T}}_h} \eta_{F,K}^2\right)^{\frac{1}{2}} ||\nabla\phi_{NC}||_\Omega \le \left(\sum_{K\in\tilde{\mathcal{T}}_h} \eta_{F,K}^2\right)^{\frac{1}{2}} ||\nabla\phi||_\Omega = \left(\sum_{K\in\tilde{\mathcal{T}}_h} \eta_{F,K}^2\right)^{\frac{1}{2}}.\end{aligned}$$

Then,

$$Z_2 \le \left(\sum_{K\in\tilde{\mathcal{T}}_h} \eta_{F,K}^2\right)^{\frac{1}{2}}$$

Finally, let us observe that $Z_3 = (\sigma_h, \nabla\phi_{NC})_\Omega = (*) = 0$, where $(*)$ is computed in page 127 where can have ϕ_{NC} instead of ϕ because $\nabla\cdot\phi = 0$ in the prove and we only need $\phi_{NC} = 0$ on $\partial\Omega$ and this is satisfied since ϕ and ϕ_C belong to $[H_0^1(\Omega)]^2$ and $\phi_{NC} = \phi - \phi_C$. So,

$$(p - p_h^s, \nabla\cdot\phi)_\Omega = Z_1 + Z_2 + Z_3 \le \left(\sum_{K\in\tilde{\mathcal{T}}_h} \eta_{D,K}^2\right)^{\frac{1}{2}} + \left(\sum_{K\in\tilde{\mathcal{T}}_h} \eta_{F,K}^2\right)^{\frac{1}{2}}.$$

Then,

$$||p - p_h^s||_\Omega \le \frac{1}{\beta} \sup_{\substack{\phi\in[H_0^1(\Omega)]^2 \\ ||\nabla\phi||_\Omega = 1}} (p - p_h^s, \nabla\cdot\phi)_\Omega \le \frac{1}{\beta}\left(\sum_{K\in\tilde{\mathcal{T}}_h} \eta_{D,K}^2\right)^{\frac{1}{2}} + \frac{1}{\beta}\left(\sum_{K\in\tilde{\mathcal{T}}_h} \eta_{F,K}^2\right)^{\frac{1}{2}}.$$

Finally,

$$\beta||p-p_h^s||_\Omega \leq \left(\sum_{K\in\tilde{\mathcal{T}}_h}\eta_{D,K}^2\right)^{\frac{1}{2}}+\left(\sum_{K\in\tilde{\mathcal{T}}_h}\eta_{F,K}^2\right)^{\frac{1}{2}}.$$

■

3.1.3. Local Efficiency

As our study in the previous Chapter in Section 2.1.3, we have explained why we can not be able to prove the local efficiency and you can see the reason in Remark 2.8.

3.1.4. Numerical Results

We will take in this section $RT_k = RT_2$, $\mathbb{P}_k = \mathbb{P}_2$ for the velocity and $\mathbb{P}_k = \mathbb{P}_1$ for the pressure. Moreover, the inf-sup constant β is unknown for the domain of interest, so we fix a value $\beta = 0.5$ in this section taking into account that it could be small for stretched domains. For a more detailed discussion about β, see Section 3.2.3 and Appendix C. We have obtained in Theorem 3.5 that

$$||\nabla(u-u_h^s)||_\Omega^2 \leq \sum_{K\in\tilde{\mathcal{T}}_h}\eta_{F,K}^2+\sum_{K\in\tilde{\mathcal{T}}_h}\eta_{D,K}^2,$$

$$||p-p_h^s||_\Omega \leq \frac{1}{\beta}\left\{\left(\sum_{K\in\tilde{\mathcal{T}}_h}\eta_{F,K}^2\right)^{\frac{1}{2}}+\left(\sum_{K\in\tilde{\mathcal{T}}_h}\eta_{D,K}^2\right)^{\frac{1}{2}}\right\}.$$

We plot the velocity error ErrorU $:= ||\nabla(u-u_h^s)||_\Omega = \sqrt{||\nabla(u-u')||_{\Omega'}^2+||\nabla(u-\tilde{u}_h)||_{\tilde{\Omega}}^2}$, the velocity estimator EstimatorU $:= \sqrt{\sum_{K\in\tilde{\mathcal{T}}_h}\eta_{F,K}^2+\sum_{K\in\tilde{\mathcal{T}}_h}\eta_{D,K}^2}$, the pressure error ErrorP $:= ||p-p_h^s||_\Omega$ and the pressure estimator EstimatorP $:= \frac{1}{\beta}\left\{\left(\sum_{K\in\tilde{\mathcal{T}}_h}\eta_{F,K}^2\right)^{\frac{1}{2}}+\left(\sum_{K\in\tilde{\mathcal{T}}_h}\eta_{D,K}^2\right)^{\frac{1}{2}}\right\}$ with respect to different positions of interface γ which has the position $x = x_\gamma$ in a way that x_γ goes form the position very near to the inlet i.e. $x_\gamma = x_\gamma^i = 0.1$ to the position very near to the corner of the channel i.e. $x_\gamma = x_\gamma^f = L_1 - 0.02 = 5.08$ where, x_γ^i and x_γ^f are located in Figure 3.1.

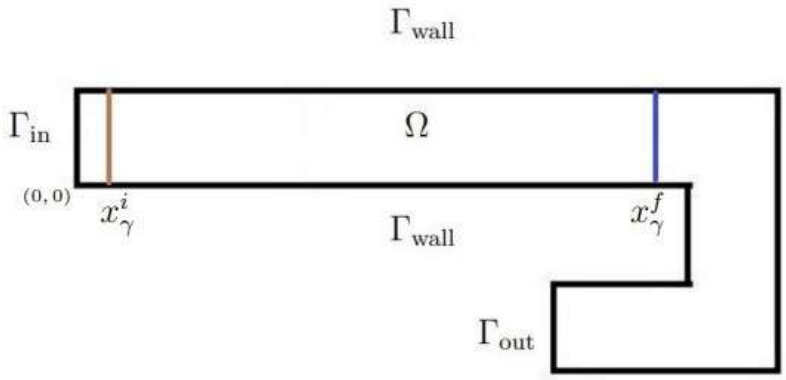

Figure 3.1.: Direction of the interface γ from the the position x_γ^i to the position x_γ^f.

For a quasi-uniform mesh with mesh size $h \approx 0.07$, we plot the error and the estimator for velocity u and pressure p in the Theorem 3.5 for different positions of the interfaces and we obtain the graph in Figure 3.2 for velocity and the graph in Figure 3.3 for pressure. Now, let us decrease the mesh size to $h \approx 0.04$ and plot the error and the estimator in the Theorem 3.5 for different positions of the interface and the graph is obtained in Figure 3.4 for velocity and Figure 3.5 for pressure.

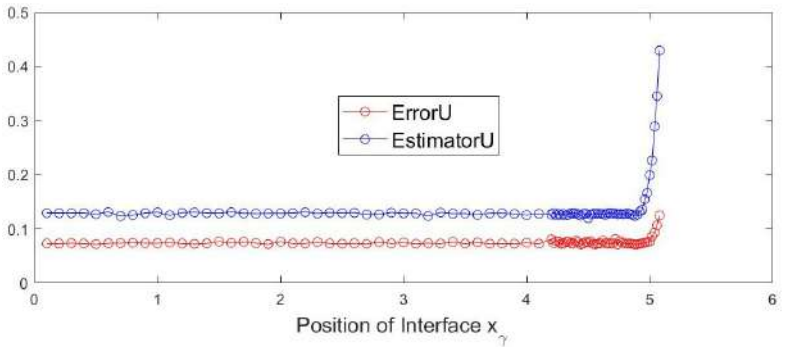

Figure 3.2.: Error on Ω and Estimator on $\tilde{\Omega}$ for velocity u for a mesh size $h \approx 0.07$

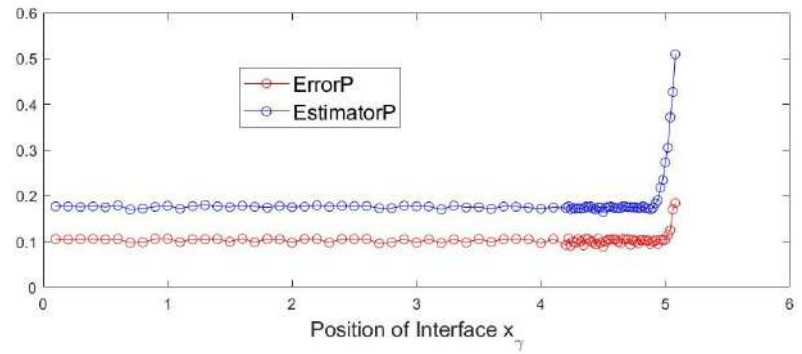

Figure 3.3.: Error on Ω and Estimator on $\tilde{\Omega}$ for pressure p for a mesh size $h \approx 0.07$

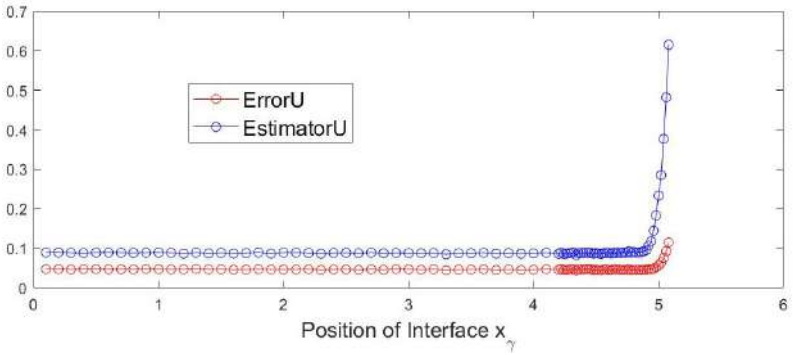

Figure 3.4.: Error on Ω and Estimator on $\tilde{\Omega}$ for velocity u for a mesh size $h \approx 0.04$

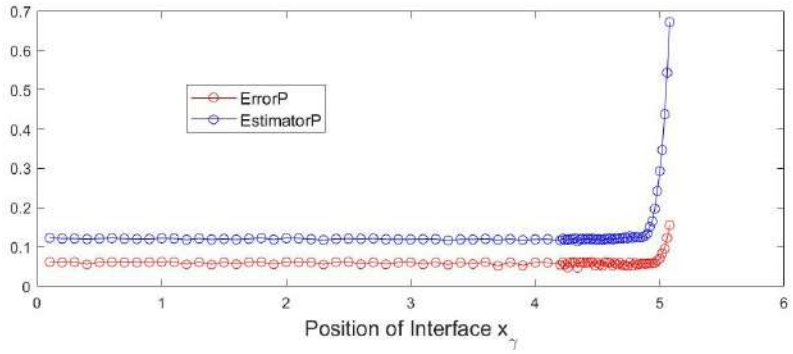

Figure 3.5.: Error on Ω and Estimator on $\tilde{\Omega}$ for pressure p for a mesh size $h \approx 0.04$

In Figures 3.2-3.5, we see that the errors and the estimators become much bigger as the interface becomes near to the corner and this is due to the dominance of the 2D affects in the corner. We must specify some tolerance in order to detect the suitable position of the interface. We will introduce an error indicator similar to **Indicator2** in Section 2.2.3 to detect the suitable position of the interface. To detect such interface we choose to introduce these two indicators on a region ω^γ for the velocity and the pressure which are defined respectively by

$$\eta_U^\gamma := ||\nabla(\tilde{u}_h - u')\psi_h^\gamma||_{\omega^\gamma}, \tag{3.6}$$

$$\eta_P^\gamma := ||(\tilde{p}_h - p')\psi_h^\gamma||_{\omega^\gamma}, \tag{3.7}$$

where ω^γ as in Figure 2.2. We plot η_U^γ and η_P^γ defined in (3.6) and (3.7) with respect to different positions of the interface γ for a mesh size $h \approx 0.07$ in Figure 3.6. We see that we can deduce a suitable interface position once a tolerance for these indicators is fixed. Now, let us fix the position of the interface at $x_\gamma = 4$ (others interface positions are possible, but the behavior would be the same). We plot in Figure 3.8 the indicator of velocity η_U^γ and in Figure 3.9 of the pressure η_P^γ with respect to different mesh sizes. We find that η_U^γ takes values between $1.19754e-06$ and $3.39165e-06$ for different mesh sizes which is approximately of the same tolerance 10^{-6} (but not constant) and η_P^γ takes values between $2.71508e-06$ and $9.27647e-06$ for different mesh sizes which is approximately of the same tolerance 10^{-6} (but not constant).

Now, let us define the total indicator for the velocity and pressure on ω^γ by

$$\eta^\gamma := \sqrt{(\eta_U^\gamma)^2 + (\eta_P^\gamma)^2}. \tag{3.8}$$

We plot η^γ defined in (3.8) with respect to different positions of the interface γ for a mesh size $h \approx 0.07$ in Figure 3.7. We plot in Figure 3.10 the total estimators η^γ on ω^γ with respect to different mesh sizes. We find that η^γ takes values between $2.96745e-06$ and $9.87705e-06$ for different mesh sizes which is approximately of the same tolerance 10^{-6} (but not constant). Finally, η^γ can be taken as an indicator for the position of the interface but it can be improved to be constant for different mesh sizes when we fix the position of the interface x_γ. This improvement is done if we introduce a new definition of reconstructing the flux which will be studied in the following section.

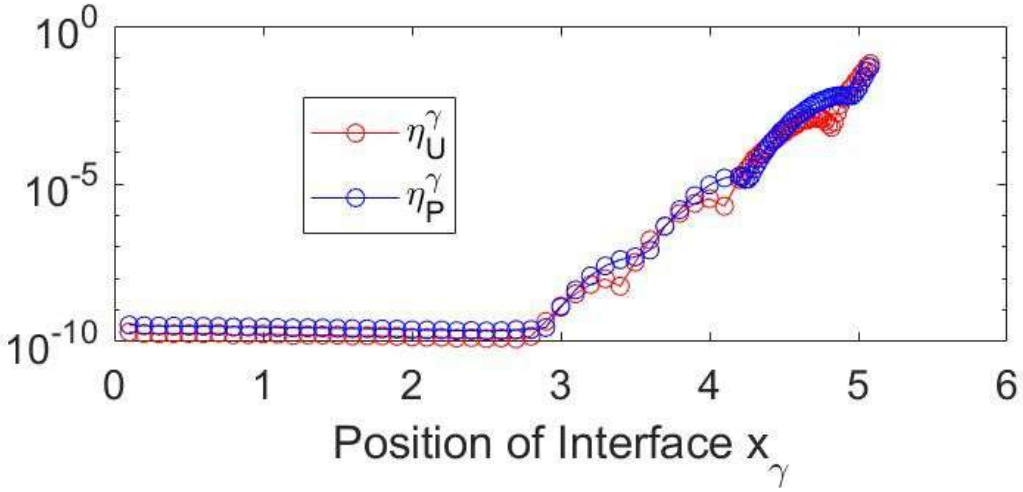

Figure 3.6.: Indicators η_U^γ and η_P^γ on ω^γ in semilogy scale with respect to different positions of the interface γ

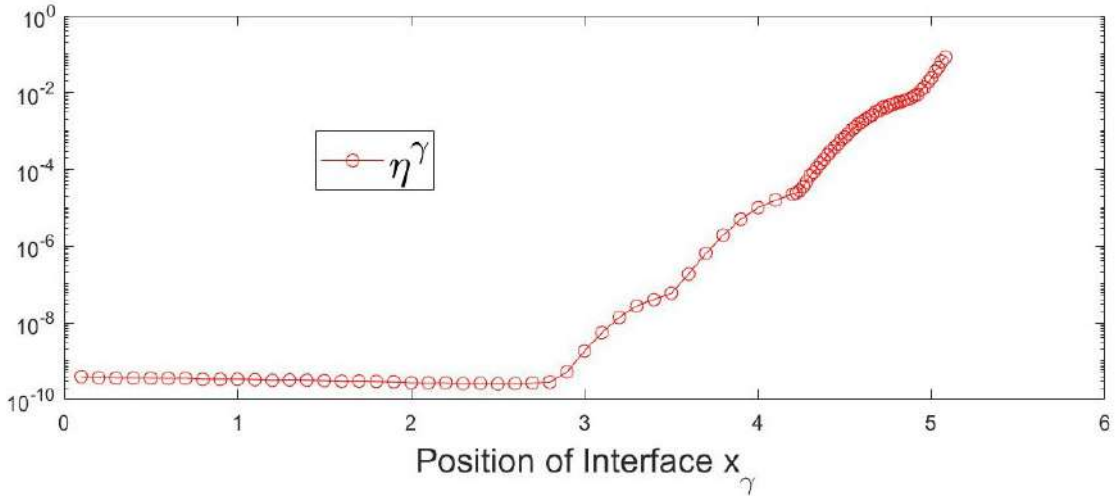

Figure 3.7.: Indicator η^{γ} on ω^{γ} in semilogy scale with respect to different positions of the interface γ

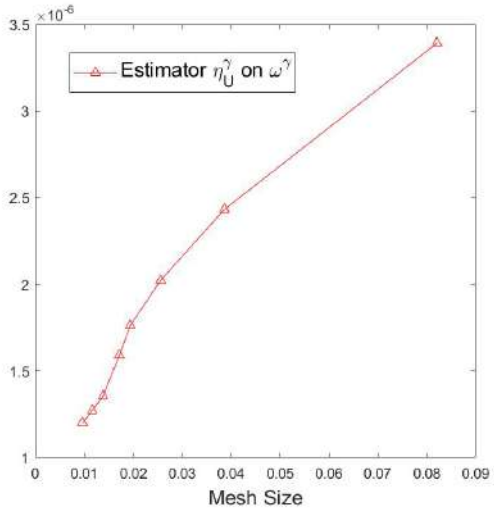

Figure 3.8.: Indicator η_U^{γ} w.r.t. different mesh sizes for a fixed interface at $x_{\gamma} = 4$

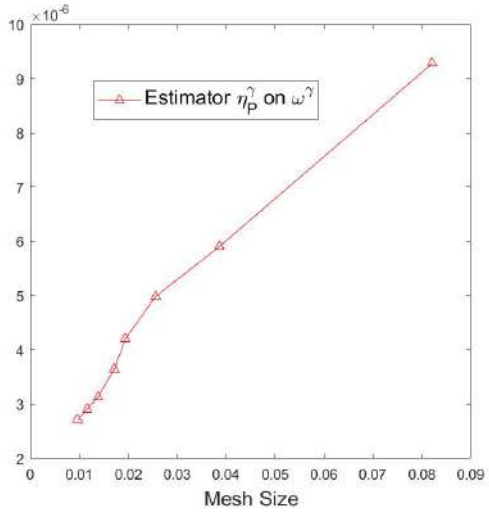

Figure 3.9.: Indicator η_P^γ w.r.t. different mesh sizes for a fixed interface at $x_\gamma = 4$

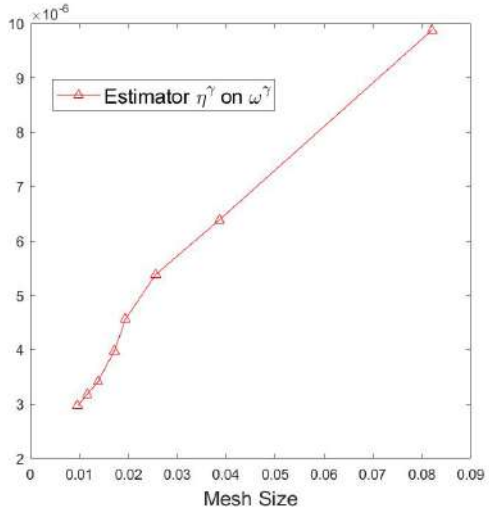

Figure 3.10.: Indicator η^γ w.r.t. different mesh sizes for a fixed interface at $x_\gamma = 4$

To conclude the section, we want to plot the errors of velocity and pressure on Ω' which are represented by:

$$||\nabla(u - u')||_{\Omega'}, \tag{3.9}$$

$$||(p - p')||_{\Omega'}. \tag{3.10}$$

The graph for the errors on Ω' with respect to different positions of the interface is represented in Figure 3.11 by the velocity and pressure errors on Ω' given by (3.9) and (3.10) respectively. We deduce from Figure 3.11 that the errors of the velocity and pressure on Ω' become more bigger when the interface position moves towards the corners of the domain. We also see that our indicator η^γ in Figure 3.7 detects that the suitable position of the interface is at $x_\gamma = 3$ and we conclude from Figure 3.11 that our indicator reasonable since the error of the velocity and pressure on Ω' begin its sharp increasing at $x_\gamma \approx 3$ also.

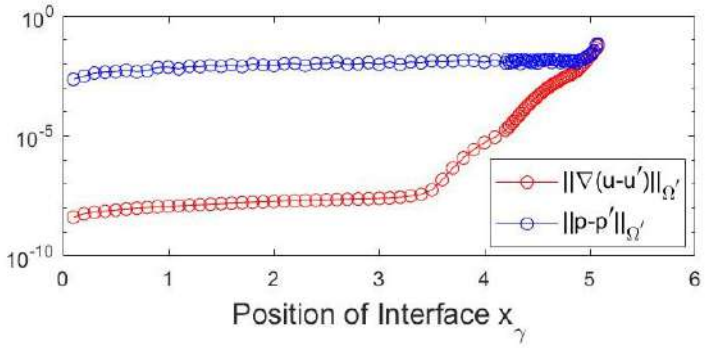

Figure 3.11.: Errors of the velocity and pressure on Ω' in semilogy scale with respect to different positions of the interface γ

Conclusions We have verified in this section that the errors and the estimators of pressure and velocity become much bigger near the corner. We have introduced an indicator in order to find a suitable position of the interface. The drawbacks of this definition of the flux are that we can not prove the efficiency (lower bound) and that for a fixed position of the interface, we find that the estimator η^γ, which is defined in (3.8), vary **a little bit** for different mesh sizes. These drawbacks will be solved in the following section by introducing the new definition of the flux reconstruction.

3.2. A posteriori estimator with upper and lower bounds

In this section we will make a new partition of unity of Ω and we will make a new definition of the stress reconstruction in order to be able to introduce an *a posteriori* error analysis with guaranteed reliability and provable efficiency as we did for Poisson in Section 2.2.

3.2.1. A posteriori error indicator

We now introduce the *a posteriori* error indicator with guaranteed reliability and provable efficiency. Let the position of the interface $x_\gamma \in [0.1, L_1 - R]$. To this end, consider the continuous function on Ω, named ψ^γ, defined on rectangular portion $[0, x_\gamma + R] \times [0, R]$ of the channel by

$$\psi^\gamma(x) = \begin{cases} 1, & \text{for} \quad x < x_\gamma \\ \frac{x_\gamma + R - x}{R}, & \text{for} \quad x \in [x_\gamma, x_\gamma + R] \\ 0, & \text{for} \quad x > x_\gamma + R \end{cases} \tag{3.11}$$

and extended by 0 everywhere else. Here, x_γ is the x-coordinate of the interface γ and we assume that $x_\gamma + R$ is still in the rectangular portion of the channel. We also introduce a piecewise affine (on mesh $\tilde{\mathcal{T}}_h$) version of ψ^γ:

$$\psi_h^\gamma(x) = \sum_{a \in \mathcal{V}_h} \psi^\gamma(a)\psi^a(x) \quad \text{for x} \in \tilde{\Omega} \tag{3.12}$$

and $\psi_h^\gamma = 1$ on Ω', where ψ^a is a hat function i.e. a polynomial of degree 1 that takes the value 1 at the node a and 0 on the other nodes different from a and $\mathcal{V}_h$ represents all

vertices that belongs to $\tilde{\Omega}$. Note the partition of unity on Ω

$$1 = \psi_h^\gamma + \sum_{a \in \mathcal{V}_h^*} (1 - \psi^\gamma(a))\psi^a,$$

recalling that $\mathcal{V}_h^*$ represents all vertices that belongs to $\tilde{\Omega} \setminus \gamma$. We define then the stress on whole $\Omega = \tilde{\Omega} \cup \Omega' \cup \gamma$ as

$$\sigma_h = \sigma_h^\gamma + \sum_{a \in \mathcal{V}_h^*} (1 - \psi^\gamma(a))\sigma_h^a + (\nabla u' - p'I)\mathbb{1}_{\Omega'}. \tag{3.13}$$

We will divide the stress into two stresses. The first stress is defined on Ω' by

$$\sigma'_h = \nabla u' - p'_h I \tag{3.14}$$

and the second stress is defined on $\tilde{\Omega}$ by

$$\tilde{\sigma}_h = \sigma_h^\gamma + \sum_{a \in \mathcal{V}_h^*} (1 - \psi^\gamma(a))\sigma_h^a. \tag{3.15}$$

Here σ_h^a is defined on all patches $\omega^a = \text{supp}(\psi_h^a) \cap \tilde{\Omega}$ for all nodes $a \in \mathcal{V}_h^*$ as follows: $\sigma_h^a \in \Sigma_h^a$ and $p_h^a \in Q_h^a$ such that for all $\tau_h \in \Sigma_h^a$ and $q_h \in Q_h^a$

$$\int_{\omega^a} \sigma_h^a \cdot \tau_h + \int_{\omega^a} p_h^a \text{div}\tau_h = \int_{\omega^a} (\nabla \tilde{u}_h - \tilde{p}_h I)\psi^a \cdot \tau_h, \tag{3.16}$$

$$\int_{\omega^a} q_h \text{div}\sigma_h^a = \int_{\omega^a} ((\nabla \tilde{u}_h - \tilde{p}_h I) \cdot \nabla \psi^a)\, q_h. \tag{3.17}$$

Similarly, σ_h^γ is defined on the patch $\omega^\gamma = \text{supp}(\psi_h^\gamma) \cap \tilde{\Omega}$ as follows: $\sigma_h^\gamma \in \Sigma_h^\gamma$ and $p_h^\gamma \in Q_h^\gamma$ such that for all $\tau_h \in \Sigma_h^{\gamma,0}$ and $q_h \in Q_h^\gamma$

$$\int_{\omega^\gamma} \sigma_h^\gamma \cdot \tau_h + \int_{\omega^\gamma} p_h^\gamma \text{div}\tau_h = \int_{\omega^\gamma} (\nabla \tilde{u}_h - \tilde{p}_h I)\psi_h^\gamma \cdot \tau_h, \tag{3.18}$$

$$\int_{\omega^\gamma} q_h \text{div}\sigma_h^\gamma = \int_{\omega^\gamma} \left((\nabla \tilde{u}_h - \tilde{p}_h I) \cdot \nabla \psi_h^\gamma\right) q_h. \tag{3.19}$$

To fix the approximation spaces let us consider the following cases.

Case 1: a in an internal node of $\tilde{\Omega}$

$\Sigma_h^a := \{\sigma_h \in [RT_2(\omega^a)]^2, \sigma_h n = 0 \quad \text{on} \quad \partial\omega^a\}$
$Q_h^a := \{q_h \in [L^2(\omega^a)]^2, q_h|_K \in [\mathbb{P}_1(K)]^2, \forall K \in \omega^a, \int_{\omega^a} q_h = 0\}$

Case 2: a on the wall of $\tilde{\Omega} \setminus \gamma$

$\Sigma_h^a := \{\sigma_h \in [RT_2(\omega^a)]^2, \sigma_h n = 0 \quad \text{on} \quad \partial\omega^a \setminus \partial\tilde{\Omega}\}$
$Q_h^a := \{q_h \in [L^2(\omega^a)]^2, q_h|_K \in [\mathbb{P}_1(K)]^2, \forall K \in \omega^a\}$

Case 3: $a = \gamma$

$\Sigma_h^\gamma := \{\sigma_h \in [RT_2(\omega^\gamma)]^2, \sigma_h n = 0 \quad \text{on} \quad \partial\omega^\gamma \setminus \partial\tilde{\Omega} \quad \text{and} \quad \sigma_h n = (\nabla u' - p'_h I)n \quad \text{on} \quad \gamma\}$
$\Sigma_h^{\gamma,0} := \{\sigma_h \in [RT_2(\omega^\gamma)]^2, \sigma_h n = 0 \quad \text{on} \quad \partial\omega^\gamma \setminus \partial\tilde{\Omega} \quad \text{and} \quad \text{on} \quad \gamma\}$
$Q_h^\gamma := \{q_h \in [L^2(\omega^\gamma)]^2, q_h|_K \in [\mathbb{P}_1(K)]^2, \forall K \in \omega^\gamma\}$

Lemma 3.6. *We have $\tilde{\sigma}_h := \sigma_h^\gamma + \sum_{a \in \mathcal{V}_h^*}(1 - \psi^\gamma(a))\sigma_h^a$ on $\tilde{\Omega}$, then $\nabla \cdot \tilde{\sigma}_h = 0$ on $\tilde{\Omega}$ and consequently $\nabla \cdot \sigma_h = 0$ on Ω.*

Proof. Straightforward computations give the result as we did before in the proof of **Proposition 3.4** Page 125. ■

3.2.2. Main theorem and the proof

Theorem 3.7. *Let (u,p) be the weak solution defined by (1.17). Let (u_h^s, p_h^s) and σ_h defined as in (1.40)–(1.41) and (3.13) respectively. Let us define the local flux estimator by*

$$\eta_{F,K} := ||\nabla \tilde{u}_h - \tilde{p}_h I - \tilde{\sigma}_h||_K$$

and the local divergence estimator by:

$$\eta_{D,K} := \frac{||\nabla \cdot \tilde{u}_h||_K}{\beta}.$$

Then, we have the upper bounds for velocity and pressure

$$||\nabla(u-u_h^s)||_\Omega^2 \leq ||\nabla u_h^s - p_h^s I - \sigma_h||_\Omega^2 + \frac{||\nabla \cdot u_h^s||_\Omega^2}{\beta^2} =: \sum_{K\in\tilde{\mathcal{T}}_h} \eta_{F,K}^2 + \sum_{K\in\tilde{\mathcal{T}}_h} \eta_{D,K}^2, \quad (3.20)$$

$$||p-p_h^s||_\Omega \leq \frac{1}{\beta}\left\{ \left(\sum_{K\in\tilde{\mathcal{T}}_h} \eta_{F,K}^2 \right)^{\frac{1}{2}} + \left(\sum_{K\in\tilde{\mathcal{T}}_h} \eta_{D,K}^2 \right)^{\frac{1}{2}} \right\}, \quad (3.21)$$

and the lower bound is

$$||\nabla u_h^s - p_h^s I - \sigma_h||_\Omega^2 \leqslant C\|\nabla u - pI - (\nabla u_h^s - p_h^s I)\|_\Omega^2 \quad (3.22)$$

with a constant C depending only on the mesh regularity.

Proof. The proof of the reliability (3.20) and (3.21) is completely the same of the proof of Theorem 3.5 since we have used the conditions $\sigma_h \in H(\mathrm{div},\Omega)$ and $\nabla \cdot \sigma_h = 0$ and the stress σ_h defined by (3.13) also satisfies these conditions. Now, the proof of (3.22) is organized in several steps.

Step 1: error caused by the interface, prior to discretization. Let us begin with a "continuous " version of our "simplified " problem: we search for $(\tilde{u},\tilde{p})$ on $\tilde{\Omega}$ such that

$$-\Delta\tilde{u} + \nabla\tilde{p} = 0 \text{ in } \tilde{\Omega}$$

$$\mathrm{div}\,\tilde{u} = 0 \text{ in } \tilde{\Omega}$$

$$\tilde{u} = u' \text{ on } \gamma, \tilde{u} = u_{out} \text{ on } \Gamma_{out} \text{and } \tilde{u} = 0 \text{ on } \Gamma_{wall}.$$

Moreover:

$$u^s = \begin{cases} u', \text{ on } \Omega' \\ \tilde{u}, \text{ on } \tilde{\Omega} \end{cases}$$

and

$$p^s = \begin{cases} p_h', \text{ on } \Omega' \\ \widetilde{p}, \text{ on } \tilde{\Omega} \end{cases}$$

with

$$\int_{\tilde{\Omega}} \widetilde{p} = \int_{\tilde{\Omega}} \widetilde{p}_h.$$

Here, p^s is just an auxiliary tool: the theorem is about p_h^s and not p^s. We want to study $\|\nabla u - pI - (\nabla u^s - p^s I)\|_\Omega$ which is the error introduced by the interface itself, without

discretizing the problem on $\tilde{\Omega}$. More precisely, we want to relate it to the continuous version of $\|\sigma_h^\gamma - (\nabla\tilde{u}_h - \tilde{p}_h I)\psi_h^\gamma\|_{\omega^\gamma}$. We thus introduce the continuous version of σ_h^γ: find $\sigma^\gamma \in H(\mathrm{div},\omega^\gamma)^2, p^\gamma \in L^2(\omega^\gamma)^2$ with $\omega^\gamma = \mathrm{supp}(\psi_h^\gamma)\cap\tilde{\Omega}$ such that $\sigma^\gamma n = -p_h' n$ on γ and for all $\tau^\gamma \in H(\mathrm{div},\omega^\gamma)^2, q^\gamma \in L^2(\omega^\gamma)^2$ with $\tau^\gamma n = 0$ on γ

$$\int_{\omega^\gamma} \sigma^\gamma\cdot\tau^\gamma + \int_{\omega^\gamma} p^\gamma \mathrm{div}\tau^\gamma = \int_{\omega^\gamma} (\nabla\tilde{u} - \tilde{p}I)\cdot\tau^\gamma, \tag{3.23a}$$

$$\int_{\omega^\gamma} q^\gamma \mathrm{div}\sigma^\gamma = 0. \tag{3.23b}$$

We want to prove

$$\|\nabla\tilde{u} - \tilde{p}I - \sigma^\gamma\|_{\omega^\gamma} \le C\,\|\nabla u - pI - \nabla u^s + p^s I\|_\Omega\ . \tag{3.24}$$

To this end, let $\omega_R^\gamma = \mathrm{supp}(\psi^\gamma)\cap\tilde{\Omega}$ with $\gamma_R = \partial\omega_R^\gamma \cap \{x = x_\gamma + R\}$. Introduce $\theta \in H^1(\omega_R^\gamma)^2$:

$$\Delta\theta = 0 \text{ on } \omega_R^\gamma$$

$$\nabla\theta\cdot n = [\nabla u^s - p^s I]n \text{ on } \gamma$$

$$\nabla\theta\cdot n = 0 \text{ on } \gamma_R$$

$$\theta = 0 \text{ on the wall}$$

Here, $[\nabla u^s - p^s I]$ stands for the jump on γ. Let $\tau^c \in H\left(\mathrm{div},\omega^\gamma\right)^2$ defined by $\tau^c = \nabla\theta$ on ω_R^γ and $\tau^c = 0$ on $\omega^\gamma \setminus \omega_R^\gamma$ (note that $\omega_R^\gamma \subset \omega^\gamma$) so that $\mathrm{div}\tau^c = 0$ on ω^γ. Now set $\tau^\gamma = \sigma^\gamma - (\nabla\tilde{u} - \tilde{p}I) + \tau^c$ and observe that $\mathrm{div}\tau^\gamma = 0$ a.e. on ω^γ and $\tau^\gamma n = 0$ on γ. We can thus use this τ^γ as the test function in (3.23). Since $\int_{\omega^\gamma} p^\gamma \mathrm{div}\tau^\gamma = 0$, this gives

$$\int_{\omega^\gamma} (\sigma^\gamma - (\nabla\tilde{u} - \tilde{p}I))\cdot(\sigma^\gamma - (\nabla\tilde{u} - \tilde{p}I) + \tau^c) = 0$$

so that

$$\|\sigma^\gamma - (\nabla\tilde{u} - \tilde{p}I)\|_{\omega^\gamma} \leqslant \|\tau^c\|_{\omega^\gamma} = \|\nabla\theta\|_{\omega_R^\gamma}.$$

We prove in Lemma 2.13

$$\|\nabla\theta\|_{\omega_R^\gamma} \leqslant C_1 \|[\nabla u^s - p^s I]n\|_{-1/2,\gamma}$$

with $C_1 > 0$ which does not depend on R and the norm $\|\cdot\|_{-1/2,\gamma}$ defined in the Lemma. Thus,

$$\|\sigma^\gamma - (\nabla\tilde{u} - \tilde{p}I)\|_{\omega^\gamma} \leqslant C_1 \|[\nabla u^s - p^s I]n\|_{-1/2,\gamma}.$$

Now, we return to bound the error $\|\nabla u - \nabla u^s\|_\Omega$ from below. To this end, observe that $\Delta(u - u^s) - \nabla(p - p^s) = 0$ in Ω, $\mathrm{div}(u - u^s) = 0$ in Ω, $u - u^s = 0$ on $\partial\Omega$, and $[(\nabla(u - u^s) - (p - p^s)I)n] = [\nabla u^s - p^s I]n$ on γ. By integration by parts

$$\int_\Omega (\nabla(u - u^s) - (p - p^s)I)\cdot\nabla v = \int_\gamma [\nabla u^s - p^s I]n\cdot v.$$

By Lemma 2.14, $\forall\eta \in H^{1/2}(\gamma)$ $\exists v \in H^1(\Omega)$ vanishing on $\partial\Omega$ such that $v_{|_\gamma} = \eta$ and

$$\|\nabla v\|_\Omega \leqslant C_2 \|\eta\|_{1/2,\gamma}$$

with C_2 that does not depend on the geometrical parameters. It suffices to take $v = \theta$ from Lemma on ω_R^γ and as the mirror image of θ to the left of γ. We have thus $\forall \eta \in H^{1/2}(\gamma)$

$$\int_\gamma [\nabla u^s - p^s I] n \cdot v \leqslant C_2 \|\eta\|_{1/2,\gamma} \|\nabla(u - u^s) - (p - p^s) I\|_\Omega$$

so that

$$\|[\nabla u^s - p^s I] n\|_{-1/2,\gamma} \leqslant C_2 \|\nabla u - pI - (\nabla u^s - p^s I)\|_\Omega$$

and finally (3.24) is obtained with $C = C_1 C_2$.

Step 2: error caused by the interface, adding the discretization. We want now to discretize (3.24), i.e. to prove

$$\|\sigma_h^\gamma - (\nabla \tilde{u}_h - \tilde{p}_h I)\psi_h^\gamma\|_{\omega^\gamma} \leqslant C \left(\|\nabla u - pI - (\nabla u^s - p^s I)\|_\Omega + \|\nabla \tilde{u} - \tilde{p} I - (\nabla \tilde{u}_h - \tilde{p}_h I)\|_{\omega^\gamma}\right) \tag{3.25}$$

We repeat the trick with the mirror image, i.e. introduce $\omega^{\gamma,m}$ as in Poisson case. A small technical difficulty is now that $\sigma_h^\gamma n \neq 0$ on γ. We have rather $\sigma^\gamma n = -p_h' n$ on γ. We take this into account by introducing $p^\gamma = p'_{h|_\gamma}$ and

- $\tilde{u}_h^m$ as the function on $\omega^{\gamma,m}$, symmetric wrt γ, and $\tilde{u}_h^m = \tilde{u}_h$ on ω^γ;
- $\tilde{p}_h^m$ as the function on $\omega^{\gamma,m}$, antisymmetric wrt γ, and $\tilde{p}_h^m = \tilde{p}_h - p^\gamma$ on ω^γ;
- $\tilde{\sigma}_h^m$ as the function on $\omega^{\gamma,m}$, antisymmetric wrt γ, and $\tilde{\sigma}_h^m = \tilde{\sigma}_h^\gamma - \tilde{\sigma}_h^{p^\gamma}$ on ω^γ where $\tilde{\sigma}_h^{p^\gamma}$ is the solution to (3.18)–(3.19) with $\tilde{u}_h = 0$, $\tilde{p}_h = -p^\gamma$ (note in particular that $\tilde{\sigma}_h^m n = 0$ on γ).

We introduce a "semi-discrete" version of the flux σ^γ: find $\hat{\sigma}^\gamma \in H(\mathrm{div}, \omega^\gamma)^2$, $\hat{p}^\gamma \in L^2(\omega^\gamma)$ such that $\hat{\sigma}^\gamma n = -p_h' n$ on γ and $\forall \tau^\gamma \in H(\mathrm{div}, \omega^\gamma)^2, \forall q^\gamma \in L^2(\omega^\gamma)^2$ with $\tau^\gamma \cdot n = 0$ on γ

$$\int_{\omega^\gamma} \hat{\sigma}^\gamma \cdot \tau^\gamma + \int_{\omega^\gamma} \hat{p}^\gamma \,\mathrm{div}\, \tau^\gamma = \int_{\omega^\gamma} (\nabla \tilde{u}_h - \tilde{p}_h I) \cdot \tau^\gamma, \tag{3.26a}$$

$$\int_{\omega^\gamma} q^\gamma \,\mathrm{div}\, \hat{\sigma}^\gamma = 0 \quad . \tag{3.26b}$$

We then extend it, similar as above

- $\hat{\sigma}^m$ as the function on $\omega^{\gamma,m}$, antisymmetric wrt γ, and $\hat{\sigma}^m = \hat{\sigma}^\gamma + p^\gamma I$ on ω^γ.

We then identify the minimums in Theorem 1.2 of [37], applied on $\omega^{\gamma,m}$ with these $\tilde{\sigma}_h^m$ and $\hat{\sigma}^m$. Using the symmetry and the fact that the terms with p^γ cancel out, we arrive at

$$\|\sigma_h^\gamma - (\nabla \tilde{u}_h - \tilde{p}_h I)\psi_h^\gamma\|_{\omega^\gamma} \leqslant C \|\hat{\sigma}^\gamma - (\nabla \tilde{u}_h - \tilde{p}_h I)\|_{\omega^\gamma}.$$

This entails by the triangle inequality

$$\|\sigma_h^\gamma - (\nabla \tilde{u}_h - \tilde{p}_h I)\psi_h^\gamma\|_{\omega^\gamma} \leqslant C \left(\|\hat{\sigma}^\gamma - \sigma^\gamma\|_{\omega^\gamma} + \|\sigma^\gamma - (\nabla \tilde{u} - \tilde{p} I)\|_{\omega^\gamma} + \|(\nabla \tilde{u} - \tilde{p} I) - (\nabla \tilde{u}_h - \tilde{p}_h I)\|_{\omega^\gamma}\right)$$

We can now derive (3.25) as in Poisson case.

Step 3: discretization error inside $\tilde{\Omega}$. We have at all the nodes a of the mesh $\tilde{\mathcal{T}_h}$

$$\|\sigma_h^a - (\nabla \tilde{u}_h - \tilde{p}_h I)\psi^a\|_{\omega^a} \leqslant C\|\nabla\tilde{u} - \tilde{p}I - (\nabla\tilde{u}_h - \tilde{p}_h I)\|_{\omega^a} \tag{3.27}$$

This is completely standard and can be proven by using Theorem 1.2 of [37] on ω^a.

Step 4: putting everything together. Using the partition of unity and (3.25), (3.27) we arrive at (cf. the details in Poisson case)

$$\|\sigma_h - (\nabla u_h^s - p_h^s I)\|_\Omega^2 = \|\tilde{\sigma}_h - (\nabla\tilde{u}_h - \tilde{p}_h I)\|_{\tilde{\Omega}}^2$$

$$\leqslant C\left(\|\nabla u - pI - (\nabla u^s - p^s I)\|_\Omega^2 + \|\nabla\tilde{u} - \tilde{p}I - (\nabla\tilde{u}_h - \tilde{p}_h I)\|_{\tilde{\Omega}}^2\right)$$

$$\leqslant C\left(\|\nabla u - \nabla u^s\|_\Omega^2 + \|p - p^s\|_{\tilde{\Omega}}^2 + \|\nabla\tilde{u} - \nabla\tilde{u}_h\|_{\tilde{\Omega}}^2 + \|\tilde{p} - \tilde{p}_h\|_{\tilde{\Omega}}^2\right)$$

Observe that we have

$$\|p - p^s\|_{\tilde{\Omega}}^2 \leq \frac{1}{\tilde{\beta}^2}\|\nabla u - \nabla u^s\|_{\tilde{\Omega}}^2 + \langle p - \tilde{p}_h\rangle_{\tilde{\Omega}}^2|\tilde{\Omega}| \tag{3.28}$$

where $\tilde{\beta}$ is the inf-sup constant for $\tilde{\Omega}$ and $\langle\cdot\rangle_{\tilde{\Omega}} = \frac{1}{|\tilde{\Omega}|}\int_{\tilde{\Omega}}\cdot$ denotes the average over $\tilde{\Omega}$. Indeed, taking any $\tilde{v} \in [H_0^1(\tilde{\Omega})]^2$ as a test function in (1.23) and (1.17), we get

$$(\nabla\tilde{u}, \nabla\tilde{v})_{\tilde{\Omega}} - (\nabla\cdot\tilde{v}, p^s)_{\tilde{\Omega}} = 0$$

and

$$(\nabla u, \nabla\tilde{v})_{\tilde{\Omega}} - (\nabla\cdot\tilde{v}, p)_{\tilde{\Omega}} = 0$$

then using the above two weak formulations, we get

$$\int_{\tilde{\Omega}}(p - p^s - \langle p - p^s\rangle_{\tilde{\Omega}})\operatorname{div}\tilde{v} = \int_{\tilde{\Omega}}(p - p^s)\operatorname{div}\tilde{v} = \int_{\tilde{\Omega}}(\nabla u - \nabla\tilde{u})\cdot\nabla\tilde{v}. \tag{3.29}$$

Indeed,

$$\begin{aligned}\int_{\tilde{\Omega}}(p - p^s - \langle p - p^s\rangle_{\tilde{\Omega}})\operatorname{div}\tilde{v} &= \int_{\tilde{\Omega}}\left(p - p^s - \frac{1}{|\tilde{\Omega}|}\int_{\tilde{\Omega}}(p - p^s)\right)\operatorname{div}\tilde{v}\\ &= \int_{\tilde{\Omega}}(p - p^s)\operatorname{div}\tilde{v} - \frac{1}{|\tilde{\Omega}|}\int_{\tilde{\Omega}}(p - p^s)\int_{\tilde{\Omega}}\operatorname{div}\tilde{v}\end{aligned}$$

Now, we have $\int_{\tilde{\Omega}}\operatorname{div}\tilde{v} = \int_{\partial\tilde{\Omega}}\tilde{v}\cdot n = 0$ as $\tilde{v} \in [H_0^1(\tilde{\Omega})]^2$, then

$$\int_{\tilde{\Omega}}\left(p - p^s - \langle p - p^s\rangle_{\tilde{\Omega}}\right)\operatorname{div}\tilde{v} = \int_{\tilde{\Omega}}(p - p^s)\operatorname{div}\tilde{v},$$

but for any $q \in L_0^2(\tilde{\Omega})$

$$\tilde{\beta}\|q\|_{\tilde{\Omega}} \leq \int_{\tilde{\Omega}}(p - \tilde{p})\operatorname{div}\tilde{v}\sup_{v\in[H_0^1(\tilde{\Omega})]^2}\frac{(q, \nabla\cdot\tilde{v})_{\tilde{\Omega}}}{||\nabla\tilde{v}||_{\tilde{\Omega}}}.$$

Since $\inf_{q\in L^2_0(\tilde{\Omega})}\sup_{\tilde{v}\in[H^1_0(\tilde{\Omega})]^2}\frac{(q,\nabla\cdot\tilde{v})_{\tilde{\Omega}}}{||q||_{\tilde{\Omega}}||\nabla\tilde{v}||_{\tilde{\Omega}}}=\tilde{\beta}>0$, then for any $q\in L^2_0(\tilde{\Omega})$, we have

$$\tilde{\beta}\|q\|_{\tilde{\Omega}}\leq\sup_{\tilde{v}\in[H^1_0(\tilde{\Omega})]^2}\frac{(q,\nabla\cdot\tilde{v})_{\tilde{\Omega}}}{||\nabla\tilde{v}||_{\tilde{\Omega}}} \tag{3.30}$$

and noting that

$$\|p-p^s\|^2_{\tilde{\Omega}}=\|p-p^s-\langle p-p^s\rangle_{\tilde{\Omega}}\|^2_{\tilde{\Omega}}+\|\langle p-p^s\rangle_{\tilde{\Omega}}\|^2_{\tilde{\Omega}} \tag{3.31}$$

since

$$\begin{aligned}\Big(p-p^s-\langle p-p^s\rangle_{\tilde{\Omega}},\langle p-p^s\rangle_{\tilde{\Omega}}\Big)_{\tilde{\Omega}}&=\int_{\tilde{\Omega}}\Big(p-p^s-\frac{1}{|\tilde{\Omega}|}\int_{\tilde{\Omega}}(p-p^s)\Big)\Big(\frac{1}{|\tilde{\Omega}|}\int_{\tilde{\Omega}}(p-p^s)\Big)\\&=\Big(\int_{\tilde{\Omega}}p-p^s-\int_{\tilde{\Omega}}p-p^s\Big)\Big(\frac{1}{|\tilde{\Omega}|}\int_{\tilde{\Omega}}(p-p^s)\Big)\\&=0\end{aligned}$$

and $\langle p-p^s\rangle_{\tilde{\Omega}}=\langle p-\tilde{p}_h\rangle_{\tilde{\Omega}}$. Indeed, $|\tilde{\Omega}|\langle p^s\rangle_{\tilde{\Omega}}=-|\Omega'|\langle p_h^{'}\rangle_{\Omega'}=|\tilde{\Omega}|\langle\tilde{p}_h\rangle_{\tilde{\Omega}}$.
We also have

$$\|\tilde{p}-\tilde{p}_h\|_{\tilde{\Omega}}\leq\left(\frac{1}{\tilde{\beta}^2}\|\nabla u-\nabla u^s\|^2_{\tilde{\Omega}}+\langle p-\tilde{p}_h\rangle^2_{\tilde{\Omega}}\,|\tilde{\Omega}|\right)^{\frac{1}{2}}+\|p-\tilde{p}_h\|_{\tilde{\Omega}}. \tag{3.32}$$

Indeed, we have

$$\|\tilde{p}-\tilde{p}_h\|_{\tilde{\Omega}}\leq\|p-\tilde{p}\|_{\tilde{\Omega}}+\|p-\tilde{p}_h\|_{\tilde{\Omega}}. \tag{3.33}$$

Now let us bound $\|p-\tilde{p}\|_{\tilde{\Omega}}$, we have $\big(p-p^s-\langle p-p^s\rangle_{\tilde{\Omega}}\big)\in L^2_0(\Omega)$ and using (3.30) and (3.29) we get

$$\begin{aligned}\tilde{\beta}\left\|p-p^s-\langle p-p^s\rangle_{\tilde{\Omega}}\right\|_{\tilde{\Omega}}&\leq\sup_{\tilde{v}\in[H^1_0(\tilde{\Omega})]^2}\frac{\big(p-p^s-\langle p-p^s\rangle_{\tilde{\Omega}},\nabla\cdot\tilde{v}\big)_{\tilde{\Omega}}}{||\nabla\tilde{v}||_{\tilde{\Omega}}}\\&=\sup_{\tilde{v}\in[H^1_0(\tilde{\Omega})]^2}\frac{\big(\nabla u-\nabla\tilde{u},\nabla\tilde{v}\big)_{\tilde{\Omega}}}{||\nabla\tilde{v}||_{\tilde{\Omega}}}\leq\|\nabla u-\nabla\tilde{u}\|_{\tilde{\Omega}}.\end{aligned}$$

Then,

$$\tilde{\beta}^2\left\|p-p^s-\langle p-p^s\rangle_{\tilde{\Omega}}\right\|^2_{\tilde{\Omega}}\leq\|\nabla u-\nabla\tilde{u}\|^2_{\tilde{\Omega}}.$$

Now, using (3.31) and $\|\langle p-p^s\rangle_{\tilde{\Omega}}\|^2_{\tilde{\Omega}}=|\tilde{\Omega}|\langle p-\tilde{p}_h\rangle^2_{\tilde{\Omega}}$, we have

$$\tilde{\beta}^2\Big(\|p-p^s\|^2_{\tilde{\Omega}}-|\tilde{\Omega}|\langle p-\tilde{p}_h\rangle^2_{\tilde{\Omega}}\Big)\leq\|\nabla u-\nabla\tilde{u}\|^2_{\tilde{\Omega}},$$

then

$$\|p-\tilde{p}\|^2_{\tilde{\Omega}}\leq\frac{1}{\tilde{\beta}^2}\|\nabla u-\nabla\tilde{u}\|^2_{\tilde{\Omega}}+|\tilde{\Omega}|\langle p-\tilde{p}_h\rangle^2_{\tilde{\Omega}}.$$

Finally, we get (3.28) i.e.

$$\|p-\tilde{p}\|_{\tilde{\Omega}}\leq\left(\frac{1}{\tilde{\beta}^2}\|\nabla u-\nabla\tilde{u}\|^2_{\tilde{\Omega}}+|\tilde{\Omega}|\langle p-\tilde{p}_h\rangle^2_{\tilde{\Omega}}\right)^{\frac{1}{2}}. \tag{3.34}$$

Now, we substitute (3.34) in (3.33) we get (3.32).
Now, assuming that $\tilde{\beta}$ is uniformly bounded from below and incorporating it in the constants C. Using (3.28) and (3.32)

$$\|\sigma_h-(\nabla u_h^s-p_h^s I)\|_\Omega^2 \leq C\left(\|\nabla u-\nabla u^s\|_\Omega^2+\|\nabla\tilde{u}-\nabla\tilde{u}_h\|_{\tilde{\Omega}}^2+\|p-p_h'\|_{\Omega'}^2+\|p-\tilde{p}_h\|_{\tilde{\Omega}}^2+\langle p-\tilde{p}_h\rangle_{\tilde{\Omega}}^2|\tilde{\Omega}|\right). \tag{3.35}$$

Let us introduce a divergence free reconstruction s_h of $\tilde{u}_h$, i.e. $\operatorname{div} s_h = 0$ on $\tilde{\Omega}$ and $s_h \in H_0^1(\tilde{\Omega})$ such that

$$\|\nabla s_h-\nabla\tilde{u}_h\|_{\tilde{\Omega}} \leq C\|\operatorname{div}\tilde{u}_h\|_{\tilde{\Omega}}. \tag{3.36}$$

We have

$$(\nabla u-\nabla u^s,\nabla\tilde{u}-\nabla s_h)_{\tilde{\Omega}}=(\nabla u-\nabla u^s-(p-p^s)I,\nabla\tilde{u}-\nabla s_h)_{\tilde{\Omega}}=0,$$

so that

$$\|\nabla u-\nabla\tilde{u}\|_{\tilde{\Omega}}^2+\|\nabla\tilde{u}-\nabla s_h\|_{\tilde{\Omega}}^2=\|\nabla u-\nabla s_h\|_{\tilde{\Omega}}^2\leqslant\left(\|\nabla u-\nabla\tilde{u}_h\|_{\tilde{\Omega}}+C\|\operatorname{div}\tilde{u}_h\|_{\tilde{\Omega}}\right)^2. \tag{3.37}$$

Hence, using (3.35), adding and subtracting ∇s_h in $\|\nabla\tilde{u}-\nabla\tilde{u}_h\|_{\tilde{\Omega}}^2$, using(3.37) and (3.36) we get

$$\|\sigma_h-(\nabla u_h^s-p_h^s I)\|_\Omega^2 \leq C\left(\|\nabla u-\nabla u_h^s\|_\Omega^2+\|\operatorname{div}\tilde{u}_h\|_{\tilde{\Omega}}^2+\|p-p_h^s\|_{\Omega'}^2+\langle p-\tilde{p}_h\rangle_{\tilde{\Omega}}^2|\tilde{\Omega}|\right). \tag{3.38}$$

We also have $\|\operatorname{div}\tilde{u}_h\|_{\tilde{\Omega}}=\|\operatorname{div}u_h^s\|_\Omega=\|\operatorname{div}(u-u_h^s)\|_\Omega\leq\|\nabla(u-u_h^s)\|_\Omega$. Hence, it remains to deal with $\langle p-\tilde{p}_h\rangle_{\tilde{\Omega}}^2|\tilde{\Omega}|$.
To this end, let us take a function $\mathbf{v}_h\in H_0^1(\Omega)^2$ such that $\mathbf{v}_{h|_{\tilde{\Omega}}}\in\tilde{V}_h$ and

$$\mathbf{v}_h = S(y)n \operatorname{on}\gamma. \tag{3.39}$$

The coupling condition (1.38) entails

$$\int_\Omega(\nabla(u-u_h^s)-(p-p_h^s)I)\cdot\nabla\mathbf{v}_h=0$$

which can be rewritten as

$$\begin{aligned}\int_{\Omega'}\langle p-p_h'\rangle_{\Omega'}\operatorname{div}\mathbf{v}_h+\int_{\tilde{\Omega}}\langle p-\tilde{p}_h\rangle_{\tilde{\Omega}}\operatorname{div}\mathbf{v}_h&=\int_\Omega(\nabla u-\nabla u_h^s)\cdot\nabla\mathbf{v}_h\\&-\int_{\Omega'}\left(p-p_h'-\langle p-p_h'\rangle_{\Omega'}\right)\operatorname{div}\mathbf{v}_h-\int_{\tilde{\Omega}}\left(p-p_h^s-\langle p-\tilde{p}_h\rangle_{\tilde{\Omega}}\right)\operatorname{div}\mathbf{v}_h.\end{aligned}$$

Observe that

$$-\int_{\Omega'}\operatorname{div}\mathbf{v}_h=\int_{\tilde{\Omega}}\operatorname{div}\mathbf{v}_h=\int_\gamma S(y)=u_{\mathrm{av}}R$$

thus,

$$u_{\mathrm{av}}R\left(\langle p-\tilde{p}_h\rangle_{\tilde{\Omega}}-\langle p-p_h'\rangle_{\Omega'}\right)\leqslant C(\|\nabla u-\nabla u_h^s\|_\Omega+\|p-p_h^s\|_\Omega)\|\nabla\mathbf{v}_h\|_\Omega.$$

Since $|\tilde{\Omega}|\langle p-\tilde{p}_h\rangle_{\tilde{\Omega}}+|\Omega'|\langle p-p_h'\rangle_{\Omega'}=0$ we have

$$\langle p-\tilde{p}_h\rangle_{\tilde{\Omega}}-\langle p-p_h'\rangle_{\Omega'}=\frac{|\Omega|}{|\Omega'|}\langle p-\tilde{p}_h\rangle_{\tilde{\Omega}}.$$

Hence

$$\langle p-\tilde{p}_h\rangle_{\tilde{\Omega}} \leqslant C\frac{|\Omega'|}{|\Omega|}(\|\nabla u-\nabla u_h^s\|_\Omega+\|p-p_h^s\|_\Omega)\frac{\|\nabla \mathbf{v}_h\|_\Omega}{u_{\text{av}}R}.$$

Now, we want to minimize $\|\nabla \mathbf{v}_h\|_\Omega$ under the constraint (3.39). The minimum can be identified with the solution to Poisson equation on Ω' and the discrete approximation to Poisson equation on $\tilde{\Omega}$. Using the Lemma 2.14 in Chapter 2 about the traces in $H^{1/2}$ and a FE interpolation on $\tilde{\Omega}$ gives

$$\|\nabla \mathbf{v}_h\|_\Omega \leqslant C\|v_h\|_{1/2,\gamma} \leqslant Cu_{\text{av}}$$

Hence

$$\langle p-\tilde{p}_h\rangle_{\tilde{\Omega}}^2|\tilde{\Omega}| \leqslant C\frac{|\tilde{\Omega}|}{R^2}(\|\nabla u-\nabla u_h^s\|_\Omega^2+\|p-p_h^s\|_\Omega^2)$$

Assuming that $|\tilde{\Omega}| \leqslant CR^2$ and substituting this into (3.38) gives the desired lower estiamate.

Remark 3.8. *The assumption $|\tilde{\Omega}| \leqslant CR^2$ in the previous proof is reasonable since the last aim from coupling the domain into 0D/2D coupled model is to put the interfaces as much as possible near the corners of the domain where we have 2D model is more dominance. After fixing the interfaces ,as much as possible near the corners, we can achieve the assumption $|\tilde{\Omega}| \leqslant CR^2$. If we want to be far from the corners such that the assumption $|\tilde{\Omega}| \leqslant CR^2$ is not satisfied, then we need to add that the constant C in Theorem 3.7 depends on the mesh regularity and on the factor $\frac{|\tilde{\Omega}|}{R^2}$.*

■

3.2.3. Numerical Results

We have a 0D/2D model for the Stokes model and in the following we will use **Appendiix B** in order to approximate β since it is unknown for us. We will make a comparison between the coupled 0D/2D Stokes model and the non-coupled 2D Stokes model in order to see that our simplified model is good. We will also observe that our β is around 0.123 which is very small and it gives a big index of efficiency for pressure. We also observe that the index of efficiency becomes smaller as β becomes near 1 and for this reason we will make a new study and change the L^2-norm of pressure to $H^{-1}-$norm and make a new study of *a posteriori* error in order to get a good index of efficiency. Let us define the estimator of velocity in (3.20) by

$$\eta_U := \left(||\nabla u_h^s - p_h^s I-\sigma_h||_\Omega^2+\frac{||\nabla\cdot u_h^s||_\Omega^2}{\beta^2}\right)^{\frac{1}{2}}$$

and the estimator of pressure in (3.21) by

$$\eta_P := \frac{1}{\beta}\left(||\nabla u_h^s - p_h^s I-\sigma_h||_\Omega+\frac{||\nabla\cdot u_h^s||_\Omega}{\beta}\right). \tag{3.40}$$

These estimators η_U and η_P depend on the inf-sup constant β and we want to take different values of $\beta \in [0,1]$ in order to prove that the index of efficiency becomes near to 1 when β becomes near 1 which is not our case since we have a long channel and we know that $\beta \approx 0.123$. Let us define the index of efficiency for the velocity $I_U := \frac{\eta_U}{\|\nabla u-\nabla u_h^s\|_\Omega}$, the index of efficiency for pressure $I_P := \frac{\eta_P}{\|p-p_h^s\|_\Omega}$ and the total efficiency $I := \frac{\eta_U+\eta_P}{\|\nabla u-\nabla u_h^s\|_\Omega+\|p-p_h^s\|_\Omega}$.

Comparison between the coupled 0D/2D Stokes and the non-coupled 2D Stokes

Now, we want to make the comparison between the coupled 0D/2D model and the 2D non-coupled model of Stokes on the portion domain $\Omega := \Omega' \cup \gamma \cup \tilde{\Omega}$ (i.e. see Figure 1.4). First, we will approximate β using the strategy in **Appendix B.** in order to find that $\beta \approx 0.123$ for our domain Ω. Then, We will make a uniform refinement and compare the error and the estimator of the coupled 0D/2D model and non-coupled model of Stokes in order to validate that the problem of large index of pressure comes from the fact that the domain has a long channel (where β is small) and does not come from our proposed simplified 0D/2D model.
Now, by making the uniform refinement, the non-coupled Stokes model gives the following results.

Mesh Size	$\|\nabla(u-u_h^s)\|_\Omega$	η_U	$\|p-p_h^s\|_\Omega$	η_P	I_U	I_P	I
0.125139	0.0931641	0.541811	0.0151024	0.600682	5.81566	39.7739	10.5526
0.0648431	0.065334	0.396398	0.0109697	0.436303	6.06725	39.7737	10.913
0.0345792	0.0380296	0.2728	0.0056509	0.303376	7.17337	53.6863	13.1907

and the coupled 0D/2D Stokes model with $x_\gamma = 4.5$ gives the following results.

Mesh Size	$\|\nabla(u-u_h^s)\|_\Omega$	η_U	$\|p-p_h^s\|_\Omega$	η_P	I_U	I_P	I
0.120389	0.0911146	0.568324	0.0160873	0.627702	6.23747	39.0185	11.1568
0.0635345	0.0660111	0.407955	0.0121931	0.448857	6.18009	36.8126	10.9561
0.0320899	0.0416264	0.261487	0.00529808	0.290947	6.28176	54.9155	11.7728

If we compare the above results in the tables, we see that the coupled 0D/2D Stokes model and the non coupled Stokes model have approximately the same results and this suggests that the index of efficiency of the pressure comes from the geometry of the domain since the estimator of pressure is multiplied by the big factor $\frac{1}{\beta}$ in (3.40). Now, let us try to see what happen if β becomes near 1. We expect that the index of efficiency must become better.

Different values of β for coupled 0D/2D Stokes

Now let us make a quasi-uniform refinement, fix the interface position at $x_\gamma = 4$ and the mesh size $h \approx 0.08$ in order to see the variation of the total index I with respect to different values of β where $\beta \in [0, 1]$ and the data are showed in the following table. We observe from the table that the total index of efficiency I becomes very closed to 1 when β becomes near 1 as seen in the table below.

β	$\|\nabla(u-u_h^s)\|_\Omega$	η_U	$\|p-p_h^s\|_\Omega$	η_P	I
0.1	0.074236	0.543022	0.096732	5.90379	37.7077
0.2	0.074236	0.274892	0.096732	1.60002	10.9665
0.3	0.074236	0.186957	0.096732	0.766265	5.57545
0.4	0.074236	0.144009	0.096732	0.462043	3.54483
0.5	0.074236	0.118994	0.096732	0.315559	2.54172
0.6	0.074236	0.102886	0.096732	0.232924	1.96417
0.7	0.074236	0.0918186	0.096732	0.181257	1.59723
0.8	0.074236	0.0838571	0.096732	0.146529	1.34754
0.9	0.074236	0.0779302	0.096732	0.121903	1.16884
1	0.074236	0.0733976	0.096732	0.103705	1.03588

From the above table we can see that the index of efficiency becomes better when $\beta \in [0.6, 1]$. Now, let us consider the following two cases in order to see that as the interface position becomes near the corner as the error and the estimator becomes bigger.

Case 1: $\beta = 0.7$

First of all, we fix the mesh size and we change the position of the interface to obtain the graphs of the error $\|\nabla u - \nabla u_h^s\|_\Omega$ and estimator η_U in (3.20) with respect to different positions of interface in Figure 3.12 and the graphs of the error $\|p - p_h^s\|_\Omega$ and estimator η_P in (3.21) with respect to different positions of interface in Figure 3.13. We take the mesh sizes $h \approx 0.06$, $h \approx 0.03$ by making a quasi-uniform mesh refinement. In the proofs we suppose that the position x_γ of the interface must be located in the interval $x_\gamma \in [0.1, L_1 - R]$ and here $L_1 - R = 4.6$ (see Figure 1.4) but in order to see what happens after the interface position $x_\gamma = L_1 - R$, we take $x_\gamma \in [0, L_1 - 0.02]$. We conclude from Figure 3.12 and Figure 3.13 that as the interface position becomes near the corner as the estimator and error of the velocity and pressure become bigger.

Case 2: $\beta = 1$

Now, let us consider $\beta = 1$ and fix a mesh size, then we change the position of the interface to obtain the graphs of the error $\|\nabla u - \nabla u_h^s\|_\Omega$ and estimator η_U in (3.20) with respect to different positions of interface in Figure 3.14 and the graphs of the error $\|p - p_h^s\|_\Omega$ and estimator η_P in (3.21) with respect to different positions of interface in Figure 3.15. We take the mesh sizes $h \approx 0.06$, $h \approx 0.03$ by making a quasi-uniform mesh refinement. We conclude from Figure 3.14 and Figure 3.15 that as the interface position becomes near the corner as the estimator and error of the velocity and pressure become bigger.

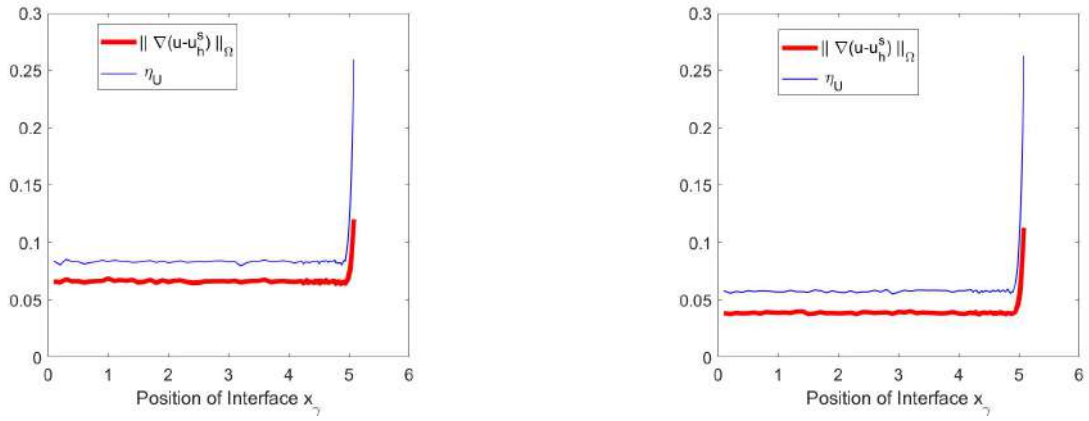

(a) $h \approx 0.06$ (b) $h \approx 0.03$

Figure 3.12.: Error and Estimator η_U of the velocity w.r.t. different positions of the interface for different mesh sizes h and for $\beta = 0.7$

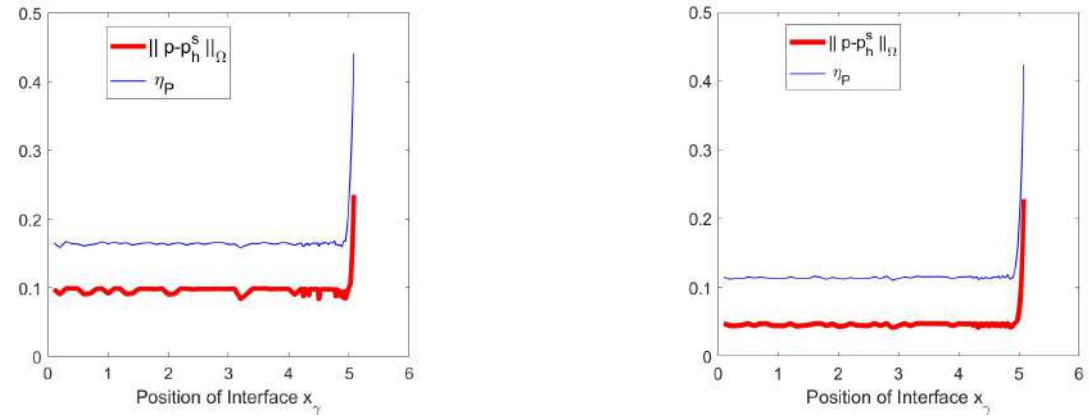

(a) $h \approx 0.06$ (b) $h \approx 0.03$

Figure 3.13.: Error and Estimator η_P of the pressure w.r.t. different positions of the interface for different mesh sizes h and for $\beta = 0.7$

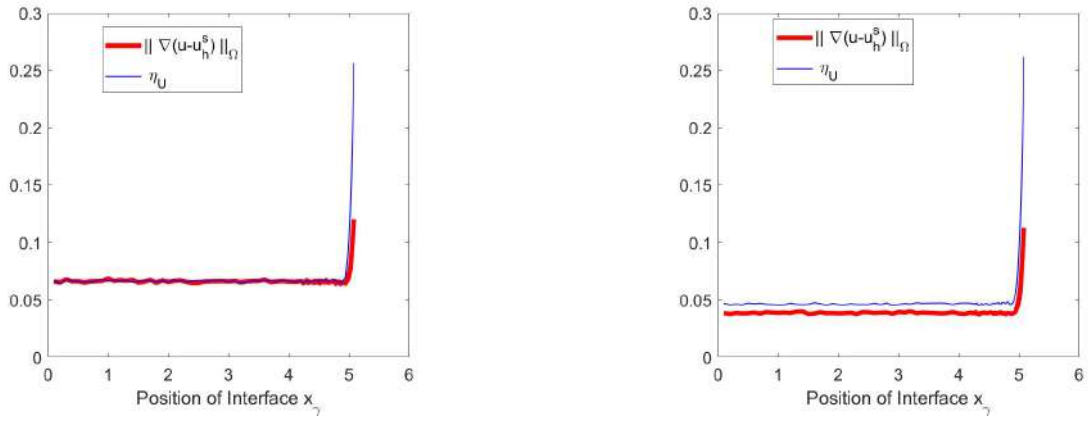

(a) $h \approx 0.06$ (b) $h \approx 0.03$

Figure 3.14.: Error and Estimator η_U of the velocity w.r.t. different positions of the interface for different mesh sizes h and for $\beta = 1$

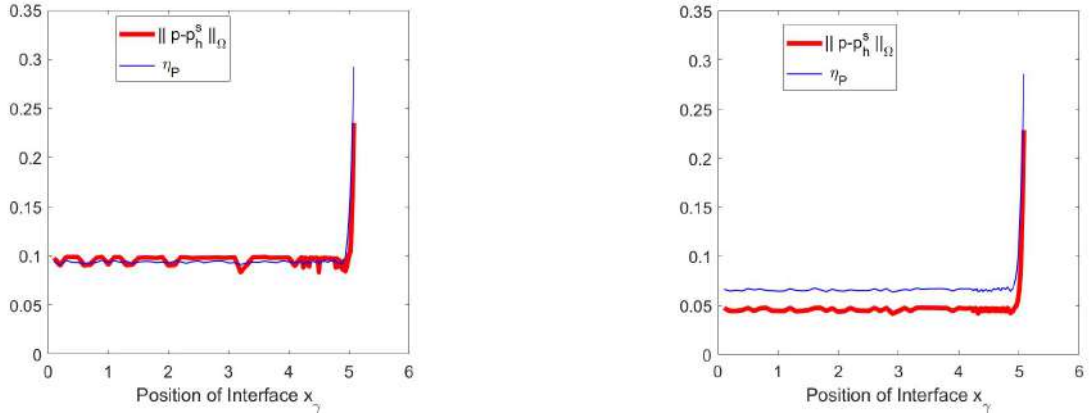

(a) $h \approx 0.06$ (b) $h \approx 0.03$

Figure 3.15.: Error and Estimator η_P of the pressure w.r.t. different positions of the interface for different mesh sizes h and for $\beta = 1$

Now, let us fix the interface at $x_\gamma = 4$ and $\beta = 0.7$, then we want to make a successive uniform refinement and compare the errors and the estimators of the velocity and pressure in order to see the convergence of the error and the estimator and calculate the indices as it is shown in the following table. We conclude from the table that we have a convergence for the error and estimator and the estimator is good as the indices are near one but we do not have an optimal convergence since we have singularity in the corners of the domain and to achieve the optimal convergence we must make mesh adaptation as we did in the Poisson.

Mesh Size	$\|\nabla(u - u_h^s)\|_\Omega$	η_U	$\|p - p_h^s\|_\Omega$	η_P	I_U	I_P	I
0.0821206	0.074236	0.0999717	0.096732	0.20101	1.34667	2.07801	1.76046
0.0386236	0.0459076	0.0696881	0.0606603	0.140202	1.51801	2.31127	1.96955
0.0194314	0.0303558	0.0486253	0.0379088	0.0977843	1.60185	2.57946	2.14474
0.0115897	0.00618741	0.0333611	0.00559242	0.0670828	5.39176	11.9953	8.52677

We suppose that the last Indices are big since we do not have exact solution and we have a reference solution.

New estimator with good index of efficiency

In **Appendix C** we make a new study for the non-coupled 2D Stokes model in order to obtain *a posteriori* estimates which does not depend on β. Instead of β we have a C_{div} constant (see Theorem C.5 in **Appendix C**) and we estimate numerically this constant, that is $C_{div} \approx 1$. In this case, repeating the same numerical tests, we find that the total index is equal to 1.03588, that is the same index for the previous study with $\beta = 1$.

3.3. Conclusion and perspectives

In this thesis we developed a numerical methodology in view to propose efficient and accurate simulations for the gaz dynamic in the cathod bipolar plate present in a PEMFC (see Figure 1.2 page 18). In the multi-physical PEMFC model [12], we focused only on the fluidic domain model. Moreover, the domain of the bipolar plate was considered as a 2D domain, as showed in Figure 2.36 page 105. In this domain, it was reasonable, as first attempt of a quite realistic study, to consider the Stokes equation, because we supposed that [12] the gaz is ideal, the gaz flow is incompressible (even more: the density constant) and laminar and that the fluid is only in the gaz phase. Another important assumption was that the channels of the plate are considered without curved bend, in the sens that the corners of the bend are modelised by a polygonal boundary (cf. Figure 2.36 page 105).

The starting idea of the presented work was to make a simplification in the resolution of the equation of interest in the bipolar plate, relying on the specific geometry of the channels of the plate. This simplification had to make a faster resolution with respect to a classical numerical computation on the whole domain, meanwhile we had to be able to control the error to calibrate a suitable accuracy. So that, we splitted the domain of the plate in a part where an analytical computation was possible and in a part where a numerical resolution was needed. Throughout the thesis, the analytical resolution was called "0D model" and the numerical one was called "2D model", which was the Finite Element

method. The goal was to make *a posteriori* estimates for the energetic norm of the discretization error of the coupled model to be able to drive the choice of the interface position between the 0D and the 2D model and the choice of an adapted mesh, for a given tolerance.

Even if the purpose was to deal with the Stokes equation, we started with the Poisson equation to fix some main ideas. In this first part, we choose a simple coupling condition (continuity of the solution) at the interface, and we developed a guaranteed error estimator in order to choose the interface postion and an adapted mesh in fonction of a suitable tolerance. For this error estimator we proved the reliability and the efficiency. The originality of this work was a new contribution of the estimator, called η^γ, built in order to guide the choice of the interface position (for a given tolerance for accuracy). The mathematical hurdle was to prove the efficiency. Numerical tests confirmed theoretical results and an adaptive algorithm was proposed to restore an optimal rate of convergence. This work is actually submitted to a journal.

In a second part, we dealt with the Stokes equation. We proposed a similar approach as the one for the Poisson equation and we obtained a guaranteed error estimator with proved reliability and efficiency. In this case, we propose a sort of natural variational coupled condition, which represent a continuity condition of the average of the stress at interface This new coupled model is essential to verify the efficiency. Here the problem was that in the estimator (see Theorem 3.7 page 138) there is the inf-sup constant β, indeed there is $\frac{1}{\beta}$. This β depends on the domain geometry and it is in general unknown, but it is known that it could be very small if the domain is stretched, and this is the case of the channel of the bipolar plate. The problem does not come from the 0D/2D approach, but is more general, the estimator is not very good for our domain since we have the factor $\frac{1}{\beta}$ that gives an over estimation once β is small and far from 1. An idea to solve this problem is to deal with the dual norm for the error for pressure instead of the L^2-norm. We try this way to estimate for the case of Stokes equation for the non-coupled problem, and this led to *a posteriori* estimates without β. We remark that another constant is in the estimate, but it can be approximated numerically, so we get the order of magnitude of the theoretical constant, that is for the problem of interest equal to 1. Finally that the upper bound in this case is guaranteed with constant equal to 1 and the estimator is completely known.

This work has many perspectives. First of all, we could extend the study of Stokes equation to the incompressible Navier-Stokes equation, we could use the Newton method to make the linearalization of the non linear term, and we can try also the compressible Navier-Stokes equation assuming that the density ρ is linear. Secondly, in order to deal with real channels, we can extend the study for real bends that is take into account a curved boundary for corners. In this sense, we can develop the theoretical study [56] in **Appendix D** in order to deal with the curved boundary by making a boundary correction. The numerical part in **Appendix D.3** gives a better *a postriori* error estimation for our curved domain as shown in the Figure D.2. Thirdly, we could calibrate the mathematical model in the whole and real domain to the realistic physical model for the PEMFC as in [51].

A. Appendix A: Adaptive algorithms in FreeFEM

Let us consider a mesh adaptation strategy on the example of Poisson problem in the Numerical Results section 1.4.1

$$-\Delta u = f \text{ in } \Omega$$

$$u = u_e \text{ on } \partial\Omega$$

with the exact solution u_e written, in polar coordinates, as

$$u_e(r,\theta) = r^{\frac{2}{3}} sin(2\theta/3)$$

discretized with $\mathbb{P}_k$ finite elements. We shall call u_h the FE solution on a mesh $\mathcal{T}_h$ and suppose that we have an *a posteriori* error estimator η_K, $K \in \mathcal{T}_h$ s.t.

$$|u - u_h|^2_{1,\Omega} \approx \sum_{K\in\mathcal{T}_h} \eta_K^2 \tag{A.1}$$

where $\eta_K^2 := \|\sigma_h + \nabla u_h\|^2_K$ and σ_h is the reconstructed approximated flux which can be defined as Vohralik did in [39]. Our goal is to compare several adaptive strategies.

A.1. Adaptive algorithm via Dörfler marking

We fix $\theta \in (0,1)$. On a given mesh, we mark certain triangles to be refined, i.e. introduce the subset $\mathcal{T}_h^M$ by

$$\sum_{K\in\mathcal{T}_h^M} \eta_K^2 \geqslant \theta \left(\sum_{K\in\mathcal{T}_h} \eta_K^2 \right)$$

keeping in $\mathcal{T}_h^M$ the triangles with highest estimators. In the original Dörfler's algorithm, one would split the marked triangles into smaller triangles and leave the unmarked triangles essentially unchanged. Under FreeFEM, we cannot do exactly that. Rather, we should introduce the desired sizes of the new mesh and then "`adaptmesh`" will try to construct the mesh with approximately these cell sized. In this spirit, we set h_{new} as the $\mathbb{P}_0$ FE function on the current mesh by

$$h_{\text{new}}|_K = \begin{cases} \frac{1}{R} h_K, & \text{for } K \in \mathcal{T}_h^M \\ h_K, & \text{otherwise} \end{cases}$$

where $R > 1$ is the fixed parameter (the refining factor). Then we give this h_{new} to FreeFEM function `adaptmesh` with `IsMetric=1`.

The command for the mesh adaptation in FreeFEM is

```
Th = adaptmesh(Th, NewMeshh, IsMetric=1, keepbackvertices=0, nbvx=1000000);
```

Here, `NewMeshh` is the $\mathbb{P}_0$ FE function containing h_{new}. According to the FreeFEM documention, the section on option `IsMetric=1`, "if only one function (i.e. `NewMeshh`) is given, then it represents the isotropic mesh size at every point." We choose `keepbackvertices=0`, because the alternative `keepbackvertices=1` works slightly worse.

A.2. Adaptive algorithm "hopt"

To introduce an alternative adaptive algorithm, let us characterize any imaginable mesh $\mathcal{T}_h$ by the meshsize distrubution $h(x)$ such that $h(x)$ at a point x inside a triangle $K \in \mathcal{T}_h$ is approximately equal to h_K. Moreover, suppose that the the FEM error on such a mesh is

$$|u - u_h|^2_{1,\Omega} \approx \int_\Omega h^{2\delta}(x) c^2(x)\,\mathrm{dx} \tag{A.2}$$

with some a priori unknown $c(x)$ and the order parameter δ chosen once for all. This is reasonable for example for $\mathbb{P}_1$ FEM with $\delta = 1$, $c(x) \sim |D^2 u|(x)$, i.e. the norm of the second order derivatives at x, provided u is sufficiently smooth. Note also that the number of DOFs is approximately given in 2D case by

$$N_{\text{DOF}} \sim \int_\Omega \frac{\mathrm{dx}}{h^2(x)}$$

since a triangle of size $h(x)$ occupies the area of order $h^2(x)$. Let us imagine first that we know $c(x)$ and we want to construct an optimal mesh (with the minimal possible N_{DOF}) to achieve a given error tolerance, i.e. $|u - u_h|_{1,\Omega} = \text{tol}$. This is a constrained minimization problem for the mesh size distribution $h(x)$:

$$\min_{\substack{h \in L^2(\Omega) \\ \int_\Omega h^{2\delta}(x) c^2(x)\,\mathrm{dx} = \text{tol}^2}} \int_\Omega \frac{\mathrm{dx}}{h^2(x)}.$$

The minimum is achieved on a stationary point of the Lagrangian

$$L(h, \lambda) = \int_\Omega \frac{\mathrm{dx}}{h^2(x)} + \lambda \left(\int_\Omega h^{2\delta}(x) c^2(x)\,\mathrm{dx} - \text{tol}^2 \right)$$

with $h \in L^2(\Omega)$ and $\lambda \in \mathbb{R}$. Taking the variations yields

$$-\int_\Omega \frac{2v(x)\,\mathrm{dx}}{h^3(x)} + \lambda \int_\Omega 2\delta h^{2\delta-1}(x) v(x) c^2(x)\,\mathrm{dx} = 0, \quad \forall v = v(x)$$

so that the optimal mesh size distribution is

$$h_{\text{opt}}(x) = \frac{\text{tol}^{1/\delta}}{\left(\int_\Omega c^{2/(\delta+1)}(x)\,\mathrm{dx}\right)^{1/(2\delta)}} \frac{1}{(c(x))^{1/(\delta+1)}}$$

Of course, $c(x)$ is not known in practice. But, on a given mesh $\mathcal{T}_h$, we have *a posteriori* error estimates of the form (A.1). Let us reinterpret this in the form (A.2),

$$\sum_{K \in \mathcal{T}_h} \int_K h^{2\delta}(x) c^2(x)\,\mathrm{dx} \sim \sum_{K \in \mathcal{T}_h} \eta_K^2.$$

This suggests to approximate $c(x)$ on any triangle $K \in \mathcal{T}_h$ by

$$c(x) \approx \frac{\eta_K}{h_K^\delta \sqrt{|K|}} \quad \text{for } x \in K.$$

This gives

$$h_{\text{opt}}(x) = \frac{\text{tol}^{1/\delta}}{\left(\sum_{K \in T_h} \eta_K^{2/(\delta+1)} h_K^{-2\delta/(\delta+1)} |K|^{\delta/(\delta+1)}\right)^{1/(2\delta)}} \frac{h_K^{\delta/(\delta+1)} |K|^{1/(2\delta+2)}}{\eta_K^{1/(\delta+1)}} \quad \text{for } x \in K. \tag{A.3}$$

Now, rather then trying to achieve the target tolerance, let us adapt the mesh by aiming to diminish the current error estimate R_{tol} times (i.e. set $\text{tol} = \text{Est}\,/R_{\text{tol}}$) with given $R_{\text{tol}} > 1$ on each iteration of the algorithm. So, the "hopt" algorithm is

1. Given the mesh $\mathcal{T}_h$, set current desired tolerance to

$$\text{tol} = \frac{1}{R_{\text{tol}}} \left(\sum_{K \in \mathcal{T}_h} \eta_K^2 \right)^{1/2}$$

2. Set h_{new} as the $\mathbb{P}_0$ FE function on the current mesh by $h_{\text{new}} = h_{\text{opt}}$ using (A.3).

3. Give this h_{new} to FreeFEM function `adaptmesh` with `IsMetric=1`. Redo the same on the new mesh.

A.3. Numerical comparisons

We do the usual L-shape test using $\mathbb{P}_2$ FEM and the equilibrated flux a posteriori estimators with RT_2 fluxes. We have compared the following algorithms:

- The original implementation, i.e. using `adaptmesh` with `IsMetric=0` (15 iterations),
- "Dörfler" algorithm with $\theta = 0.8$, $R = 4$ (18 iterations),
- "hopt" algorithm with $\delta = 1$, $R_{\text{tol}} = 4$ (8 iterations),
- "hopt" algorithm with $\delta = 1.5$, $R_{\text{tol}} = 5$ (10 iterations),
- "hopt" algorithm with $\delta = 2$, $R_{\text{tol}} = 5$ (13 iterations).

We have tried to achieve the error below 10^{-4} with all the strategies, did not always succeed (either the mesh became too heavy, or encountered some mesh generation problems, or other). This is why the number of iteration differs from one variant to another. Any way, when we look at Errors vs. DOFs, all the methods look roughly similar in Figure (A.1).

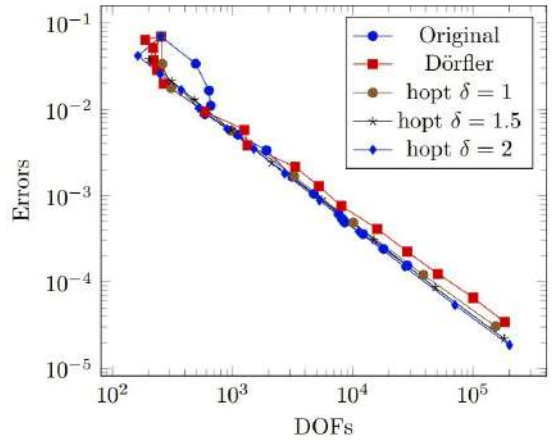

Figure A.1.: Errors with respect to degrees of freedom DOFs

The same if we look at the estimators in Figure (A.2).

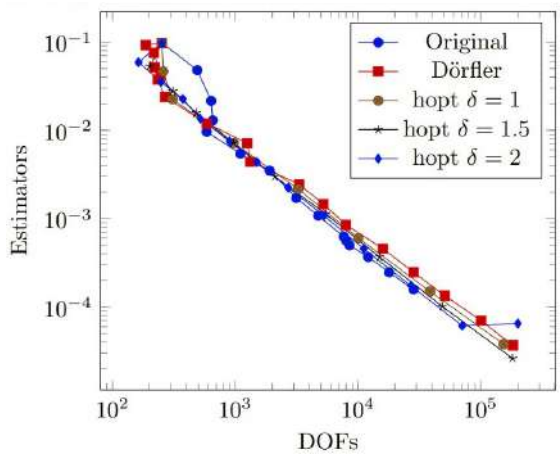

Figure A.2.: Estimators with respect to degrees of freedom DOFs

Rather surprisingly, we can conclude that all the approaches give the meshes of more or less the same quality. Hence, to distinguish between the variants, we can now look at the evolution of the error on iterations in Figure (A.3).

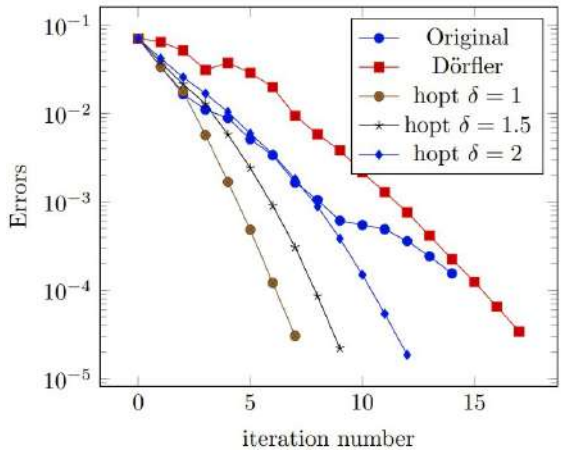

Figure A.3.: Errors with respect to number of iterations

And the winner is: "hopt" algorithm with $\delta = 1$, $R_{\text{tol}} = 4$.

B. Appendix B: Approximation of the inf-sup constant using Crouzeix-Raviart FE for the velocity

Let $\mathcal{T}_h$ be a sequence of regular meshes indexed by $h \to 0$, on a convex polygon Ω. Let

$$\beta = \inf_{p \in Q} \sup_{v \in V} \frac{(p, \operatorname{div} v)_\Omega}{\|p\|_{0,\Omega} |v|_{1,\Omega}}$$

and

$$\beta_h = \inf_{p_h \in Q_h} \sup_{v_h \in V_h} \frac{(p_h, \operatorname{div} v_h)_\Omega}{\|p_h\|_{0,\Omega} |v_h|_{1,\Omega}}$$

where $V = H_0^1(\Omega)^d$, $Q = L_0^2(\Omega)$, V_h is the $\mathbb{P}_1$ non-conforming Crouzeix-Raviart FE space on $\mathcal{T}_h$ ($V_h \not\subset V$), and $Q_h \subset Q$ the $\mathbb{P}_0$ discontinuous FE space on $\mathcal{T}_h$.

Lemma B.1. *We have $\beta_h \geqslant \beta$ on every $\mathcal{T}_h$ and*

$$\lim_{h \to 0} \beta_h = \beta.$$

Proof. To prove $\beta_h \geqslant \beta$, introduce the standard interpolation to Crouzeix-Raviart FE by

$$\forall v \in V \quad \text{let} \quad I_h(v) = v_h \in V_h \quad \text{be such that} \quad \int_E v_h = \int_E v$$

on all the facets of the mesh $E \in \mathcal{E}_h$. This implies

$$\forall K \in \mathcal{T}_h : \int_K \operatorname{div} I_h(v) = \int_K \operatorname{div} v$$

and $|I_h(v)|_{1,\Omega} \leqslant |v|_{1,\Omega}$. Thus, for any $p_h \in Q_h$ and any $v \in V$

$$\frac{(p_h, \operatorname{div} I_h(v))_\Omega}{\|p_h\|_{0,\Omega} |I_h(v)|_{1,\Omega}} = \frac{(p_h, \operatorname{div} v)_\Omega}{\|p_h\|_{0,\Omega} |I_h(v)|_{1,\Omega}} \geqslant \frac{(p_h, \operatorname{div} v)_\Omega}{\|p_h\|_{0,\Omega} |v|_{1,\Omega}}$$

i.e. for any $p_h \in Q_h$

$$\sup_{v_h \in V_h} \frac{(p_h, \operatorname{div} v_h)_\Omega}{\|p_h\|_{0,\Omega} |v_h|_{1,\Omega}} \geqslant \sup_{v \in V} \frac{(p_h, \operatorname{div} I_h(v))_\Omega}{\|p_h\|_{0,\Omega} |I_h(v)|_{1,\Omega}} \geqslant \sup_{v \in V} \frac{(p_h, \operatorname{div} v)_\Omega}{\|p_h\|_{0,\Omega} |v|_{1,\Omega}} \geqslant \beta.$$

Taking the inf over $p_h \in Q_h$ gives $\beta_h \geqslant \beta$.

To go further, let us first assume that inf in the definition of β is achieved on some $\bar{p} \in H^1(\Omega)$, i.e.

$$\exists \bar{p} \in H^1(\Omega) \cap Q \,\text{with}\, \|\bar{p}\|_{0,\Omega} = 1 \quad \text{and} \quad \beta = \sup_{v \in V} \frac{(\bar{p}, \operatorname{div} v)_\Omega}{|v|_{1,\Omega}}$$

Actually the sup above is also achieved on $\bar{v} \in V$ such that

$$(\nabla \bar{v}, \nabla w)_\Omega = (\bar{p}, \operatorname{div} w)_\Omega \quad \forall w \in V$$

i.e. $\bar{v} \in H^2(\Omega)$, $|\bar{v}|_{2,\Omega} \leqslant C|\bar{p}|_{1,\Omega}$

$$-\Delta \bar{v} = \nabla \bar{p} \text{ on } \Omega, \quad \bar{v} = 0 \text{ on } \partial\Omega.$$

Take $\bar{p}_h \in Q_h$ as the orthogonal projection of $\bar{p}$ on Q_h then

$$\|\bar{p}_h - \bar{p}\| \leqslant Ch|\bar{p}|_{1,\Omega}$$

Note that the supremum in

$$\sup_{v_h \in V_h} \frac{(\bar{p}_h, \operatorname{div} v_h)_\Omega}{|v_h|_{1,\Omega}}$$

is achieved on $\bar{v}_h \in V_h$ such that

$$(\nabla \bar{v}_h, \nabla w_h)_\Omega = (\bar{p}_h, \operatorname{div} w_h)_\Omega \quad \forall w_h \in V_h.$$

Taking any $w_h \in V_h$, we get by IPP element by element

$$(\nabla \bar{v}, \nabla w_h)_\Omega = (\bar{p}, \operatorname{div} w_h)_\Omega + \sum_{E \in \mathcal{E}_h} \int_E (\nabla \bar{v} - \bar{p} I) n \cdot [w_h].$$

Hence

$$(\nabla(I_h(\bar{v}) - \bar{v}_h), \nabla w_h)_\Omega = (\nabla(I_h(\bar{v}) - \bar{v}), \nabla w_h)_\Omega + (\bar{p} - \bar{p}_h, \operatorname{div} w_h)_\Omega + \sum_{E \in \mathcal{E}_h} \int_E (\nabla \bar{v} - \bar{p} I) n \cdot [w_h].$$

Taking $w_h = I_h(\bar{v}) - \bar{v}_h$ and using $\int_E [w_h] = 0$ on every $E \in \mathcal{E}_h$, and $|\bar{v}|_{2,\Omega} \leqslant C|\bar{p}|_{1,\Omega}$, we get

$$|\bar{v} - \bar{v}_h|_{1,\Omega} \leqslant C(|\bar{v} - I_h(\bar{v})|_{1,\Omega} + \|\bar{p} - \bar{p}_h\|_{0,\Omega} + h|\bar{v}|_{2,\Omega} + h|\bar{p}|_{1,\Omega}) \leqslant C_1 h|\bar{p}|_{1,\Omega}.$$

All this leads to

$$\sup_{v_h \in V_h} \frac{(\bar{p}_h, \operatorname{div} v_h)_\Omega}{\|\bar{p}_h\|_{0,\Omega}|v_h|_{1,\Omega}} = \frac{|\bar{v}_h|_{1,\Omega}}{\|\bar{p}_h\|_{0,\Omega}} \leqslant \frac{|\bar{v}|_{1,\Omega} + C_1 h|\bar{p}|_{1,\Omega}}{1 - Ch|\bar{p}|_{1,\Omega}} = \frac{\beta + C_1 h|\bar{p}|_{1,\Omega}}{1 - Ch|\bar{p}|_{1,\Omega}}.$$

Thus

$$\beta \leqslant \beta_h \leqslant \frac{\beta + C_1 h|\bar{p}|_{1,\Omega}}{1 - Ch|\bar{p}|_{1,\Omega}}$$

so that we get $\lim_{h \to 0} \beta_h = \beta$ as announced, and morever the error $|\beta_h - \beta|$ is of order h.

In the general case, i.e. without supposing that the inf in the definition of β is achieved on some $\bar{p} \in H^1(\Omega)$, we still have the same convergence result (without order of convergence). Indeed, by the density of H^1 in L^2, we have $\forall \varepsilon > 0$

$$\exists \bar{p}_\varepsilon \in H^1(\Omega) \cap Q \text{ with } \|\bar{p}_\varepsilon\|_{0,\Omega} = 1 \quad \text{and} \quad \sup_{v \in V} \frac{(\bar{p}_\varepsilon, \operatorname{div} v)_\Omega}{|v|_{1,\Omega}} \leqslant \beta + \varepsilon.$$

By the same arguments as above we get then

$$\beta \leqslant \beta_h \leqslant \frac{\beta + \varepsilon + C_1 h|\bar{p}_\varepsilon|_{1,\Omega}}{1 - Ch|\bar{p}_\varepsilon|_{1,\Omega}},$$

so, by takin ε sufficiently small, and then h sufficiently small, we obtain β_h arbitrarily close to β. ■

Numerical experiments To calculate β_h numerically, we note that $\beta = \sqrt{\lambda_{\min}}$ where $\lambda_{\min}$ is the smallest (non-zero) eigen value of the Shur complement

$$S = B_h A_h^{-1} B_h^T$$

where B_h is the discretization of the operator div and A_h is the discretization of $-\Delta$ with 0 boundary conditions. Note that the eigen problem (with M_h the mass matrix)

$$Sp = \lambda M_h p$$

can be rewritten as the generalized eigen problem

$$\begin{pmatrix} A_h & -B_h \\ B_h & 0 \end{pmatrix} \begin{pmatrix} u \\ p \end{pmatrix} = \lambda \begin{pmatrix} 0 & 0 \\ 0 & M_h \end{pmatrix} \begin{pmatrix} u \\ p \end{pmatrix}$$

We programmed this problem in FreeFem, noting that the matrix on the LHS is not symmetric, and the matrix on the RHS is not positive definite. Nevertheless, the FreeFEM function EigenValue with option sym=true seems to work. It gives the following approximations to β on rectangles $(0, L) \times (0, 1)$:

L	β
1	0.49458
2	0.389852
4	0.218723
8	0.112451
16	0.0566144
32	0.0284483

We observe indeed $\beta \to 0$ as $L \to \infty$ like $\beta \sim \frac{1}{L}$. This is consistent with observations (both theoretical and numerical) from [27].

C. Appendix C: On LBB dependence of the a posteriori error estimates à la Vohralik

Consider the problem posed in a domain $\Omega \subset \mathbb{R}^d$ with $d = 2$ or 3:

$$-\Delta u + \nabla p = f \quad \text{in } \Omega$$

$$\operatorname{div} u = 0 \quad \text{in } \Omega$$

$$u = 0 \quad \text{on } \partial\Omega$$

We suppose $f \in L^2(\Omega)$ and Ω a bounded polygonal/polyhedral domain. The pressure p is defined up to an additive constant. To make the solution unique, we impose $\int_\Omega p = 0$. Let $\mathcal{T}_h$ be a regular mesh on Ω consisting of triangles/tetrahedral. Let V_h be the usual $\mathbb{P}_k$ finite element space on this mesh (the space of continuous functions on Ω given by polynomials of degree $\leqslant k$ on every $K \in \mathcal{T}_h$). The functions in V_h are supposed to vanish on the boundary of Ω. Let moreover M_h be the usual $\mathbb{P}_{k-1}$ finite element space on the same mesh. The discrete problem is to find $u_h \in V_h$ and $p_h \in M_h$ such that for any $v_h \in V_h$, $q_h \in M_h$

$$\begin{aligned} \int_\Omega \nabla u_h \cdot \nabla v_h - \int_\Omega p_h \operatorname{div} v_h &= \int_\Omega f v_h, \\ \int_\Omega q_h \operatorname{div} u_h &= 0. \end{aligned} \tag{C.1}$$

Several *a posteriori* error estimates are available for the problem above [33, 73, 80]. We are interested in the estimates based on equilibrated fluxes as in the course by Vohralík [79], that have the form:

$$\|\nabla u - \nabla u_h\|_\Omega \leqslant \left(\|\sigma_h + \nabla u_h - p_h I\|_\Omega^2 + \frac{1}{\beta^2} \|\operatorname{div} u_h\|_\Omega^2 \right)^{\frac{1}{2}} + h.o.t., \tag{C.2}$$

$$\|p - p_h\|_{0,\Omega} \leqslant \frac{1}{\beta} \|\sigma_h + \nabla u_h - p_h I\|_\Omega + \frac{1}{\beta^2} \|\operatorname{div} u_h\|_\Omega + h.o.t., \tag{C.3}$$

where σ_h is the equilibrated flux reconstruction (a computable approximation to $-\nabla u + pI$), found in practice by solving local problems in Raviart-Thomas spaces on mesh element patches around each node, and *h.o.t.* stands for higher order terms which are negligible, at least when f and the solution are regular enough. The attractive feature of this estimator is that it provides a guaranteed upper bound of the error in the natural norms and this estimate contains explicit constants, namely the inf-sup (LBB) constant

$$\beta = \beta(\Omega) = \inf_{q \in L^2_0(\Omega)} \sup_{v \in H^1_0(\Omega)^d} \frac{(q, \operatorname{div} v)}{\|q\|_\Omega \|\nabla v\|_\Omega}.$$

The downside is that β is difficult to evaluate in practice. Moreover, $\beta(\Omega)$ can be very small if Ω is very elongated (such as long channels), cf. [27, 31]. In this appendix, we propose an alternative estimator, indeed this estimate:

$$\|\nabla u - \nabla u_h\|_\Omega \leqslant \left(\|\sigma_h + \nabla u_h - p_h I\|_\Omega^2 + C_{div}^2 \|\operatorname{div} u_h\|_\Omega^2\right)^{\frac{1}{2}} + h.o.t. \tag{C.4}$$

$$\|\nabla(p - p_h)\|_{-1,\Omega} \leqslant \|\sigma_h + \nabla u_h - p_h I\|_\Omega + C_{div} \|\operatorname{div} u_h\|_\Omega + h.o.t. \tag{C.5}$$

which is LBB-free, i.e. does not involve the LBB constant $\beta(\Omega)$, but involves instead a constant C_{div}, which will be proven to depend only on the mesh regularity, and thus independent of Ω. We do not attempt here to evaluate C_{div} theoretically. We provide instead some numerical tests which suggest that C_{div} is close to 1 (the constant C_{div} can be defined in fact through by a maximazation problem over patches of mesh elements around a node, and then numerically approximated by discretizing these problems).

Apart from the dependence on the LBB constant, the main differences between the original estimates (C.2)–(C.3) and the new ones (C.4)–(C.5) is in the treatment of the error in pressure. It is no longer measured in the traditional $L^2(\Omega)$ norm. Following [82], we adopt here the $H^{-1}(\Omega)$ norm of the pressure gradient, that is:

$$\|\nabla p\|_{-1,\Omega} = \sup_{v \in H_0^1(\Omega)} \frac{(\nabla p, v)}{|v|_{1,\Omega}}. \tag{C.6}$$

Note that, if a good approximation of $\beta = \beta(\Omega)$ is available, one can return to the original error measure via the bound $\|p - p_h\|_\Omega \leqslant \frac{1}{\beta}\|\nabla(p - p_h)\|_{-1,\Omega}$. The new estimate (C.5) gives then a sharper upper bound than the old one (C.3) if $\beta << 1$. Moreover, the $H^{-1}(\Omega)$ norm of the pressure gradient can be used for certain other quantities of interest. For example, if one is interested in the pressure on a subdomain $\omega \subset \Omega$ and ω is of simple form so that $\beta(\omega)$ can be assumed known, then one calculates easily $\|p - p_h\|_\omega \leqslant \frac{1}{\beta(\omega)}\|\nabla(p - p_h)\|_{-1,\Omega}$. A previous work [52] is important but it treats only with Crouzeix-Raviart spaces. [65] introduces the idea of employing LBB constants on subdomains, rather than on the whole Ω.

The main goal of the appendix is to get red of the inf-sup constant β. This appendix is organized as follows: firstly, we give an informal motivation and derivation of our estimator which does not contain the inf-sup constant β. Then, we prove the reliability and efficiency of the estimates. Finally, we approximate the constant C_{div} in (C.4)–(C.5) numerically. For completeness, we describe in Appendix our approach to this evaluation, following mostly [27].

C.1. Informal derivation of the estimator

First of all, we note the following bound: for any $\sigma \in H_{\operatorname{div}}(\Omega)^d$ such that $\operatorname{div}\sigma = f$ on Ω, and any $s \in H_0^1(\Omega)^d$ with $\operatorname{div} s = 0$, we have

$$\|\nabla u - \nabla u_h\|_\Omega^2 \leqslant \|\sigma + \nabla u_h - p_h I\|_\Omega^2 + \|\nabla u_h - \nabla s\|_\Omega^2 \tag{C.7}$$

Indeed,

$$\|\nabla u - \nabla u_h\|_\Omega^2 = \|\nabla u - \nabla u_h^0\|_\Omega^2 + \|\nabla u_h^0 - \nabla u_h\|_\Omega^2 \tag{C.8}$$

where u_h^0 is the H_0^1-orthogonal projection of u_h to the subspace of $H_0^1(\Omega)^d$ of divergence-free functions, i.e. $u_h^0 \in Z = \{v \in H_0^1(\Omega)^d : \operatorname{div} v = 0\}$. Setting $e = u - u_h^0$ we observe $e \in Z$ and $(\nabla(u_h - u_h^0), \nabla e)_\Omega = 0$. Hence,

$$\begin{aligned}\|\nabla e\|_\Omega^2 = (\nabla(u-u_h^0), \nabla e)_\Omega = (\nabla u - pI, \nabla e)_\Omega - (\nabla u_h^0 - p_h I, \nabla e)_\Omega = (f, e)_\Omega - (\nabla u_h^0 - p_h I, \nabla e)_\Omega \\ = (\operatorname{div}\sigma, e)_\Omega - (\nabla u_h - p_h I, \nabla e)_\Omega = -(\sigma + \nabla u_h - p_h I, \nabla e)_\Omega\end{aligned}$$

so that $\|\nabla(u-u_h^0)\|_\Omega \leqslant \|\sigma + \nabla u_h - p_h I\|_\Omega$. Moreover, $\|\nabla u_h - \nabla u_h^0\|_\Omega \leqslant \|\nabla u_h - \nabla s\|_\Omega^2$ since u_h^0 is the best divergence-free approximation to u_h. This establishes (C.7) as a consequence to (C.8).

The idea of what follows is to give a recipe to construct σ with $\operatorname{div}\sigma \approx f$ in a way easily implementable on a computer, and also to construct $s \in Z$, on the theoretical level only (the divergence-free reconstruction s here is not meant to be computed in practice, it is only an auxiliary theoretical notion that helps to bound one of the contributions to the error through a constant C_{div}, which will be evaluated numerically once for all). Another thing to keep in mind is that this σ should be kept as close as possible to $-\nabla u_h + p_h I$, and s should be kept as close as possible to u_h, in order to minimize the over-prediction of the error in (1.48).

We start by choosing a good candidate for the flux σ. An ideal flux (of no practival use) would be $\sigma^{\text{ideal}} = -\nabla u + pI$. Now, let us introduce the localized version of σ^{ideal} : $\sigma^a = (-\nabla u + pI)\psi^a$ where ψ^a is the $\mathbb{P}_1$ finite element basis function (the hat function) associated to any mesh node a. This σ^a satisfies on the patch $\omega^a = \operatorname{supp}(\psi^a)$

$$\sigma^a = (-\nabla u + pI)\psi^a \operatorname{on}\omega^a$$

$$\operatorname{div}\sigma^a = f\cdot\psi^a + (-\nabla u + pI)\cdot\nabla\psi^a \operatorname{on}\omega^a$$

$$\sigma^a \cdot n = 0 \operatorname{on}\partial\omega^a \setminus \partial\Omega$$

Note that $\sigma^{\text{ideal}} = \sum_a \sigma^a$ on Ω since $\sum_a \psi^a = 1$ (we imply the summation over all the mesh nodes in such expressions).

Let us discretize the problem for σ^a. Introduce the FE spaces

$$\Sigma_h^a = \{\sigma_h \in H_{\operatorname{div}}(\omega^a), \sigma_h|_K \in \mathrm{RT}_k(K) \quad \forall K \in \omega^a,\ \sigma_h\cdot n = 0 \operatorname{on}\partial\omega^a \setminus \partial\Omega\}$$

and

$$Q_h^a = \operatorname{div}\Sigma_h^a = \left\{q_h \in L^2(\omega^a), q_h|_K \in \mathbb{P}_k(K) \quad \forall K \in \omega^a, \quad \text{and} \int_{\omega^a} q_h = 0 \text{ if } a \text{ is an interior node}\right\}$$

Here $\mathbb{P}_k(K)$ is the set of polynomials of degree $\leqslant k$ on K, and $\mathrm{RT}_p(K)$ is the set of Raviart-Thomas (vector-valued) finite elements on a cell K. Note that $\Sigma_h^a \subset H_{\operatorname{div}}(\omega^a)$, which is the natural space for σ^a. Note also that the boundary conditions for σ^a are already encoded in the definition of Σ_h^a. The constraint $\int_{\omega^a} q_h = 0$ is introduced in Q_h^a in accordance with $\sigma_h \cdot n = 0$ on $\partial\omega^a$ in the definition of Σ_h^a. This happens on the internal nodes only.

Now, an approximation to σ^a can be constructed as $\sigma_h^a \in \Sigma_h^a$ such that

$$\sigma_h^a = \arg \min_{\substack{\tau_h^a \in \Sigma_h^a \\ \operatorname{div}\tau_h^a = P_{Q_h^a}(f\cdot\psi^a + (-\nabla u_h + p_h I)\nabla\psi^a)}} \|\tau_h^a - (-\nabla u_h + p_h I)\psi^a\|_{\omega^a} \tag{C.9}$$

The Euler-Lagrange equations for the solution to (C.9) are as follows: find $\sigma_h^a \in \Sigma_h^a$ and $\pi_h^a \in Q_h^a$ such that for all $\tau_h \in \Sigma_h^a$ and $\chi_h \in Q_h^a$

$$\int_{\omega^a} \sigma_h^a : \tau_h + \int_{\omega^a} \pi_h^a \cdot \operatorname{div} \tau_h = \int_{\omega^a} (-\nabla u_h + p_h I)\psi^a : \tau_h \tag{C.10}$$

$$\int_{\omega^a} \chi_h \cdot \operatorname{div} \sigma_h^a = \int_{\omega^a} (f\psi^a + (-\nabla u_h + p_h I)\nabla\psi^a) \cdot \chi_h \tag{C.11}$$

Existence of the solution to this problem is well-known, cf. [78, Theorem 6.64]. Finally, the flux reconstruction is defined as

$$\sigma_h = \sum_a \sigma_h^a \tag{C.12}$$

Let us turn now to the divergence free velocity reconstruction s mimicking the above construction of the flux σ_h. The ideal candidate for s would be $s^{\text{ideal}} = u$. Let us introduce the localized version of s^{ideal} : $s^a = u\psi^a$. This s^a satisfies on the patch $\omega^a = \operatorname{supp}(\psi^a)$

$$\operatorname{div} s^a = u \cdot \nabla\psi^a \operatorname{on} \omega^a$$

$$s^a = 0 \operatorname{on} \partial\omega^a$$

Note that $s^{\text{ideal}} = \sum_a s^a$ on Ω. Let us "discretize" the problem for s^a (we put "discretize" in quotes since the "discrete" version s_h^a of s^a will be a solution to a PDE, used only in theory but not constructed in practice). We thus introduce $s_h^a \in H_0^1(\omega^a)$ such that

$$s_h^a = \arg \min_{\substack{t_h^a \in H_0^1(\omega^a) \\ \operatorname{div} t_h^a = u_h \cdot \nabla\psi^a}} \|\nabla(t_h^a - u_h\psi^a)\|_{\omega^a} \tag{C.13}$$

The Euler-Lagrange equations for this problem read: find $s_h^a \in H_0^1(\omega^a)$ and $p_h^a \in L_0^2(\omega^a)$ such that

$$\int_{\omega^a} \nabla s_h^a \cdot \nabla t + \int_{\omega^a} p_h^a \operatorname{div} t = \int_{\omega^a} \nabla(u_h\psi^a) \cdot \nabla t, \quad \forall t \in H_0^1(\omega^a) \tag{C.14}$$

$$\int_{\omega^a} q \operatorname{div} s_h^a = \int_{\omega^a} (u_h \cdot \nabla\psi^a) q, \quad \forall q \in L_0^2(\omega^a) \tag{C.15}$$

This probelm is a weak formulation of Stokes equations on ω^a. It is thus well-posed. The velocity reconstruction s_h is now defined by

$$s_h = \sum_a s_h^a \tag{C.16}$$

with s^a given by (C.14)–(C.15). It is indeed divergence-free, since

$$\operatorname{div} s_h = \sum_a \operatorname{div} s_h^a = u_h \cdot \nabla \left(\sum_a \psi^a \right) = 0 \tag{C.17}$$

C.2. LBB-free *a posteriori* error estimates

Lemma C.1. *Let $u_h \in V_h$ and $s_h^a \in H_0^1(\omega^a)$ be given by (C.14)–(C.15). Then*

$$\|\nabla(s_h^a - u_h\psi^a)\|_{\omega^a} \leqslant \tilde{C}_{div}\|\sqrt{\psi^a}\,\mathrm{div}\,u_h\|_{\omega^a} \tag{C.18}$$

with $\tilde{C}_{div} > 0$ depending only on the mesh regularity and the polynomial degree k.

Proof. Introducing the new unknown $\hat{s}_h^a = s_h^a - u_h\psi^a$, the problem (C.14)–(C.15) can be rewritten as

$$\int_{\omega^a} \nabla\hat{s}_h^a \cdot \nabla t + \int_{\omega^a} p_h^a \,\mathrm{div}\, t = 0, \quad \forall t \in H_0^1(\omega^a) \tag{C.19}$$

$$\int_{\omega^a} q\,\mathrm{div}\,\hat{s}_h^a = -\int_{\omega^a} q\psi^a\,\mathrm{div}\,u_h \quad \forall q \in L_0^2(\omega^a) \tag{C.20}$$

It is thus clear that if $\mathrm{div}\,u_h = 0$ on ω^a then $\hat{s}_h^a = 0$ by uniqueness of the solution to (C.19)–(C.20), which is the weak formulation of the usual Stokes equations. Thus, it is sufficient to consider the case $\mathrm{div}\,u_h \neq 0$, and, by homogeneity $\|\sqrt{\psi^a}\,\mathrm{div}\,u_h\|_{\omega^a} = 1$, $\mathrm{diam}(\omega^a) = 1$. The statement now follows by maximizing

$$\Phi(u_h, \omega^a) = \|\nabla\hat{s}_h^a\|_{\omega^a}$$

under these constraints. This maximum is indeed attained since it is taken over a bounded set in a finite dimensional space and Φ is a continuous function of u_h and ω^a. ■

Remark C.2. *We do not attempt here to give a theoretical bound for $\tilde{C}_{div}$. However, our numerical experiments suggest that it is close to* 1.95 *in the case $k = 2$, cf. Section C.2.1. We conjecture $C_{div} \leqslant 2$.*

Lemma C.3. *Let $u_h \in V_h$ and $s_h^a \in H_0^1(\omega^a)$ be given by (C.14)–(C.15). Then, for any cell $K \in \mathcal{T}_h$, and taking the sums over all the nodes a, it holds*

$$\|\sum_a \nabla(s_h^a - u_h\psi^a)\|_K^2 \leqslant C_{\mathrm{int}}^2 \sum_a \|\nabla(s_h^a - u_h\psi^a)\|_K^2 \tag{C.21}$$

with $0 < C_{\mathrm{int}} < \sqrt{d+1}$ depending only on the mesh regularity and the polynomial degree k.

Proof. The bound (C.21) with $C_{\mathrm{int}} = \sqrt{d+1}$ follows easily from the inequality between the mean and the quadratic mean, taking into account that there are at most $(d+1)$ nodes that contribute into the sum on a given cell K. In fact, the optimal value of C_{int} is smaller than $\sqrt{d+1}$. Otherwise, if it were equal to $\sqrt{d+1}$, there would exist a mesh, a cell K, and u_h such that corresponding $\hat{s}_h^a$ are the same on K for all the vertices a of K. This is impossible. ■

Lemma C.4 (Poincaré-Wirtinger inequality with the optimal constant from [13])**.** *For any $K \in \mathcal{T}_h$ andies any $u \in H^1(K)$ such that $\int_K u = 0$, there holds*

$$\|u\|_K \leqslant \frac{h_K}{\pi}\|\nabla u\|_K \tag{C.22}$$

C. Appendix C: On LBB dependence of the a posteriori error estimates à la Vohralik

Theorem C.5. *The error estimator* $\|\sigma_h+\nabla u_h\|_\Omega$ *with* σ_h *defined by (C.10)-(C.11)-(C.12) satisfies*

$$\|\nabla u - \nabla u_h\|_\Omega \leqslant \left(\|\sigma_h + \nabla u_h - p_h I\|_\Omega^2 + C_{div}^2 \|\operatorname{div} u_h\|_\Omega^2\right)^{\frac{1}{2}} + \frac{1}{\pi}\operatorname{osc}_{\mathcal{T}_h}(f) \tag{C.23}$$

$$\|\nabla(p-p_h)\|_{-1,\Omega} \leqslant \|\sigma_h + \nabla u_h - p_h I\|_\Omega + C_{div}\|\operatorname{div} u_h\|_\Omega + \frac{1}{\pi}\operatorname{osc}_{\mathcal{T}_h}(f) \tag{C.24}$$

with $C_{div} = \tilde{C}_{div} C_{int}$ *the combination of constants from constant from (C.18) and* (C.21)

$$(\operatorname{osc}_{\mathcal{T}_h}(f))^2 = \sum_{K\in\mathcal{T}_h} h_K^2 \|f - \Pi_h^k f\|_K^2$$

where Π_h^k *is the orthogonal projection on the space of (discontinues) piecewise polynomials of degree* $\leqslant k$ *on mesh* $\mathcal{T}_h$*.*

Moreover, we have the local lower bounds on any $K \in \mathcal{T}_h$

$$\|\sigma_h + \nabla u_h - p_h I\|_K \leqslant C(\|\nabla u - \nabla u_h\|_{\omega_K} + \|\nabla(p-p_h)\|_{-1,\omega_K} + \widetilde{\operatorname{osc}}_{\omega_K}(f)) \tag{C.25}$$

$$\|\operatorname{div} u_h\|_K \leqslant C\|\nabla u - \nabla u_h\|_K \tag{C.26}$$

and the global lower estimate

$$\|\sigma_h + \nabla u_h - p_h I\|_\Omega + \|\operatorname{div} u_h\|_\Omega \leqslant C(\|\nabla u - \nabla u_h\|_\Omega + \|\nabla(p-p_h)\|_{-1,\Omega} + \widetilde{\operatorname{osc}}_{\mathcal{T}_h}(f)) \tag{C.27}$$

In the last 3 inequalities $C > 0$ *stand for constants depending only on the mesh regularity. The oscillations* $\widetilde{\operatorname{osc}}$ *are defined as*

$$(\widetilde{\operatorname{osc}}_{\mathcal{T}_h}(f))^2 = \sum_{a\in\mathcal{V}_h} h_a^2 \|f\psi^a - \Pi_h^{k-1}(f\psi^a)\|_K^2$$

and similarly for $\widetilde{\operatorname{osc}}_{\omega_K}$ *with the sum over the vertices of* K*.*

Remark C.6. *If* f *is sufficiently smooth, then* $\operatorname{osc}_{\mathcal{T}_h}(f)$ *is of order* h^{k+2} *and* $\widetilde{\operatorname{osc}}_{\mathcal{T}_h}(f)$ *is of order* h^{k+1}*. They can be thus neglected in comparison with other terms, which are of order* h^k*.*

Proof. The upper estimate (C.23) is already almost proved, cf. (C.7) and Lemma C.1. However, we do not have exactly $\operatorname{div}\sigma_h = f - \nabla p_h$, but rather $\operatorname{div}\sigma_h = f_h - \nabla p_h$ with f_h described in the statement above. To see this, we recall (C.11) which is valid for all piecewise $\mathbb{P}_k$ polynomials q_h if a is a boundary node. If a is interior node, then (C.11) is valid only under the constrait $\int_{\omega^a} q_h = 0$. However, (C.11) is also satisfied with $q_h = e_i$, i.e. the i-th vector of the canonical basis of $\mathbb{R}^d$. Indeed,

$$\int_{\omega^a} e_i\cdot\operatorname{div}\sigma_h^a = 0 = \int_{\omega^a}(f\cdot\psi^a e_i - \nabla u_h : \nabla(\psi^a e_i) + p_h \operatorname{div}(\psi^a e_i)) = \int_{\omega^a}(f\cdot\psi^a e_i + (-\nabla u_h + p_h I)\cdot\nabla(\psi^a e_i))$$

since $\sigma_h^a n = 0$ on $\partial\omega^a$ and thanks to (C.1) with $v_h = \psi^a e_i$. Thus, (C.11) is valid for any piecewise $\mathbb{P}_k$ polynomial χ_h without constraints. We can also write it separately on any mesh cell $K \in \mathcal{T}_h$ since χ_h are discontinuous:

$$\int_K \chi_h \cdot \operatorname{div}\sigma_h^a = \int_K \chi_h \cdot (f\psi^a + (-\nabla u_h + p_h I)\cdot\nabla\psi^a), \quad \forall \chi_h \in \mathbb{P}_k(K)$$

Summing this over all the vertices a gives, cf (1.53),

$$\int_K \chi_h \cdot \operatorname{div} \sigma_h = \int_K \chi_h \cdot f, \quad \forall \chi_h \in \mathbb{P}_k(K)$$

so that $\operatorname{div} \sigma_h = f_h$ on K. We now modify the proof of (C.7): introducing $\bar{e}_K$ as the mean of $e = u - s$ on K

$$\|\nabla u - \nabla s\|_\Omega^2 = (\nabla u - \nabla s, \nabla e) = (f - f_h, e) + (f_h - \nabla p_h, e) - (\nabla s, \nabla e)$$

$$= (f - f_h, e) + (\operatorname{div} \sigma_h - \nabla p_h, e) - (\nabla s, \nabla e) = \sum_{K \in \mathcal{T}_h} (f - f_h, e - \bar{e}_K)_K - (\sigma_h + p_h I + \nabla s, \nabla e)$$

$$\leqslant \left(\sum_{K \in \mathcal{T}_h} h_K^2 \|f - f_h\|_K^2 \right)^{\frac{1}{2}} \left(\sum_{K \in \mathcal{T}_h} \frac{1}{h_K^2} \|e - \bar{e}_K\|_K^2 \right)^{\frac{1}{2}} + \|\sigma_h + \nabla s + p_h I\|_\Omega \|\nabla e\|_\Omega$$

This proves (C.23) since $\|e - \bar{e}_K\|_K \leqslant \frac{h_K}{\pi} \|\nabla e\|_K$ and

$$\|\nabla(s - u_h)\|_\Omega \leqslant C_{div} \|\operatorname{div} u_h\|_\Omega$$

with $C_{\mathrm{div}} = C_{\mathrm{int}} \tilde{C}_{div}$.To prove the last bound, we recall Lemma C.3:

$$\|\nabla(s - u_h)\|_K^2 = \|\sum_a \nabla(s_h^a - u_h \psi^a)\|_K^2 \leqslant C_{\mathrm{int}}^2 \sum_a \|\nabla(s_h^a - u_h \psi^a)\|_K^2$$

sum this over all $K \in \mathcal{T}_h$, and use Lemma C.1

$$\|\nabla(s - u_h)\|_\Omega^2 \leqslant C_{\mathrm{int}}^2 \sum_a \|\nabla(s_h^a - u_h \psi^a)\|_{\omega^a}^2 \leqslant C_{\mathrm{int}}^2 \tilde{C}_{div}^2 \sum_a \int_{\omega^a} \psi^a |\operatorname{div} u_h|^2 = C_{\mathrm{int}}^2 \tilde{C}_{div}^2 \|\operatorname{div} u_h\|_\Omega^2 \tag{C.28}$$

To prove the upper bound for the error in pressure (C.24), we take any $v \in H_0^1(\Omega)$ with $\|\nabla v\|_\Omega = 1$ and decompose

$$v = z + w$$

where z is divergence-free, i.e. $z \in Z = \{v \in H_0^1(W)^d : \operatorname{div} v = 0\}$, and w is in the orthogonal complement of Z, i.e. $w \in Z^\perp = \left\{ r \in H_0^1(W)^d : (\nabla r, \nabla z)_\Omega = 0 \quad \forall z \in Z \right\}$. We have then $\|\nabla w\|_\Omega \leqslant 1$ since

$$\|\nabla w\|_\Omega^2 = (\nabla w, \nabla w + \nabla z)_\Omega = (\nabla w, \nabla v)_\Omega \leqslant \|\nabla w\|_\Omega \|\nabla v\|_\Omega = \|\nabla w\|_\Omega$$

Using again $\operatorname{div} z = 0$, $w \in Z^\perp$ and the variational formulation of the Stokes equations, we get

$$\int_\Omega \nabla(p - p_h) \cdot v = -\int_\Omega (p - p_h) \operatorname{div} w = -\int_\Omega \nabla u : \nabla w + \int_\Omega f \cdot w - \int_\Omega \nabla p_h \cdot w$$

$$= -\int_\Omega \nabla s : \nabla w + \int_\Omega (f - f_h) \cdot w + \int_\Omega (\operatorname{div} \sigma_h - \nabla p_h) \cdot w$$

$$= \int_\Omega (\nabla u_h - \nabla s) : \nabla w + \int_\Omega (f - f_h) \cdot w - \int_\Omega (\sigma_h + \nabla u_h - p_h I) \cdot \nabla w$$

$$\leqslant \|\nabla u_h - \nabla s\|_\Omega \|\nabla w\|_\Omega + \|\sigma_h + \nabla u_h - p_h I\|_\Omega \|\nabla w\|_\Omega + \left(\sum_{K \in \mathcal{T}_h} h_K^2 \|f - f_h\|_K^2 \right)^{\frac{1}{2}} \left(\sum_{K \in \mathcal{T}_h} \frac{1}{h_K^2} \|w - \bar{w}_K\|_K^2 \right)^{\frac{1}{2}}$$

with $\bar{w}_K$ the average of w on K. Using (C.28), Lemma C.4, and $\|\nabla w\|_\Omega \leqslant 1$, we arrive at

$$\int_\Omega \nabla(p-p_h)\cdot v \leqslant C_{\rm div}\|\operatorname{div} u_h\|_\Omega + \|\sigma_h + \nabla u_h - p_h I\|_\Omega + \frac{1}{\pi}\operatorname{osc}_{\mathcal{T}_h}(f)$$

This gives (C.24) by the the definition of the H^{-1} norm of $\nabla(p-p_h)$ as the supremum over all $v \in H^1_0(\Omega)$ with $|v|_{1,\Omega}=1$.

We turn now to the lower bounds. Thanks to Theorem 7 of [15], in the 2D case, for any interior node a, there exists a matrix-valued field c_h^a on ω^a such that $c_h^a|_K \in (\mathrm{RT}_k(K))^2$ on all the mesh triangles in ω^a, $c_h^a n = 0$ on $\partial\omega^a$,

$$\operatorname{div} c_h^a|_K = r_K \text{ on all } K \subset \omega^a, \quad [[c_h^a]]|_E n = r_E \text{ on all } E \in \mathcal{F}^a$$

where $\mathcal{F}^a$ denotes the set of mesh facets inside ω^a and r_K, r_E are the residuals

$$r_K = \Pi_{Q_h^a}(f\psi^a) + (\Delta u_h - \nabla p_h)\psi^a, \quad r_E = [[\nabla u_h - p_h I]]_F \psi^a.$$

Moreover,

$$\|c_h^a\|_{\omega^a} \leqslant C\|r\|_{\left[[H^1(\omega^a)/\mathbb{R}]^2\right]^*} = C \sup_{v\in H^1(\omega^a)/\mathbb{R}} \frac{\sum_{K\subset\omega^a}\int_K r_K\cdot v + \sum_{E\in\mathcal{F}^a}\int_K r_K\cdot v}{\|\nabla v\|_{\omega^a}}$$

Setting

$$\tau_h = \sigma_h^a + (\nabla u_h - p_h I)\psi^a + c_h$$

we see that $\tau_h \in \Sigma_h^a$ and $\operatorname{div}\tau_h = 0$. Using this τ_h in (C.10) as a test function leads to

$$\|\sigma_h^a + (\nabla u_h - p_h I)\psi^a\|_{\omega^a} \leqslant C\|c_h\|_{\omega^a} \leqslant C$$
$$\sup_{v\in[H^1(\omega^a)/\mathbb{R}]^2} \frac{\int_{\omega^a}(\Pi_{Q_h^a}(f\psi^a) - f\psi^a)v + \sum_{K\subset\omega^a}\int_K (f+\Delta u_h - \nabla p_h)\psi^a\cdot v + \sum_{E\in\mathcal{F}^a}\int_E [[\nabla u_h - p_h I]]_F\psi^a\cdot v}{\|\nabla v\|_{\omega^a}}$$

Recalling that $f = -\Delta u + \nabla p$ and integrating by parts, we conclude

$$\begin{aligned}\|\sigma_h^a + (\nabla u_h - p_h I)\psi^a\|_{\omega^a} &\leqslant C \sup_{v\in[H^1(\omega^a)/\mathbb{R}]^2} \frac{\int_{\omega^a}(\Pi_{Q_h^a}(f\psi^a) - f\psi^a)v + \int_{\omega^a}(\nabla(u-u_h) - (p-p_h)I) : \nabla(\psi^a v)}{\|\nabla v\|_{\omega^a}} \\ &\leqslant C(h_a\|f\psi^a - \Pi_h^{k-1}(f\psi^a)\|_{\omega^a} + \|\nabla(u-u_h)\|_{\omega^a} + \|p-p_h)\|_{-1,\omega^a}) \quad \text{(C.29)}\end{aligned}$$

since $\|v\|_{\omega^a} \leqslant Ch_a\|\nabla v\|_{\omega^a}$ for any $v \in [H^1(\omega^a)/\mathbb{R}]^2$ by Poincaré inequality, and consequently $\|\nabla(\psi^a v)\|_{\omega^a} \leqslant \|\nabla v\|_{\omega^a} + \frac{C}{h_a}\|v\|_{\omega^a} \leqslant C\|\nabla v\|_{\omega^a}$. The orthogonal projector $\Pi_{Q_h^a}$ above can be replaced with Π_h^{k-1} since the test functions v are orthogonal to constants. The same bound (C.29) holds for the nodes a on the boundary $\partial\Omega$ by a straiforward adaptation of the proof in [15] (one should replace then $H^1(\omega^a)/\mathbb{R}$ by the subspace of $H^1(\omega^a)$ of functions vanishing on $\partial\omega^a \cap \partial\Omega$). In the 3D case, the same holds by Theorem 2.3 of [40]. Thus, (C.29) holds in all the cases of interest.

We can now establish (C.25): take any $K \in \mathcal{T}_h$ and sum (C.29), squared on both sides, over all the vertices a of K. To deal with the pressure error, we need the following observation

$$\sum_{a:\text{ vertices of } K} \|\nabla(p-p_h)\|^2_{-1,\omega^a} \leqslant (d+1)\|\nabla(p-p_h)\|^2_{-1,\omega_K} \quad \text{(C.30)}$$

Indeed, for any $\eta > 1$ and any node a there exists $v^a \in H_0^1(\omega^a)$ such that

$$\|\nabla v^a\|_{1,\omega^a} = \|\nabla(p - p_h)\|_{-1,\omega^a} \quad \text{and} \quad \|\nabla(p - p_h)\|^2_{-1,\omega^a} \leqslant \eta(\nabla(p - p_h), \nabla v^a)_{\omega^a}$$

Extending all these functions by 0 outside of their respective domains, we can write (assuming the summation over $d+1$ vertices of K, denoted by a)

$$\begin{aligned}\sum_a \|\nabla(p - p_h)\|^2_{-1,\omega^a} &\leqslant \eta \sum_a \int_{\omega^a} \nabla(p - p_h) \cdot \nabla v^a \\ &= \eta \int_{\omega_K} \nabla(p - p_h) \cdot \sum_a \nabla v^a \leqslant \eta \|\nabla(p - p_h)\|_{-1,\omega_K} \left\| \sum_a \nabla v^a \right\|_{\omega_K} \\ &\leqslant \eta \|\nabla(p - p_h)\|_{-1,\omega_K} (d+1) \left(\sum_a \|\nabla(p - p_h)\|^2_{-1,\omega^a} \right)^{\frac{1}{2}}\end{aligned}$$

Passing to the limit $\eta \to 1$ gives (C.30). This establishes (C.25).

The other local lower estimate (C.26) is trivial since

$$\| \operatorname{div} u_h\|_K = \| \operatorname{div}(u - u_h)\|_K \leqslant \sqrt{d} \|\nabla(u - u_h)\|_K$$

Summing (C.29) over all the nodes of the mesh and dealing again with the pressure error in a manner similar to (C.30), replacing $(d+1)$ by a constant C related to the maximum number of overlaps between patches ω^F which depends only on the mesh regularity, gives the global lower estimate (C.27). ■

C.2.1. A numerical evaluation of the constant $\tilde{C}_{div}$ in Lemma C.1.

In this section we want to evaluate the constant C_{div} in Lemma C.1. Let ω^a be a patch of elements around a node of the mesh $\mathcal{T}_h$ and $V_h(\omega^a)$ the restriction of the velocity finite element space V_h on ω^a. As suggested by formulation (C.19)-(C.20), the first task in evaluating the constant $\tilde{C}_{\text{div}}$ on ω^a is to construct a basis of a subspace of $V_h(\omega^a)$ complementary to the subspace of divergence-free functions. To this end, we construct the matrix $\mathbf{D}$ of the bilinear form

$$D(u_h, v_h) = \int_{\omega^a} \psi^a \, (\operatorname{div} u_h) \, (\operatorname{div} v_h)$$

on the natural basis of $V_h(\omega^a)$ and solve the eigen-value problem

$$\mathbf{D}\vec{u}_i = \lambda_i \vec{u}_i$$

We then select only the positive eigen-values, say $\lambda_1, \ldots, \lambda_M$, with the corresponding eigenvectors $\vec{u}_i$ representing the finite element functions $u_{h,i} \in V_h(\omega^a)$, which form a basis for the orthogonal complement to the kernel of the bilinear form D. We can normalize $u_{h,i}$ so that $D(u_{h,i}, u_{h,j}) = \delta_{ij}$.

We now introduce a fine mesh $\mathcal{T}_{\tilde{h}}$ on ω^a splitting every element of ω^a into $R \times R$ smaller triangles, cf. FIg. C.1. We then discretize problem (C.19)-(C.20) as: find $\hat{s}^a_{\tilde{h}} \in V_{\tilde{h}}(\omega^a), p^a_{\tilde{h}} \in Q_{\tilde{h}}(\omega^a)$ such that

$$\int_{\omega^a} \nabla \hat{s}^a_{\tilde{h}} \cdot \nabla t_h + \int_{\omega^a} p^a_{\tilde{h}} \operatorname{div} t_h = 0 \quad \forall t_{\tilde{h}} \in V_{\tilde{h}}(\omega^a) \tag{C.31}$$

$$\int_{\omega^a} q_{\tilde{h}} \operatorname{div} \hat{s}^a_{\tilde{h}} = -\int_{\omega^a} \psi^a q_{\tilde{h}} \operatorname{div} u_h \quad \forall q_{\tilde{h}} \in Q_{\tilde{h}}(\omega^a) \tag{C.32}$$

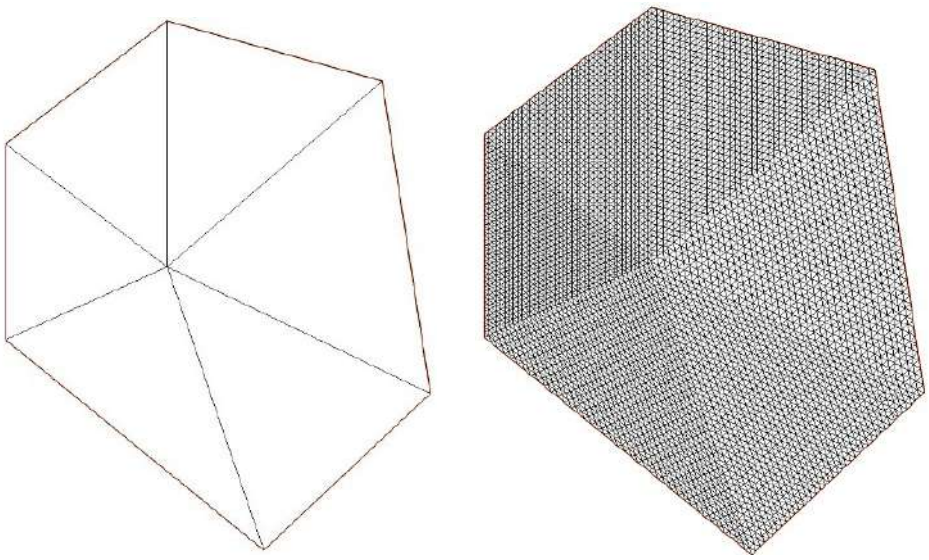

Figure C.1.: Introduce a fine mesh on patch ω^a

where $V_{\tilde{h}}(\omega^a) \subset H_0^1(\omega^a)$, $Q_{\tilde{h}}(\omega^a) \subset L_0^2(\omega^a)$ are (respectively) $\mathbb{P}_2$ and $\mathbb{P}_1$ finite elements on mesh $\mathcal{T}_{\tilde{h}}$. The constant $\tilde{C}_{\mathrm{div}}^2$ in inequality (C.18) on ω^a is approximated be the maximum of

$$\frac{\int_{\omega^a} \nabla \hat{s}_{\tilde{h}}^a : \nabla \hat{s}_{\tilde{h}}^a}{\int_{\omega^a} \psi^a \left(\operatorname{div} u_h\right)^2}$$

over the span of $\{u_{h,1}, \ldots, u_{h,M}\}$. To find this maximum, we solve (C.31) for every $u_h = u_{h,i}$, $i = 1, \ldots, M$. Denoting the obtained solutions by $\hat{s}_{\tilde{h},i}^a$, it remains to form the matrix A of size $M \times M$ by$A_{ij} = \int_{\omega^a} \nabla \hat{s}_{\tilde{h},i}^a : \nabla \hat{s}_{\tilde{h},j}^a$ and to calculate the largest eigen-value of A. It gives the maximum of the ratio above.

D. Appendix D: Curved Boundary

An important limitation of all the *a posteriori* error estimates developed so far in this thesis, is that they apply only to the finite element approximation in polygonal domains. Dealing with problems posed in domains with curved boundaries is of course also very important. In this appendix, we rely on a finite element discretization in such domains proposed in the Master thesis of Claire Marin [56] and designed having in mind the ease of implementation in FreeFEM. The hypothesis is that the mesh is composed of triangular elements with straight edges (which is the only mesh type available in FreeFEM), and the boundary conditions on the approximated polygonal boundary are deduced from the actual boundary conditions on the exact boundary thanks to a Taylor expansion. This approach is very close to *Boundary-Value Corrections* method of [17]. We present here the main results on the *a priori* error analysis from [56] for the Dirichlet-Poisson problem. Then we test numerically an equilibrated flux *a posteriori* estimator making a comparison between the boundary correction model and the model without boundary correction. We do not have any theoretical justification for our *a posteriori* estimator, but we observe that it describes the error of the finite element approximation very accurately if the boundary correction trick was used to compute this approximation.

D.1. A Priori Error

D.1.1. Notations

Let Ω be a bounded domain in $\mathbb{R}^2$ with a smooth boundary $\partial\Omega$. We consider the Poisson problem which is: find $u \in H^2(\Omega)$ satisfying

$$\begin{cases} -\Delta u = f & \text{in} \quad \Omega \\ u = g & \text{on} \quad \partial\Omega \end{cases} \tag{D.1}$$

where $f \in L^2(\Omega)$ and $g \in H^{\frac{3}{2}}(\partial\Omega)$. We introduce a triangular mesh $\mathcal{T}_h$ on Ω such that the nodes at the boundary are all on $\partial\Omega$ while the boundary edges are not. The triangulation is supposed to be a classical one, with straight sides. Then, in general, the boundary edges do not match exactly $\partial\Omega$. Let Ω_h be the domain formed by the mesh, i.e. :

$$\overline{\Omega_h} = \cup_{K \in \mathcal{T}_h} K$$

and a mapping $\phi : \mathbb{R}^2 \to \mathbb{R}^2$ that associates for each $x_h \in \partial\Omega_h$ to a point $\phi(x_h) = x \in \partial\Omega$ and then, the gap function δ defined by $\delta(x_h) = \phi(x_h) - x_h, \ \forall x_h \in \partial\Omega_h$.

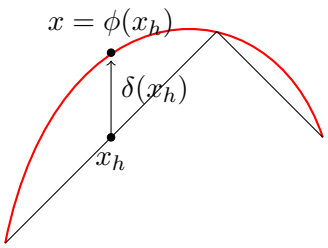

We suppose that ϕ is a $\mathcal{C}^2$ mapping and we consider a $\mathbb{P}_k$ finite elements to approximate the problem. we will introduce the first order corrections on $\partial\Omega_h$ in order to have optimal convergence :

$$\forall x_h \in \partial\Omega_h, \quad u(x_h) \simeq g(\phi(x_h)) - \delta(x_h) \cdot \nabla u(x_h).$$

Let V_h be the space of (continuous) piecewise $\mathbb{P}_k$ polynomial functions on $\mathcal{T}_h$, and V_h^0 the subspace of V_h containing the functions that vanish on $\partial\Omega_h$. Now, we want to find $u_h \in V_h$ such that

$$\begin{cases} \int_{\Omega_h} \nabla u_h \cdot \nabla v_h \, \mathrm{d}\Omega = \int_{\Omega_h} f v_h \, \mathrm{d}\Omega, \quad \forall v_h \in V_h^0 \\ \int_{\partial\Omega_h} (u_h + \delta \cdot \nabla u_h) v_h \, \mathrm{d}\Gamma = \int_{\partial\Omega_h} (g \circ \phi) v_h \, \mathrm{d}\Gamma, \quad \forall v_h \in V_h \end{cases}. \tag{D.2}$$

Discretization

We will do a Taylor expansion of order $l \leq k$ near the boundary, with $l \in \mathbb{N}$. Let $\{\mathcal{T}_h\}_h$ be triangular mesh of Ω with the mesh size h. Let Ω_h be the domain formed by the mesh, i.e. $\overline{\Omega_h} = \cup_{K \in \mathcal{T}_h} K.$, let $\mathcal{T}_h^b$ be the set of triangles that intersects the boundary $\partial\Omega_h$, and let $\mathcal{E}_h$ be the set of boundary edges. We suppose that $\{\mathcal{T}_h\}_h$ is :

Hypothesis 1 : regular We suppose that there exists a constant C such that, for all $h > 0$ and for all $T \in \mathcal{T}_h$,

$$\frac{h_T}{\rho_T} \leqslant C.$$

Hypothesis 2 : Quasi-uniform There exists a constant C depending on Ω such that

$$\min_{T \in \mathcal{T}_h} \rho_T \geqslant Ch.$$

We consider the following problem : find $u_h \in V_h$ such that :

$$\begin{cases} \displaystyle\int_{\Omega_h} \nabla u_h \cdot \nabla v_h \, \mathrm{d}\Omega = \int_{\Omega_h} f v_h \, \mathrm{d}\Omega, \quad \forall v_h \in V_h^0 \\ \displaystyle\int_{\partial\Omega_h} \left(\sum_{|s| \leqslant l} \frac{\partial^s u_h}{s!} \delta^s \right) v_h \, \mathrm{d}\Gamma = \int_{\partial\Omega_h} (g \circ \phi) v_h \, \mathrm{d}\Gamma, \quad \forall v_h \in V_h \end{cases}. \tag{D.3}$$

Here $s = (s_1, s_2)$ is a couple of non-negative integers, $|s| = s_1 + s_2$, $s! = s_1! s_2!$, $\partial^s u_h = \dfrac{\partial^{|s|} u_h}{\partial x^{s_1} \partial y^{s_2}}$ and $\delta^s = (\delta_1, \delta_2)^s = {\delta_1}^{s_1} {\delta_2}^{s_2}$.
We suppose that all the generic constants C are different from an equation to another

and depend on the mesh regularity only. We are going to put the theorem about the optimal order of convergence of H^1 error semi-norm of $u - u_h$ for an appropriate order of approximation of the boundary and order of the finite elements.

Theorem D.1. *Let u be the solution of the problem* (D.1)*, and u_h the solution of the problem* (D.3)*. Assume that $u \in H^{k+1}(\Omega) \cap W^{l+1,\infty}(\Omega)$, $k \geqslant l \geqslant \frac{k}{2} - \frac{3}{4}$. There exists a constant C depending only on the regularity of the mesh and the domain Ω such that for h small enough :*

$$| u - u_h |_{H^1(\Omega_h)} \leqslant Ch^k | u |_{H^{k+1}(\Omega) \cap W^{l+1,\infty}(\Omega)},$$

where we denote by $| u |_{H^{k+1}(\Omega) \cap W^{l+1,\infty}(\Omega)}$ the quantity $| u |_{H^{k+1}(\Omega)} + | u |_{W^{l+1,\infty}(\Omega)}$.

Now, we want to put the theorem about the optimal order of convergence of L^2 norm of $u - u_h$.

Theorem D.2. *Assume that the solution u of the problem* (D.3) *is in $H^{k+1}(\Omega)$, and $l \geqslant \frac{k}{2} - \frac{1}{4}$. There exists a constant C depending only on the regularity of the mesh and the domain Ω such that for h small enough :*

$$\| u - u_h \|_{L^2(\Omega_h)} \leqslant Ch^{k+1} | u |_{H^{k+1}(\Omega) \cap W^{l+1,\infty}(\Omega)}$$

Proof. See [56]. ■

Now, let us present the numerical part of *a posteriroi* error using the idea of Claire for defining the approximated solution u_h as in (D.3)

P2 finite elements

Now, we want to implement the scheme (D.2). We remark that the Dirichlet boundary conditions are imposed in FreeFEM++ via penalization even in standard situation of FEM on a polygonal domain. So, the simplest way to implement in FreeFEM++ is to find $u_h \in V_h$ such that for all $v_h \in V_h$

$$\int_{\Omega_h} \nabla u_h \cdot \nabla v_h \, \mathrm{d}\Omega + \frac{1}{\varepsilon} \int_{\partial\Omega_h} (u_h + \delta \cdot \nabla u_h) \, v_h \, \mathrm{d}\Gamma = \int_{\Omega_h} f v_h \, \mathrm{d}\Omega + \frac{1}{\varepsilon} \int_{\partial\Omega_h} (g \circ \phi) v_h \, \mathrm{d}\Gamma, \quad \text{(D.4)}$$

with $\varepsilon \ll 1$.

In the following figures, we compare the method (D.4) with the results without doing any approximation of the boundary, that is to say by implementing :

$$\int_{\Omega_h} \nabla u_h \cdot \nabla v_h \, \mathrm{d}\Omega + \frac{1}{\varepsilon} \int_{\partial\Omega_h} u_h v_h \, \mathrm{d}\Gamma = \int_{\Omega_h} f v_h \, \mathrm{d}\Omega + \frac{1}{\varepsilon} \int_{\partial\Omega_h} (g \circ \phi) v_h \, \mathrm{d}\Gamma. \quad \text{(D.5)}$$

D.2. A Posteriori Error

The weak formulation of system (D.1) is:

Find $u \in H^1_g(\Omega)$ such that:

$$(\nabla u, \nabla v)_\Omega = (f, v)_\Omega \quad \forall v \in H^1_0(\Omega) \quad \text{(D.6)}$$

Where,

$$f = \frac{12u_{av}}{R^2}$$

$$H_0^1(\Omega) := \{u \in H^1(\Omega); \quad u = 0 \quad \text{on} \quad \partial\Omega\}$$

,

$$H_g^1(\Omega) := \{u \in H^1(\Omega); \quad u = g \quad \text{on} \quad \partial\Omega\}$$

and

$$g = \begin{cases} u = u_{in} & \text{on} \quad \Gamma_{\text{in}}, \\ u = u_{out} & \text{on} \quad \Gamma_{\text{out}}, \\ u = 0 & \text{on} \quad Wall, \end{cases}$$

Let u_h be the approximate solution defined as in scheme (D.2). We look for stress $\sigma_h \in \Sigma_h \subset H(\text{div}, \Omega)$ such that:

$$\sigma_h^{\text{ideal}} := \underset{\substack{v_h \in \Sigma_h, \\ \text{div } v_h = \Pi_{Q_h}(f) = f \text{on } \Omega}}{\arg\min} ||\nabla u_h + v_h||_{L^2(\Omega)} \tag{D.7}$$

In practice, Σ_h will be RT_1 on Ω and and Q_h will be $\mathbb{P}_1(\mathcal{T}_h)$ on Ω. Computing σ_h as the solution of eq (D.7): σ_h^{ideal} would be too costly, so we localize this minimization. For each vertex $a \in \Omega$ we consider a patch ω_a to be the collection of all triangles that share this vertex a. Now, relies on the partition of unity by the hat functions ψ_a and finds the following local minimizers:

$$\sigma_h^a := \underset{\substack{v_h \in \Sigma_h^a, \\ \text{div } v_h = \Pi_{Q_h^a}(\psi_a f - \nabla\psi_a \cdot \nabla u_h)}}{\arg\min} ||\psi_a \nabla u_h + v_h||_{L^2(\omega_a)} \tag{D.8}$$

Let $\mathcal{V}_h$ be the set of vertices of the mesh $\mathcal{T}_h$

$$\sigma_h = \sum_{a \in \mathcal{V}_h} \sigma_h^a \tag{D.9}$$

Conjecture D.3 (A general a posterior error estimate)**.** *Let u be the weak solution defined by system (D.6). When we make approximation of the curved boundary, we define u_h as in (D.2), and when we do not make approximation of the curved boundary, we define u_h as in (D.5) and σ_h defined as (D.9) . $\forall K \in \mathcal{T}_h$ define:*

- *Flux estimator:* $\eta_{F,K} := ||\nabla u_h + \sigma_h||_K$
- *Total estimator* $\eta^2 := \sum_{K \in \mathcal{T}_h} \eta_{F,K}^2$

Then,

$$||\nabla(u - u_h)||_\Omega^2 \leq \eta^2 \tag{D.10}$$

D.3. Numerical results

Let us consider the following problem:

$$\begin{cases} -\Delta u = f & \text{in} \quad \Omega \\ u = g & \text{on} \quad \partial\Omega \end{cases}$$

Where Ω is defined in the Figure D.1 below, $f = 1$, $R_1 = 0.7$, $R_2 = 1$ and

$$g = \begin{cases} u = u_e & \text{on} \quad \Gamma_{\text{in}}, \\ u = u_e & \text{on} \quad \Gamma_{\text{out}}, \\ u = 0 & \text{on} \quad Wall, \end{cases}$$

$u_e = A + B\frac{ln(x^2+y^2)}{2} - \frac{(x^2+y^2)}{4}$ where, $A = \frac{R_2^2 ln(R_1) - R_1^2 ln(R_2)}{4ln(\frac{R_1}{R_2})}$and $B = \frac{R_2^2 - R1^2}{4ln(\frac{R_2}{R_1})}$

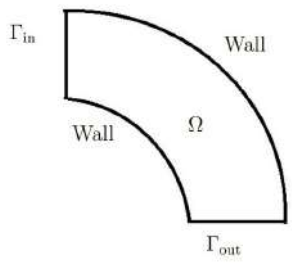

Figure D.1.: Domain Ω with curved boundary

Now, we will compare the error and estimator in (D.10) between taking u_h as solution of non correction boundary in scheme (D.5) and between the solution of corrected boundary in scheme (D.2). We conclude from this comparison in Figure D.2 that the correction of the boundary gives less error and estimator than the non corrected one. Also, when we do not make the correction of the boundary, then the estimator is less that the error as you see in Figure D.2 and this contradicts the posterior error estimation in Theorem D.3. To see more the results we introduce the data for non corrected boundary in the table below and as you see the estimator is less than the error which lead to index of efficiency Index $= \frac{\eta}{\text{Error}} = 0.8$.

Mesh size	Error	η	Index
0.0469192	0.000262393	0.000221949	0.845865
0.0232701	9.1345e-05	7.9358e-05	0.868773
0.0126408	3.20462e-05	2.81435e-05	0.878215
0.00702287	1.12396e-05	9.92078e-06	0.882665

While when we make the correction of the boundary, we get that the error is less than the estimator which lead to index of efficiency Index $= \frac{\eta}{\text{Error}} = 1.019$ as you see in the following table

Mesh size	Error	η	Index
0.0469192	5.8102e-05	5.9233e-05	1.01947
0.0232701	1.31804e-05	1.33805e-05	1.01518
0.0126408	3.56757e-06	3.6359e-06	1.01916
0.00702287	8.9232e-07	9.09405e-07	1.01915

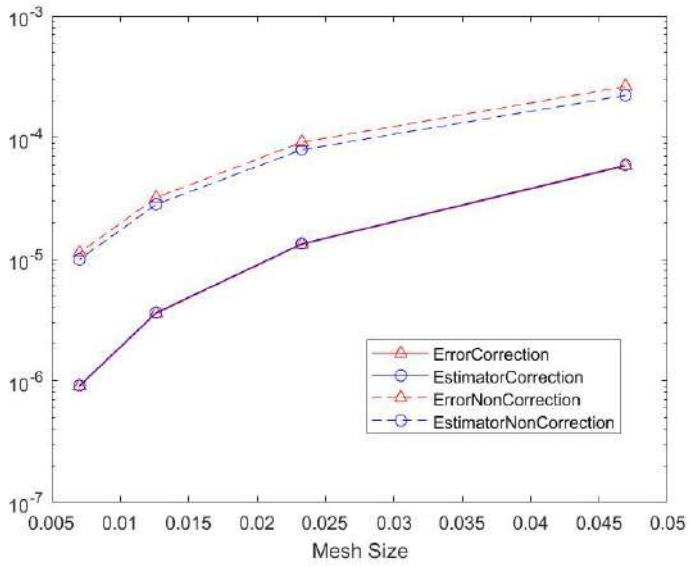

Figure D.2.: Errors and Estimator for the corrected boundary and the non corrected one

We conclude from the above results that the correction of the boundary for the curved domains is important since without making this correction we obtain an estimator η less than the error $\|u - u_h\|_\Omega$ which does not confirm what we have in Theorem D.3 while after making the correction of the boundary as in (D.4), the estimator η becomes greater than the error $\|u - u_h\|_\Omega$ which confirm the Theorem D.3 and the index of efficiency improved from Index $= \frac{\eta}{\text{Error}} = 0.8$ (when we do not make correction of the boundary) to Index $= \frac{\eta}{\text{Error}} = 1.019$ (when we make a correction of the boundary).

Bibliography

[1] Mark Ainsworth and J Tinsley Oden. A posteriori error estimation in finite element analysis. *Computer methods in applied mechanics and engineering*, 142(1-2):1–88, 1997.

[2] Mark Ainsworth and J.Tinsley Oden. A posteriori error estimation in finite element analysis. *Computer Methods in Applied Mechanics and Engineering*, 142(1):1–88, 1997.

[3] Ivo Babuška, Ricardo Durán, and Rodolfo Rodríguez. Analysis of the efficiency of an a posteriori error estimator for linear triangular finite elements. *SIAM journal on numerical analysis*, 29(4):947–964, 1992.

[4] Ivo Babuška and Werner C Rheinboldt. A-posteriori error estimates for the finite element method. *International Journal for Numerical Methods in Engineering*, 12(10):1597–1615, 1978.

[5] Ivo Babuska and Werner C. Rheinboldt. Analysis of optimal finite element meshes in r1. *Mathematics of Computation*, 33:435–435, 1979.

[6] Ivo Babuška and Werner C Rheinboldt. On the reliability and optimality of the finite element method. *Computers & Structures*, 10(1-2):87–94, 1979.

[7] Ivo Babuska and Werner C Rheinboldt. A posteriori error analysis of finite element solutions for one-dimensional problems. *SIAM Journal on Numerical Analysis*, 18(3):565–589, 1981.

[8] Ivo Babuška and Theofanis Strouboulis. *The finite element method and its reliability*. Oxford university press, 2001.

[9] I Babuvška and Werner C Rheinboldt. Error estimates for adaptive finite element computations. *SIAM Journal on Numerical Analysis*, 15(4):736–754, 1978.

[10] Saumya Bajpai and Debendra Kumar Swain. A priori error estimates of a three-step two-level finite element galerkin method for a 2d-boussinesq system of equations. *Computers & Mathematics with Applications*, 146:137–164, 2023.

[11] Randolph E Bank and R Kent Smith. A posteriori error estimates based on hierarchical bases. *SIAM Journal on Numerical Analysis*, 30(4):921–935, 1993.

[12] Frano Barbir, H Gorgun, and Xinting Wang. Relationship between pressure drop and cell resistance as a diagnostic tool for pem fuel cells. *Journal of Power Sources*, 141(1):96–101, 2005.

[13] Mario Bebendorf. A note on the Poincaré inequality for convex domains. *Zeitschrift für Analysis und ihre Anwendungen*, 22(4):751–756, 2003.

[14] Dietrich Braess, Veronika Pillwein, and Joachim Schöberl. Equilibrated residual error estimates are p-robust. *Computer Methods in Applied Mechanics and Engineering*, 198(13-14):1189–1197, 2009.

[15] Dietrich Braess, Veronika Pillwein, and Joachim Schöberl. Equilibrated residual error estimates are *p*-robust. *Comput. Methods Appl. Mech. Engrg.*, 198(13-14):1189–1197, 2009.

[16] Dietrich Braess and Joachim Schöberl. Equilibrated residual error estimator for edge elements. *Mathematics of Computation*, 77(262):651–672, 2008.

[17] James H Bramble, Todd Dupont, and Vidar Thomée. Projection methods for dirichlet's problem in approximating polygonal domains with boundary-value corrections. *Mathematics of Computation*, 26(120):869–879, 1972.

[18] Carsten Carstensen. All first-order averaging techniques for a posteriori finite element error control on unstructured grids are efficient and reliable. *Mathematics of Computation*, 73(247):1153–1165, 2004.

[19] Carsten Carstensen. A unifying theory of a posteriori finite element error control. *Numerische Mathematik*, 100:617–637, 2005.

[20] Carsten Carstensen, Michael Feischl, Marcus Page, and Dirk Praetorius. Axioms of adaptivity. *Computers & Mathematics with Applications*, 67(6):1195–1253, 2014.

[21] Carsten Carstensen and Stefan A Funken. Constants in clément-interpolation error and residual based a posteriori estimates in finite element methods. *East-West J. Numer. Math*, 8(3):153–175, 2000.

[22] Carsten Carstensen and Roland Klose. A posteriori finite element error control for the p-laplace problem. *SIAM Journal on Scientific Computing*, 25(3):792–814, 2003.

[23] Carsten Carstensen and Christian Merdon. Estimator competition for poisson problems. *Journal of Computational Mathematics*, pages 309–330, 2010.

[24] Paul Castillo, Bernardo Cockburn, Ilaria Perugia, and Dominik Schötzau. An a priori error analysis of the local discontinuous galerkin method for elliptic problems. *SIAM Journal on Numerical Analysis*, 38(5):1676–1706, 2000.

[25] Paul Castillo, Bernardo Cockburn, Dominik Schötzau, and Christoph Schwab. Optimal a priori error estimates for the hp-version of the local discontinuous galerkin method for convection–diffusion problems. *Mathematics of computation*, 71(238):455–478, 2002.

[26] MJ Castro-Díaz, Frédéric Hecht, Bijan Mohammadi, and O Pironneau. Anisotropic unstructured mesh adaption for flow simulations. *International Journal for Numerical Methods in Fluids*, 25(4):475–491, 1997.

[27] Evgenii V Chizhonkov and Maxim A Olshanskii. On the domain geometry dependence of the LBB condition. *ESAIM: Mathematical Modelling and Numerical Analysis*, 34(5):935–951, 2000.

[28] Patrick Ciarlet and Martin Vohralík. Localization of global norms and robust a posteriori error control for transmission problems with sign-changing coefficients. *ESAIM: Mathematical Modelling and Numerical Analysis*, 52(5):2037–2064, 2018.

[29] Philippe G. Ciarlet. *The finite element method for elliptic problems*. Studies in Mathematics and its Applications, Vol. 4. North-Holland Publishing Co., Amsterdam-New York-Oxford, 1978.

[30] Philippe Destuynder and Brigitte Métivet. Explicit error bounds in a conforming finite element method. *Mathematics of Computation*, 68(228):1379–1396, 1999.

[31] Manfred Dobrowolski. On the LBB constant on stretched domains. *Mathematische Nachrichten*, 254(1):64–67, 2003.

[32] Vit Dolejsi, Alexandre Ern, and Martin Vohralík. hp-adaptation driven by polynomial-degree-robust a posteriori error estimates for elliptic problems. *SIAM Journal on Scientific Computing*, 38(5):A3220–A3246, 2016.

[33] Willy Dörfler and Mark Ainsworth. Reliable a posteriori error control for nonconforming finite element approximation of stokes flow. *Mathematics of computation*, 74(252):1599–1619, 2005.

[34] Alexandre Ern and Jean-Luc Guermond. *Finite Elements I: Approximation and Interpolation*. Springer, February 2021.

[35] Alexandre Ern and Jean-Luc Guermond. *Finite Elements II: Galerkin Approximation, Elliptic and Mixed PDEs*. Springer, April 2021.

[36] Alexandre Ern and Jean-Luc Guermond. Finite elements iii, 2021.

[37] Alexandre Ern, Iain Smears, and Martin Vohralík. Discrete p-robust H(div)-liftings and a posteriori estimates for elliptic problems with H^{-1} source terms. *Calcolo*, 54(3):1009–1025, January 2017.

[38] Alexandre Ern, Iain Smears, and Martin Vohralík. Guaranteed, locally space-time efficient, and polynomial-degree robust a posteriori error estimates for high-order discretizations of parabolic problems. *SIAM Journal on Numerical Analysis*, 55(6):2811–2834, 2017.

[39] Alexandre Ern and Martin Vohralík. Polynomial-degree-robust a posteriori estimates in a unified setting for conforming, nonconforming, discontinuous galerkin, and mixed discretizations. *SIAM Journal on Numerical Analysis*, 53(2):1058–1081, 2015.

[40] Alexandre Ern and Martin Vohralík. Stable broken H^1 and $H(\mathrm{div})$ polynomial extensions for polynomial-degree-robust potential and flux reconstruction in three space dimensions. *Math. Comp.*, 89(322):551–594, 2020.

[41] Francesca Fierro and Andreas Veeser. A posteriori error estimators, gradient recovery by averaging, and superconvergence. *Numerische Mathematik*, 103(2):267–298, 2006.

[42] Luca Formaggia, Jean-Frédéric Gerbeau, Fabio Nobile, and Alfio Quarteroni. On the coupling of 3d and 1d navier–stokes equations for flow problems in compliant vessels. *Computer methods in applied mechanics and engineering*, 191(6-7):561–582, 2001.

[43] Luca Formaggia, Fabio Nobile, Alfio Quarteroni, and Alessandro Veneziani. Multiscale modelling of the circulatory system: a preliminary analysis. *Computing and visualization in science*, 2(2):75–83, 1999.

[44] Pascal-Jean Frey and Frédéric Alauzet. Anisotropic mesh adaptation for cfd computations. *Computer methods in applied mechanics and engineering*, 194(48-49):5068–5082, 2005.

[45] J.-F. Gerbeau and B. Perthame. Derivation of viscous Saint-Venant system for laminar shallow water; numerical validation. *Discrete Contin. Dyn. Syst. Ser. B*, 1(1):89–102, 2001.

[46] Jean-Frédéric Gerbeau and Benoît Perthame. Derivation of Viscous Saint-Venant System for Laminar Shallow Water; Numerical Validation. Research Report RR-4084, INRIA, 2000. Projet M3N.

[47] Vivette Girault and Pierre-Arnaud Raviart. *Finite element methods for Navier-Stokes equations: theory and algorithms*, volume 5. Springer Science & Business Media, 2012.

[48] Weimin Han. *A posteriori error analysis via duality theory: with applications in modeling and numerical approximations*, volume 8. Springer Science & Business Media, 2004.

[49] F. Hecht. New development in freefem++. *J. Numer. Math.*, 20(3-4):251–265, 2012.

[50] Stefan Hüeber and Barbara I Wohlmuth. An optimal a priori error estimate for nonlinear multibody contact problems. *SIAM Journal on Numerical Analysis*, 43(1):156–173, 2005.

[51] Suvi Karvonen, Tero Hottinen, Jaakko Saarinen, and Olli Himanen. Modeling of flow field in polymer electrolyte membrane fuel cell. *Journal of power sources*, 161(2):876–884, 2006.

[52] Kwang-Yeon Kim. Fully computable a posteriori error estimates for the Stokes equation without the global inf-sup constant. *Comput. Math. Appl.*, 67(3):681–691, 2014.

[53] Sergey Korotov. Two-sided a posteriori error estimates for linear elliptic problems with mixed boundary conditions. *Applications of Mathematics*, 52(3):235–249, 2007.

[54] Pierre Ladeveze and Dominique Leguillon. Error estimate procedure in the finite element method and applications. *SIAM Journal on Numerical Analysis*, 20(3):485–509, 1983.

[55] Robert Luce and Barbara I Wohlmuth. A local a posteriori error estimator based on equilibrated fluxes. *SIAM Journal on Numerical Analysis*, 42(4):1394–1414, 2004.

[56] Claire Marin. Finite elements on non-polygonal domains in FreeFEM++. Master's thesis, LmB, Université de Franche-Comté, 2018.

[57] Edie Miglio, Simona Perotto, and Fausto Saleri. Model coupling techniques for free-surface flow problems: Part i. *Nonlinear Analysis: Theory, Methods & Applications*, 63(5-7):e1885–e1896, 2005.

[58] Pekka Neittaanmäki and Sergey R Repin. *Reliable Methods for Computer Simulation: Error Control and Posteriori Estimates*. Elsevier, 2004.

[59] G. P. Panasenko. Method of asymptotic partial decomposition of domain. *Math. Models Methods Appl. Sci.*, 8(1):139–156, 1998.

[60] Jan Papež, Zdeněk Strakoš, and Martin Vohralík. Estimating and localizing the algebraic and total numerical errors using flux reconstructions. *Numerische Mathematik*, 138(3):681–721, 2018.

[61] William Prager and John L Synge. Approximations in elasticity based on the concept of function space. *Quarterly of Applied Mathematics*, 5(3):241–269, 1947.

[62] Serge Prudhomme, Frédéric Pascal, J Tinsley Oden, and Albert Romkes. A priori error estimate for the baumann–oden version of the discontinuous galerkin method. *Comptes Rendus de l'Académie des Sciences-Series I-Mathematics*, 332(9):851–856, 2001.

[63] Alfio Quarteroni and Luca Formaggia. Mathematical modelling and numerical simulation of the cardiovascular system. *Handbook of numerical analysis*, 12:3–127, 2004.

[64] Sergey Repin. *A posteriori estimates for partial differential equations*. Walter de Gruyter, 2008.

[65] Sergey Repin. Estimates of the distance to the set of solenoidal vector fields and applications to a posteriori error control. *Comput. Methods Appl. Math.*, 15(4):515–530, 2015.

[66] Sergey I Repin. A posteriori error estimation for nonlinear variational problems by duality theory. *Journal of Mathematical Sciences*, 99:927–935, 2000.

[67] Béatrice Rivière, Mary F Wheeler, and Vivette Girault. A priori error estimates for finite element methods based on discontinuous approximation spaces for elliptic problems. *SIAM Journal on Numerical Analysis*, 39(3):902–931, 2001.

[68] Rajen Kumar Sinha and Bhupen Deka. A priori error estimates in the finite element method for nonself-adjoint elliptic and parabolic interface problems. *Calcolo*, 43:253–277, 2006.

[69] John Lighton Synge. *The hypercircle in mathematical physics: a method for the approximate solution of boundary value problems*. Cambridge University Press, 2012.

[70] Manel Tayachi, Antoine Rousseau, Eric Blayo, Nicole Goutal, and Véronique Martin. Design and analysis of a schwarz coupling method for a dimensionally heterogeneous problem. *International Journal for Numerical Methods in Fluids*, 75(6):446–465, 2014.

[71] Andreas Veeser and Rüdiger Verfürth. Explicit upper bounds for dual norms of residuals. *SIAM journal on numerical analysis*, 47(3):2387–2405, 2009.

[72] Tomáš Vejchodskỳ. Guaranteed and locally computable a posteriori error estimate. *IMA Journal of Numerical Analysis*, 26(3):525–540, 2006.

[73] Rüdiger Verfürth. A posteriori error estimators for the stokes equations. *Numerische Mathematik*, 55(3):309–325, 1989.

[74] Rüdiger Verfürth. A posteriori error estimation and adaptive mesh-refinement techniques. *Journal of Computational and Applied Mathematics*, 50(1-3):67–83, 1994.

[75] Rüdiger Verfürth. Robust a posteriori error estimators for a singularly perturbed reaction-diffusion equation. *Numerische Mathematik*, 78:479–493, 1998.

[76] Rüdiger Verfürth. Robust a posteriori error estimates for stationary convection-diffusion equations. *SIAM journal on numerical analysis*, 43(4):1766–1782, 2005.

[77] Rüdiger Verfürth. *A posteriori error estimation techniques for finite element methods*. OUP Oxford, 2013.

[78] Martin Vohralík. A posteriori error estimates for efficiency and error control in numerical simulations. *Lecture Notes. Paris: Université Pierre et Marie Curie*, 2013.

[79] Martin Vohralík. A posteriori error estimates for efficiency and error control in numerical simulations. Lecture notes, Course NM497, 2018.

[80] Junping Wang, Yanqiu Wang, and Xiu Ye. A posteriori error estimate for stabilized finite element methods for the stokes equations. *International Journal of Numerical Analysis & Modeling*, 9(1), 2012.

[81] Chi-Yung Wen, Anh Dinh Le, Kun-Tsan Jeng, and Bin-Tsang Tsai. A numerical model of the cathode of a proton exchange membrane fuel cell with experimental validation. *Int. J. Numer. Anal. Model. Ser. B*, 1(2):123–146, 2010.

[82] Matthias Wohlmuth and Manfred Dobrowolski. Numerical analysis of Stokes equations with improved LBB dependency. *Electronic Transactions on Numerical Analysis*, 32:173–189, 2008.

[83] Daming Zhou. *Modeling and Multi-Dimensional Analysis of a Proton Exchange Membrane Fuel Cell*. PhD thesis, Bourgogne Franche-Comté, 2017.

[84] Olgierd C Zienkiewicz and Jian Z Zhu. A simple error estimator and adaptive procedure for practical engineerng analysis. *International journal for numerical methods in engineering*, 24(2):337–357, 1987.